CHARACTERISATION OF PASTES IN CHOCOLATE PROCESSING

by

CHARLOTTE LOUISE IOSSON

A thesis submitted to the
University of Birmingham
for the degree of
DOCTOR OF ENGINEERING

School of Chemical Engineering
College of Engineering and Physical Sciences
University of Birmingham
September 2018

UNIVERSITY OF
BIRMINGHAM

University of Birmingham Research Archive

e-theses repository

This unpublished thesis/dissertation is copyright of the author and/or third parties. The intellectual property rights of the author or third parties in respect of this work are as defined by The Copyright Designs and Patents Act 1988 or as modified by any successor legislation.

Any use made of information contained in this thesis/dissertation must be in accordance with that legislation and must be properly acknowledged. Further distribution or reproduction in any format is prohibited without the permission of the copyright holder.

ABSTRACT

The initial process step to combine the ingredients that form chocolate, prior to refining of the particle size, produces a thick paste resembling wet sand. Currently, experienced operators are relied upon to assess differences between batches. Pastes containing high volumes of large particles are challenging to measure using existing rheological techniques. A back extrusion technique is developed which produces comparable measurements of pastes containing small particles to existing rheological techniques. Repeatable measurements have also been achieved of chocolate pastes, containing 74 vol% solids up to 1000 μm. These chocolate pastes display shear thinning behaviour and many exhibit a yield stress. Increasing the fat content reduces the yield stress and shear thinning behaviour, generating a paste with properties closer to a Newtonian fluid. Increasing the temperature of the paste also reduces the overall paste viscosity and refining warmer pastes produces smaller particles, similarly to increasing the fat content. Measuring the power draw of the mixer, although specific to the mixing geometry, provides an indication of differences between pastes which correlate with viscosity measurements. Additionally, the particle size of the refined material correlates strongly with the power measured on the refiner rolls, offering a supplementary method of assessing the particle sizes online.

ACKNOWLEDGEMENTS

Firstly, I would like to thank my lead supervisor, Dr. Andy Ingram, for his continuous academic and, at times emotional, support throughout my EngD. Without our extensive discussions and thorough feedback, I would not have reached this stage. I would also like to thank Prof. Serafim Bakalis for providing me with this opportunity to work on an industrial project. Within Mondelēz International, I am extremely grateful for the supervision of Dr. Beccy Smith and Anthony Brown throughout this project who have given up much of their time and helped to ensure that the research remains industrially relevant.

I am also grateful for the support of Dr. Richard Greenwood and Prof. Mark Simmons, along with his research group, for their views and advice. Furthermore, I thank Stuart Blackburn for the use of his lab and assistance from John Wedderburn.

I would like to show my greatest appreciation for all the help from colleagues at Mondelēz International for assistance with trials. In particular, Stuart and Ollie who have been extraordinarily tolerant and supportive of all my requests over the years.

Furthermore, I would like to thank those people who have kept me sane during this entire endeavour: early on, I appreciated both the intellectual support and friendship from Tim, Federico and John; in particular, Tom and Iain have continually helped as both friends and academics; additionally, I am appreciative for those friends, both within and outside of the department, who have helped me enjoy my additional 4 years in Birmingham.

Special thanks go to my parents, Jackie and Andy, and particularly my sister Vicki, who have always been supportive and understanding. Finally, I am ever grateful to Stefan for surviving my madness and providing me with my all-important writing desk.

TABLE OF CONTENTS

TABLE OF CONTENTS ..... **I**

LIST OF FIGURES ..... **VI**

LIST OF TABLES ..... **XXI**

NOMENCLATURE ..... **XXIX**

1 INTRODUCTION **1**

1.1 BUSINESS CASE 1

1.2 OUTLINE OF THE MANUFACTURING PROCESS 2

1.3 IMPACT OF PASTING 5

1.4 AIMS 6

2 LITERATURE REVIEW **8**

2.1 INGREDIENTS 8

2.1.1 Dairy powders *8*

2.1.2 Sucrose *14*

2.1.3 Fat *15*

2.1.4 Non-fat cocoa solids *16*

2.1.5 Crumb *16*

2.1.6 Emulsifiers *17*

2.1.7 Effect of fat additions on chocolate properties *20*

2.2 RHEOLOGICAL BEHAVIOUR OF PARTICULATE SYSTEMS 21

2.2.1 Viscosity of continuous phase *21*

2.2.2 Packing of particles *22*

2.2.3 Particle shape *25*

2.2.4 Effective solid volume content *25*

2.2.5 Aggregation and deaggregation affecting immobilised fat *26*

2.2.6 Particle interactions *27*

2.2.7 Specific effects on the shear thinning behaviour of suspensions *27*

2.2.8 Specific effects on the yield stress *28*

2.3 EFFECT OF PROCESSING ON SUSPENSIONS 29

2.3.1 Mechanisms of particle wetting *30*

2.3.2 Particle size changes during processing *32*

2.3.3 Identifying homogeneity *33*

2.4 METHODS FOR MEASURING RHEOLOGY OF PASTES 35

2.4.1 Cone and plate or parallel plate rheology *36*

2.4.2 Concentric cylinders *37*

2.4.3 Vane rheology *39*

2.4.4 Capillary extrusion *41*

2.4.5 Back extrusion *43*

2.4.6 Penetrometers and vanes used for soils *45*

2.4.7 Slump test *46*

2.4.8 Bostwick consistometer *46*

2.4.9 FT4 powder rheometer *47*

2.4.10 Measuring rheology in mixers *47*

3 MATERIALS AND METHODS 50

3.1 INTRODUCTION 50

3.2 METHODS: EQUIPMENT 50

3.2.1 Mixing *51*

3.2.2 Refining *54*

3.3 METHODS: MEASURING TECHNIQUES 56

3.3.1 Operator ranking *56*

3.3.2 Particle size distribution *57*

3.3.3 FT4 powder rheometer *60*

3.3.4 Parallel plate rheology *61*

3.3.5 Vane rheology *61*

3.3.6 Simplified back extrusion technique *62*

3.3.7 Finalised back extrusion technique *62*

3.3.8 Density *64*

3.3.9 X-Ray computer tomography *64*

3.4 METHODS: STATISTICAL ANALYSIS 65

3.4.1 Predictive models *65*

3.4.2 Principal component analysis *66*

3.5 MATERIALS 66

4 METHODS TRIALLED TO CHARACTERISE PASTES 69

4.1 INTRODUCTION 69

4.2 PARALLEL PLATE RHEOLOGY 72

4.2.1 Steady shear tests *72*

4.2.2 Oscillatory shear tests *74*

4.3 VANE RHEOLOGY 80

4.3.1 Steady shear tests *81*

4.3.2 Oscillatory shear tests *82*

4.4 FT4 POWDER RHEOMETER 87

4.5 MIXER POWER 89

4.6 CONCLUSIONS 90

5 ANALYSING THE SUITABILITY OF THE BACK EXTRUSION TECHNIQUE 93

5.1 INTRODUCTION 93

5.2 PRINCIPLE OF THE TECHNIQUE 94

5.2.1 Initial motion of the probe *96*

5.2.2 End of the probe motion *99*

5.2.3 Shape of force increase *100*

5.2.4 Probe hold within the sample *108*

5.2.5 Comparisons of raw data *110*

5.3 FITTING TO RHEOLOGICAL MODELS 112

5.3.1 Calculating the flow behaviour index *114*

5.3.2 Sensitivity *119*

5.3.3 Rheological measurements of suspensions *121*

5.3.4 Effect of probe ratio *129*

5.3.5 Shear rates relevant within the manufacturing process *133*

5.4 CONCLUSION 135

6 IMPACT OF FORMULATION AND PROCESSING CONDITIONS ON PASTE CONSISTENCY 137

6.1 INTRODUCTION 137

6.2 TRIAL 1: INFLUENCE OF FAT CONTENT, LECITHIN CONTENT, MIXING TIME AND MIXING SPEED 140

6.2.1 Comparisons of the techniques to quantify paste consistency *142*

6.2.2 Significant effects on the Herschel-Bulkley model parameters measured using the back extrusion technique *145*

6.2.3 Significant effects on the online measuring techniques *148*

6.2.4 Significant effects on the particle size distributions *154*

6.2.5 Can the change in consistency due to fat content be replicated by longer mixing time? *161*

6.2.6 Discussion *163*

6.3 TRIAL 2: INFLUENCE OF FAT CONTENT, LECITHIN CONTENT, MIXING TIME AND TEMPERATURE 165

6.3.1 Back extrusion technique *168*

6.3.2 Significant Effects on the Particle Size Distributions *180*

6.3.3 Comparing consistency with particle size distribution *184*

6.3.4 What process settings can be used to change the consistency instead of additional fat? *185*

6.3.5 Discussion *187*

6.4 COMPARISONS BETWEEN THE TWO TRIALS 188

6.5 CONCLUSIONS 189

7 IMPACT OF FORMULATION AND PROCESSING CONDITIONS ON REFINING 193

7.1 INTRODUCTION 193

7.2 TRIAL 1: PRE-REFINED PASTE 194

7.2.1 Particle size distributions of pre-refined paste *194*

7.2.2 Consistency of pre-refined paste *202*

7.2.3 Discussion *214*

7.3 TRIAL 1: REFINED FLAKE 215

7.3.1 Refined particle sizes *216*

7.3.2 Comparing Refiner Flake PSD with Paste Consistency *221*

7.3.3 Comparing Refiner Flake PSD with Pre-Refined Paste Consistency *222*

7.3.4 Contrasting additional fat with more intensive mixing of the paste *223*

7.3.5 Impact of lecithin *224*

7.3.6 Discussion *228*

7.4 TRIAL 2 229

7.4.1 Refiner performance *230*

7.4.2 Particle Size Distributions of the Refined Paste *239*

7.4.3 Discussion *252*

7.5 CONCLUSIONS 255

8 CONCLUSIONS AND FUTURE WORK 259

8.1 QUANTIFYING CHOCOLATE PASTE RHEOLOGY 259

8.2 INFLUENCING PASTE CONSISTENCY 261

8.3 IMPACT ON DOWNSTREAM PERFORMANCE 262

8.4 FUTURE WORK 263

8.4.1 Back extrusion technique *263*

8.4.2 Chocolate paste processing *264*

REFERENCES 267

APPENDIX 1 276

APPENDIX 2 292

LIST OF FIGURES

Figure 1.1: Summary of the main two manufacturing processes a) powder chocolate, generally manufactured for the continental Europe market and b) crumb chocolate, used most prolifically for British chocolate 4

Figure 2.1: Dimpled surfaces on spray dried milk powder particles (Kaláb, 2010)..... 11

Figure 2.2: Highly agglomerated spray dried milk powder particle (Kaláb, 2010) 11

Figure 2.3: Pore structure within a broken spray dried milk powder particle (Kaláb, 2010) 12

Figure 2.4: Location of fat within a spray dried milk powder particle (Vignolles et al., 2007)..... 13

Figure 2.5: Results taken from Farris (1968) comparing the relative viscosities of particle suspensions over a range of solid volume fractions for monomodal and multimodal distributions of particles. 23

Figure 2.6: Results taken from Ancey et al. (2001) detailing the yield stress,τC, as a function of solids concentration of the coarse fraction using bimodal particles of 0.3 and 3 mm. ξ is the volume occupied by the small particles to the total volume of the coarse fraction..... 24

Figure 2.7: Effect of the particle shape on yield stress and consistency of suspensions when the solid volume fraction is increased (Hafid et al., 2016)..... 25

Figure 2.8: Diagram of the ConTec Visco5 used by Heirman et al. (2008). Labelled are: (1) top ring, (2) outer cylinder, (3) test material, (4) free upper section of inner cylinder, (5) fixed bottom of inner cylinder..... 40

Figure 2.9: 2D MRI of a 40 % suspension of 250 µm particles within a yield stress fluid after 1 hour of shearing in a vane rheometer, taken from Ovarlez (2011). Lighter areas are regions of higher suspending fluid concentration..... 41

Figure 3.1: Mixing blades within the 200kg capacity Buhler mixer. Base situated the top left corner of the image opens to release the paste into the pre-refiner. 52

Figure 3.2: Current draw of the mixing shaft motor over the duration of the production of one chocolate paste batch..... 52

Figure 3.3: Side on and birds eye view images of the Aoustin mixer with two z-blade mixing shafts..... 54

Figure 3.4: Diagrams of the three different refiner layouts that have been used in chapter 7 56

Figure 3.5: Mean particle size distribution of four batches of pastes with the same formulation, each measured three times. The error bars represent one standard deviation. 59

Figure 3.6: Mean particle size distribution of four batches of pastes with the same formulation, each measured three times, compared with the mean model PSD computed in two ways: 1) each paste is modelled and the mean of the volume distribution within each sieve size is plotted and 2) the mean is taken of each PSD model parameter used to describe each run and then a PSD is reconstructed. *60*

Figure 3.7: XRCT of two model pastes containing sugar, skimmed milk powder, cocoa powder and vegetable oil a) MCP1 and b) MCP2 (see Table 4.1 for formulations). Samples are encased in a circular straw section. Darkest areas are low density (air pockets), lighter areas have higher densities. Large sugar particles can easily be distinguished however the mixture of oil, milk powder and cocoa is too difficult to differentiate. *65*

Figure 4.1: Shear sweep tests of three model chocolate paste formulations tested on a 40mm parallel plate rheometer. Error bars represent the standard error. *73*

Figure 4.2: Failure points of the three chocolate paste formulations during the parallel plate shear sweep tests, $R^2 = 0.9923$ *74*

Figure 4.3: Storage and loss moduli from a strain sweep of MCP3 using a parallel plate geometry. Frequency is $10\ rad\ s^{-1}$ *77*

Figure 4.4: Storage and loss moduli from a frequency sweep of MCP3 using a parallel plate geometry. Strain is 0.005 % *77*

Figure 4.5: Storage and loss moduli from a strain sweep of MCP2 using a parallel plate geometry. Frequency is $10\ rad\ s^{-1}$ *77*

Figure 4.6: Storage and loss moduli from a frequency sweep of MCP2 using a parallel plate geometry. Strain is 0.005 % *77*

Figure 4.7: Storage and loss moduli from a strain sweep of MCP1 using a parallel plate geometry. Frequency is $10\ rad\ s^{-1}$ *78*

Figure 4.8: Storage and loss moduli from a frequency sweep of MCP1 using a parallel plate geometry. Strain is 0.005 % *78*

Figure 4.9: Viscosity and complex viscosity of MCP1 calculated from linear shear and oscillation tests, respectively, on a 40 mm parallel plate. *79*

Figure 4.10: Viscosity and complex viscosity of MCP2 calculated from linear shear and oscillation tests, respectively, on a 40 mm parallel plate. *79*

Figure 4.11: Viscosity and complex viscosity of MCP3 calculated from linear shear and oscillation tests, respectively, on a 40 mm parallel plate. *80*

Figure 4.12: Results of shear ramp tests using a vane rheometer to measure the three model chocolate pastes . *81*

Figure 4.13: Storage and loss moduli from a strain sweep of MCP1 using a vane in cup geometry. Frequency is 10 rad s^{-1} *83*

Figure 4.14: Storage and loss moduli from a frequency sweep of MCP1 using a vane in cup geometry *83*

Figure 4.15: Storage and loss moduli from a strain sweep of MCP2 using a vane in cup geometry. Frequency is 10 rad s^{-1} *83*

Figure 4.16: Storage and loss moduli from a frequency sweep of MCP2 using a vane in cup geometry *83*

Figure 4.17: Storage and loss moduli from a strain sweep of MCP2 using a vane in cup geometry. Frequency is 10 rad s^{-1} *84*

Figure 4.18: Storage and loss moduli from a frequency sweep of MCP3 using a vane in cup geometry *84*

Figure 4.19: Viscosity and complex viscosity of MCP1 calculated from linear shear and oscillation tests, respectively, using a vane in cup geometry *85*

Figure 4.20: Viscosity and complex viscosity of MCP2 calculated from linear shear and oscillation tests, respectively, using a vane in cup geometry *85*

Figure 4.21: Viscosity and complex viscosity of MCP3 calculated from linear shear and oscillation tests, respectively, using a vane in cup geometry *85*

Figure 4.22: Comparisons of viscosity and complex viscosity of MCP1 from steady shear and oscillatory shear tests, respectively, where a) parallel plate geometry and b) vane in cup geometry *86*

Figure 4.23: Comparisons of viscosity and complex viscosity of MCP2 from steady shear and oscillatory shear tests, respectively, where a) parallel plate geometry and b) vane in cup geometry *87*

Figure 4.24: Comparisons of viscosity and complex viscosity of MCP3 from steady shear and oscillatory shear tests, respectively, where a) parallel plate geometry and b) vane in cup geometry *87*

Figure 4.25: Flow energy of three pastes measured on the FT4 powder rheometer. Results of a students t-test showed that all three results are statistically significant. *88*

Figure 4.26: Current measured on the mixing shaft during paste manufacture of a standard chocolate recipe in a 200 kg capacity vessel. Error bars are the standard error of three repeated batches. *90*

Figure 5.1: Idealise force response produced during a single test run of the back extrusion technique. The force increases initially as the probe is plunged into the sample (A-B) until it reaches a set distance (B). The probe then stops remains stationary for 60 seconds. The material has a short relaxation period where the meniscus relaxes before reaching a steady force at C. *96*

Figure 5.2: Initial force increase at 0.46 seconds after the probe begins to move into the sample. *97*

Figure 5.3: Force measured at 0.46 seconds into test phase (black markers) and force calculated from probe mass × acceleration. Reuslts are plotted against the probe velocity set for the test using four probe diameters. Linear trend lines go through the intercept. Results of raw data from testing SMP47. ..... *98*

Figure 5.4: Velocities of the probe as the BET begins. Results at four different probe velocities are shown when testing SMP47 using a 30 mm diameter probe within a 90 mm diameter vessel (three repeats at each speed are shown, all tests were on the same sample). *99*

Figure 5.5: Slowing of the probe velocity as the test approaches the time of maximum plunged distance. The test time is normalised with respect to the point where the plunger has moved 50 mm. The data shown is from tests on SMP47 although similar results are seen for all fluids. *100*

Figure 5.6: Slowing of the probe velocity as the test approaches the maximum plunged distance. The distance moved by the probe is normalised with respect to the point where the plunger has moved 50 mm. The data shown is from tests on SMP47 although similar results are seen for all fluids. *100*

Figure 5.7: Force over time data of three materials, normalised between 0 – 1. Tests were run using a 30 mm diameter probe at 16 mm s^{-1} *101*

Figure 5.8: Average deviations from linearity over four different probe diameters, averaged over four probe velocities. Error bars are standard error of 3 repeated measurements on each sample..... *102*

Figure 5.9: Average deviations from linearity over four different probe diameters, averaged over four probe velocities. Error bars are standard error of 3 repeated measurements on each sample..... *102*

Figure 5.10: Average deviations from linearity over four different test velocities. Error bars are standard error of 3 repeated measurements on each sample at four probe diameters. *102*

Figure 5.11: Average deviations from linearity over four different test velocities. Error bars are standard error of 3 repeated measurements on each sample at four probe diameters. *102*

Figure 5.12: Average deviations from linearity for IS57 and CP74 over four different probe diameters using smooth and roughened (R) walls. Error bars are standard error of 3 repeated measurements on each sample at four probe diameters. *104*

Figure 5.13: Average deviations from linearity for CP68 and GS60 over four different probe diameters using smooth and roughened (R) walls. Error bars are standard error of 3 repeated measurements on each sample at four probe diameters. *104*

Figure 5.14: Normalised force of CP74, plotted against the normalised time, comparing the results using smooth and roughened surfaces (30 mm diameter probe at 16 mm s^{-1}*)* *105*

Figure 5.15: Average deviations from linearity for IS57 and CP74 over four different test velocities using smooth and roughened (R) walls. Error bars are standard error of 3 repeated measurements on each sample at four probe diameters. *106*

Figure 5.16: Average deviations from linearity for CP68 and GS60 over four different test velocities using smooth and roughened (R) walls. Error bars are standard error of 3 repeated measurements on each sample at four probe diameters. *106*

Figure 5.17: Peak forces of three chocolate pastes at four probe velocities with error bars representing the standard error *112*

Figure 5.18: Relaxation forces of three chocolate pastes at four probe velocities. The dashed line represents the average value of the buoyancy force of the probe for all three pastes (484 ± 5.14 mN) *112*

Figure 5.19: Examples of the velocity profiles created within the gap between the probe and the vessel wall as the probe is plunged down into the sample and the material is forced back up through the annulus. Velocities are relative to the vessel wall. R is the radius of the vessel and ξ *is the dimensionless radius of the vessel.* *113*

Figure 5.20: Example of the coefficients of variance which occur for the consistency coefficients when different values of flow behaviour indices are analysed *115*

Figure 5.21: Shear stress plotted against shear rate for CP62, comparing the results when two techniques (T1 or T2) have been used to determine the flow behaviour indices using four different probe diameters (20 - 35 mm) *116*

Figure 5.22: Shear stress plotted against shear rate for CP68, comparing the results when two techniques (T1 or T2) have been used to determine the flow behaviour indices using four different probe diameters (20 - 35 mm) *117*

Figure 5.23: Shear stress plotted against shear rate for CP74, comparing the results when two techniques (T1 or T2) have been used to determine the flow behaviour indices using four different probe diameters (20 - 35 mm) *118*

Figure 5.24: Shear stress vs shear rate of a 5% CMC solution when the physical inputs are altered by +/- 5% *121*

Figure 5.25: Rheological behaviour of a CMC solution measured using a parallel plate and the BET (40mm diameter vessel) *123*

Figure 5.26: Rheological behaviour of SMP32 measured using a parallel plate and the BET (40mm diameter vessel) *123*

Figure 5.27: Rheological behaviour of SMP43 measured using a parallel plate and the BET (90mm diameter vessel) *124*

Figure 5.28: Rheological behaviour of SMP47 measured using a parallel plate and the BET (90mm diameter vessel) *124*

Figure 5.29: Rheological behaviour of SMP56 measured using a parallel plate and the BET (90mm diameter vessel) *125*

Figure 5.30: Rheological behaviour of IS57 measured using a parallel plate and the BET (90mm diameter vessel) *125*

Figure 5.31: Rheological behaviour of GS60 measured using a parallel plate and the BET (90mm diameter vessel) *127*

Figure 5.32: Rheological behaviour of CP62 measured using a parallel plate and the BET (90mm diameter vessel) *127*

Figure 5.33: Rheological behaviour of CP68 measured using a parallel plate and the BET (90mm diameter vessel) *127*

Figure 5.34: Rheological behaviour of CP74 measured using a parallel plate and the BET (90mm diameter vessel) *127*

Figure 5.35: Consistency coefficients of each measurement of three chocolate pastes. Comparison circles are shown on the right which indicate that all three formulations are significantly different. *129*

Figure 5.36: Yield stresses of each measurement of three chocolate pastes. Comparison circles are shown on the right which indicate that the yield stress of CP74 is significantly different to the yield stresses of CP62 and CP68. ..... *129*

Figure 5.37: Flow behaviour indices of each measurement of three chocolate pastes. Comparison circles are shown on the right which indicated all three formulations are significantly different. *129*

Figure 5.38: Shear stresses, at a shear rate of 10 s^{-1} of each measurement of three chocolate pastes. Comparison circles are shown on the right which indicated all three formulations are significantly different. *129*

Figure 5.39: Rheological behaviour of CP62 measured using four probes with different diameters *132*

Figure 5.40: Rheological behaviour of CP68 measured using four probes with different diameters *132*

Figure 5.41: Rheological behaviour of CP74 measured using four probes with different diameters *133*

Figure 6.1: Loading plots of the first two principal components which describe 76.6 % of the variation between the operator rank, mixing shaft current, flow behaviour index, consistency coefficient, yield stress and the shear stress at a shear rate of 10 s^{-1} (final four measured using the BET) *145*

Figure 6.2: Yield stresses of the pastes which were produced in trial 1 ..... *146*

Figure 6.3: Interaction between fat and mixing time significantly impacts the current measured onthe mixer. The results from the predictive model are plotted and the error bars are the standard deviation. *149*

Figure 6.4: Temperatures of the pastes which were produced in trial 1. Temperatures at the beginning were established from the raw ingredients and temperatures were measured using a temperature probe at the end of the mixing duration. Some gaps exist where the temperature was not recorded. *150*

Figure 6.5: Interaction between fat content and mixing time significantly impacts the temperatures of pastes. The results from the predictive model are plotted and the error bars are the standard deviation. *152*

Figure 6.6: Temperatures of the pastes plotted against the consistency measurements. A line of best fit has been drawn and the value of R^2 is quoted. *153*

Figure 6.7: Average particle size distribution of all the pastes produced in trial 1 ..... *155*

Figure 6.8: Influence of the fat content on the paste PSDs using the average model parameters from the least squares fit ($SSA_{low\ fat}$ = 271.6 $m^2\ kg^{-1}$, $SSA_{high\ fat}$ = 260.0 $m^2\ kg^{-1}$) *156*

Figure 6.9: Influence of the mixing time on the paste PSDs using the average model parameters from the least squares fit *156*

Figure 6.10: Influence of the mixing speed on the paste PSDs using the average model parameters from the least squares fit ($SSA_{low\ speed}$ = 256.1 $m^2\ kg^{-1}$, $SSA_{high\ speed}$ = 275.6 $m^2\ kg^{-1}$) *156*

Figure 6.11: Influence of the mixing time and mixing speed on the paste PSDs using the average model parameters from the least squares fit *157*

Figure 6.12: Influence of the fat content and mixing speed on the paste PSDs using the average model parameters from the least squares fit ($SSA_{29.5\%\ fat,\ 14\ rpm}$ = 268.5 $m^2\ kg^{-1}$, $SSA_{29.5\%\ fat,\ 37\ rpm}$ = 274.8 $m^2\ kg^{-1}$, $SSA_{34.5\%\ fat,\ 14\ rpm}$ = 243.6 $m^2\ kg^{-1}$, $SSA_{34.5\%\ fat,\ 37\ rpm}$ = 276.3 $m^2\ kg^{-1}$) *158*

Figure 6.13: Influence of the lecithin content and mixing time on the paste PSDs using the average model parameters from the least squares fit *158*

Figure 6.14: Current of the mixer measured at the end of the mixing time of pastes produced in trial 1, varying in fat content, lecithin content, mixing time and mixing speed. *163*

Figure 6.15: Shear stress of pastes, at a shear rate of 10 s^{-1}, produced in trial 1, based on the Herschel-Bulkley parameters measured on the BET, varying in fat content, lecithin content, mixing time and mixing speed. *163*

Figure 6.16: Measured yield stresses plotted against values from the predictive model. The plot on the left shows the entire data set where p-$value_{ANOVA}$ = 0.0016 and p-$value_{LoF}$ = 0.005. The outlier is removed and the plot on the right shows the actual and predicted data of the new model with a p-$value_{ANOVA}$ = 0.0114 and p-$value_{LoF}$ = 0.84. ..... *170*

Figure 6.17: Interaction between fat and mixing time significantly impacts the yield stresses of pastes. The results from the predictive model are plotted and the error bars are the standard deviation. *172*

Figure 6.18: Interaction between temperature and mixing time significantly impacts the yield stresses of pastes. The results from the predictive model are plotted and the error bars are the standard deviation. *173*

Figure 6.19: The fat content significantly impacts the flow behaviour indices of the pastes. The results from the predictive model are plotted and the error bars are the standard deviation. *174*

Figure 6.20: Interaction between temperature and mixing time significantly impacts the flow behaviour index of the pastes, plus there is a significant curvature of the temperature. The results from the predictive model are plotted and the error bars are the standard deviation *175*

Figure 6.21: The fat content significantly impacts the consistency coefficient of the pastes. The results from the predictive model are plotted and the error bars are the standard deviation. *177*

Figure 6.22: The mixing time significantly impacts the consistency coefficient of the pastes, plus there is a significant curvature of the mixing time. The results from the predictive model are plotted and the error bars are the standard deviation. *177*

Figure 6.23: The fat content significantly impacts the shear stress of pastes at a shear rate of 10 s^{-1}. The results from the predictive model are plotted and the error bars are the standard deviation. *179*

Figure 6.24: The mixing time significantly impacts the shear stress of pastes at a shear rate of 10 s^{-1}. The results from the predictive model are plotted and the error bars are the standard deviation. *179*

Figure 6.25: Interaction between fat and the lecithin content significantly impacts the shear stress of the pastes, at a shear rate of 10 s^{-1}. The results from the predictive model are plotted and the error bars are the standard deviation. *179*

Figure 6.26: Influence of the mixing time on the paste PSDs using the average model parameters from the least squares fit *181*

Figure 6.27: Loading plots of the first three principal components which describe 79.3% of the variation between the particle size parameters of the three log-normal distributions (mean, M, standard deviation, S, and weight, W), the specific surface areas (SSA) and the results measured using the BET (flow behaviour index, consistency coefficient, yield stress and the shear stress at a shear rate of 10 s^{-1}). The log-normal peak containing the smallest particles is labelled 1, the largest particles are within the log-normal peak labelled 3. ..... *184*

Figure 6.28: Comparing how shear stress at a shear rate of 10 s^{-1} changes depending on the fat content and mixing time when the lecithin content is 0 vol%. The results from the predictive model are plotted and the error bars are the standard deviation. *186*

Figure 6.29: Comparing how shear stress at a shear rate of 10 s^{-1} changes depending on the fat content, mixing time when the lecithin content is 0.14 vol%. The results from the predictive model are plotted and the error bars are the standard deviation. *186*

Figure 6.30: Average particle size distributions of the pastes produced in trial 1 and trial 2 using the average model parameters from the least squares fit *189*

Figure 7.1: Average particle size distributions of the pastes and pre-refined pastes produced in trial 1 using the average model parameters from the least squares fit *195*

Figure 7.2: Influence of the fat content on the pre-refined paste PSDs using the average model parameters from the least squares fit *197*

Figure 7.3: Loading plots of the first three principal components which describe 78.4% of the variation between the particle size parameters of the three log-normal distributions (mean, M, standard deviation, S, and weight, W) for the pastes (P) and the pre-refined pastes (PR). The log-normal peak containing the smallest particles is labelled 1, the largest particles are within the log-normal peak labelled 3. ..... *201*

Figure 7.4: Loading plots of the first three principal components which describe 61 % of the variation between the results of the pastes measured using the BET (flow behaviour index, consistency coefficient, yield stress and the shear stress at a shear rate of 10 s^{-1}), the operator ranks of the pastes, the values of current measured at the end of mixing and the particle size parameters of the three log-normal distributions describing the pre-refined pastes (mean, M, standard deviation, S, and weight, W). The log-normal peak containing the smallest particles is labelled 1, the largest particles are within the log-normal peak labelled 3. ..... *202*

Figure 7.5: Loading plots of the first two principal components which describe 82.9 % of the variation between the results of the pre-refined pastes measured using the BET (flow behaviour index, consistency coefficient, yield stress and the shear stress at a shear rate of 10 s^{-1}) and the operator rank of the pre-refined pastes. *205*

Figure 7.6: The fat content significantly impacts the shear stress of pre-refined paste at a shear stress of 10 s^{-1}. The results from the predictive model are plotted and the error bars are the standard deviation. *206*

Figure 7.7: Interaction between mixing time and mixing speed significantly impacts the shear stress of pre-refined paste at a shear stress of 10 s^{-1}. The results from the predictive model are plotted and the error bars are the standard deviation. *206*

Figure 7.8: Yield stresses of the pre-refined pastes which were produced in trial 1 ..... *207*

Figure 7.9: The fat content significantly impacts the operator rank of pre-refined paste. The results from the predictive model are plotted and the error bars are the standard deviation. *207*

Figure 7.10: The lecithin content significantly impacts the operator rank of pre-refined paste. The results from the predictive model are plotted and the error bars are the standard deviation. *207*

Figure 7.11: Interaction between lecithin content and mixing time significantly impacts the operator rank of pre-refined paste. The results from the predictive model are plotted and the error bars are the standard deviation. *208*

Figure 7.12: Interaction between lecithin content and mixing time significantly impacts the SSA of pre-refined paste. The results from the predictive model are plotted and the error bars are the standard deviation. *208*

Figure 7.13: Consistency parameters of the paste and pre-refined pastes based on the predictive models for the Herschel-Bulkley model parameters and the shear stress at a shear rate of 10 s^{-1}. The results from the predictive model are plotted and the error bars are the standard deviation. *211*

Figure 7.14: Loading plots of the first three principal components which describe 71.1 % of the variation between the results of the pre-refined pastes measured using the BET (flow behaviour index, consistency coefficient, yield stress and the shear stress at a shear rate of 10 s^{-1}), the operator ranks of the pre-refined pastes and the particle size parameters of the three log-normal distributions describing the pre-refined pastes (mean, M, standard deviation, S, and weight, W). The log-normal peak containing the smallest particles is labelled 1, the largest particles are within the log-normal peak labelled 3. ..... *212*

Figure 7.15: Shear stress at a shear rate of 10 s^{-1} of pre-refined pastes produced in trial 1, based on the Herschel-Bulkley parameters measured on the BET, varying in fat content, lecithin content, mixing time and mixing speed. The points are staggered within each mixing category in order to see each of the points clearly. *213*

Figure 7.16: Influence of the fat content on the refiner flake PSDs using the average model parameters from the least squares fit..... *217*

Figure 7.17: Influence of the mixing time and mixing speed on the refined flake PSDs using the average model parameters from the least squares fit *218*

Figure 7.18: Influence of the fat content and mixing speed on the refined flake PSDs using the average model parameters from the least squares fit *219*

Figure 7.19: Loading plots of the first two principal components which describe 77.8 % of the variation between the results of the pastes measured using the BET (flow behaviour index, consistency coefficient, yield stress and the shear stress at a shear rate of 10 s^{-1}), the operator rank of the pastes, the mixing shaft current and the particle size parameters of the two log-normal distributions describing the refined flake (mean, M, standard deviation, S, and weight, W). The log-normal peak containing the smallest particles is labelled 1, the largest particles are within the log-normal peak labelled 2. ..... *222*

Figure 7.20: Loading plots of the first two principal components which describe 85.4 % of the variation between the results of the pre-refined pastes measured using the BET (flow behaviour index, consistency coefficient, yield stress and the shear stress at a shear rate of 10 s^{-1}), the operator rank of the pre-refined pastes and the particle size parameters of the two log-normal distributions describing the refined flake (mean, M, standard deviation, S,

and weight, W). The log-normal peak containing the smallest particles is labelled 1, the largest particles are within the log-normal peak labelled 2. ..... *223*

Figure 7.21: Plot of the refined flake PSD comparing low fat flakes which were pasted at intensive conditions and high fat flakes which were gently pasted based on the predictive models of each PSD parameter. Note: the lecithin content is at an average value = 0.075 vol% *224*

Figure 7.22: Plot of the refiner flake PSD based on the predictive models of each PSD parameter, comparing low fat flakes which were pasted at intensive conditions and high fat flakes which were gently pasted at 0 vol% lecithin. *225*

Figure 7.23: Plot of the refiner flake PSD based on the predictive models of each PSD parameter, comparing low fat flakes which were pasted at intensive conditions and high fat flakes which were gently pasted with 0.15 vol% lecithin. *225*

Figure 7.24: Plot of the pre-refined paste consistency measurements on the BET based on the predictive models over a range of the lecithin contents, comparing results of a low fat paste mixed for 18 minutes at 37 rpm and a low fat paste mixed for 2 minutes at 14 rpm. *226*

Figure 7.25: Plot of the shear stress and shear rate of two pastes which do not contain lecithin at 1) a high fat content and low mixing time/speed and 2) a high mixing time/speed and a low fat content. The highlighted region is where the behaviour of the paste is similar to what has been observed for refined flakes. *227*

Figure 7.26: Plot of the shear stress and shear rate of two pastes which contain 0.15 vol% lecithin at 1) a high fat content and low mixing time/speed and 2) a high mixing time/speed and a low fat content. The highlighted region is where the behaviour of the paste is similar to what has been observed for refined flakes. *228*

Figure 7.27: Measured times taken to refine plotted against values from the predictive model (p-value$_{LoF}$ = 0.0049). *231*

Figure 7.28: Average current measured on the first refiner roll plotted against values from the predictive model (p-value$_{LoF}$ = 0.0142). *231*

Figure 7.29: The fat content significantly impacts the time taken to refine. The results from the predictive model are plotted and the error bars are the standard deviation. *232*

Figure 7.30: The fat content significantly impacts the average current measured on the first refiner roll. The results from the predictive model are plotted and the error bars are the standard deviation. *232*

Figure 7.31: Interaction between fat content and temperature had marginally significance on the yield stresses of pastes (p-value = 0.0513). The results from the predictive model are plotted and the error bars are the standard deviation. *233*

Figure 7.32: Interaction between fat content and temperature significantly impacts the time taken to refine. The results from the predictive model are plotted and the error bars are the standard deviation. *233*

Figure 7.33: Influence of the fat and temperature on the paste PSDs using the average model parameters from the least squares fit *233*

Figure 7.34: Influence of the fat and lecithin content on the yield stress of the pastes, the shear stress of the pastes and the time taken to refine a batch of paste. The results from the predictive model are plotted and the error bars are the standard deviation. *235*

Figure 7.35: Interaction between lecithin content and temperature significantly impacts the time taken to refine. The results from the predictive model are plotted and the error bars are the standard deviation. *235*

Figure 7.36: Interaction between lecithin content and temperature significantly impacts the average current measured on the first refiner roll. The results from the predictive model are plotted and the error bars are the standard deviation. *235*

Figure 7.37: Significant curvature is measured for the fat content, mixing time and temperature. The results from the predictive model are plotted and the error bars are the standard deviation. *236*

Figure 7.38: Loading plots of the first three principal components which describe 84.8 % of the variation between the time taken for the batch to refine, the average current on the first roll of the refiner and the particle size parameters of the three log-normal distributions describing the pastes (mean, M, standard deviation, S, and weight, W). The log-normal peak containing the smallest particles is labelled 1, the largest particles are within the log-normal peak labelled 3. ..... *237*

Figure 7.39: Loading plots of the first two principal components which describe 85.6 % of the variation between the time taken for the batch to refine, the average current on the first roll of the refiner, flow behaviour index, consistency coefficient, yield stress and the shear stress at a shear rate of 10 s^{-1} (final four measured using the BET) *238*

Figure 7.40: Average particle size distributions of the pastes and refined pastes produced in trial 2 using the average model parameters from the least squares fit *240*

Figure 7.41: Influence of the fat content on the refined paste PSDs using the average model parameters from the least squares fit. At 29.9 vol% fat, d_{90} = 123.0 µm, SSA = 682.1 $m^2 kg^{-1}$. At 34.9 vol% fat, d_{90} = 107.5 µm, SSA = 730.9 $m^2 kg^{-1}$. *243*

Figure 7.42: The fat content and mixing time significantly impact the SSA of refined pastes. The results from the predictive model are plotted and the error bars are the standard deviation. *243*

Figure 7.43: Influence of the mixing time on the refined paste PSDs using the average model parameters from the least squares fit *244*

Figure 7.44: Influence of the fat content and temperature on the refined paste PSDs using the average model parameters from the least squares fit. *245*

Figure 7.45: Influence of lecithin content and temperature on the shear stress of the paste at a shear rate of 10 s^{-1}. The results from the predictive model are plotted and the error bars are the standard deviation. *246*

Figure 7.46: Influence of lecithin content and temperature on the time taken to refine and the current measured on the first roll of the refiner. The results from the predictive model are plotted and the error bars are the standard deviation. *246*

Figure 7.47: Influence of lecithin content and temperature on the d_{90} and the SSA of the refined paste. The results from the predictive model are plotted and the error bars are the standard deviation. *247*

Figure 7.48: Loading plots of the first two principal components which describe 61.5 % of the variation between the particle size parameters of the log-normal distributions (mean, M, standard deviation, S, and weight, W) for the pastes (P) and the refined pastes (R). The log-normal peak containing the smallest particles is labelled 1. The pastes are modelled by three log-normal distributions and the refined pastes are only modelled by two. *248*

Figure 7.49: Relationships between the shear stresses of the pastes and the SSA of the pre-refined paste when data is separated by each of the DoE factors *249*

Figure 7.50: Loading plots of the first three principal components which describe 86.6 % of the variation between the time taken for the batch to refine, the average current on the first roll of the refiner with the SSA, d_{90} and the particle size parameters of the two log-normal distributions describing the pastes (mean, M, standard deviation, S, and weight, W) and. The log-normal peak containing the smallest particles is labelled 1, the largest particles are within the log-normal peak labelled 3. ..... *250*

Figure 7.51: Relationships between the current measured on the first refiner rolls and the SSA of the refined paste when data is separated by each of the DoE factors *251*

Figure 7.52: Values of SSA of the refined paste based on the results from the predictive model, comparing pastes at high and low levels of each of the four factors: fat content, lecithin content, mixing time and temperature. . 252

LIST OF TABLES

Table 2.1: Typical compositions of milk powders, taken from (Bylund, 2015) *9*

Table 2.2: Fatty acid composition of cocoa butter (Szydłowska-Czerniak et al., 2017) and dairy fat (Beckett, 2009)..... *15*

Table 3.1: Techniques used to manufacture the pastes which will be presented within this Thesis..... *50*

Table 3.2: Base values of current measured on the mixer at each of the speeds using in this design of experiments, when empty...... *53*

Table 3.3: Values of refractive index used to test each material using laser diffraction..... *57*

Table 3.4: Physical properties of the solids from commercial suppliers...... *68*

Table 3.5: Physical properties of the liquids from commercial suppliers. *68*

Table 3.6: Average formulations of the chocolate pastes manufactured during two pilot plant trials..... *68*

Table 4.1: Formulations of model chocolate pastes (MCP). Ratios of solid components are maintained...... *71*

Table 4.2: Details of the techniques which were not capable of measuring the rheological properties of chocolate pastes and were not used past preliminary testing..... *71*

Table 4.3: Techniques which were able to measure some elements of the paste..... *72*

Table 4.4: Herschel-Bulkley model parameters describing the three model chocolate paste formulations measured using 40mm parallel plate..... *80*

Table 4.5: Herschel-Bulkley model parameters describing the three model chocolate paste formulations measured using a vane in cup geometry..... *86*

Table 5.1: Formulations of the suspensions used within this chapter, in vol% (calculated from densities, discussed in section 3.3.8) and the grit size of the sandpaper used for roughening in section 5.2.3 ..... *94*

Table 5.2: The force measured at 0.46 seconds into the test at four different test speeds using four different diameter probes. Averages of the raw data from testing SMP47 are shown with the standard deviation of three measurements. *98*

Table 5.3: Linear trend lines are fitted to the residual force as a 30 mm probe was held stationary within the sample for 60 seconds. The yield stresses are the values measured when the residual forces are averaged over the 60 seconds and the Herschel-Bulkley model is applied. All of the results for the gradient and the yield stress are averaged across three repeats at four different speeds for each fluid. It is important to note that practically,

materials which have been measured to have negative yield stresses are then only modelled using a power law model. *109*

Table 5.4: Measured densities, based on the weight of a known volume, of chocolate pastes *111*

Table 5.5: Peak and relaxation forces of three model chocolate pastes at four different probe velocities (probe diameter = 30mm, vessel diameter = 90 mm). Average value of the buoyancy force of the probe for all three pastes = 484 ± 5.14 mN *111*

Table 5.6: Parameters of the Herschel-Bulkley model when four different diameter probes are used to test CP62, comparing the values when the power-law theory is used to calculate n and when the variation in k is at a minimum. *116*

Table 5.7: Parameters of the Herschel-Bulkley model when four different diameter probes are used to test CP68, comparing the values when the power-law theory is used to calculate n and when the variation in k is at a minimum. *117*

Table 5.8: Parameters of the Herschel-Bulkley model when four different diameter probes are used to test CP74, comparing the values when the power-law theory is used to calculate n and when the variation in k is at a minimum. *117*

Table 5.9: Calculated values of the Herschel-Bulkley parameters of a 5% CMC solution when the probe and vessel diameters, fluid density and the plunge distance are altered by ± 5%. The R^2 value of the flow behaviour index fit for all samples is 0.99. ..... *120*

Table 5.10: Rheological parameters of fluids and suspensions measured using the parallel plate and back extrusion technique (with both smooth and roughened walls). *122*

Table 5.11: Results of nine ANOVAs investigating whether there are statistically significant differences between the yield stress, consistency coefficient and shear stress at a shear rate of 10 s^{-1} for the three chocolate pastes when measured at four different probe diameters. Values of p-value are shown and are considered significant if they are below 0.05. ..... *130*

Table 5.12: Connecting letters report from a Tukey HSD test of the consistency coefficients of CP62 measured using four different probe diameters. *131*

Table 5.13: Connecting letters report from a Tukey HSD test of the shear stresses, measured at a shear rate of 10 s^{-1} of CP62 measured using four different probe diameters. *131*

Table 5.14: Connecting letters report from a Tukey HSD test of the consistency coefficients of CP68 measured using four different probe diameters. *131*

Table 5.15: Connecting letters report from a Tukey HSD test of the yield stresses of CP68 measured using four different probe diameters. *131*

Table 5.16: Connecting letters report from a Tukey HSD test of the shear stresses, measured at a shear rate of 10 s^{-1}, of CP68 measured using four different probe diameters. *131*

Table 5.17: Connecting letters report from a Tukey HSD test of the consistency coefficients of CP74 measured using four different probe diameters. *131*

Table 5.18: Connecting letters report from a Tukey HSD test of the yield stresses of CP74 measured using four different probe diameters. *131*

Table 5.19: Connecting letters report from a Tukey HSD test of the shear stresses, measured at a shear rate of 10 s^{-1}, of CP74 measured using four different probe diameters. *131*

Table 5.20: Estimated shear rates between the blade and the walls in the mixers which are used to produce the pastes discussed in Chapter 6. ..... *134*

Table 5.21: Estimated shear rate between the second and third refiner rolls of the Lehmann refiner based upon producing particles with a diameter of 117 µm. *134*

Table 6.1: Heat balance on the components of an average paste formulation used for trial 1, disregarding any heat losses to the environment or gains from the heating jacket *140*

Table 6.2: List of high, low and control points that were used in the full factorial DoE of paste *141*

Table 6.3: Levels of each factor used for the runs of the DoE in trial 1 ..... *142*

Table 6.4: Measured peak and relaxation forces using the simplified back extrusion technique, values of the current at the end of mixing and operator ranks for each paste produced in trial 1 ..... *143*

Table 6.5: Calculated values of Herschel-Bulkley model parameters based upon the measured values using the simplified BET for each paste produced in trial 1 ..... *144*

Table 6.6: Significance of factors and interactions on the shear stress at a shear rate of 10 s^{-1} of paste ($p\text{-value}_{ANOVA} = 0.012$) *147*

Table 6.7: Significance of factors and interactions on the operator rank of paste *148*

Table 6.8: Significance of factors and interactions on the current draw of the mixer *149*

Table 6.9: Significance of factors and interactions on the paste temperature *151*

Table 6.10: Model PSD parameters averaged over all of the pastes produced in trial 1 ..... *155*

Table 6.11: Significance of factors and interactions on the standard deviation of the first paste PSD peak (p-value = 0.57) *159*

Table 6.12: Significance of factors and interactions on the mean of the first paste PSD peak (p-value = 0.032) *159*

Table 6.13: Significance of factors and interactions on the weighting of the first paste PSD peak (p-value = 0.025)..... *159*

Table 6.14: Significance of factors and interactions on the standard deviation of the second paste PSD peak (p-value = 0.83) *159*

Table 6.15: Significance of factors and interactions on the mean of the second paste PSD peak (p-value = 0.88) *160*

Table 6.16: Significance of factors and interactions on the weighting of the second paste PSD peak (p-value = 0.71) *160*

Table 6.17: Significance of factors and interactions on the standard deviation of the third paste PSD peak (p-value = 0.57) *160*

Table 6.18: Significance of factors and interactions on the mean of the third paste PSD peak (p-value = 0.31) *160*

Table 6.19: Significance of factors and interactions on the weighting of the third paste PSD peak (p-value = 0.19) *161*

Table 6.20: Significance of factors and interactions on the specific surface area of the paste (p-value = 0.0240) *161*

Table 6.21: List of high, low and control points that were used in the DoE of paste..... *167*

Table 6.22: Levels of each factor used for the runs of the DoE in trial 2 ..... *168*

Table 6.23: Calculated values of Herschel-Bulkley model parameters based upon the measured values using the BET for each paste produced in trial 2 ..... *169*

Table 6.24: Significance of factors and interactions on the yield stress of pastes when the largest outlier is removed (p-value$_{ANOVA}$ = 0.0114)..... *170*

Table 6.25: Significance of factors and interactions on the flow behaviour index (p-value$_{ANOVA}$ = 0.05) *174*

Table 6.26: Significance of factors and interactions on the consistency coefficient of pastes ($p\text{-value}_{ANOVA}$ = 0.0252) *176*

Table 6.27: Significance of factors and interactions on the shear stress at a shear rate of 10 s^{-1} of pastes ($p\text{-value}_{ANOVA}$ = 0.011) *178*

Table 6.28: Model PSD parameters averaged over all of the pastes produced in trial 2 ..... *180*

Table 6.29: Significance of factors and interactions on the mean of the first paste PSD peak ($p\text{-value}_{ANOVA}$ = 0.1199) *181*

Table 6.30: Significance of factors and interactions on the standard deviation of the first paste PSD peak ($p\text{-value}_{ANOVA}$ = 0.1094) *181*

Table 6.31: Significance of factors and interactions on the weighting of the first paste PSD peak ($p\text{-value}_{ANOVA}$ = 0.6105) *182*

Table 6.32: Significance of factors and interactions on the mean of the second paste PSD peak ($p\text{-value}_{ANOVA}$ = 0.0597) *182*

Table 6.33: Significance of factors and interactions on the standard deviation of the second paste PSD peak ($p\text{-value}_{ANOVA}$ = 0.3293) *182*

Table 6.34: Significance of factors and interactions on the weighting of the second paste PSD peak ($p\text{-value}_{ANOVA}$ = 0.7316) *182*

Table 6.35: Significance of factors and interactions on the mean of the third paste PSD peak ($p\text{-value}_{ANOVA}$ = 0.4611) *183*

Table 6.36: Significance of factors and interactions on the standard deviation of the third paste PSD peak ($p\text{-value}_{ANOVA}$ = 0.3984) *183*

Table 6.37: Significance of factors and interactions on the weighting of the third paste PSD peak ($p\text{-value}_{ANOVA}$ = 0.5361) *183*

Table 6.38: Significance of factors and interactions on the specific surface area of the paste ($p\text{-value}_{ANOVA}$ = 0.9799) *183*

Table 7.1: Mean values of the parameters used to model the PSD and the SSA of the pastes to the pre-refined pastes (± the standard deviation). *195*

Table 7.2: Comparing the mean values of paste and pre-refined paste SSA from the predictive models at high and low levels of lecithin content and mixing speed ± the standard deviation *197*

Table 7.3: Factors which significantly impact the mean of the first pre-refined paste PSD peak (p-value$_{ANOVA}$ = 0.11) *198*

Table 7.4: Factors which significantly impact the standard deviation of the first pre-refined paste PSD peak (p-value$_{ANOVA}$ = 0.26) *198*

Table 7.5: Factors which significantly impact the weight of the first pre-refined paste PSD peak (p-value$_{ANOVA}$ = 0.25) *198*

Table 7.6: Factors which significantly impact the mean of the second pre-refined paste PSD peak (p-value$_{ANOVA}$ = 0.31) *198*

Table 7.7: Factors which significantly impact the standard deviation of the second pre-refined paste PSD peak (p-value$_{ANOVA}$ = 0.70) *199*

Table 7.8: Factors which significantly impact the weight of the second pre-refined paste PSD peak (p-value$_{ANOVA}$ = 0.61) *199*

Table 7.9: Factors which significantly impact the mean of the third pre-refined paste PSD peak (p-value$_{ANOVA}$ = 0.11) *199*

Table 7.10: Factors which significantly impact the standard deviation of the third pre-refined paste PSD peak (p-value$_{ANOVA}$ = 0.46) *199*

Table 7.11: Factors which significantly impact the weight of the third pre-refined paste PSD peak (p-value$_{ANOVA}$ = 0.52) *200*

Table 7.12: Factors which significantly impact the specific surface area of the pre-refined paste (p-value$_{ANOVA}$ = 0.0261)* *200*

Table 7.13: Measurements of peak and relaxation forces using the simplified back extrusion technique and the operator ranks for each pre-refined paste produced in trial 1 ..... *203*

Table 7.14: Calculated values of Herschel-Bulkley model parameters based upon the measured values using the simplified BET for each pre-refined paste produced in trial 1 ..... *204*

Table 7.15: Significance of factors and interactions on the operator ranking of the pre-refined paste (p-value$_{ANOVA}$ = 0.0043)* *209*

Table 7.16: Significance of factors and interactions on the flow behaviour index of the pre-refined paste (p-value$_{ANOVA}$ = 0.0977) *209*

Table 7.17: Significance of factors and interactions on the consistency coefficient of the pre-refined paste (p-value$_{ANOVA}$ = 0.0990) *209*

Table 7.18: Significance of factors and interactions on the yield stress of the pre-refined paste (p-value$_{ANOVA}$ = 0.1172) *209*

Table 7.19: Significance of factors and interactions on the shear stress, at a shear rate of 10s-1, of the pre-refined paste (p-value$_{ANOVA}$ = 0.0251)* *210*

Table 7.20: Significance of factors and interactions on the mean of the first refined flake PSD peak (p-value$_{ANOVA}$ = 0.136) *219*

Table 7.21: Significance of factors and interactions on the standard deviation of the first refined flake PSD peak (p-value$_{ANOVA}$ = 0.0849) *219*

Table 7.22: Significance of factors and interactions on the weight of the first refined flake PSD peak (p-value$_{ANOVA}$ = 0.328) *220*

Table 7.23: Significance of factors and interactions on the mean of the second refined flake PSD peak (p-value$_{ANOVA}$ = 0.173) *220*

Table 7.24: Significance of factors and interactions on the standard deviation of the second refined flake PSD peak (p-value$_{ANOVA}$ = 0.162) *220*

Table 7.25: Significance of factors and interactions on the d_{90} of the refined flake PSD (p-value$_{ANOVA}$ = 0.142) *220*

Table 7.26: Significance of factors and interactions on the SSA of the refined flake PSD (p-value$_{ANOVA}$ = 0.158) *221*

Table 7.27: Significance of factors and interactions on the time taken for pastes to refine (p-value$_{ANOVA}$ = 0.0007) *231*

Table 7.28: Significance of factors and interactions on the average current on the first refiner roll (p-value$_{ANOVA}$ = 0.0113). *231*

Table 7.29: Significance of factors and interactions on the standard deviation of the first refined paste PSD peak (p-value$_{ANOVA}$ = 0.2697) *240*

Table 7.30: Significance of factors and interactions on the mean of the first refined paste PSD peak (p-value$_{ANOVA}$ = 0.1470) *240*

Table 7.31: Significance of factors and interactions on the standard deviation of the second refined paste PSD peak (p-value$_{ANOVA}$ = 0.8433) *241*

Table 7.32: Significance of factors and interactions on the mean of the second refined paste PSD peak (p-value$_{ANOVA}$ = 0.0134) *241*

Table 7.33: Significance of factors and interactions on the weight of the first refined paste PSD peak (p-value$_{ANOVA}$ = 0.3644). *241*

Table 7.34: Significance of factors and interactions on the d_{90} of the refined paste PSD (p-value$_{ANOVA}$ = 0.0039). *241*

Table 7.35: Significance of factors and interactions on the SSA of the refined paste PSD (p-value$_{ANOVA}$ = 0.0009). *242*

Table 7.36: Comparing the mean values of the paste yield stress and the refined paste SSA and d_{90} from the predictive models at high and low levels of fat content and temperature ± the standard deviation *244*

NOMENCLATURE

a	Probe radius	m
B	Einstein coefficient	-
c_p	Specific heat capacity	J/kg.°C
F_b	Buoyancy force	N
F_{cb}	Peak force corrected for buoyancy	N
F_t	Peak force	N
F_{te}	Residual Force	N
G'	Storage modulus	Pa
G''	Loss modulus	Pa
G^*	Complex modulus	Pa
K	Consistency coefficient	Pa.s
L	Plunged distance	m
m	Mass	kg
M	Mean of the log-normal distribution	µm
n	Flow behaviour index	-
P	Pressure drop per unit length	Pa/m
ΔP_d	Pressure difference within a capillary	Pa
Q	Volumetric flow rate of fluid displaced by the probe	m^3/s
r	Radial coordinate from centre of the probe and vessel	m
r_C	Capillary radius	m
R	Vessel radius	m
S	Standard deviation of the log-normal distribution	µm
t	Time	s
T	Temperature	°C
T_o	Dimensionless yield stress	-
T_w	Dimensionless shear stress at the wall	-
U	Linear velocity of surface	m/s
v_p	Probe velocity	m/s
V_{sif}	Volume of surface immobilised fat	m^3
V_{vif}	Volume of immobilised fat within pores	m^3
W	Weighting of each log-normal distribution	-
x	Average sieve size	µm
γ	Interfacial tension	N/m
$\dot{\gamma}$	Shear rate	s^{-1}
$\dot{\gamma}_c$	Characteristic shear rate	s^{-1}

δ	Phase angle	rad
ε	Measured strain	-
ε_0	Strain amplitude	-
η_{app}	Apparent viscosity	Pa.s
η_r	Relative viscosity	Pa.s
η_0	Continuous phase viscosity	Pa.s
η^*	Complex viscosity	Pa.s
θ	Contact angle	rad
κ	Probe ratio, a/R	-
λ	Value of $\xi$where shear stress is zero	-
λ_+ , λ_-	Limits of plug flow region	-
ξ	Width along the vessel diameter, r/R	-
ρ	Sample density	kg m^{-3}
σ_{HB}	Herschel-Bulkley shear stress	Pa
σ_{PL}	Power law shear stress	Pa
σ_y	Yield stress	Pa
σ_V	Vocadlo shear stress	Pa
σ_w	Shear stress at the wall	Pa
τ	Applied stress	Pa
τ_0	Stress amplitude	Pa
υ_w	Dimensionless velocity at the probe wall	-
$\frac{d\Upsilon}{d\xi}$	Dimensionless shear rate	-
Υ	Dimensionless volumetric flow rate through the annulus	-
φ	Solids volume fraction	-
φ_{eff}	Effective solids volume content	-
φ_{hifi}	Proportion of hydrodynamically immobilised fat	-
φ_m	Maximum packing fraction	-
φ_{sif}	Proportion of surface immobilised fat	-
φ_{vif}	Proportion of immobilised fat within pores	-
Ψ	Aggregation ratio	-
ω	Angular frequency	rad/s

1 INTRODUCTION

1.1 Business Case

Approximately 300 tonnes per hour of chocolate are produced throughout the year at the factory owned by Mondelēz in Bournville, UK, which is just one of the 156 manufacturing sites that Mondelēz own across 57 countries. In 2014 the UK was the fourth largest consumer of chocolate per capita in the entire world; each Briton consumed 11 kg of chocolate per year, therefore it is of commercial importance to optimise efficiency of the production lines.

The chocolate manufacturing process has remained much the same since 1905, when Fry's was first produced and sold in the UK. There is still a lack of understanding about the impact of each process step on the quality of the final product (Beckett, 2009) but as chocolate is a low cost good, the throughput of lines is critical and little research has been carried out to understand the macro-scale properties of the chocolate at all process stages.

There are four key stages to chocolate production: mixing, pre-refining, refining and conching. Raw ingredients are first combined together in the mixing stage to form a thick paste resembling wet sand. In an entire book which is considered to be the complete guide to chocolate making, Beckett (2008) discusses this mixing of raw ingredients in only one line; "It is important to turn this mixture [of raw ingredients] into a uniform paste with the appropriate consistency in order for the milling to proceed correctly". The consistency of the paste is frequently seen to change between batches yet the particle size reduction which occurs in the subsequent milling stages, performed by roll refiners, is dependent on how much the paste opposes the forces of the rolls. Currently there is no procedure to assess whether the

mixed paste has achieved the "*appropriate consistency*" before it is refined, no practise to alter the paste consistency during the mixing stage and no standardised method of altering the downstream process based on the consistency.

1.2 Outline of the Manufacturing Process

Chocolate is a mixture of sugar, milk powder and non-fat cocoa solids in a matrix of milk and cocoa fats. The raw ingredients can be combined together in two different ways:

1. A single mixing step can be used to combine the sugar and milk powder with the fat and cocoa liquor. This is the simple route which is most commonly used to manufacture powder chocolates.
2. In some regional areas, condensed milk, sugar and cocoa liquor are cooked together, forming a solid material known as crumb. The crumb is then combined with the fat in a similar mixing step as above. This technique was first established to ensure a steady supply of chocolate whilst milk prices fluctuated during the year however it is now relied upon to create the distinctive flavour profiles of established brands (Haylock and Dodds, 2009).

The diagram in Figure 1.1 shows a summary of the manufacturing processes when chocolate is manufactured from either powder ingredients or a crumb base.

The mixed ingredients form a thick paste with a broad particle size distribution (PSD). Research has shown that particles below 30μm cannot be detected on the tongue therefore the particles must be refined to below this size so that the chocolate will be perceived as smooth (Beckett, 2009). For large scale manufacture, roll refiners are commonplace. Hollow steel rolls are held parallel to each other and are designed to compress, shear and elongate the particles to reduce the particle size.

The research presented within this thesis relates to a two stage refining process. The paste falls from the mixer, via a hopper, into a two-roll refiner where the largest particles are broken to around 300µm. This material is then steadily transferred into a five-roll refiner which reduces the particle size to the desired chocolate PSD. Each consecutive roll of the five-roll refiner turns in the opposite direction and the speed of each roll becomes progressively faster. There are two approaches to how a roll refiner can be operated; gap driven or pressure driven.

Gap driven: A gap is set between the rolls and a high pressure is maintained. Particles cannot pass through the gap unless they are small enough to get through that particular gap. Smaller gap settings result in smaller particles.

Pressure driven: The rolls are completely touching when the pressure is applied at either end of the rolls. The material must then force the gap open in order to pass through. Higher pressures result in a lower particle size and faster roll speeds can be used to encourage a greater amount of material through.

The performance of the refiners determines the particle size distribution which directly impacts the rheological properties of the final chocolate. For sensorial reasons, it is beneficial to get the PSD below 30µm however if the particles are too small, there will be a much higher surface area for the fat phase to coat and the viscosity of the chocolate will be increased.

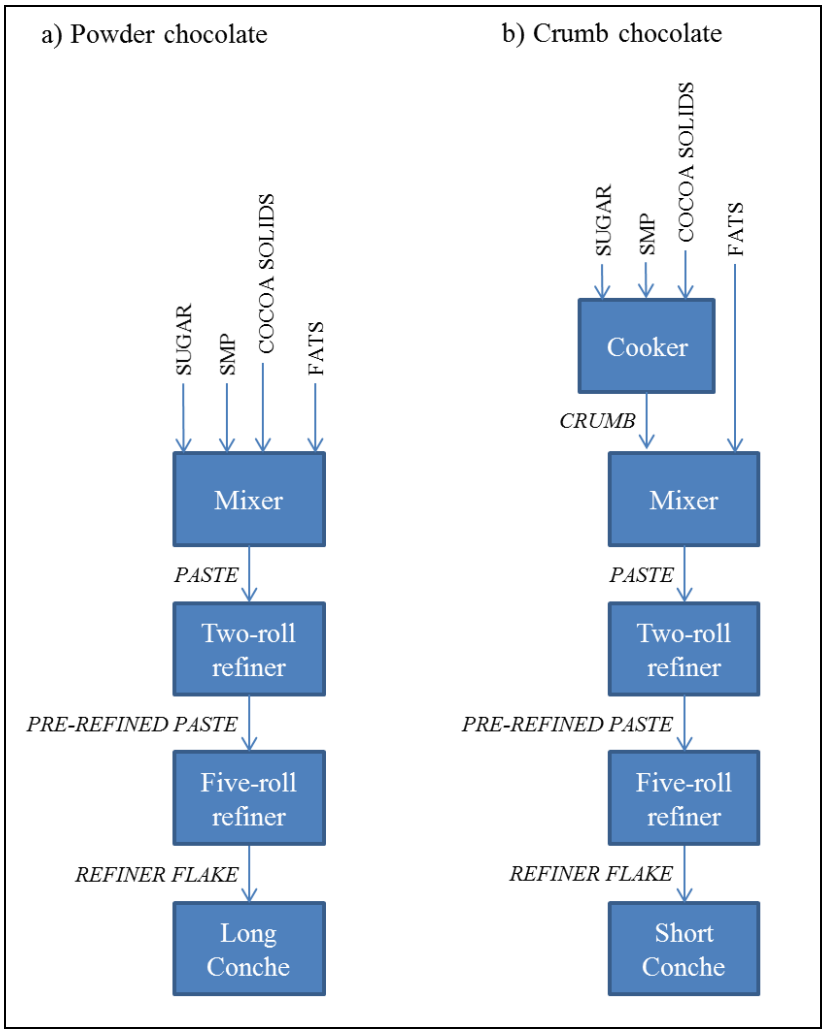


Figure 1.1: Summary of the main two manufacturing processes a) powder chocolate, generally manufactured for the continental Europe market and b) crumb chocolate, used most prolifically for British chocolate

The final fat content of the chocolate is always maintained; based on how much fat has been added into the paste, the remaining cocoa butter is added to the refiner flake along with emulsifiers and any flavouring during a conching stage. Conching is a mixing stage designed to liquefy the fine chocolate flake with these additional ingredients and remove the unwanted volatiles which have come from earlier fermentation of the cocoa beans. Through controlling the heating during this step, distinctive flavour profiles which can be specific to brands are created within conching (Beckett, 2009). Often cooked, caramel flavours are developed in the manufacture of crumb so the conching process may be primarily focussed on evenly

distributing the fat and removing of volatiles. It is desirable to add most of the fat into this stage because the viscosity is seen to reduce further than when fat is added during pasting.

1.3 Impact of Pasting

Much of the research that has involved chocolate production focusses on manipulating the ingredients or developing the refining and conching steps, recently the work by Bolenz et al. (2014), Glicerina et al. (2015), and Middendorf et al. (2016). To be able to optimise the efficiency of these energy intensive process steps, it is important to be able to produce a consistent paste of the raw ingredients. The paste forces the rolls of the refiner apart which will impact on the refiner flake PSD. Stiffer pastes will exert more force on the rolls, push them further apart, allowing more paste through the gap and will produce a refiner flake with a high PSD. Thinner pastes will not be able to push the rolls as far apart so the particles will have to become much smaller to get through the refiner rolls. The pasting step can take less than 10 minutes to combine the ingredients although small changes in paste consistency will impact on the PSD of the refiner flake if the settings of the refiners are left unchanged. When less paste is able to force its way through the gaps between the rolls, the throughput from this process step is decreased.

Currently, skilled operators are relied upon to manually control operating conditions of the refiner in order to produce a refiner flake with the correct particle size. They visually evaluate the coverage on the rolls; even coverage of material over the rolls indicates a good throughput and stable running conditions and any patterns on the rolls can be indicative of which settings of the refiners need to be altered. Each production line will be run by different operators who have their own preferences for which settings of the refiner to alter, potentially resulting in difference chocolate properties.

1.4 Aims

The objectives of this research are:

- to develop a method which can quantify differences between paste batches that could be used alongside a production line,
- to quantify how much the process settings of the mixer and formulation can influence the paste consistency,
- to record the impact that varying paste consistency has on the downstream processes, with the aim of quantifying what the ideal paste consistency is.

The chapters are structured in the following way:

Chapter 2: Literature Review

An overview of the physical properties of ingredients typically found within chocolate is given. The many physical properties which can contribute towards the viscosities of pastes are discussed and techniques which have been used to characterise how the pastes flow are critically reviewed.

Chapter 3: Materials and Methods

Three sections detail the equipment used to manufacture pastes, the methods used to characterise these pastes and the physical properties of the ingredients.

Chapter 4: Methods trialled to characterise pastes

The results and issues of using conventional techniques to measure chocolate pastes are discussed.

Chapter 5: Developing and analysing the suitability of a method to measure the rheological properties of chocolate paste

In-depth development of the back extrusion technique involves discussions of the fundamental implications of the raw data and compares results to conventional rheological techniques for appropriate fluids.

Chapter 6: Impact on paste consistency

Chocolate pastes have been produced on a pilot plant scale, based on two statistical designs, to investigate how the paste consistency is influenced by both the formulation and the mixing conditions and explore the suitability of online measurements techniques.

Chapter 7: Impact on refining

The particle sizes of refined chocolate pastes and the conditions of the roll refiners are evaluated at constant refiner settings, referring back to the factors of the statistical designs established in chapter 6.

The knowledge gained through this research can then be provided to manufacturing and R&D lines so that they are able to constantly manipulate the settings of the mixing step in order to maintain a constant paste consistency enabling a consistent product to be manufactured.

2 LITERATURE REVIEW

This chapter critically reviews the literature which is relevant to the topics within this thesis. Firstly, the individual components of chocolate paste are discussed, considering the structural properties and how the ingredients may interact within the system. The second section explores how the consistencies of pastes and suspensions are affected by the solids. The third sections discusses how processing conditions will also affect the material rheological properties. Finally, the fourth section compares techniques which have been used to measure the consistency of pastes and suspensions in many different industries.

2.1 Ingredients

Powder chocolate paste generally comprises skimmed milk powder (SMP), sweet whey powder (SWP), granulated sugar (sucrose), cocoa liquor (CL), cocoa butter (CB), anhydrous milk fat (AMF), vanillin and could contain lecithin. The solids have different surface chemistries which dictates how they will interact with the fats that are present. They will also have different elastic behaviours which determines how much they may break during the processing.

2.1.1 Dairy powders

Dairy is an important component in all milk and white chocolates. As milk has such a short shelf life, drying at relatively low temperatures (≈ 85 °C) offers a greatly improved shelf life whilst ensuring the taste is unchanged through processing (Bylund, 2015). Skimmed milk, whole milk and whey are dried to produce skimmed milk powder, whole milk powder and

sweet whey powder, respectively. Table 2.1 outlines the typical compositions of these three powders which will alter the physical and organoleptic properties of the final chocolate.

Table 2.1: Typical compositions of milk powders, taken from (Bylund, 2015)

	Skimmed Milk Powder	Whole Milk Powder	Sweet Whey Powder
Protein	34.0 – 37.0	24.5 – 27.0	11.0 – 14.5
Lactose	49.5 – 52.0	36.0 – 38.5	63.0 – 75.0
Fat	0.6 – 1.5	26.0 – 40.0	1.0 – 1.5
Ash	8.2 – 8.6	5.5 – 6.5	8.2 – 8.8
Moisture	3.0 – 4.0	2.0 – 4.5	3.5 – 5.0

The process of roller drying dairy products between hot metal rolls was first patented in 1906 by Just and Hatmaker (Beckett, 2008). Pasteurised milk is added above two heated rotating drums. Here the water is quickly driven off, the solids are carried through the gap between the drums and then scraped off to produce roller dried milk powder. The main advantage of this material is that each particle is a long flat flake which has a very high level of free fat (90g/100g) (Auty et al., 2001). Higher levels of free fat will contribute to lubricating particles within the chocolate, lowering the final viscosity (Bolenz et al., 2003). Unfortunately, these machines are expensive to run due to the large heat losses and create difficulties maintaining food safety standards (Beckett, 2008).

Demand for milk powders increased by the end of WWII and spray drying became a more economical technique (Vignolles et al., 2007). Spray drying produces particles which will easily dissolve in comparison to roller dried milk powder, which has a much lower solubility due to its chemical composition and physical morphology (solubility of spray dried milk powder > 99%, solubility of roller dried milk powders = 85%) (Sharma et al., 2012). The milk powder industry is presently led by products that require milk powders to quickly dissolve within aqueous systems. This has led to spray drying to become the leading technology and

therefore is generally lower cost. Despite the benefits offered by using roller dried milk powders, mainly regarding free fat content, it is now far more economical to use low fat spray dried milk powders, supplemented with additional milk fat to increase the free fat content, aiding lubrication of the particles.

Spray drying can be operated at a range of temperatures; low temperature can be around 145/85°C (Kim et al., 2009) up to a high temperature of 254/100°C (Jones et al., 2013) where the two values represent the inlet and outlet temperatures, respectively. The differences in temperature are some of the main drivers which influence the moisture content, density and fat location in these powders. These properties will impact how the particles interact with the other chocolate paste ingredients and could affect final chocolate quality (Sharma et al., 2012).

The spray drying process allows properties of the powders to be manipulated which have a direct effect on how the dairy powders behave within fat suspensions. Three main properties of the dairy powders; agglomeration, porosity and location of fat are discussed below. There is a large amount of literature available discussing the impact how altering the spray drying process impacts the final chocolate properties. Most recently, Kelly et al. (2014), Sharma et al. (2012) and Kim et al. (2009).

Agglomeration

Operating conditions can result in dimpling or agglomeration of particles due to particle collisions before they are fully cooled, as can be seen from the work by Mistry et al. (1992), Kim et al. (2002) and Vignolles et al. (2007). Kaláb (2010) reports that dimpling may be caused when the particles are mainly dry but still soft; contact between two particles does not cause the particles to stick however indents are made in the surface (Figure 2.1).

Alternatively, Lay Ma et al. (2008) suggests that air expands within the particles but then escapes, leaving a collapsed region at the particle surface. When particles are still wet, collisions between particles can result in permanent attachment for the remainder of the drying process, forming agglomerates. Agglomerates will have larger pores which allows liquid to better penetrate the particles and the formation of larger particles also increases the flowability of the powder (Hogekamp and Schubert, 2003, Murrieta-Pazos et al., 2012, Bylund, 2015, Ji et al., 2016). These are very desirable qualities in many industrial applications as milk powder can be more easily transported and stored before being rehydrated on site (Selomulya and Fang, 2013). Figure 2.2 shows a highly agglomerated particle.

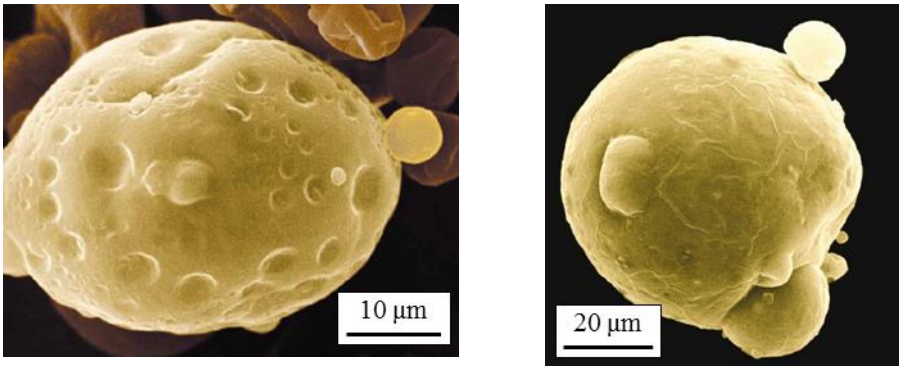


Figure 2.1: Dimpled surfaces on spray dried milk powder particles (Kaláb, 2010)

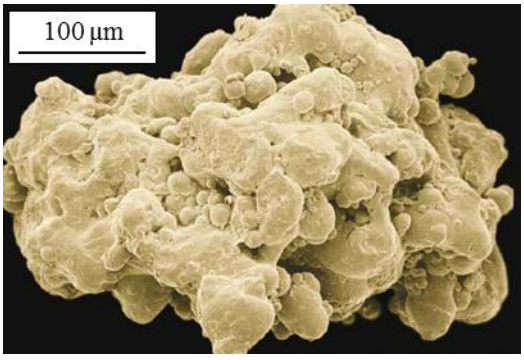


Figure 2.2: Highly agglomerated spray dried milk powder particle (Kaláb, 2010)

Porosity

The proportion of open pores, accessible from the surface, is low if SMP and SWP particles remain whole and intact. The surfaces of SMP particles can be folded whereas SWP shows a smoother surface with shallow dimples containing pools of fat (Kim et al., 2002). If the particles become broken there can be a large network of pores and large vacuoles, resulting in a greatly increased surface area (Attaie et al., 2003, Caric and Kalab, 1987, Kaláb, 2010) (Figure 2.3).

Franke and Heinzelmann (2008) used a twin screw extruder without the die to perform mechanical-thermal treatment on skimmed milk powders. This densified the particles and re-crystallised the amorphous lactose on the surface. When the densified powder was used for milk chocolate, the viscosity of the chocolate was decreased after conching.

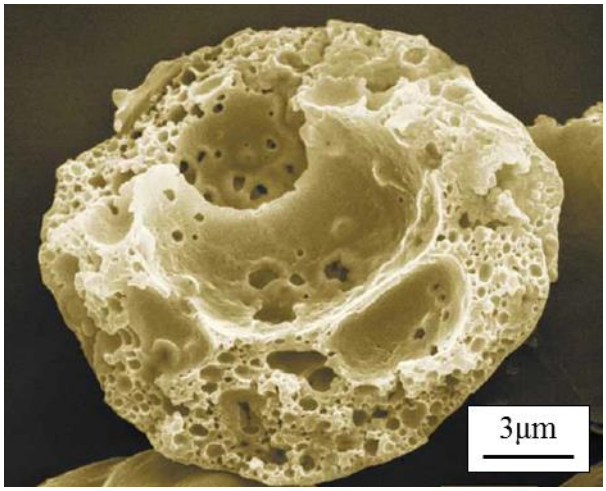


Figure 2.3: Pore structure within a broken spray dried milk powder particle (Kaláb, 2010)

Location of Fat

Buma (1971) concluded that there were four types of extractable fat from a spray dried dairy particle. Since then, Vignolles et al. (2007) have attempted to define the location of fat within

spray dried dairy powders based on the many sources available in the literature. The fat is thought to be divided between these four categories, illustrated in Figure 2.4:

1. Layers or patches of surface free fat.
2. Inner free fat held on surfaces of the matrix within capillaries or vacuoles.
3. Surface globular fat embedded in the matrix.
4. Encapsulated or coalesced globular fat within the matrix.

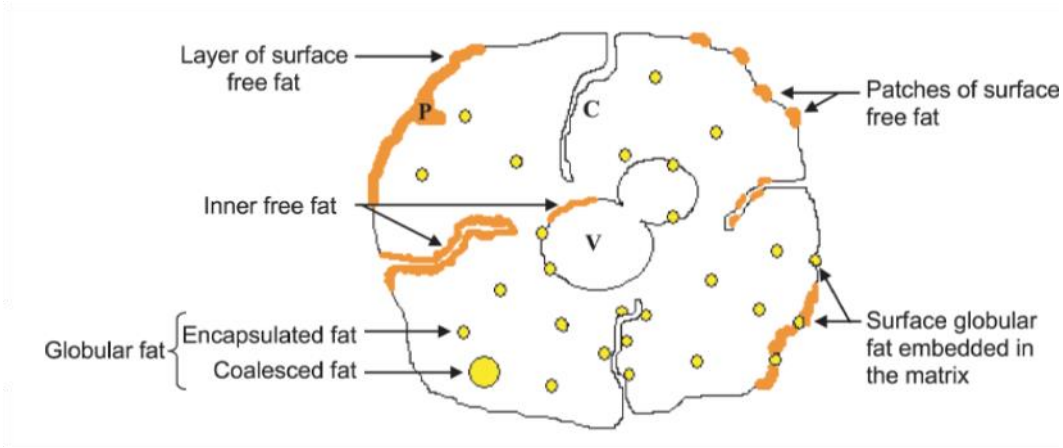


Figure 2.4: Location of fat within a spray dried milk powder particle (Vignolles et al., 2007)

When the powder particles are combined with the other chocolate ingredients, the non-emulsified fat, present on the surface and within capillaries/vacuoles (1 and 2) of milk powder particles, will mix with the other fats in the system. This contributes towards reducing the final chocolate viscosity, hence it is considered *free fat* (Vignolles et al., 2007, Palanuwech et al., 2003). The remainder of the fat, globular fat (3 and 4), will not separate from the particle. This is often undesirable as it will contribute towards the total fat content of a product but will not offer any benefits to the sensorial properties (Bolenz et al., 2003). Liang and Hartel (2004) compared chocolate made with spray dried whole milk powder, which has a high level of fat trapped in globules (total fat content 29.4 %), to chocolate with the same total fat content but made with spray dried skimmed milk powder (total fat content 1.0 %) and additional

anhydrous milk fat. The chocolate containing whole milk powder is measured to have a dramatically higher viscosity as very little of the total fat content contributes towards lubricating the particles.

The proportion of fat in each of these locations will vary depending on many processing factors, for example nozzle design of the atomiser, inlet and outlet temperatures to the spray drier and mechanical stresses from drying cyclones (Kelly et al., 2002). The location of fat is also at risk of changing based on seasonal effects, as discussed by Twomey et al. (2000).

2.1.2 Sucrose

Sucrose can be manufactured from either sugar cane or sugar beet. Sugar beet requires high temperatures and several crystallisation stages in order to extract the maximum quantity of sucrose whereas sugar cane can be treated at lower temperatures (Beckett, 2009). Sugars typically make up 50% of milk chocolate, most of which are sucrose.

The crystallised sucrose used within powder chocolate production is usually classified as medium fine, with a particle size between 0.6 – 1 mm, bulk density of 850 kg/m^3 and purity of 99.9 % (Beckett, 2009). The granules are brittle and the particles will break where there are small structural flaws. Within the food industry, particle sizes above 30 µm are detected as gritty on the tongue thus particles larger than this must be reduced.

There has been some speculation that amorphous sucrose may be being produced during the refining stages. Niedrick (1981) suggests that 30-90 % of the sugar becomes amorphous. On the other hand, Martin (1988) discusses the difficulties of estimating this value as the amorphous sucrose is highly hygroscopic and will rapidly absorb moisture and flavour compounds, causing recrystallization. Unfortunately, no further work is known to be published which has gone on to research this effect, as had been hoped by Martin.

2.1.3 Fat

2.1.3.1 Cocoa butter

Cocoa butter is the main fat component used within chocolate mass, manufactured by pressing the processed cocoa beans to release the fat. Table 2.2 describes the fatty acid composition of cocoa butter which is mainly comprised of oleic, stearic and palmitic acids. Depending on the cooling profile, there are six polymorphic forms that cocoa butter can take once solidified.

Table 2.2: Fatty acid composition of cocoa butter (Szydłowska-Czerniak et al., 2017) and dairy fat (Beckett, 2009)

Fatty Acid	Cocoa Butter, Weight %	Dairy Fat, Weight %
C4:0 Butyric	-	4.10
C6:0 Caproic	-	2.40
C8:0 Caprylic	-	1.40
C10:0 Capric	-	2.90
C10:1 Caproleic	-	0.30
C12:0 Lauric	-	3.50
C14:0 Mysteric	0.11	11.40
C15:0 Pentadecylic	0.03	-
C16:0 Palmitic	26.51	23.30
C16:1 Palmitoleic	0.02	-
C17:0 Margaric	0.23	-
C18:0 Stearic	35.59	12.40
C18:1 Oleic	32.86	25.20
C18:2 Linoleic	2.92	2.60
C18:3 Linolenic	0.18	0.90
C20:0 Arachidic	1.07	-
C20:1 Paullinic	0.05	-
C22.0 Behenic	0.20	-
Other	-	10.00
Trans	0.02	-

2.1.3.2 Dairy fat

Milk fat in chocolate is most commonly anhydrous milk fat (AMF) which is manufactured from fresh cream or butter by removing the water phase. It is made up of many different fatty acids, listed in Table 2.2, and is much softer than cocoa butter. For comparison, the enthalpy required to melt a sample of cocoa butter is 14.2 cal/g whereas anhydrous milk fat requires only 3.3 cal/g. Mixing the two together will soften the fat overall; a 1:1 ratio by weight of each fat requires a melting enthalpy of 5.8 cal/g (Ali and Dimick, 1994).

2.1.3.3 Interaction of fats

Cocoa butter and milk fat mix fully together once molten, however once they solidify, they retain different stable crystal forms. When added below 50 % (typically there is less than 30 % milk fat within milk chocolate), milk fat will not alter the polymorphic form of cocoa butter (Beckett, 2009).

2.1.4 Non-fat cocoa solids

Cocoa nibs can be separated from the shells by breaking cocoa beans, generally using a centrifuge to impact the beans against a plate. The pieces are then winnowed to separate the husks from the cocoa nibs. The nibs must then be ground to below 30 μm using roll refiners, pin mills and ball mills. This allows most of the fat to be extracted from the cocoa solids, producing cocoa liquor. By pressing this liquor, the cocoa butter is extracted, leaving behind a press cake of non-fat cocoa powder (Gutiérrez, 2017).

2.1.5 Crumb

Due to the short storage life of fresh milk in the 1870's, Daniel Peter and Henri Nestlé in Switzerland designed a process to dry milk, sugar and cocoa liquor together to prevent mould from developing. This material, crumb, was then introduced to the UK and US markets within

the 20th Century due to the limited supply of good quality milk powder but an abundance of fresh milk (Wells, 2009). The chocolate manufactured from crumb has distinctive flavour profiles due to Maillard reactions occurring at high temperatures during crumb production (Haylock and Dodds, 2009).

Other than its original intended benefit, the cooking of crumb also results in a large amount of the amorphous lactose and sucrose becoming crystalline. This results in a less sticky consistency which is better for storage and also reduces the amount of fat which would be trapped due to the presence of amorphous, glassy sugar (Wells, 2009).

Crumb chocolate has a more limited market (mainly in the UK) therefore this thesis will focus mainly on chocolates produced from powder ingredients.

2.1.6 Emulsifiers

Emulsifiers are commonly added to chocolate in order to reduce the final viscosity of the conched liquid chocolate so that less cocoa butter, an expensive ingredient, is required. There are many different emulsifiers that are used in chocolate manufacturing; commonly soy lecithin, polyglycerol polyricinoleate (PGPR) or ammonium phosphatide are used, each altering the viscosity of chocolate mass in different ways (Beckett, 2008). These rheological properties are important for both a consumer sensory perspective (behaviour as the chocolate melts in the mouth) and for accuracy of process operations such as depositing the correct amount of chocolate in moulds, creating chocolate shells of a specific thickness or enrobing fillings with a certain amount of chocolate.

It is common that the majority of the emulsifiers are added to the conched chocolate however at some manufacturing sites and for some processes, a small quantity of lecithin is added into the initial mixing stage. There is not, however, thought to be any literature available which

compares chocolate quality or processing performance when lecithin is added into the mixing stage or not. Each lecithin molecule, usually produced from soy or sunflowers, has a hydrophilic polar head and a lipophilic tail. In the presence of a sugar particle within a fat phase, the head attaches to the hydrophilic sucrose and the tail will extend out into the fat phase. The tails stretching out into the surrounding fat is intended to prevent the particles from aggregating, which could have otherwise trapped fat within the voids. Instead, particles can flow past each other freely, reducing the viscosity of the suspension (Middendorf et al., 2016). Through centrifugation, Middendorf et al. (2016) found that soy lecithin immobilised less fat at the surfaces of sugar than sunflower lecithin, however they published no information comparing this to the quantity of immobilized fat when there was no emulsifier present at all. Using atomic force microscopy, the layers of fat absorbed at the surfaces were found to be similar for both types of lecithin but again there was no comparison to the system without any emulsifier.

Arnold et al. (2013) also used atomic force microscopy to examine the repulsion forces between sugar particles within soybean oil. When sugar surfaces were covered with soy lecithin molecules, the adhesion forces were weakened however there were no differences between the repulsive forces of sugar particles whether lecithin molecules were present or not.

When suspensions of SMP and fat are studied, Millqvist-Fureby and Smith (2007) found no difference between the settling velocity of the solids, expected to be indicative of the suspension rheology, when lecithin was present in the fat phase or not. As the surfaces of the SMP particles are already hydrophobic, this result suggests that within a hydrophobic environment, SMP particles prefer to be coated by the fat than interact with the lecithin molecules.

From publications regarding the impact of lecithin on conched chocolate, adding up to 0.5 wt% lecithin into the conched chocolate will reduce the plastic viscosity and yield stress of the suspension. The hydrophilic end of the lecithin molecules will adsorb at the solid surfaces, increasing the dispersion of the particles within the fat and preventing aggregation. At lecithin contents above 0.6 wt%, the plastic viscosity is no longer affected but the yield stress begins to increase again (Nebesny and Żyżelewicz, 2005). Garti and Aserin (2012) hypothesise that when there is an excess of phospholipid lecithin molecules, either micelles of the lecithin molecules form within the bulk or multiple layers of lecithin molecules are built up on the solid particles which hinders the flow of particles through the fat and causes the increase in yield stress.

Although lecithin can have a desirable effect by reducing the viscosity of chocolate, it will also impact how sensitive the chocolate is to temperature or moisture during storage, affecting the shelf life of the product (Schantz et al., 2003).

There is some speculation by Bolenz and Manske (2013) suggesting that when lecithin was added in the early stages of ball-milling, some of the functionality is thought to have been lost as it may have been absorbed into particles. Bolenz and Manske do not indicate which particles however based on the review of literature earlier in this section, it is anticipated that they are referring to the milk powder particles. There is no follow up around this point but in industry it is possible to find processes which either add lecithin into the mixer and the conche, or processes which only add it in the conche. No information can be found surrounding the differences for why this is, other than it may have begun as a personal preference and has now become established as standard practice.

In spite of lecithin being a widely used material, all of these sources highlight that although the effect that lecithin has on the final chocolate is known, the fundamental interactions between the solids and fat with the lecithin are still unknown and the literature remains speculative.

2.1.7 Effect of fat additions on chocolate properties

A small amount of fat must be added to the dry ingredients prior to roll refining to prevent and material being thrown from the rolls (Beckett, 2009). Once the particles are reduced in size, the remaining fat necessary to suspend the solids is added during the final conching stage. As there is a slight moisture content within the refined material, the first aim of the conching step is to reduce the moisture content since it would undesirably increase the viscosity of chocolate. Any emulsifiers that are present may also hinder the moisture from leaving. Equally, if there is too much fat present, it will coat the particles so that the moisture cannot leave (Beckett, 2009). Additionally, Beckett (2008) describes that it is also beneficial to shear the material between the walls to increase the number of particles which become coated in the fat. If the fat content was higher, then the material would instead flow out of the way.

Once the moisture has been driven off a sufficient amount, the remaining fat can be added so that the solids are suspended within a continuous fat phase. The viscosity can be manipulated by the quantity of fat added or addition of emulsifiers, depending on the intended use (i.e. forming solid chocolate bars, creating the exterior shells of filled chocolates or enrobing of other filling such as biscuit) (Beckett, 2008).

The author is not aware of any literature which investigates the effect of manipulating the fat content prior to the material being refined, specifically related to chocolate production.

Generally it is only considered important to achieve a texture of chocolate paste which is able to be easily transferred through the rolls of the refining step. No consideration is given to how the paste texture may impact the refining process or how the presence of additional fat may impact the particle size reduction.

2.2 Rheological behaviour of particulate systems

Particles within suspensions contribute to the overall viscosity of the material. As there are multiple different solids ranging from 10 - 3000 μm within the paste, there are many factors that can impact how the paste will flow:

- Viscosity of the continuous phase
- Packing of particles
- Particle shape
- Effective solids volume content
- Aggregation or deaggregation of solids
- Particle interactions

These factors are discussed in more detail below.

2.2.1 Viscosity of continuous phase

The Krieger-Dougherty equation (equation 2.12.1) is commonly used to calculate the viscosity of Newtonian concentrated suspensions. The relative viscosity, η_r , is used to isolate the influence of the particle phase on the apparent viscosity, η_{app} by separating the continuous phase viscosity term, η_0 (Dörr et al. (2013)). From the equation it is possible to see that the viscosity of the suspension, η_{app}, is directly related to the viscosity of the

suspending liquid, and the maximum packing fraction, φ_m, which accounts for a range of particle sizes and shapes (Barnes et al., 1989).

$$\eta_r = \frac{\eta_{app}}{\eta_0} = \left(1 - \frac{\varphi}{\varphi_m}\right)^{-B\varphi_m} \quad (2.1)$$

where B is the Einstein coefficient (constant based on the aspect ratio of the particles) and φ is the volume fraction of particles.

There are many other correlations, discussed by J. Stickel and L. Powell (2005), which predict the viscosities of suspensions considering other physical factors and similarly will consider the viscosity of the continuous phase.

2.2.2 Packing of particles

If the particles have a narrow PSD then, irrelevant of the actual particle size, there are large amounts of voids that require a large quantity of liquid to fill (Hafid et al., 2016). In this case, increasing the volume fraction of solids within a suspension will cause the material to display stronger non-Newtonian behaviour.

It is possible to increase the solids volume content of a suspension yet reduce the overall viscosity; Farris (1968) showed that if the additional solids are much smaller than the existing particles in the suspension, they will fill the voids between the large particles, freeing the fat which was previously trapped within voids so that it is now able to lubricate the suspension. In Figure 2.5 it is possible to see that the same relative viscosity as a monomodal suspension can be achieved when the volume fraction of solids is higher so long as the system is multimodal.

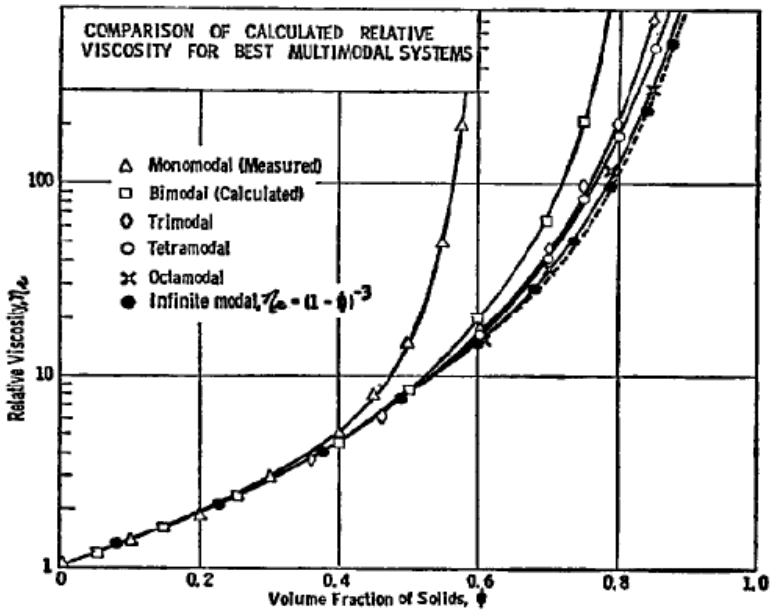


Figure 2.5: Results taken from Farris (1968) comparing the relative viscosities of particle suspensions over a range of solid volume fractions for monomodal and multimodal distributions of particles.

Additionally to considering the relative viscosity, Ancey et al. (2001) have discussed that the yield stress of clay dispersions diverge when the volume of solids approaches the maximum packing fraction (Figure 2.6). When the PSDs are polydisperse, this alters the maximum packing fraction and therefore impacts on the yield stress of the material.

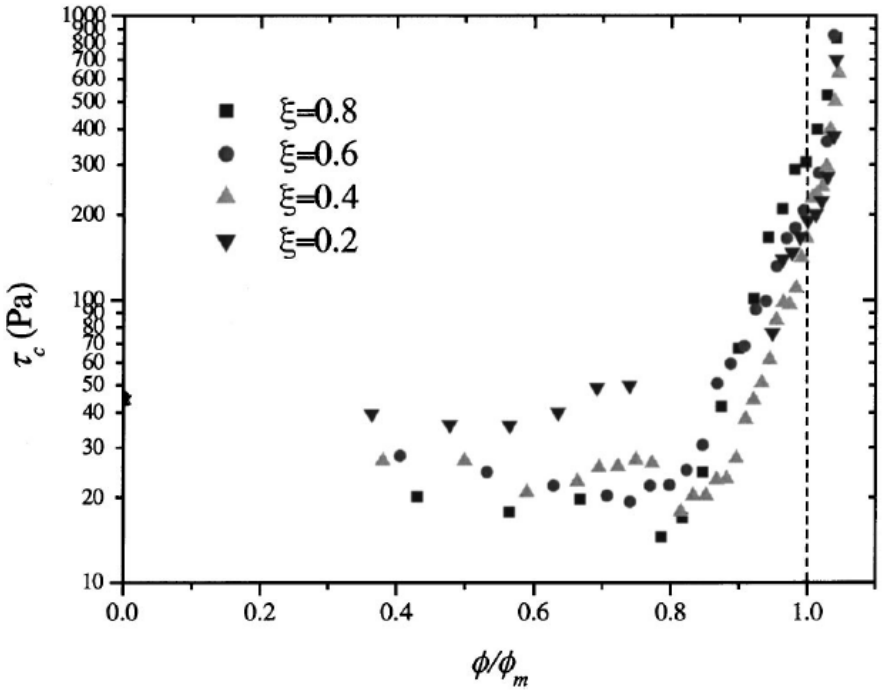


Figure 2.6: Results taken from Ancey et al. (2001) detailing the yield stress,τ_C, as a function of solids concentration of the coarse fraction using bimodal particles of 0.3 and 3 mm. ξ is the volume occupied by the small particles to the total volume of the coarse fraction.

There are some models available which estimate the apparent viscosity of polydisperse suspensions assuming that large particles are suspended in a continuous phase formed from particles 7-10 times smaller. This can be repeated for larger particles 7-10 times larger in order to predict the rheology of a suspension of multiple size classes of monodisperse solids (Farris, 1968, Brouwers, 2010, Mwasame et al., 2016).

There are also several groups which have developed computational models based upon for binary, ternary and quaternary mixtures of particles (Liu and Ha, 2002, Yuan et al., 2018). Most recently, Yuan et al. (2018) have been able to estimate the volume fraction of polydisperse particles based on a partly empirical model. This also can incorporate the shape variation of particles but most models mainly rely on the assumption that particles are spherical (Mehdipour and Khayat, 2017).

2.2.3 Particle shape

Hafid et al. (2016) classified sand particles based upon their shape and measured the rheology of suspensions made with particles from each category. Figure 2.7 shows how the relative yield stresses and Herschel-Bulkley consistencies vary when the solids volume fraction is increased, depending on the shapes of the particles. When the particles are shaped more irregularly, both the yield stress and the consistency increase more rapidly as the solid volume fraction is increased. Similar results were also seen by Kabagire et al. (2017), who compared smooth spherical glass beads to crushed limestone sands with a much rougher surface.

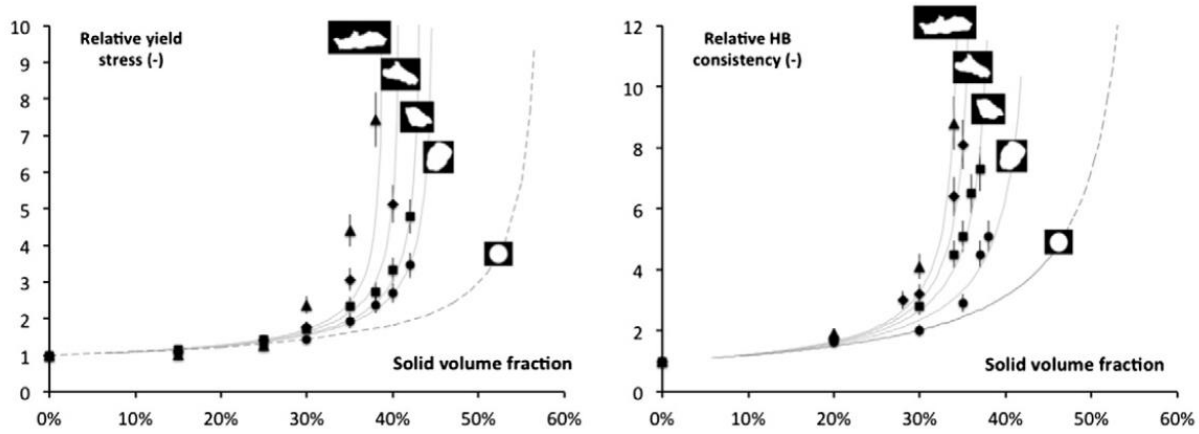


Figure 2.7: Effect of the particle shape on yield stress and consistency of suspensions when the solid volume fraction is increased (Hafid et al., 2016)

2.2.4 Effective solid volume content

In order to decrease the viscosity of suspensions, there must be an increase in the volume of fat which is available to flow in between the particles (Mukherjee and Pisupati, 2015). Rather than solely consider the volume of particles in comparison to the volume of liquid within the suspension, Windhab (2000) considers it important to take into account the fat immobilised at surface of the particles, fat that has been absorbed into the volume of the particles pores, and the "hydrodynamically immobilised" fat. Hydrodynamically immobilised fat exists if particles

are irregularly shaped and continually rotate so that fat within the effective sphere that is taken up by the particle is not available to move freely within the suspension (Mueller et al., 2009, Xu et al., 2018). These three situations result in an effective solid content of a suspension, φ_{eff}, which can be quantified by equation 2.2. Windhab (2000)uses this equation to establish a theoretical viscosity is able to draw comparisons with experimental measurements for suspensions with solids volume contents up to 0.3.

$$\varphi_{eff} = \varphi_{sif} + \varphi_{vif} + \varphi_{hifi} \quad (2.2)$$

where φ_{eff} is the effective solid content, φ_{sif} is the surface immobilised fat, φ_{vif} is the volume immobilised fat and φ_{hifi} is the hydrodynamically immobilised fat.

2.2.5 Aggregation and deaggregation affecting immobilised fat

When fat is immobilised either within particles or at the surface of particles, it is not available to assist flow. If loose aggregates within pastes are broken up, there is likely to be a reduction in the effective solid volume fraction as more fat will be released from within the voids of the aggregate than is then necessary to coat the new interfaces that now exist. If, however, dense aggregates are broken down then there may be an increase in the effective solid volume content as more fat will be required to coat the particles than was contained within voids of the aggregate.

Aggregation or deaggregation may be a permanent phenomenon which occurs during the mixing of the pastes. Windhab (2000) discusses that this effect could also occur during the testing of a sample. The impact that this will have on a suspension can be calculated by understanding the volume ratios of surface immobilised fat, V_{sif}, and volume immobilised fat, V_{vif} (equation 2.32.3). If Ψ is > 1 then aggregation of particles will lead to a shear thinning

and thixotropic material, however if Ψ < 1 then aggregation will produce a shear thickening and rheopectic material.

$$\Psi = \frac{\Delta V_{sif}}{\Delta V_{vif}} \qquad (2.3)$$

2.2.6 Particle interactions

Hydrodynamic interactions between solids can change based on the shear that is being applied. At low shear rates, aggregates will trap more liquid as interparticle forces are dominant. As the shear rate increases, hydrodynamic forces increase and the liquid between particles reduces until the shear rate reaches a point where the aggregate is broken completely (Dabak and Yucel, 1986, Zhou et al., 1995).

Jánosi et al. (1997) found that long range hydrodynamic forces are dominant when suspensions settle however when the suspensions are sheared, these forces are found to be minimal and could even reduce the degree of particle dispersion (Metzger and Butler, 2010). Interestingly, the follow up of this study concluded that the contacting of particles is the most influential factor, increasing chaotic dispersion of particles within suspensions (Pham et al., 2015).

2.2.7 Specific effects on the shear thinning behaviour of suspensions

There is still no clear understanding of why shear thinning occurs within suspensions but there have been several theories discussed; When the continuous phase is Newtonian, Vázquez-Quesada et al. (2017) discusses that as shear rates of the tests are increased, the friction between particles reduces, causing shear thinning behaviour. It is also possible that between particles the shear rate is higher than the bulk. This could result in the material between particles thinning, thus lowering the overall bulk viscosity (Vázquez-Quesada et al., 2017).

Similarly, Mueller et al. (2009) hypothesises that the strain rate between the particles is higher than the bulk, causing *viscous heating*. When the gap is sufficiently small, the heat can no longer dissipate and the continuous phase warms, reducing its' viscosity.

There is a further hypothesis that slip may be occurring at the surfaces of particles. This study agrees that between particles, there is a higher shear rate than within the bulk, but suggests that there is a slip layer which increases with particle roughness and also with shear rate (Kroupa et al., 2017, Moon et al., 2015).

2.2.8 Specific effects on the yield stress

Whether a material can have a true yield stress is a topic which has been frequently deliberated in the literature for over 35 years. The conventional view has been that at low shear stresses, some fluids can behave as solids. As shear rate increase, the material continues to display elastic solid-like behaviour until a yield stress is reached. At which point, the material transitions to display liquid properties (Møller et al., 2009, Ovarlez et al., 2013).

Barnes published a paper in 1985 arguing that all fluids, given enough time, will flow and that yield stresses are only observed as artefacts when the sensitivity of the measuring equipment is not adequate at such low shear rates (Barnes and Walters, 1985). There is a belief that at low shear rates, there is a Newtonian plateau at a very high viscosity which can appear like a yield stress. Many authors do not firmly agree or disagree with Barnes, however for assessing the fluid behaviour within the time scales that are industrially and practically appropriate, the yield stress is considered to be an adequate model parameter of the observable fluid behaviour (Barnes, 2007, Fischer and Windhab, 2011, Reeve, 2010).

Within conched chocolates, Mongia and Ziegler (2000)and Windhab (2000) both discuss that the surface area, roughness, and shape of particles correlate with the yield stresses. The

difference, however is that these particles are much smaller than those present in chocolate pastes.

Yu et al. (2016) developed a relationship for debris flows containing particles between 375 – 9500 µm. The equivalent volumetric solid concentration is considered to be a function of the volumetric solid content, the volume average diameter, a shape factor and a material coefficient dependent on the type of material. Comparing experimental data for concentrations with volumetric concentrations of particles up to 0.75, they find a positive relationship between the equivalent volumetric solid concentration and the yield stresses.

Conversely to Yu et al. (2016), Mahaut et al. (2008) finds that yield stresses of suspensions of larger particles, between 80 - 2000 µm, at a solids volume content of up to 0.6, correlate well with the volume fraction of solids but are independent of the particle size, shape and roughness. Several studies have similarly concluded that increasing the solid content in suspensions will result in higher values of yield stress for particles up to 10 mm diameter (Subbanna et al., 1998, Heymann et al., 2002, Alejo and Barrientos, 2009). There are also papers discussing that specifically increasing the number of fines (< 75 µm) will increase the yield stress (Banfill, 1994, Yu et al., 2016).

2.3 Effect of processing on suspensions

The process by which the solids are mixed with the liquids may influence the resulting rheological behaviour of the suspension. Discussed below are the mechanisms by which the particles are wet by the liquid phase, how the mixing process could be altering the sizes of the particles and the importance of determining how homogeneous a batch is.

2.3.1 Mechanisms of particle wetting

The chocolate pastes contain particles with a wide range of sizes which have solids volume contents of up to 0.7. These suspensions can either be formed from combining dry materials together and subsequently adding the liquid to the mixture or the solids can be added into a reservoir of the liquid.

If a particle is added to a large quantity of liquid, Barnes and Holbrook (1993) discuss the process of how that particle is wet; first, there is *adhesional wetting* where the particle initially contacts the surface of the liquid; the solid-air interface of the particle and the liquid-air interface of the fluid begin to be replaced by one solid-liquid interface. As the particle begins to sink, *immersional wetting* occurs as further solid-liquid interfaces are created which replace the solid-air interfaces. For the particle to become submerged, the third stage, *spreading wetting*, involves a solid-liquid interface replacing the entire solid-air interface.

In practice, the solids are added all together and so particles are likely to hit the liquid surface with other particles. Particles which are touching may not allow new interfaces to be formed around the entirety of each particle resulting in aggregates. There is then a fourth stage, *penetration*, which requires the air now contained within interparticle passages to be displaced by liquid and the particle surfaces to be completely wetted, forming a paste (Scicolone et al., 2016). Barnes and Holbrook suggest that each passage between the particles can be modelled as a capillary and the pressure to force a liquid through each capillary is:

$$\Delta P_d = \frac{-2\gamma \cos\theta}{r_c} \qquad (2.4)$$

where r_c is the radius of the capillary, γ is the interfacial tension and θ is the contact angle.

If the wetting of aggregates can be modelled using this equation, it might then be possible to assess whether the addition of emulsifiers at this point would be beneficial. Emulsifiers can

reduce the contact angle between a solid and a liquid, however they increase the interfacial tension of the liquid which could negatively impact the ease that aggregates can be broken up.

Debacker et al. (2014) have recently published work which suggests there are three stages to aggregate imbibition if particles are left unmixed within a continuous liquid phase. This work highlights how the Washburn equation (equation 2.5) can initially apply, although as the air cannot easily escape from the pores once the aggregate is submerged in liquid, a build-up of air pressure will resist the flow of liquid through the capillaries. After submersion, the first stage of the imbibition is considered to be when the liquid quickly wets the outside layer of the aggregate within a few minutes. In the second stage, the infiltration of the liquid into the aggregate stops as the aggregate becomes saturated. Finally, after some time, the remaining pores are saturated with the liquid and complete imbibition is reached.

$$h^2 = \frac{r\,\gamma\,cos\,\theta}{2\,\eta}\,t \qquad (2.5)$$

where h is the distance into the capillary, r is the pore radius, γ is the surface tension of the liquid, θ is the contact angle, η is the liquid dynamic viscosity and t is the time.

Alternatively, it is possible to add the powders to the mixer and then feed in the liquid. If the liquid is added steadily, there are four stages of wetting; initially, the *pendular state* is where liquid bridges begin to be formed between individual particles. Once more liquid is added, the *funicular state* is then where interparticle voids begin to become replaced by liquid. When there are no longer any voids within the aggregation of particles, this can be described as the *capillary state.* Any further liquid added beyond this point results in the particles being fully dispersed within a continuous phase, forming a paste (Pietsch, 1997). Many groups have been able to use measurements of torque or power consumption to recognise these stages of wetting (Goldszal and Bousquet, 2001, Leuenberger and Betz, 2007, Leuenberger et al., 2009).

Using either of these techniques, it is desirable for the solids become fully dispersed within the liquids otherwise aggregates of particles will remain, potentially trapping air within voids. These aggregates will alter the effective solids content of the mixture, which as has been discussed within section 2.2.4, will impact the rheology of the suspensions. Aggregates may also be problematic when samples are measured if they become disrupted due to the test conditions. As discussed within section 2.2.5, this would falsely indicate the material may be shear thinning/thickening.

2.3.2 Particle size changes during processing

The mixing stage is designed primarily to homogenise the ingredients however there may be changes to the size of particles, particularly the sugar. Rumpf (1959) discusses three mechanisms for crushing solids:

1. Two solid surfaces – compression crushing
2. Solid surface or particle-particle collisions – impact crushing
3. Shearing from surrounding material

The mixing blades which are used for this stage of chocolate manufacture are not standardised and so the likelihood of these three crushing phenomenon occurring may vary depending on the geometry. It is well known that finer particles require more energy to fracture/break than coarse material which suggests that the coarse sugar particles may be more susceptible to breakage than smaller milk powder or cocoa particles (Tavares and King, 1998, Shi, 2016). If milk powder or whey powder were to fracture then the internal closed pore network is very large and would dramatically increase the surface area that the fat must coat.

Currently, there is not thought to be any relevant literature which has attempted to model undesirable particle size reduction within solid-liquid mixing processes. Cullen (2009)

discusses that is mechanical damage in food processes is thought to be wide-spread however literature is almost entirely focussed on breakages during crystallisation.

2.3.3 Identifying homogeneity

As has been discussed in section 2.3.1, ideally all of the particles would be distributed evenly throughout the mixture. If there are regions which remain unmixed, there will be localised regions where the viscosity may be higher due to the effects described in sections 2.2.2 and 2.2.5.

To assess the homogeneity of a mixture, it is important to identify a scale of scrutiny at which the homogeneity should be assessed at. This is considered by Harnby (2000) to be the one of the most important elements in assessing the quality of a product. The scale of scrutiny cannot be smaller than the largest particles within the suspension and can be determined by understanding the impact of homogeneity on downstream processes or the finished product (Muthukumarappan, 2009).

Image analysis of materials is frequently used as a straightforward method of assessing the homogeneity of a product. For batch processes, the product must be sampled at either a specific location or at a range of locations within the vessel in order to identify variation within the batch. Matuszek and Wojtkiewicz (2017) stained particles with fluorescent dye and used a Student t-test to identify whether there were statistically significant differences between then proportions of fluorescent particles between the samples that were taken. Ten random samples were taken but it is unclear how they ensured these were representative of the bulk. For continuous processes, several groups have used image analysis techniques to film the product across a width of a belt. Ammarcha et al. (2017) used image analysis to continually assess the homogeneity of dry material which had been fed onto a belt placed at

the outlet of a continuous mixer. They compare the coefficient of variance (defined as the standard deviation of each sample divided by the mean) for each sample and calculated a homogeneity ratio to calculate the changes over time. Berthiaux et al. (2006) similarly assessed the homogeneity of powders on a conveyor belt over time. They also used principal component analysis as an alternative to standard variance methods. The results, however, were not used for anything further so it is unclear whether this additional knowledge would be beneficial. These techniques are reliant on having images with good contrast in order to assess homogeneity.

There are also techniques which have been used to visualise the flow of liquid or particles suspended within a liquid. Mavros (2001) and Huang and Kuo (2014) review many of the techniques that have been used to visualise flow in mixing vessels, such as particle image velocimetry, laser-induced fluorescence and magnetic resonance imaging . Many of these may be useful for studying the impact of specific processing conditions in a laboratory environment however they involve the addition of specific particles which would be inappropriate to introduce into a food processing line (Ayazi Shamlou and Koutsakos, 1989, Montante et al., 2001, Magelli et al., 1990).

To study the concentration of particles, it may be more appropriate to use a tomography technique, such as electrical resistance tomography (ERT) (Harrison et al., 2012, Hosseini et al., 2010, Stanley and Bolton, 2008). ERT relies on the window that is being examined to be continuously full of the sample. Within an open mixing vessel where the surface distorts as the mixing shaft rotates, the results would not be representative (Sharifi and Young, 2013).

2.4 Methods for measuring rheology of pastes

As has been discussed, the viscosity of chocolate paste can vary between batches due to the many interactions which occur between the particles and the fluid, plus inherent variation of the natural materials used to produce chocolate. It is hoped that quantifying the rheological behaviour will distinguish pastes from one another and relate to the performance of downstream processes. It will then be possible to understand whether downstream processes can be altered to accommodate for varying consistencies of paste or whether process settings can be altered within mixing in order to produce a paste with reliable consistency.

Many problems exist when trying to measure the rheology of materials containing high volumes of large solids. Firstly, it is likely that there will be an *effective slip* where the particles roll and slide close to the wall (Koos et al., 2012). Due to the presence of the wall, it is also impossible to achieve the same particle arrangement at the wall as is present in the bulk (Barnes et al., 1989). Additionally, as suspensions are sheared, it is easier for the liquid to move and the solids will avoid areas of high shear. The depletion in solids at the wall due to packing and phase migration of liquid towards the walls results in a less viscous layer close to the wall (Larson, 1999, Shauly et al., 1998). The shear stress within this layer will be different to the bulk and will mean that when the velocity profile of the bulk is extrapolated to the wall, there will be a different velocity to that of the boundary, referred to as the *apparent slip velocity* (Jana et al., 1995). This layer has been approximated within many publications and is estimated to be around the diameter of one particle, assuming a monomodal PSD of the solids (Koos et al., 2012).

Most rheological techniques rely on assumptions that there is no slip at the wall, denoting that at the contacting boundaries of the geometry, the material should adhere to the surface in

order to correctly predict the strain field (Barnes et al., 1989). To counteract the effective and apparent wall slip, it is common to roughen the walls so that the surface roughness is of a similar length scale to the particles. This can be done through sticking similar particles to those held within the suspension onto the walls, using sandpaper as a roughened surface or sandblasting (Mezger, 2006, Koos et al., 2012, Ewoldt et al., 2015).

At low solids volume contents, it is accepted by the rheological community that ideally a gap size of 10 times the largest particle should be used when measuring suspensions. At solid volumes content above 0.25, Barnes proposes that a gap size of 100 times the size of the largest particle is required in order to minimise the impact that particle depletion at the wall has on the bulk measurement (Barnes, 2000, Barnes et al., 1989).

2.4.1 Cone and plate or parallel plate rheology

The cone of a cone and plate rheometer has an angle less than 8° (Hou, 1981), generating a constant shear rate in the sample gap. The centre of the cone is commonly truncated so that there is no abrasion or friction between the cone and the plate but generally, the gap is below 50 μm (Mezger, 2006). This means that it is completely unsuitable for measuring suspensions of particles which are larger than 50 μm as they risk becoming jammed at the truncation. In order to adhere to the common practice that the gap sizes must be at least 10 times the size of the particles, it is unwise to use this method to test suspensions containing particles above 5 μm.

The flat plates of a parallel plate rheometer can be operated at a maximum of 4000 μm apart, which would allow particles of up to 400 μm within a dilute suspension to be measured reliably (Yilmazer and Kalyon, 1989, Mezger, 2006), adhering to the rule of thumb of a 1:10 ratio. In practice, this height is also limited by the surface tension of the sample to remain

within the gap. The shear rate is highest at the edges of the plate; this value is used when discussing the shear rate of the system.

Parallel plates or cone and plates can be similarly used for steady shear tests or oscillatory shear tests. Steady shear tests are commonly used to establish the flow behaviour of fluids, however there can be problems which arise if suspensions of solids are tested. Krishnan et al. (2006) observes radial migration of particles towards the outer edge of the sample during steady shear tests within a 45 vol% solid suspension of 462 – 664 μm particles within a parallel plate. Deshpande and Shapley (2010) showed that in oscillatory shear tests of 40 vol% solid suspensions of 106 - 125 μm particles, there was an enhanced migration of particles compared to steady shear tests; agreeing with several other studies (Merhi et al., 2005, Kim et al., 2008). It is also possible that the edge will begin to distort during parallel plate or cone and plate tests. Another issue related to testing solid suspension is that the edge of the sample could fracture which results in the material leaving the gap between the plates (Keentok and Xue, 1999, Jomha and Reynolds, 1993). This can be identified by a drop in the shear stress as the shear rate increases (TA.Instruments).

2.4.2 Concentric cylinders

Concentric cylinders, also known as couette or cup and bob rheometers, are typically used for more complex fluids which take a longer time to locally equilibrate within the flow (Dontula et al., 2005). The test gap is formed between two cylinders, one positioned inside of the other. The inner cylinder rotates and the outer cylinder remains stationary and when the radii of the cylinders are large, the shear rate can be considered constant at all regions within the gap.

As surface tension of the material no longer limits the gap size, it is possible for larger annular gaps to be used, although this means that the shear stress and shear rate are not constant across the width of the gap (Chatzimina et al., 2009).

R. Abbott et al. (1991) used NMR imaging to observe the particle concentration during wide-gap couette tests of neutrally buoyant particles within concentrated suspensions ($\varphi = 0.5$). All suspensions of particles between 675 – 3175 µm showed radial migration during the test duration; larger particles more readily migrated towards the outer edges where the shear rates are lower, and a higher rate of migration was also found when the particles were polydisperse rather than monomodal. Chow et al. (1994) also reported that particles can commonly migrate to the stagnant region under the bob. Rheo-NMR was similarly used by Colbourne et al. (2018) to assess the velocity and concentration profiles of concentrated suspensions, up to $\varphi = 0.52$, in a wide-gap couette.

There is an abundant resource of literature discussing how the radial migration would be best modelled, suggesting that this is a prolific problem which affects the quality of measurements of many particle suspensions using wide-gap couette geometries (Kromkamp et al., 2006, Ingber et al., 2009, Tetlow et al., 1998, Yu et al., 2007, Mirbod, 2016).

As there is now a larger volume of fluid within the test geometry, sedimentation of the particles will influence the homogeneity of the sample that is being tested. Using Magnetic Resonance Imaging, Ovarlez et al. (2012) concluded that shearing materials will enable particles to move and this was found to induce sedimentation. They also investigate the effect of different suspensions from $\varphi = 0.05 – 0.4$ and conclude that increasing the solid fraction has two contradictory effects; the increased concentration of solids will hinder settling however it will also decrease the viscous resistance of the continuous phase because of shear

concentration between particles. There is, however, a time frame to do with this and Ovarlez found that after continually shearing a sample of 275 μm glass beads within a concentrated emulsion for 4 minutes at 8.8 s^{-1}, the sedimentation from had only moved 1 cm.

2.4.3 Vane rheology

It is possible to modify the geometry of the inner cylinder of a couette rheometer by instead using a vaned probe. This is intended to trap material between thin vanes which, when rotated, forms a cylinder of the test material with the aim of reducing the wall slip (Ewoldt et al., 2015, Dzuy and Boger, 1983, Yoshimura et al., 1987). The vane is most commonly used to measure the yield stress of materials in soil mechanics, food and bioengineering applications. More recently there has been research into using the vane rheometer to measure the rheological behaviour of samples over a range of shear rates.

From experiments, Barnes and Carnali (1990) found that when a shear thinning ($n < 0.5$) solution of 5.5 % CMC was tested, yielding of the material created a layer of material that remained within the vanes; this reduced wall slip at the inner wall and gave an accurate estimation of the rheological properties.

Using suspensions of 0.18 μm particles which were at a 50 w/w water, Fisher et al. (2007) were able to measure comparable results of the shear stress using a four-bladed vane within an infinite medium as was measured with a capillary rheometer. They found the shear stress to be highest close to the probe and it decreased as the radius increased. Within an infinite radius of material, once the shear stress lowers to the yield stress of the fluid, the material will stop moving and an interface is formed within the material. As both sides of this interface consist of the same material then they no longer found a risk of slip at the wall.

A more complex geometry is used by Heirman et al. (2008), the ConTec Visco5, which has 10 vanes (Radius = 100 mm) but rather than extending from the centre, there is a cylindrical space around the centre. A diagram of this, taken from Heirman et al. (2008), is shown in Figure 2.8. In this case the outer cylinder (Radius = 145 mm), which also has small baffles, rotates and the equipment records the torque on the stationary inner cylinder. They rely on the standard methodology used to process raw data from a Couette and they validate the results by comparing the measured torque vs rotation speed to values of calculated torque based on the predictions for the Herschel-Bulkley model (described in section 2.4.5) at each rotation speed. The technique was used to measure concretes containing aggregates that had a maximum diameter of 14 mm up to a solid volume fraction of 0.47. At shear rates below 1.1 s^{-1} they found that slip increased due to the formation of a plug, resulting in lower torque measurements than were expected. Above 11 s^{-1} they found that there was a risk of phase migration due to the higher shear rates so consequently the tests were carried out within these two values.

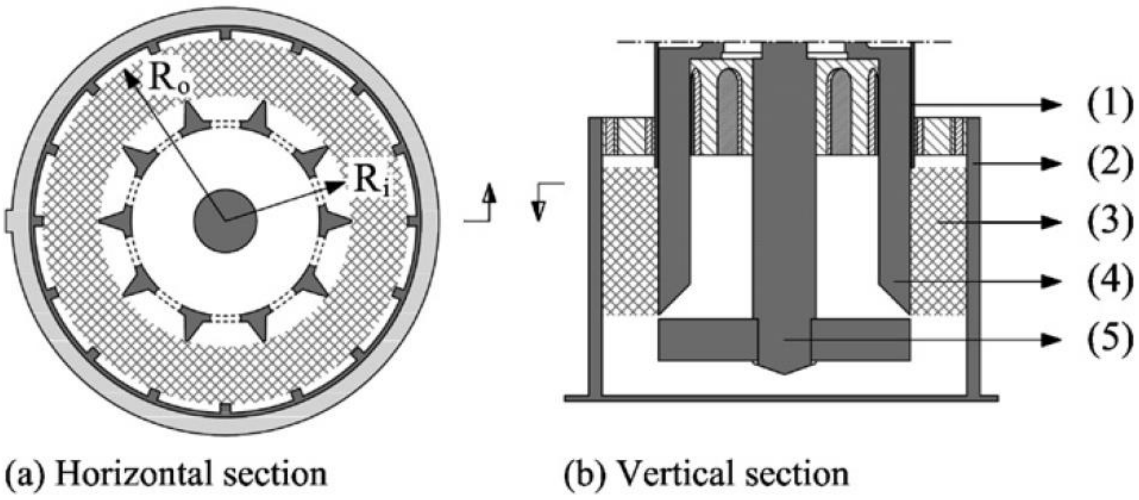


Figure 2.8: Diagram of the ConTec Visco5 used by Heirman et al. (2008). Labelled are: (1) top ring, (2) outer cylinder, (3) test material, (4) free upper section of inner cylinder, (5) fixed bottom of inner cylinder

It is clear from the literature that although Barnes and Carnali (1990), Fisher et al. (2007) and Barnes and Nguyen (2001) all mention that the vane has more recently been used to measure rheological properties of slurries, ceramic pastes and food pastes, there seems to be very few studies published which are able to conclusively measure large particle suspensions with the vane rheometer over a large range of shear rates. Out of 48 references, only one study by Yoo and Rao (1994) reports successful measurements of tomato concentrate suspensions using a vane rheometer. These contain particles as large as 710 µm up to a solids volume fraction of 0.35. They do not, however, present any raw data or discuss the issues that slip may produce.

Magnetic Resonance Imaging by Ovarlez et al. (2011) has indicated that the vane technique is not suitable for measuring suspensions of large particles. Ovarlez et al. (2011) observed rapid, irreversible depletion of particles between the gaps of each vane, which is comparable to a wall slip effect (Figure 2.9) and believes that this is a significant enough effect to invalidate the results.

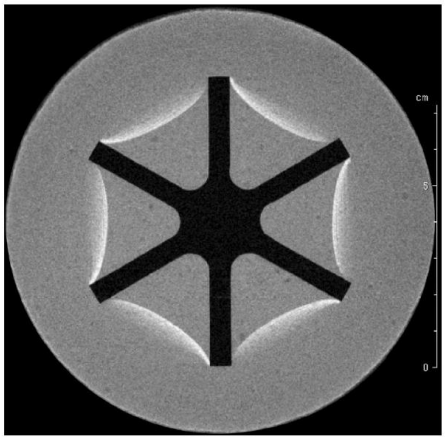


Figure 2.9: 2D MRI of a 40 % suspension of 250 µm particles within a yield stress fluid after 1 hour of shearing in a vane rheometer, taken from Ovarlez (2011). Lighter areas are regions of higher suspending fluid concentration.

2.4.4 Capillary extrusion

It is possible to determine the flow properties of materials by extrusion through dies of different length and diameter ratios. The Benbow-Bridgwater model was established in the

1980s to predict how solid suspensions would flow. Unlike other rheological measuring techniques, there are constants incorporated into the Benbow-Bridgwater equation to account for the slip at the wall.

This technique has been used for many applications such as ceramic pastes, doughs, catalyst monoliths and many other applications; summarised by Wilson and Rough (2006). Whilst this is a good technique for materials that are prone to slipping, high shear rates can lead to phase migration, where the continuous phase ends up flowing through the network of solids, rather than behaving as a homogeneous paste (Draper et al., 1999) . Yaras et al. (1994) and Bayfield et al. (1998) both discuss the occurrence of liquid paste migration whilst extruding suspensions containing 63 – 78 % vol solids (particles approximately 13 μm and a mixture of 20 μm and 200 μm particles, respectively). Liquid phase migration is more prevalent when the liquid content is lower, resulting in a layer of liquid at the walls where the shear is highest. Less phase migration was observed when the particles were smoother as they were less prone to jamming. If particles do jam, the liquid phase is likely to migrate through the network of solids so that a more concentrated suspension remains.

In geometries like this, the calculations rely on the pressure drop through the length of the die. If the layer nearest the wall is depleted of particles, there is a deviation of the local pressure gradient close to the edges (Barnes, 1995). Benbow and Bridgwater found that the thickness of this layer in capillary extrusion varied relative to the proportion of liquid available rather than the viscosity of the suspension (Benbow and Bridgwater, 1993).

Many research groups have also observed accumulation of solids at the leading edge within pipe flow, known as the meniscus, resulting in a region with higher solids content than the bulk (Karnis and Mason, 1967, Ramachandran and Leighton, 2010, Tadier et al., 2014,

Azzolini et al., 2014). There are, however, no studies involving solids volume contents above 50 %. Particles prefer to migrate to regions of lower shear; within a tube, particles have been observed to migrate towards the centre. The velocity is highest at the centre, leading to these particles moving quicker than the average suspension velocity. As the meniscus is only moving at this average velocity, particles accumulate at the meniscus. Since there are particles moving faster than the bulk towards the meniscus, there has to be radial flow of the particles towards the edges of the tube in order to maintain the mass flow rate (Karnis and Mason, 1967). Ramachandran and Leighton (2010) discuss how long it takes, measured in distance along the tube, for phase migration to occur. The length will decrease when the particles are larger, the solids concentration is higher or if the tube is smaller, an effect which is also observed by Bayfield et al. (1998).

Tadier et al. (2014) found that liquid migration could be reduced by using two different sized particles, as the particle packing was increased. As the particles are packed better, it is harder for the liquid to move through the gaps between particles.

The force measured during capillary extrusion tests reported in the literature should remain constant if the paste remains homogeneous but often the force steadily increases over the extrusion period. This cannot be explained by slip and there are no explanations or hypotheses offered within the literature for why this occurs (Tadier et al., 2014, Azzolini et al., 2014, Bayfield et al., 1998, Yaras et al., 1994).

2.4.5 Back extrusion

A cylindrical probe is pushed down at a constant speed into a contained cylinder of the test material. The material is displaced by the plunger and is forced to move upwards through the annulus. By repeating this test at multiple speeds, a range of shear rates are achieved and the

parameters which describe the behaviour of the material can be calculated. As material moves through the annulus, similarities can be drawn with capillary extrusion and filling of an empty pipe.

Based on work originally designed to test Newtonian fluids, Osorio and Steffe (1987) published a method to characterise the rheological properties of an aqueous hydroxypropyl-methyl-cellulose solution, applying the power law model. Further research was then published extending this technique to test sodium-calcium alginate solutions which were represented using the Herschel-Bulkley model (Osorio and Steffe, 1991).

Brusewitz and Yu (1996) used the technique to test mustard slurries and Gujral and Sodhi (2002) also used the technique to test wheat porridge samples with particles sized between 355-600μm. Both groups limited their research to comparisons between the raw forces measured and did not go so far as to relate the results to rheological model parameters.

This method was also used by Alviar and Reid (1990) to characterise tomato concentrates, with total solids up to 36 vol%, using a gap between the probe and the barrel of 7 mm. These concentrates were also measured on a parallel plate rheometer using a gap of 750 μm, despite risks of the particles being too large (the tomato paste was sieved through 0.033 inch sieve, approximately 840 μm). Using a power-law model, the results of shear stress show a good agreement to the parallel plate rheometer results. More recently, Perrot et al. (2011) have used the technique to measure a 50 wt% suspension of 20 μm sugar in oil. They concluded that when pushing the probe in at velocities between 0.1 – 1 mm/s, the Herschel-Bulkley model parameters are relatively close to the results using a vane rheometer in a roughened cup.

David et al. (2013) have since expanded on the analysis of the raw data using a Vocadlo model (equation 2.6) based on the raw data discussed by Osorio and Steffe (1991).

$$\sigma_V = ({\sigma_y}^{1/n} + K\dot{\gamma})^n \quad (2.6)$$

No further publications are known of which investigate the presence of slip or radial migrations, both issues which are common occurrences in the previous rheological methods reviewed here,

2.4.6 Penetrometers and vanes used for soils

For soils, it is desirable to test materials in-situ rather than taking a sample from the site. In civil engineering, there are a range of techniques which involve either penetrating the sample with a probe or by rotating a vane which is submerged in the sample.

Soils consist of particles of different sizes with water between or surrounding the solids. Soft soils show comparable behaviour to pastes and the strength of these soils can be quantified using a cone penetrometer. The tip of the cone is either placed at the surface of the sample or at a set height above the sample and is then released. The weight of the cone and the height at which it is dropped from vary the kinetic energy which is applied to the sample and the distance at which the cone has moved into the sample can be measured after a known time (Jones and Kunze, 2004).

There are many techniques similar to this involving penetration of the sample with a cylinder or cone, or rotation of a vane which has already been submerged within the soil. Unfortunately, these techniques can measure different forces (e.g. torsional, compressive, shear) but the results are all quoted as a shear strength; leading to comparisons within publications which are not appropriate (Zimbone et al., 1996). Zimbone et al. (1996) also discusses that the results from these techniques can also be very dependent on the operator.

2.4.7 Slump test

Since the development of this test by Murata (1984), the slump test (BS EN 12350-2:2009) has become common place within concrete manufacturing. Within this industry, it is desirable to quickly assess the differences between batches, these differences commonly being associated with the yield stress (Roussel and Coussot, 2005, Saak et al., 2004). The slump test involves a known amount of material held in a conical mould on top of a flat board. The mould is removed and the material will relax. If inertial effects are ignored, the material will stop moving once the shear stress becomes lower than the yield stress of the material. The distance that the material has spread and/or the height that the material has dropped will then be indicative of the yield stress. Several semi-empirical models have also been developed, for example by Ferraris and de Larrard (1998), linking the slump to both yield stress and the plastic viscosity; assuming a Bingham fluid model can apply.

2.4.8 Bostwick consistometer

As rheometers are sensitive pieces of equipment and require a relatively high level of precision and training in order to accurately measure the rheology of materials, it is often desirable to have a more rapid test despite the drawback of a lower degree of accuracy. The Bostwick consistometer involves filling a sample cell with the test material and then removing one of the sides to measure how far the material will flow as a function of time. Usually, the result is used as an empirical value to compare between samples although some research has been carried out in order to quantify the power-law model parameters of viscous fluids using the Bostwick technique. Currently, this work is limited to assessing the similarity of the experimental data and the theoretical data in order to predict the value of n (Piau and Debiane, 2005, Piau, 2006).

2.4.9 FT4 powder rheometer

Freeman Technologies developed the FT4 Powder Rheometer which is designed to characterise the flow properties of powders. Based on a patented measurement principle, a small helical blade is rotated through a sample in an upwards motion. The force and torque on the blade are continually recorded and are converted into total flow energy as an indication of how readily a powder will flow (Brockbank et al., 2015).

Scicolone et al. (2016) used this technique to characterise how the flowability of different sized glass beads changes when water is added. This work found that at 20 wt% liquid content, when they began to appear paste-like, the suspensions of 5 µm, 50 µm, 100 µm and 275 µm particles resulted in different quantities of total energy. Unfortunately, there is no work published relating these measurements of flow energy or flowability with rheological model parameters for liquids or pastes thus the results remain purely empirical and reliant on the test conditions.

2.4.10 Measuring rheology in mixers

A range of literature has been published on measuring the rheology of material within a mixer, spanning many different industries. The overall theory which seems to be applied in the majority of these papers is to establish what the equivalent geometry of a concentric cylinder rheometer is to a specific mixer. There are mainly two different arrangements discussed within the literature, either a single vertical impeller or two horizontal, adjacent blades.

Aït-Kadi et al. (2002) published research using a vertical helical blade as an analogy to a couette rheometer (sample size < 100 ml). Subsequently, for suspensions of particles (up to 800µm) which rapidly phase separate from the fluid, Guillemin et al. (2008) designed their

own impeller geometry which would keep the particles in suspension (sample size < 10 ml). Both groups found that by using the analogy of a couette, they could reliably measure the rheology of suspensions which easily settled. There have been many other papers published, reviewed by Duffy et al. (2015), which also describe impellers used to measure the Newtonian or Power-Law behaviour of fluids based on this analogy (Williams, 1979, Castell-Perez and Steffe, 1990). Similarly, there has been work using the Brabender Viscometer where a series of pins are rotated within a vessel of the sample, which can also be modelled as a concentric cylinder (Aerts and Verspaille, 2001). Unfortunately, these techniques rely on using a rheometer to establish the relationships of mixer torque and angular velocity with shear stress and shear rate, respectively. As it has been established that existing rheometers may struggle to assess concentrated suspensions, it would be difficult to establish similar relationships for measuring chocolate pastes.

There has also been a lot of research published where small mixers (< 250ml) containing two horizontal, adjacent blades are used to measure rheological behaviour (Santi et al., 2009, Hancock et al., 1994, Rowe and Sadeghnejad, 1987). For wet granulation applications, these are often known as *mixer torque rheometers* but similar geometries are established as simply *torque rheometers*. The raw data can be used alone to infer the rheological behaviour; the amplitude of the torque oscillations indicates how heterogeneous the mixture is and the increase in the torque from the start corresponds to the mean resistance of the material (Luukkonen et al., 1999). Following initial work by Goodrich and Porter (1967) based only on Newtonian fluids, Bousmina et al. (1999) showed that it was possible to measure both Newtonian and power-law behaviour of fluids in agreement to cone-and-plate and capillary rheometers.

Some research has been published based on larger scale mixing which found that the torque measured on an 80 litre mixer as three formulations of cement mortar were combined correlates strongly with the results of a slump test (Ziyi et al., 2014). Unfortunately, no research is known to have been published regarding scaling up of these small mixers to quantify the rheological properties of materials during manufacture.

3 MATERIALS AND METHODS

3.1 Introduction

This chapter is divided into four sections; the first discusses the equipment that was used on a pilot plant scale to produce chocolate pastes and subsequently process these pastes to produce molten chocolate. The second section describes the measuring techniques that were used offline to measure physical properties of the materials created throughout this project. The penultimate section explains the statistical methods which were used to analyse the data. Finally, the materials used within all of the research presented in the subsequent chapters are described.

3.2 Methods: Equipment

Pastes that are discussed within this thesis were manufactured in a variety of ways and the equipment used is detailed in Table 3.1.

Table 3.1: Techniques used to manufacture the pastes which will be presented within this Thesis

Process Stage	Preliminary pastes and suspensions	Trial 1	Trial 2
Mixing	Hand mixed	200kg capacity mixer (Buhler, Germany)	8kg capacity mixer (Aoustin, France)
Pre-Refining	-	Two roll refiner (Buhler, Germany)	Three roll refiner (Lehmann, Germany)
Refining	-	Five roll refiner (Buhler, Germany)	-

3.2.1 Mixing

3.2.1.1 Hand mixed

Pastes and suspensions which were used for the experiments in chapters 0 and 0 were manufactured at room temperature. Batches smaller than 3 kg were formulated by adding the liquid elements to the solids and hand mixing with a spatula until visibly homogeneous (approximately 3 minutes).

3.2.1.2 200 kg Capacity Buhler Mixer

Solids were first added to the mixer whilst the blades remain stationary. The machine then began to mix as the liquids were added on top. The speed and mixing time were both included as factors within the design of experiments. The vessel was open to the environment but had a water jacket which was maintained at 45°C. The base of the mixer was shaped around two horizontal mixing shafts which each had 5 mixing blades (Figure 3.1). The clearance between the blades and the vessel wall was 5 mm. Once the mixing time was complete, the mixing shaft was stopped and a section of the base was opened so that the paste could drop directly into the two roll refiner.

The current draw of the mixing blades was logged at a rate of 1 Hz, directly from the control panel, whilst the machine was in operation. Figure 3.2 shows an example of the current recorded over the mixing time of one batch. The current initially increases as the mixing shafts begin to turn which is due to the extra energy required to get the blade turning on start-up. It is also difficult for the blade to move as the fat is only in concentrated regions and therefore the friction between dry particles is high. Over the duration of the mixing, it was consistently observed that the current draw decreases which is anticipated to relate to the increasing distribution of the fat over the surfaces of the particles.



Figure 3.1: Mixing blades within the 200kg capacity Buhler mixer. Base situated the top left corner of the image opens to release the paste into the pre-refiner.

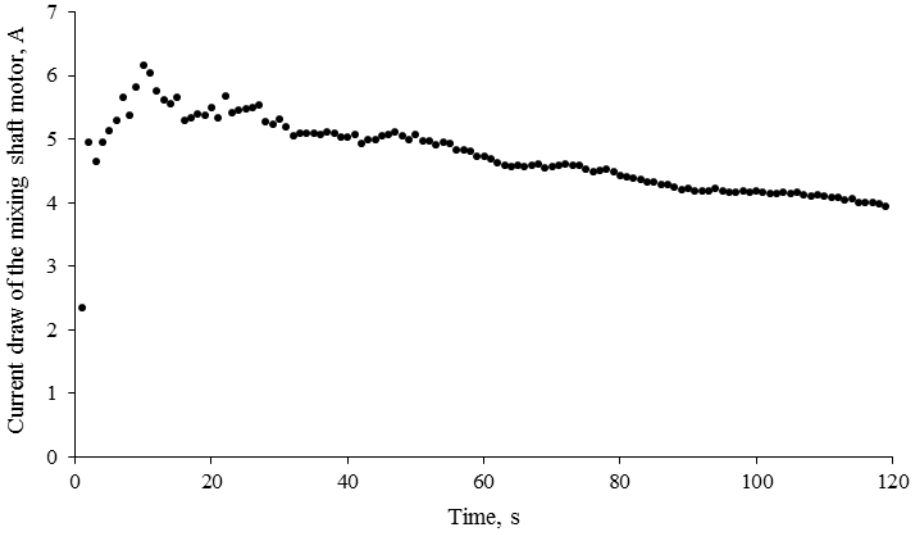


Figure 3.2: Current draw of the mixing shaft motor over the duration of the production of one chocolate paste batch

Two values can be established from this profile of current draw; firstly the final value of current at the end of the mixing duration should indicate of how much the paste is resisting the blade, i.e. the paste consistency at the end of mixing. It is also possible to calculate a value

indicating the total work done over the mixing time by summing the value of current at each second, however this quantity is strongly affected by the mixing time. As mixing time was a factor within the trials, the final value of current was a better value to compare batches.

The current of the mixing shaft moving was measured when the vessel was empty and varies when the shaft moved at different speeds. The values discussed within this thesis are all determined by subtracting these empty vessel values from the raw data. During each run, the voltage remained constant.

Table 3.2: Base values of current measured on the mixer at each of the speeds using in this design of experiments, when empty.

Mixing blade speed, rpm	14	25.5	37
Current of empty vessel, Amps	3.29	3.38	2.97

3.2.1.3 8 kg Capacity Aoustin Mixer

This was a twin z-blade mixer and each paddle was 106 mm in diameter. The solids were first put in to the mixer by hand and the mixing began as the liquid was quickly added to the mixer. The clearance between the blades and the vessel wall was 2 mm. Similarly to the larger capacity mixer, it was possible to record the current draw of the mixing shaft. Unfortunately, the capacity of the motor was much greater than the resistance of the pastes and therefore the currents recorded did not change when the paste recipe/operating conditions were varied.



Figure 3.3: Side on and birds eye view images of the Aoustin mixer with two z-blade mixing shafts

3.2.2 Refining

3.2.2.1 Two roll refining

Two refiner rolls (diameter = 400 mm) turned counter-currently as the material was dropped directly from the mixer into the nip of the two rolls. The refiner rolls were operated whilst the paster was emptied into it so the level of material above the nip of the rolls was not maintained. The second roll was rotated faster than the first with a speed ratio of 1:2.5. The rolls were pressed together with a pressure of 20 bar and the gap size was held constant (setting: 40E).

3.2.2.2 Five roll refining

Once the paste had passed through the two roll refiner, the material was held in an intermediate mixer which gently mixed the material, heated at 50°C. This ensured that the pre-refined paste could be steadily fed to the refiner.

Five rolls were stacked vertically, creating four gaps which the material was passed through. The second roll rotated at 90 rpm and each roll moved progressively faster and rotated in opposite directions. Roll 2 was fixed in place whilst the other four rolls were “floating”. A

pressure of 15 bar was applied on either side of the rolls which pushed them against roll 2. The gap setting was 345, a value which was used as calibration point and has no units.

The pre-refined paste was steadily fed into the gap between the first two rolls and a constant level of pre-refined paste within the nip was roughly maintained by an operator. The material transferred from one roll to the next at each nip. A sharp blade positioned across the fifth roll scraped the material off and the refined chocolate flake fell into a collection vessel.

3.2.2.3 Three roll refining

Material produced in a smaller 8 kg capacity mixer was reduced in particle size using a refiner containing three rolls, positioned horizontally. Similarly to the five roll refiner, the rolls rotated in opposite directions and the speed of each roll progressively increased. Each roll has a diameter of 260 mm and the speeds used were: roll 1 = 20 rpm, roll 2 = 60 rpm and roll 3 = 144 rpm. A pressure of 7 bar was applied on both sides of each roll and a one half turn was applied to each of the clocks controlling the distance between the rolls.

The pastes were pre-heated to the required temperature (specified within the trial design) before being hand fed into the nip between the first two rolls. The level of material on top of this nip was maintained fairly constant, based on the judgement of the operator. A blade pressed across the third roll scraped off the material which was collected for further analysis.

The current which was required for each roll to turn was recorded during the refining of each batch. It was also possible to determine the length of time that each batch took to refine which is an indicator of the rate of the material passing through the refining process.

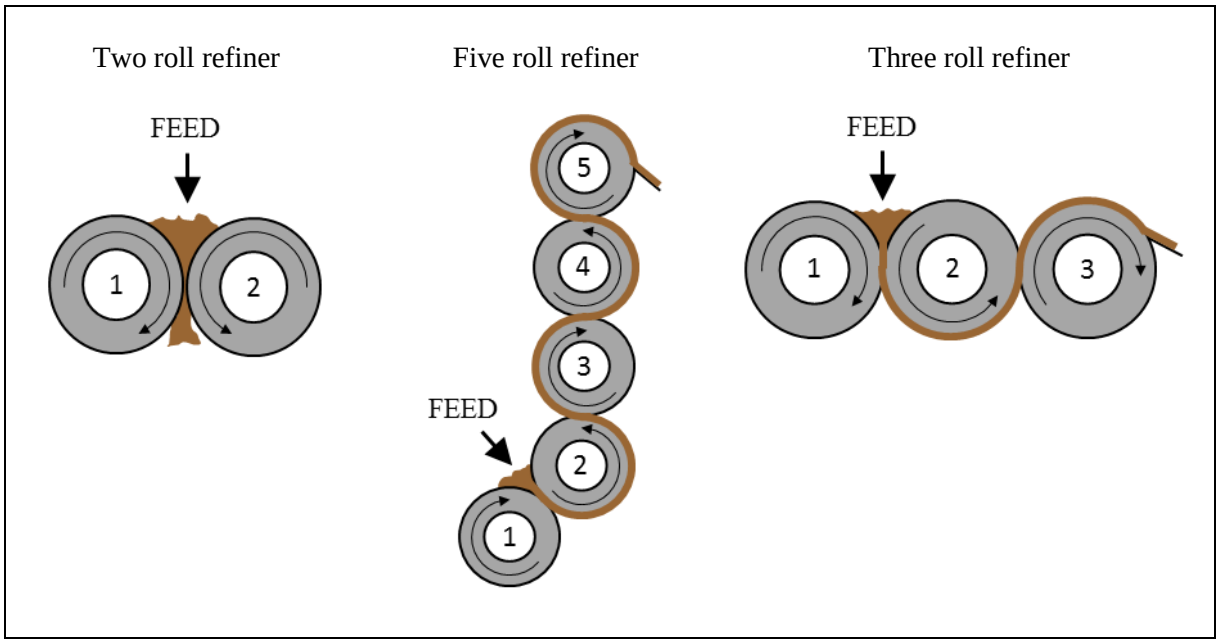


Figure 3.4: Diagrams of the three different refiner layouts that have been used in chapter 7

3.3 Methods: Measuring Techniques

3.3.1 Operator ranking

A scale was developed alongside an experienced operator from the Mondelēz pilot plant to assess the consistency of the pastes and pre-refined pastes on a scale of 0-10. The centre point of the scale represented a paste which has a consistency that is easily processed, based on the chocolate pastes which are produced on a day-to-day basis. Zero represented the thickest paste (generally with a low fat content) which would be able to be processed. Ten represented the thinnest paste (generally a high fat content) which would not fall straight through the gap between the refiner rolls.

As the surface area of the particles increased once pastes had passed through the pre-refiner, the consistency of the pastes were different to the pre-refined pastes. Therefore, they were not ranked on the same scale. Instead, the extremities of the scale were specific to the thickest and thinnest material possible at the pre-refining stage.

3.3.2 Particle size distribution

3.3.2.1 Measuring particle size distributions

Particle sizes of each component were measured with either a Mastersizer 3000 or Mastersizer 2000 (Malvern Panalytical, UK), both are generations of the same equipment. This is a laser scattering technique which uses the Frauenhofer theory to predict particle size based on the light scattering pattern (Malvern Instruments Limited). The Frauenhofer theory was used since the majority of particles are above 50 µm and within mixed solid suspensions, such as chocolate pastes, the refractive indices of the materials vary (Cilas).

The method was based upon the technique used by Afoakwa (2016); 0.2g of material was dispersed within vegetable oil by hand, followed by 2 minutes within an ultrasonic bath. At an ambient temperature, each sample was added into the Mastersizer until the obscuration reached 20 %. Table 3.3 lists the refractive indices used for these measurements.

Granulated sugar and SMP were also manually sieved for use in trials reported chapter 0. The resulting PSDs were measured using a dynamic image analysis technique (QICPIC and GRADIS combined system, Sympatec GmbH, Germany). The dry powders were fed through a 400 mm freefall shaft, with a gap height of 2 mm and a feed rate of 10 %.

Table 3.3: Values of refractive index used to test each material using laser diffraction

Material	Refractive Index
Granulated Sugar	1.54
SMP	1.54
SWP	1.54
Cocoa Powder	1.59
CCL	1.59
Paste	1.59
Flake	1.59

3.3.2.2 Modelling particle size distributions

The particle size distributions of the pastes, refined pastes, flakes and conched chocolates can all be considered as multi-modal. To compare results statistically, the PSDs were modelled by multiple log-normal curves, relative to the number of peaks the PSD has. Each of the log-normal curves, expressed by equation 3.1, were then weighted by W so that the total PSD had a volume distribution equal to 1. Using JMP 12 (SAS, UK), a standard least squares method is used to create a predictive model of each PSD parameter. This statistical analysis technique is further discussed in section 3.4. Using the predicted values for each parameter, at a specific condition, a full particle size distribution could be recreated using equation 3.1 to support the statistical analysis results discussed in chapters 6 and 7.

$$Log\text{–}Normal\ Volume\ Distribution = \frac{1}{S\sqrt{2\pi}} e^{-(\ln x - M)^2 / 2S^2} \qquad (3.1)$$

where x is the particle diameter, M is the mean of the log-normal distribution and S is the standard deviation of the log-normal distribution.

The specific surface area (SSA) was also used to evaluate differences between materials in chapters 6 and 7. This was calculated by the Malvern software. Several studies have discussed that values of SSA are sensitive to the refractive indices of the solids and that most error exists when predicting the surface areas of particles below 5 μm (Arvaniti et al., 2015, Cepuritis et al., 2017). This measurement was only used as a comparison tool between the samples and it is important to consider that, like the PSD results, assumptions have been made that the particles are all spherical and have the same refractive index.

3.3.2.3 Error of particle size distribution measurements

The chocolate pastes and pre-refined pastes contain particles which can range over a broad size (0.1 – 2000 µm). To establish what the repeatability of the technique is, four batches of chocolate pastes were manufactured, following the method described in section 3.2.1.3. Three separate samples were measured of each of these pastes, following the method described above. Based on these 12 measurements, Figure 3.5 shows the mean PSD, where the volume of particles within each sieve class have been averaged, ± one standard deviation. It is possible to see that the largest amount of variation occurs at the top of the third peak. As the laser diffraction technique produces results based on a volume distribution, the presence of one larger particle (i.e. 1000 µm) has a greater impact on the results than an additional particle which might only be 10 µm.

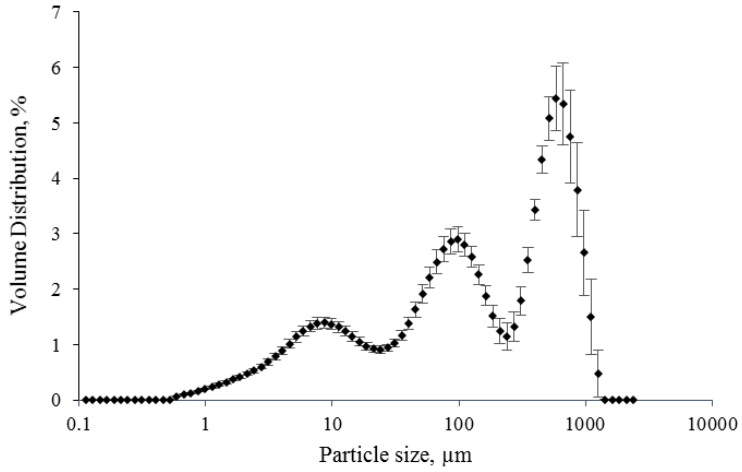


Figure 3.5: Mean particle size distribution of four batches of pastes with the same formulation, each measured three times. The error bars represent one standard deviation.

By modelling the PSD results with either two or three log-normal distributions, this will allow the curves to be compared, however this may also introduce error into the results. Based on the same four pastes compared above, each result was modelled using three log-normal distributions. The mean PSD using the values of raw data within each sieve size are compared

to two PSDs which have been computed in two ways. These are described in Figure 3.6. The model PSD produces a very similar result to the mean of the raw data. There is a slight discrepancy of the particles which fall within the first peak and the model also shows a more gradual tail off of the very largest particles. Overall, this comparison suggests that the three log-normal distribution model is capable of representing the shape of the raw data well.

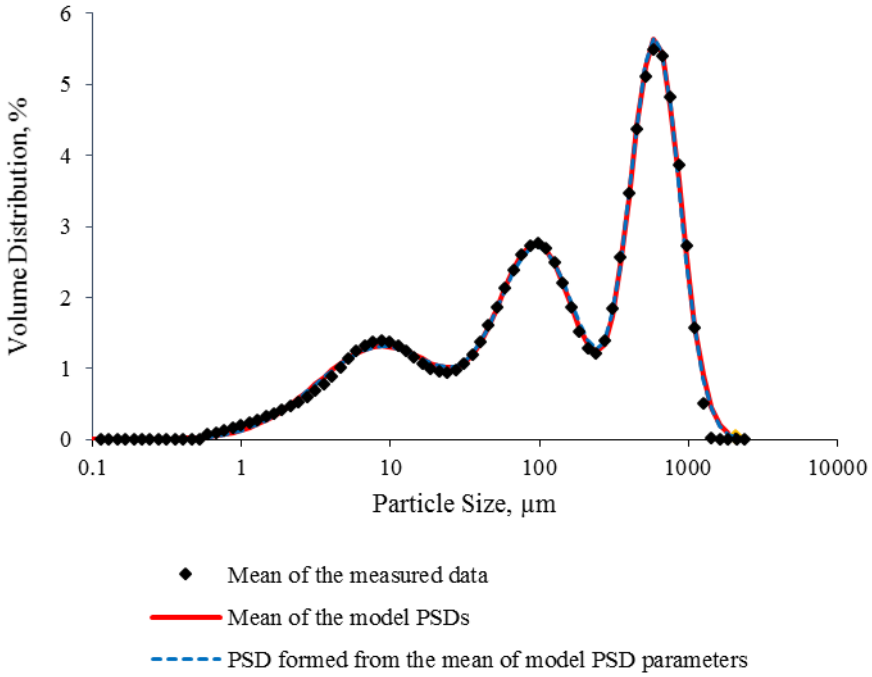


Figure 3.6: Mean particle size distribution of four batches of pastes with the same formulation, each measured three times, compared with the mean model PSD computed in two ways: 1) each paste is modelled and the mean of the volume distribution within each sieve size is plotted and 2) the mean is taken of each PSD model parameter used to describe each run and then a PSD is reconstructed.

3.3.3 FT4 powder rheometer

The FT4 rheometer (Freeman Technology, UK) is the fourth generation of a technique designed to characterise the flow of dry powders. The sample was loaded into a 200 ml cylindrical container and a conditioning step was first run; the 25 mm helical blade rotated and moved downwards into the sample which was designed to re-distribute the particles so packing of the solids was even over the whole sample. The test phase was then run as the blade moved back up through the sample at a tip speed of 40 mm s^{-1}. Three repeats were

carried out on each sample. The force and torque on the blade were continually recorded and were converted into total flow energy.

3.3.4 Parallel plate rheology

Rheological properties of fluids and suspensions were characterised using the Discovery HR-2 Rheometer (TA Instruments, USA). A 40 mm parallel plate was used for all the measurements. Model chocolate pastes, suspensions of skimmed milk powder and a CMC solution were measured with gap sizes of 1700 µm, 700 µm and 750 µm, respectively. Steady shear tests were run at 21°C between shear rates of 0.1 – 1000 s^{-1}. Strain sweeps were carried out between 0.001 – 100 % at a frequency of 10 rad s^{-1}. Frequency sweeps were carried out between 0.1 – 100 rad s^{-1} at a strain of 0.005 %. For each test condition, three repeats were carried out, each on a different sample of the same material. The shear stresses of pastes and suspensions have been modelled using both the power law and the Herschel-Bulkley rheological models, equations 4.7 and 4.8 respectively.

3.3.5 Vane rheology

The Discovery HR-2 Rheometer (TA Instruments, USA) was also used to run tests using a 28 mm diameter, 4-vaned probe contained within a 40 mm diameter cup. Steady shear tests were run between shear rates of 0.1 – 100 s^{-1} at 21°C. Strain sweeps were carried out between 0.001 – 1000 % at a frequency of 10 rad s^{-1}. Frequency sweeps were carried out between 0.1 – 100 rad s^{-1} at a strain of 0.01 %. Five measurements were done for each sample of paste and between each measurement the vane was removed, the sample was stirred and then the vane repositioned; submerged within the sample.

3.3.6 Simplified back extrusion technique

Samples reported on within this document have been tested using two versions of the back extrusion technique (BET). A simplified method was firstly used to test samples produced during trial 1 using the TA.XT plus Texture Analyser (Stable Micro Systems, UK). The results of these are discussed within sections 6.2 and 7.2. All the samples were reheated to 40°C before testing and gently stirred to counteract the effect of particle settling. The pastes were each contained within a 45 mm diameter plastic vessel with a fluid height of 40 mm. A 25 mm diameter steel probe was attached to a Texture Analyser (Stable Micro Systems, UK) and was lowered to 20 mm above the sample. Once the test program was started, it directed the probe to move downwards until a force of 1 g was first measured. This indicated that the probe had reached the surface of the test fluid. The force was then recorded as the probe moved 20 mm into the sample at a constant speed. Two speeds were used: 2 mm s^{-1} and 4 mm s^{-1} which produced two different shear rates at the wall. The probe was then held at the maximum plunged distance for 20 seconds whilst the force continued to be recorded.

After the hold time the probe was retracted out of the sample. Each sample was remixed and the probe was wiped clean. The sample was tested six times at each of the two speeds.

3.3.7 Finalised back extrusion technique

The results presented in chapter 0 describe an investigation into the fundamentals of this technique and the developments that have been made in order to establish a final back extrusion technique using a Universal Mechanical Tester (Zwick Roell, Switzerland). This final method has then been used to test samples of paste produced in Trial 2, the results of which are discussed in section 6.3.

A cylindrical, acrylic vessel with a 90 mm inside diameter (height = 200 mm) was filled with the test material. The cross head moved a 30 mm diameter, cylindrical, aluminium probe so that it is positioned at the surface of the sample (probes with 20, 25 and 35 mm diameters were also trialled within chapter 0). After zeroing the force on the probe, the probe was moved 50 mm downwards at a constant speed whilst the resistive force was measured. A gap of over 50 mm was maintained beneath the probe once it was fully submerged in order to avoid any end effects. Four different speeds were used: 4 mm s^{-1}, 8 mm s^{-1}, 16 mm s^{-1} and 30 mm s^{-1}, producing results at four different shear rates.

Once the probe had moved 50 mm, the probe was held stationary and the force was recorded for a further 60 seconds. The probe was then removed from the sample and wiped clean. The sample was gently recombined using a spatula to reduce any effects of particle settling and to remove any remaining indentation within the material remaining from the probe. Three repeats were done on the same material at each of the four speeds. From the values of force over the test duration, the rheological model parameters were determined. The complete method for achieving this is described in section 5.3 and the code that has been used to process the raw data in MATLAB can be found in APPENDIX 1.

For any given sample, a value of the flow behaviour index is calculated using the raw data from four test velocities, each velocity was tested three times. Section 5.3.1 details how these 12 results are used to establish the flow behaviour index. Based on this average value of flow behaviour index, each experimental run is then independently used to calculate the consistency coefficient and yield stress (if using a Herschel-Bulkley model). The values of consistency coefficient and yield stress which are quoted throughout the results sections are the mean values for all 12 runs. In chapter 5, when individual values of the shear stress and shear rate are plotted, the shear stresses are calculated using the mean values of the

consistency coefficient and yield stress, plus the flow behaviour index. The shear rates are the mean values of shear rate at the wall at each test velocity.

3.3.8 Density

Densities of liquids and pastes were calculated by measuring the weight of a sample of known volume. Five repeats were carried out during each measurement and a mean value was taken.

The densities of solids were taken from the literature in order to approximate the volume content of the suspensions formulated for this research.

3.3.9 X-Ray computer tomography

X-Ray computer tomography (XRCT) is a non-destructive technique used to scan and produce 3D images of the structure within a sample. Two samples of chocolate paste was tested using a SkyScan1272 High resolution Micro-CT system (Bruker, USA). The sample was loaded into a short section of plastic straw with a diameter of 4.3 mm which was mounted on a plasticine ball and centered in front of the scanner. A scan was run using an applied voltage of 35 kV and source current of 100 μA. Five hundred images were taken whilst the sample was rotated so that a 3D image of the sample could be established.

The components of the pastes all have relatively similar densities and therefore it was difficult to distinguish between the components. The milk powder particles are much smaller than the granulated sugar particles which results in a lack of definition of the small particles. An example of the result is shown in Figure 3.7.

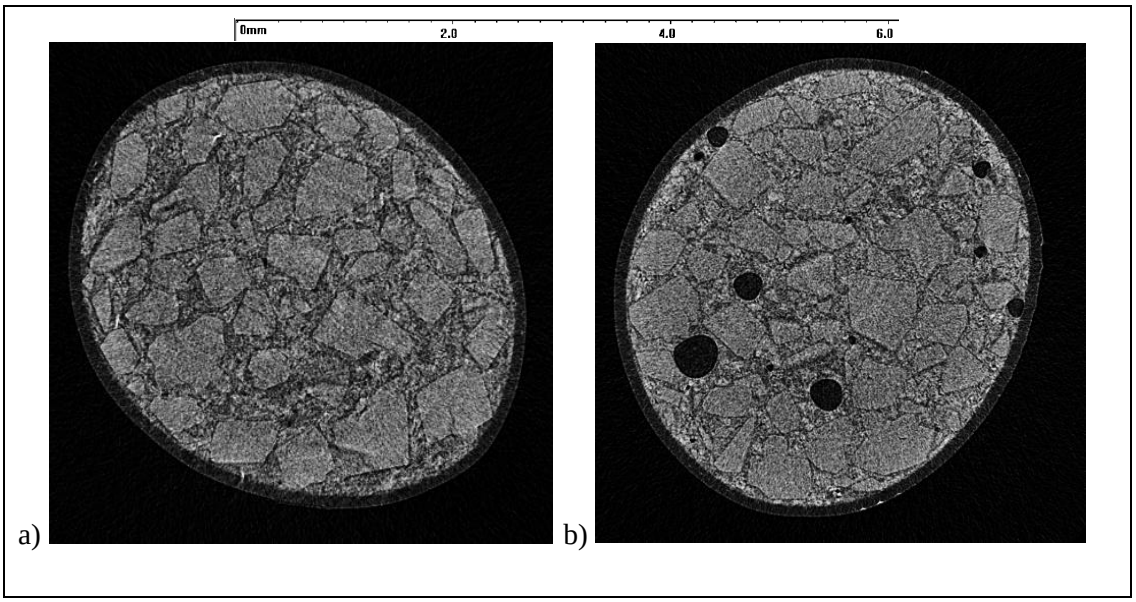


Figure 3.7: XRCT of two model pastes containing sugar, skimmed milk powder, cocoa powder and vegetable oil a) MCP1 and b) MCP2 (see Table 4.1 for formulations). Samples are encased in a circular straw section. Darkest areas are low density (air pockets), lighter areas have higher densities. Large sugar particles can easily be distinguished however the mixture of oil, milk powder and cocoa is too difficult to differentiate.

3.4 Methods: Statistical Analysis

JMP 12 (SAS, UK) was used to design two sets of experiments, one full factorial design and one response surface design, in order to investigate the effect that multiple factors have on the paste consistency and downstream processes. Details of both these designs are described within chapter 6.

3.4.1 Predictive models

To identify factors which have a statistically significant effect on the paste consistency or downstream processes, the fit model platform was utilized in JMP 12 (SAS, UK) to perform an ANOVA. This fitted general linear models of the factors (variables) to each response (measurements) using multiple linear regression. The factors or interactions of factors that had a significant effect on each response were then identified; a 95% confidence interval was used, therefore significant effects are indicated by p-values < 0.05.

When statistical differences between samples at different conditions are stated within the results sections, these have been identified using a Tukey's honestly significant difference test (HSD). This compares the differences between the means of the values produced using the predictive model, rather than comparing pairs of values, as is done within a t-test.

3.4.2 Principal component analysis

As there are many responses that are measured during the production of chocolate paste and during the processing of it downstream, it is desirable to identify responses which show similar trends. Rather than relying on linear x-y plots, principal component analysis (PCA) can be used to identify relationships between multiple measured responses.

For *n* responses, standardised so that they are equally weighted, PCA transforms the data to generate new dimensions, known as principal components, which represent the variability within the data sets. There are *n-1* principal components (PCs), each orthogonal to each other. The first principal component represents the largest amount of variability between the responses and they continue to be ranked in order of their variation. It is common to examine those principal components which represent at least 80% of the variation within the data.

Loading plots are used to represent the spread of data; the correlations between the responses and two principal components are plotted on an x-y graph. This highlights clusters of responses which vary similarly whilst responses within opposite corners may highlight a negative correlation. These results can be related to the factors, or interactions between factors, to draw conclusions about multiple sets of data.

3.5 Materials

To develop a test method capable of measuring chocolate pastes, experiments were initially performed on simple fluids before increasing the complexity of the fluids. A carboxy(methyl)

cellulose (CMC) solution, bought as powder, (Sigma Aldrich, USA) was formulated in small batches (< 2 l) by gradually adding powdered CMC to distilled water whilst continuously stirring. This was intended to have non-Newtonian properties without containing particles that would affect the rheological measurements (Benchabane and Karim, 2008).

Several suspensions were formulated of skimmed milk powder, granulated sugar and icing sugar particles within continuous phases of vegetable oil. Combinations of different solids were also formulated within a matrix of oil, containing skimmed milk powder, granulated sugar and cocoa powder, in order to recreate the consistency of chocolate pastes which could be tested at room temperature.

Once the back extrusion technique had been developed, it was adapted, incorporating a heating jacket. This enabled chocolate pastes to be tested containing fat that is solid at room temperature. These contained skimmed milk powder (SMP), sweet whey powder (SWP), granulated sugar, cocoa butter, cocoa liquor, anhydrous milk fat (AMF), lecithin and vanillin. All of these suspensions were manufactured by hand in small batches (< 1 kg) until visibly homogeneous. The physical properties of all these components are shown in Table 3.4 and Table 3.5.

Pastes that were manufactured on a pilot plant scale were based on a generalised powder chocolate recipe. The average recipes of the pastes used in trial 1 and 2 are shown in Table 3.6. The ratios between the solid components was maintained for each paste but the fat content and lecithin content were varied at different trial conditions (ratios of fat discussed in sections 6.2 and 6.3). Recipes were simplified for experimental ease during trial 2; skimmed milk powder replaced the sweet whey powder and additional cocoa butter was used in place of the anhydrous milk fat.

Table 3.4: Physical properties of the solids from commercial suppliers.

POWDER	SMP	SWP	Granulated Sugar	Icing Sugar	Cocoa Powder
Particle Size (d_{10}), µm	18.34 [a]	45.7 [a]	352.8 [a]	-	-
Particle Size (d_{90}), µm	145.5 [a]	316.2 [a]	794.8 [a]	20.00 [b]	45 [b]
Fat, %	0.60 [b]	0.90 [b]	-	-	11 [b]
Protein, %	33.19 [b]	11.08 [b]	-	-	-
Moisture, %	3.76 [b]	1.70 [b]	-	0.05	4.5 [b]
Bulk Density, g/cm^3	0.70 [b]	0.55 [b]	1.59 [b]	0.65 [b]	0.56 [b]

a: Measured using techniques discussed in section 3.3.2
b: Taken from Certificate of Analysis from Mondelēz International

Table 3.5: Physical properties of the liquids from commercial suppliers.

LIQUID	Vegetable Oil	Cocoa Butter	Cocoa Liquor	Lecithin	AMF
Viscosity, mPa.s (at 40°C, unless stated)	69.2 (@ 21°C)	50.9	$5518\dot{\gamma}^{0.854}$	12500 (@ 21°C)	31
Melting Point, °C	-17	36.4[a]	36.4[b]	-	34
Density, g/cm^3	0.92	0.86	1.06	-	0.906
Particle Size (d_{10}), µm	n/a	n/a	2.51	n/a	n/a
Particle Size (d_{90}), µm	n/a	n/a	22.6	n/a	n/a
Moisture, %	0	0.1	0.66	-	0.06
Fat, %	100.00	99.9	55.10	-	99.94

a: There are six polymorphic forms within the cocoa butter. All of them should be melted at the temperature stated here.
b: Continuous phase is cocoa butter which is not affected by solid contents

Table 3.6: Average formulations of the chocolate pastes manufactured during two pilot plant trials

	Trial 1 vol %	Trial 2 vol %
Dairy products	29.2	21.9
Cocoa products	30.4	38.0
Granulated Sugar	40.3	40.0
Lecithin	0.1	0.1
Total Solids	67.6	67.6

4 METHODS TRIALLED TO CHARACTERISE PASTES

4.1 Introduction

It is known anecdotally that the paste consistency impacts the performance of the manufacturing process; it will change the coverage of material on the refiner rolls and subsequently affects the particle size of the chocolate. After the ingredients arrive on site, the first point where the product is currently measured is after the 5-roll refiner. Experienced operators are able to manipulate the settings of the refiner, either in response to the way the paste looks and feels or based on the appearance of roll coverage on the 5-roll refiners. If the paste consistency could be quantified, it would be possible to measure how variable the paste is. Then data can be examined to understand the relationship between paste consistency and the performance of downstream processes.

This chapter discusses the techniques which were trialled for their applicability of quantifying the paste consistency. As the paste displays fluid properties, it was hoped to be able to determine the rheological properties of the material rather than relying on empirical methods that are limited to identifying differences between pastes.

As discussed in Chapter 0, pastes commonly display shear thinning behaviour. A suitable rheological model used to incorporate shear thinning behaviour would be the power law model (equation 4.7). The pastes may also have a yield stress and therefore this rheological behaviour can be described by a Herschel-Bulkley model (equation 4.8).

If the yield stress, shear thinning behaviour and apparent viscosity can be separated then one of these components may have a strong relationship with the performance of downstream

processes. It would then be desirable for future work to focus on measuring this one rheological property using a simplified online or near-line technique.

$$\sigma_{PL} = K\dot{\gamma}^n \quad (4.7)$$

$$\sigma_{HB} = \sigma_y + K\dot{\gamma}^n \quad (4.8)$$

where σ_{PL} and σ_{HB} are the shear stresses using the power law and Herschel-Bulkley models, respectively, K is the consistency coefficient, $\dot{\gamma}$ is the shear rate, n is the flow behaviour index and σ_y is the yield stress.

If the yield stress, shear thinning behaviour and apparent viscosity can be separated then one of these components may have a strong relationship with the performance of downstream processes. It would then be desirable for future work to focus on measuring this one rheological property using a simplified online or near-line technique.

During the development of a new characterisation technique, it was not practical to adapt each technique so that the cocoa butter was fully liquid by maintaining a temperature above 37°C. For the results described in this chapter, model chocolate pastes were formulated from granulated sugar, SMP, cocoa powder and vegetable oil to the ratios listed in Table 4.1. On an industrial scale, 6% differences in liquid volume content would have a huge impact on how the chocolate paste would be processed, so it was hoped that these formulations would produce very clear differences.

Table 4.1: Formulations of model chocolate pastes (MCP). Ratios of solid components are maintained.

	MCP1	MCP2	MCP3
Oil, vol%	35.8	30.0	24.0
Cocoa Powder, vol%	10.4	11.3	12.3
SMP, vol%	16.4	17.9	19.4
Sugar, vol%	37.4	40.8	44.4

Many techniques were identified in Chapter 0 that may be able to quantify consistency and measure the rheological properties of chocolate pastes. From preliminary assessments, some techniques, discussed in Table 4.2, were not suitable for the paste formulations and no further testing was done. This chapter will further discuss the successes and challenges of the remaining techniques, summarised in Table 4.3.

Table 4.2: Details of the techniques which were not capable of measuring the rheological properties of chocolate pastes and were not used past preliminary testing

Technique	Result from preliminary tests
Capillary Rheometer	Severe phase separation: large proportion of the fat extruded initially and the solids remaining jammed the geometry
Cone Penetrometer	Cone sank as material too wet Large degree of error from repeated tests
Vane Penetrometer	Manual operation caused large variability between results
Slump Test	Materials too wet to form initial slump Materials spread too much on stage
Bostwick	Loading technique is not accurate enough to give repeatable results

Table 4.3: Techniques which were able to measure some elements of the paste

Technique	Result from trials
Parallel Plate	Material failed above 20 s^{-1} in a shear ramp test
Rheology	Oscillation test could better measure rheology
- **Shear Ramp**	Oscillation test was unsuccessful for concentrated suspensions
- **Oscillation**	Large degree of error from repeated tests
Vane Rheology	Oscillation test was unsuccessful for concentrated suspensions
- **Shear Ramp**	Large degree of error from repeated tests
- **Oscillation**	Only small differences between pastes identified
FT4	Very good repeatability Disadvantage: not measuring rheology
Current Measurements	Good repeatability Advantage: Online technique Disadvantage: not measuring rheology

4.2 Parallel plate rheology

4.2.1 Steady shear tests

The results of shear ramp tests are shown in Figure 4.1 for the three model chocolate pastes. The plots of viscosity for all three formulations decreased with increasing shear rate, indicating shear thinning behaviour.

All three samples reached a peak shear stress, at which point the shear stress began to decrease. This was named the failure point. This same point was identified from the viscosity versus shear stress plots at the point where the viscosity suddenly diverged from the linear trend. These values of peak shear stress correlated with observations of instabilities forming at the outer edge of the sample and the sample leaving the gap. For polymers and suspensions, there is expected to be a critical shear rate where the edge of sample will begin to distort. A fracture is then likely to form which will spread into the sample and cause loss of some of the sample from between the gap (Jomha and Reynolds, 1993, Keentok and Xue, 1999). Literature has also shown that when suspensions of large particles are tested in parallel plate rheometers, centrifugal forces result in particles moving towards to outer edges of the sample

(Krishnan et al., 2006, Deshpande and Shapley, 2010, Shauly et al., 1998). Results in Figure 4.2 indicated that there is a linear relationship between the solids content of the pastes and the shear rate at which the materials failed. When there was a higher concentration of solids, the shear rate at which failure occurred at is lower.

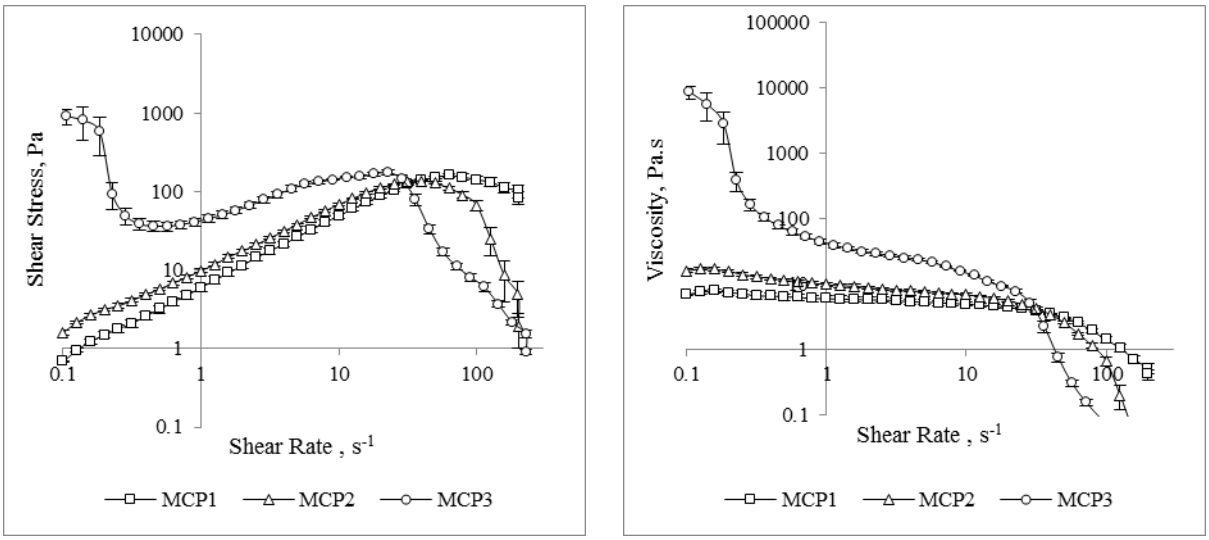


Figure 4.1: Shear sweep tests of three model chocolate paste formulations tested on a 40mm parallel plate rheometer. Error bars represent the standard error.

Prior to the point of failure, pastes with a higher solids content were measured to have higher values of shear stresses and viscosities. The differences in shear stress and viscosity did not follow a linear relationship with the solids content; MCP1 and MCP2 were much closer than MCP3, despite equivalent differences in the fat content.

At low shear rates, MCP3 showed a different initial response; the shear stress was initially much higher for the first few measurements before dropping sharply. This may indicate the presence of a yield stress; a common physical property found in suspensions when the solids content is close to the maximum packing fraction (Mueller et al., 2009).

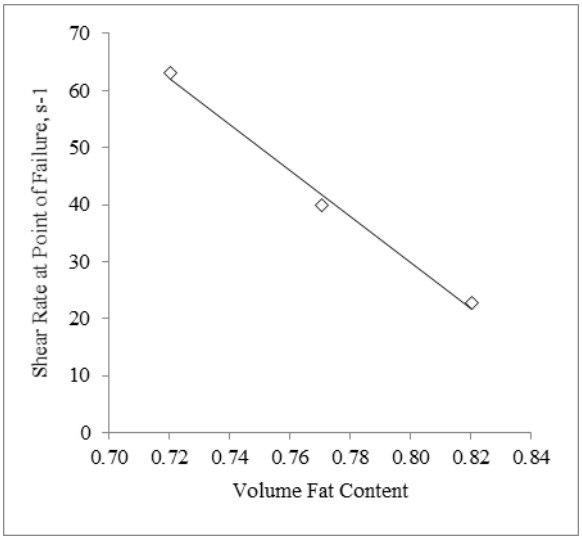


Figure 4.2: Failure points of the three chocolate paste formulations during the parallel plate shear sweep tests, $R^2 = 0.9923$

4.2.2 Oscillatory shear tests

Dynamic oscillatory measurements were carried out on materials in order to establish their viscoelastic behaviour. These tests were intended to help maintain the structure of the sample and reduce the likelihood of edge instabilities which were observed at high shear rates (Choi et al., 2016) although there have also been studies which find that radial migration of particles can be higher within oscillatory shear tests than at steady shear (Deshpande and Shapley, 2010).

Using a parallel plate geometry, stress was applied sinusoidally and the strain response of the material was measured by the rheometer. The relationship between the phase angle of the applied stress, τ, and the measured strain, γ, indicated the viscoelastic properties of the fluid (equation 4.1 and 4.2). If the phase angle, δ, = 0 ° then the response is purely elastic and the material is behaving as a Hookean solid. If $\delta = 90$ ° then the response is purely viscous (Newtonian). Generally, materials are between these two extremes, displaying both elastic and viscous behaviour (viscoelasticity) (TA.Instruments).

$$\tau = \tau_0 \cos(\omega t) \quad (4.1)$$

$$\varepsilon = \varepsilon_0 \cos(\omega t - \delta) \quad (4.2)$$

where τ_0 is the stress amplitude and ε_0 is the strain amplitude, ω is the angular frequency and δ is the phase angle.

The complex modulus, G^*, is a measure of the overall resistance to deformation (equation 4.3). This is a function of the storage (elastic) modulus, G', and the loss (viscous) modulus, G'', calculated using equations 4.4 and 4.5, respectively.

$$G^* = G' + i \cdot G'' = \sqrt{\left(G'^2 + G''^2\right)} = \frac{\tau_0}{\varepsilon_0} \quad (4.3)$$

$$G' = \left(\frac{\tau_0}{\varepsilon_0}\right) \cos\delta \quad (4.4)$$

$$G'' = \left(\frac{\tau_0}{\varepsilon_0}\right) \sin\delta \quad (4.5)$$

First, the linear visco-elastic region (LVR) must be identified from a strain sweep. This is the region where G' and G'' remain independent of the amplitude at a constant frequency. An example of this can be observed below 0.05 % strain in Figure 4.3; particularly G'' remained constant over a range of amplitudes. In this region $G' > G''$, indicating that at low strain rates, the material had a solid-like response. Materials with these properties would make start-up of moving plant equipment, i.e. pumps, more difficult. Frequency sweeps were then run between 0.1 – 100 rad s^{-1}, whilst the strain was 0.05 %. Similarly to the LVR within the strain sweeps, the frequency sweep on the MCP3 sample shows that $G' > G''$ over the entire range of frequencies tested (Figure 4.4). The moduli were fairly independent of the frequency and several studies have shown that if G' is independent of frequency, a yield stress will be present in steady shear flow (Choi et al., 2016).

The strain sweep of MCP2, Figure 4.5, indicated that the LVR may be below 0.005 % strain rate, however there was a large amount of variation between the three repeats that were run. This may have been instrument noise due to being close to the sensitivity limit of the rheometer at such low strain rates. From Figure 4.7, an LVR was not clearly identifiable from the strain sweep of MCP1. For both MCP2 and MCP1, $G'' > G'$, indicating fluid-like behaviour at all strain rates. Overall, the values of the moduli were much lower than for MCP3 which contained the least amount of fat. This might indicate that MCP3, which has a solids content of 76 %, was close to the maximum packing fraction within the paste. For completeness, frequency tests were run on MCP1 and MCP2 at the same conditions as for MCP3, as their LVRs could not be determined. MCP2 and MCP1 showed different responses to MCP3; both moduli were dependent on the frequency, indicating more fluid-like behaviour (TA.Instruments). At low frequency, $G' > G''$ which indicated that the response to deformation is dominated by elasticity. At higher frequencies, there was a crossover point which resulted in $G'' > G'$ and suggested that viscous behaviour dominated. The crossover point for MCP1 was higher than the crossover point for MCP2 (≈ 10 rad s^{-1} and ≈ 2.5 rad s^{-1}, respectively). This did not agree with the expectation that as MCP1 has a lower solids content, it should have more fluid-like properties; this result may have been a consequence of the strain rate not being within the LVR for these two samples or this may not have been a reliable measure of the suspension behaviour.

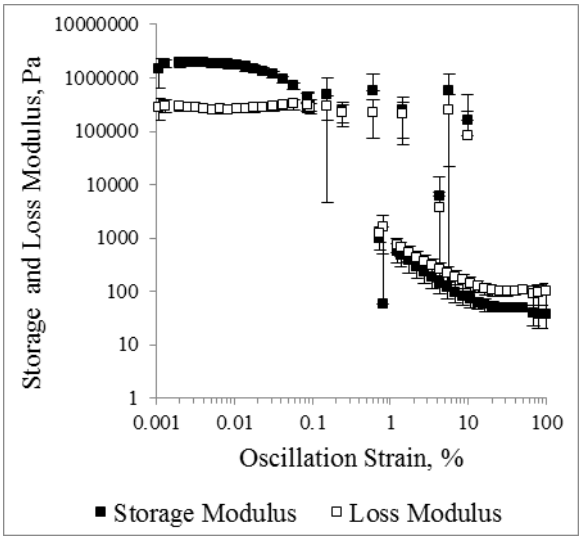


Figure 4.3: Storage and loss moduli from a strain sweep of MCP3 using a parallel plate geometry. Frequency is 10 rad s^{-1}.

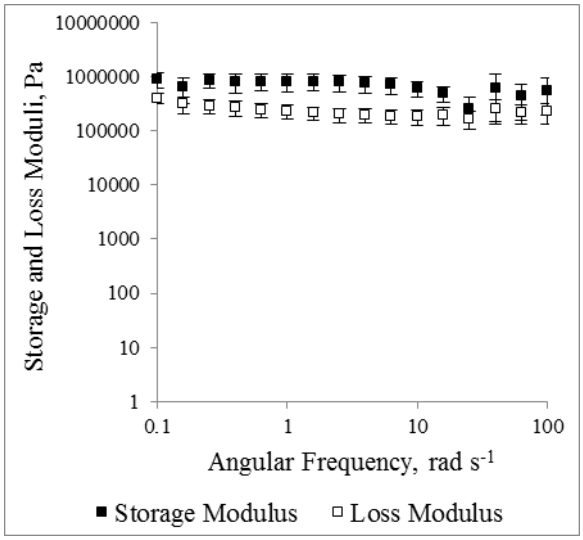


Figure 4.4: Storage and loss moduli from a frequency sweep of MCP3 using a parallel plate geometry. Strain is 0.005 %.

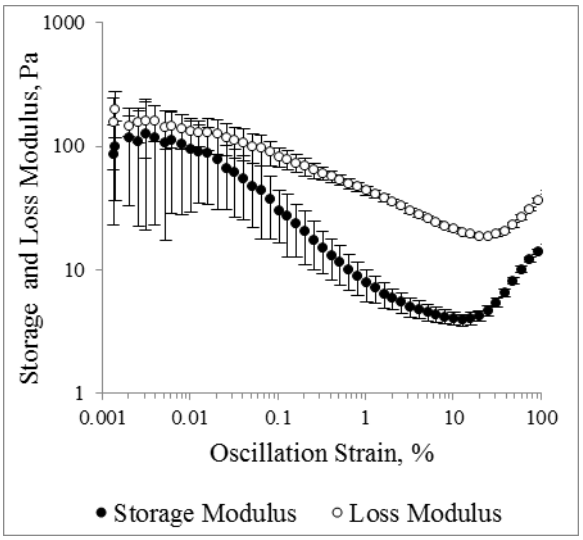


Figure 4.5: Storage and loss moduli from a strain sweep of MCP2 using a parallel plate geometry. Frequency is 10 rad s^{-1}.

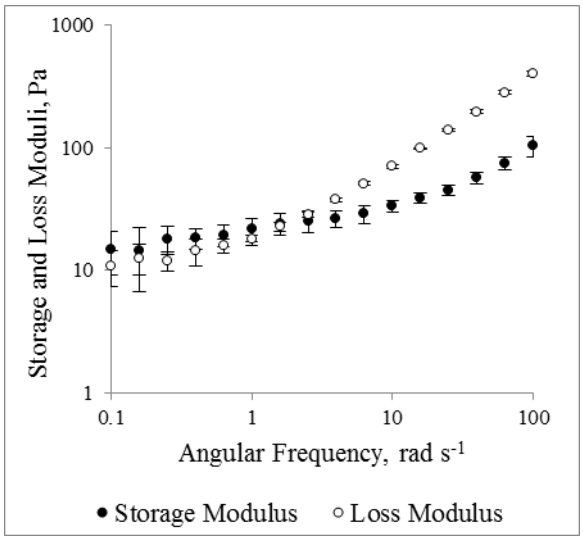


Figure 4.6: Storage and loss moduli from a frequency sweep of MCP2 using a parallel plate geometry. Strain is 0.005 %.

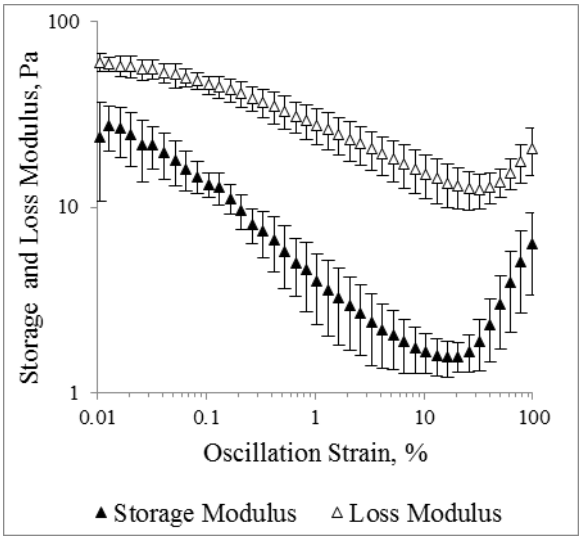


Figure 4.7: Storage and loss moduli from a strain sweep of MCP1 using a parallel plate geometry. Frequency is 10 rad s^{-1}.

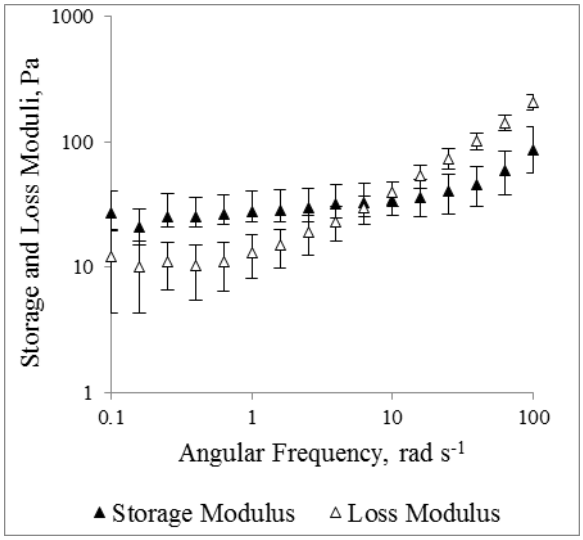


Figure 4.8: Storage and loss moduli from a frequency sweep of MCP1 using a parallel plate geometry. Strain is 0.005 %.

Sixty years ago, an empirical relationship was established to relate the results of oscillation tests to the shear rate dependence on shear viscosities (Cox and Merz, 1958). Plots of the complex viscosity (equation 4.6) at a range of angular frequencies from the oscillatory shear tests are considered to be comparable to plots of the viscosity against shear rate from steady shear tests. Many studies have confirmed that this similarity is seen for polymers however the literature suggests that this does not hold true for suspensions of particles containing more than 30 vol% solids (Winter, 2008, Gleissle and Hochstein, 2003, Nguyen et al., 2013). In order to establish whether any knowledge can be gained through use of this Cox-Merz rule, the complex viscosities were calculated using equation 4.6.

$$\eta^* = \frac{G^*}{\omega} \qquad (4.6)$$

From Figure 4.9 and Figure 4.10, it is possible to see that the complex viscosities of MCP1 and MCP2 showed higher values than the steady shear viscosities below 10 rad/s (equivalent to 10 s^{-1}). These were similar to results measured by Nguyen et al. (2013) of epoxy resins

containing 45 vol% polymer spheres that found that the Cox-Merz rule resulted in higher complex viscosities than the steady shear viscosities.

Figure 4.11 indicates that the complex viscosity calculated for MCP3 was dramatically higher than the viscosity from steady shear tests. This result agrees with the results seen in literature, previously discussed, highlighting that viscosities of these solid suspensions were not able to be approximated using the Cox-Merz rule.

Corrections to the Cox-Merz rule have been developed in several studies however they only involve suspensions of particles below 30 µm where hydrodynamic forces dominate and particle-particle interactions do not affect the rheology (Gleissle and Hochstein, 2003, Doraiswamy et al., 1991, Sumita and Manga, 2008). The very high complex viscosity of MCP3 may have been due to much more frequent particle-particle interactions which occurred due to being close to the maximum packing fraction.

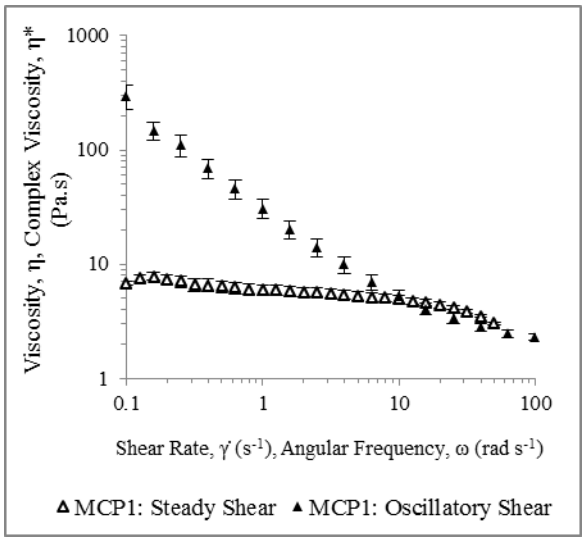


Figure 4.9: Viscosity and complex viscosity of MCP1 calculated from linear shear and oscillation tests, respectively, on a 40 mm parallel plate.

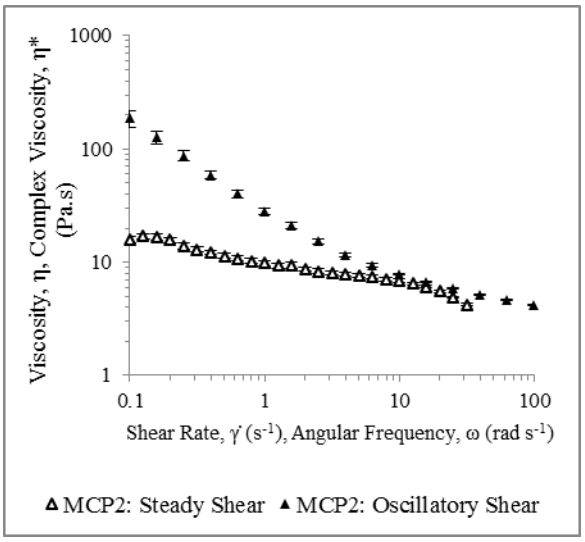


Figure 4.10: Viscosity and complex viscosity of MCP2 calculated from linear shear and oscillation tests, respectively, on a 40 mm parallel plate.

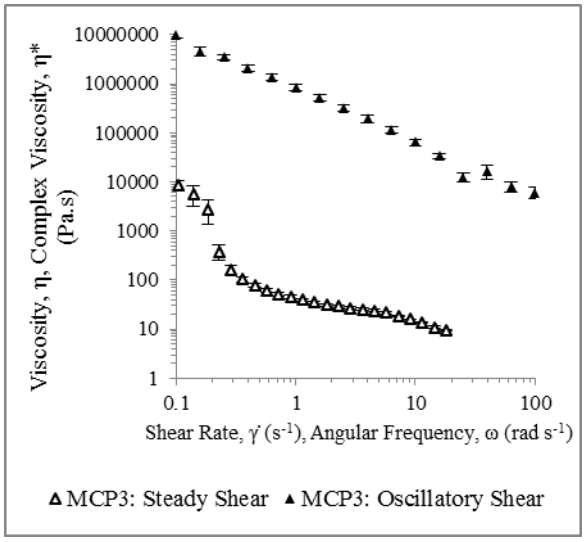


Figure 4.11: Viscosity and complex viscosity of MCP3 calculated from linear shear and oscillation tests, respectively, on a 40 mm parallel plate.

Table 4.4: Herschel-Bulkley model parameters describing the three model chocolate paste formulations measured using 40mm parallel plate

	Steady Shear (before failure of the samples)			**Oscillatory Shear**		
	Yield Stress, Pa	**Consistency Coefficient, Pa.s**	**Flow Behaviour index**	**Yield Stress, Pa**	**Consistency Coefficient, Pa.s**	**Flow Behaviour index**
MCP1	-6.79	14.21	0.62	27.36	2.97	0.91
MCP2	-8.06	20.40	0.56	18.55	9.14	0.82
MCP3	-19.63	71.87	0.34	-1.46E+08	1.46E+08	-4.20E-04

4.3 Vane Rheology

Vane rheometry has been used as a technique to measure the rheological properties of many different pastes, ranging from fruit pulps to concrete, as has been discussed within Chapter 0. Very little of the work that has been published involves suspensions of solids which are as large or as concentrated as chocolate paste. Tests were carried out using the geometry and method described in section 3.3.5, creating a 6 mm gap between the vane blades and the vessel.

4.3.1 Steady shear tests

The shear stress and viscosity measurements of the three model chocolate pastes (Figure 4.12) showed curvature at both low shear rates and as the shear rate approached 100 s^{-1}. This makes it challenging for a Herschel-Bulkley model to be fit to each of the curves. To best fit the overall trend of the data, it was only possible to include the results between 0.06 – 10 s^{-1}. The shear stresses and viscosities of MCP3 also showed some curvature around 1 s^{-1}.

As the liquid content was increased, the viscosity of the pastes decreased. Results for all three formulations, like the parallel plate results, suggested that the pastes shear thin. It was also observed that as the probe began to move, the entire body of fluid rotated at what appeared to be a similar speed to the vane rotation. The sugar particles, which make up approximately half of the solids content, were only 6 times smaller than the gap. These would be likely to jam together, causing slip and not allowing a velocity profile to develop across the width of the gap.

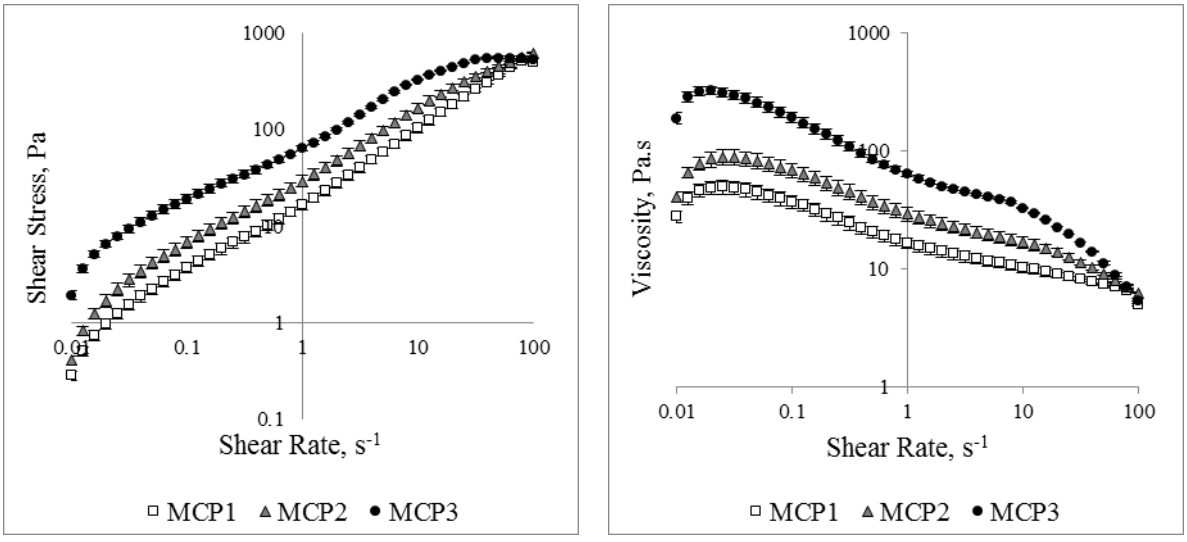


Figure 4.12: Results of shear ramp tests using a vane rheometer to measure the three model chocolate pastes

Hysteresis tests were also run to understand whether the viscosity of the pastes was affected by the structure breakdown. During all of the tests (including the steady shear tests), air was

observed to be drawn down behind each of the blades. This led to material overflowing out of the geometry during the ramp up of the shear rate, hence the same quantity of material was not tested as the shear rate decreases.

4.3.2 Oscillatory shear tests

Dynamic oscillation tests can also be carried out using the vane in cup geometry in order to maintain some of the structure and attempt to prevent the material from leaving the geometry. Stress was first applied sinusoidally whilst the frequency remained at 10 rad s^{-1}. The same equations for calculating the storage and loss moduli are valid, as in section 4.2.2. Both the storage and loss moduli of MCP1 were independent of the strain below 0.1 % (Figure 4.13). This LVR was much larger than was measured using the parallel plates. For both MCP2 and MCP3, the LVR was below 0.01 % (Figure 4.15 and Figure 4.16, respectively).

Within the LVR, G'' > G' for all three formulations indicating that they were displaying fluid-like behaviour. This differs from the parallel plates results which measured G' > G'' for MCP3. This parallel plate result measured very high values of the moduli (G' and G'' $\approx 10^6$ Pa) whereas these results from the vane rheometer were more reasonable (G' and G'' $\approx 10^3$ Pa).

Frequency sweeps were run between 0.1 – 100 rad/s, maintaining the strain at 0.01 %. Similarly to the parallel plate results, both MCP1 and MCP2 showed an increase of G' and G'' when ω increased whereas MCP3 appeared to be less dependent on the frequency. For all three formulations, G'' > G' indicating that all three showed more fluid like behaviour.

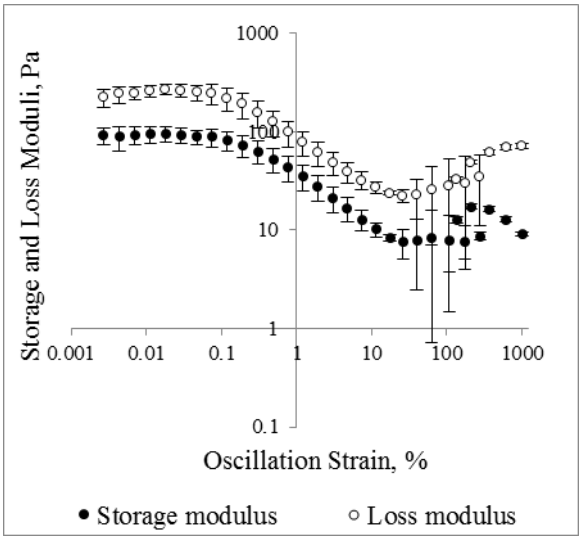


Figure 4.13: Storage and loss moduli from a strain sweep of MCP1 using a vane in cup geometry. Frequency is 10 rad s^{-1}.

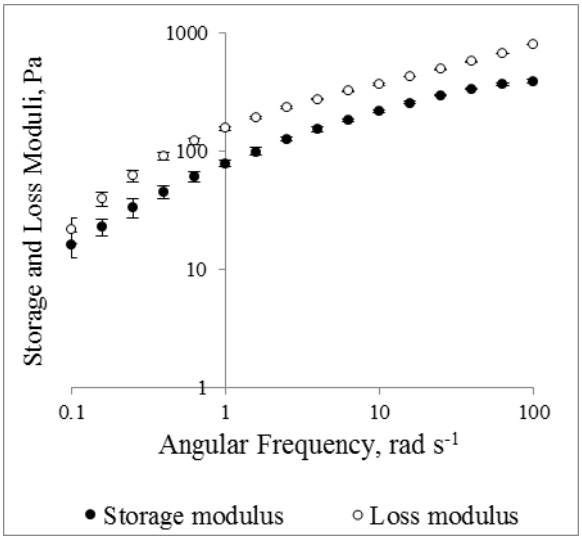


Figure 4.14: Storage and loss moduli from a frequency sweep of MCP1 using a vane in cup geometry

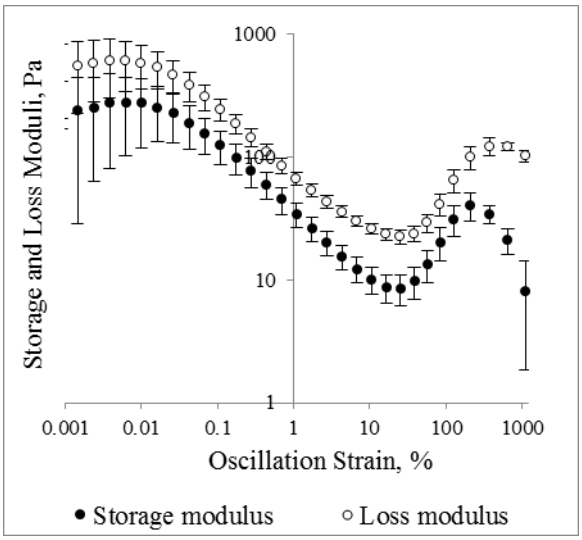


Figure 4.15: Storage and loss moduli from a strain sweep of MCP2 using a vane in cup geometry. Frequency is 10 rad s^{-1}.

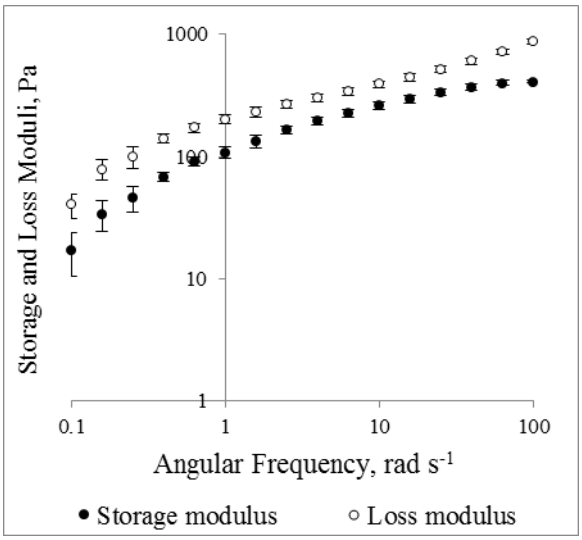


Figure 4.16: Storage and loss moduli from a frequency sweep of MCP2 using a vane in cup geometry

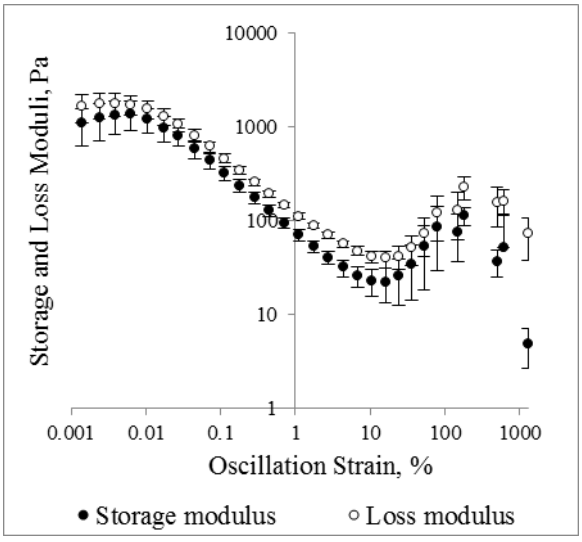


Figure 4.17: Storage and loss moduli from a strain sweep of MCP2 using a vane in cup geometry. Frequency is 10 rad s^{-1}.

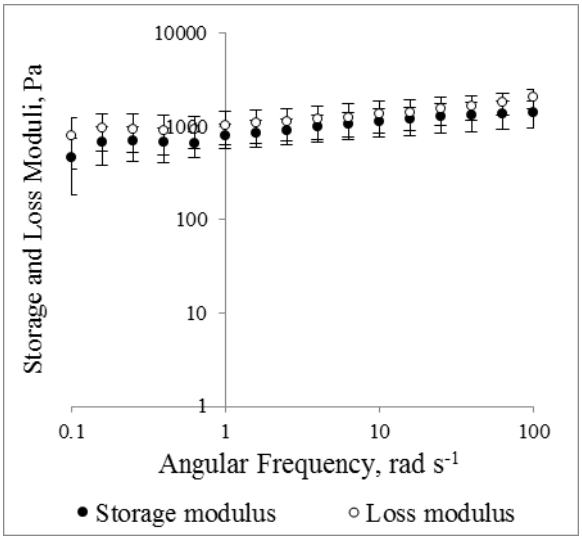


Figure 4.18: Storage and loss moduli from a frequency sweep of MCP3 using a vane in cup geometry

Although the Cox-Merz rule does not hold for these concentrated suspensions where particle-particle interactions have a significant effect on the viscosity, it was used in order to compare the oscillation and steady shear results. Figure 4.19, Figure 4.20 and Figure 4.21 show comparisons of the steady shear and oscillation shear tests using the vane rheometer. Both techniques measured shear thinning behaviour, however the values of complex viscosity, similarly to results using the parallel plate geometry, were consistently higher than the steady shear viscosity.

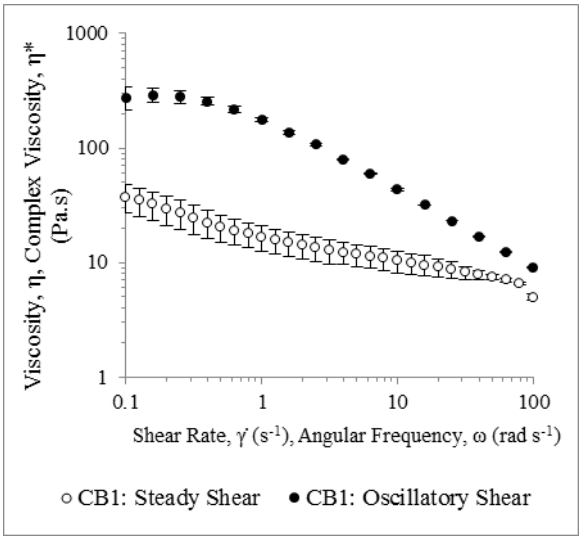


Figure 4.19: Viscosity and complex viscosity of MCP1 calculated from linear shear and oscillation tests, respectively, using a vane in cup geometry

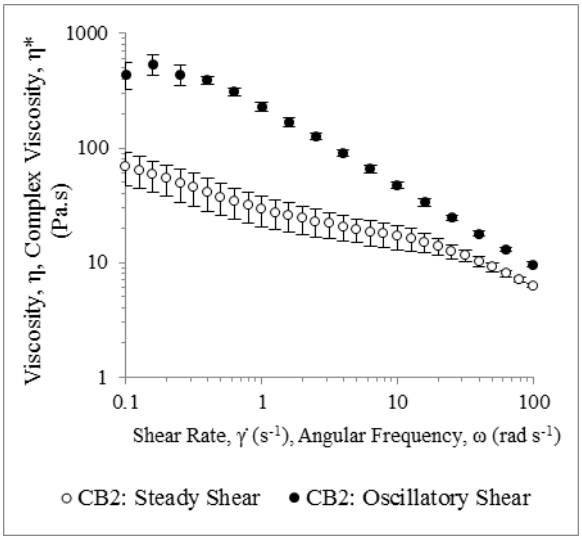


Figure 4.20: Viscosity and complex viscosity of MCP2 calculated from linear shear and oscillation tests, respectively, using a vane in cup geometry

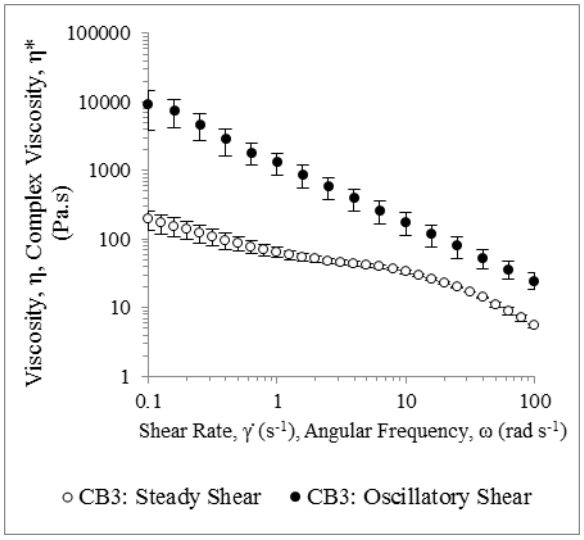


Figure 4.21: Viscosity and complex viscosity of MCP3 calculated from linear shear and oscillation tests, respectively, using a vane in cup geometry

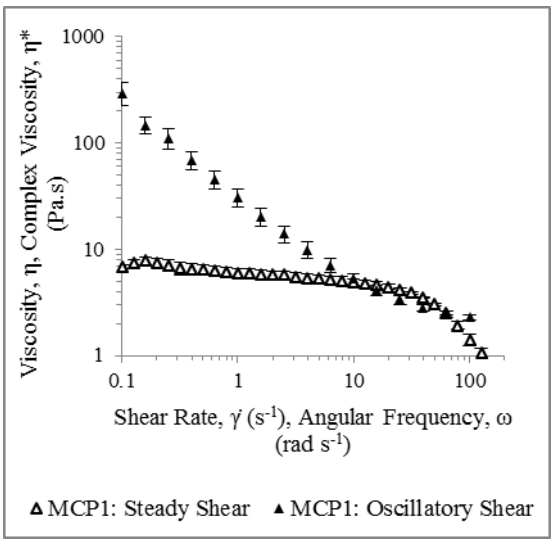
The results using the parallel plate and the vane geometries to run steady shear tests and oscillatory tests are compared in Figure 4.22, Figure 4.23 and Figure 4.24. Each of the Herschel-Bulkley parameters for the two methods are compared in Table 4.5. None of the samples were measured to have similar results using either of the geometries at steady shear or oscillation shear test conditions.

Table 4.5: Herschel-Bulkley model parameters describing the three model chocolate paste formulations measured using a vane in cup geometry

	Steady Shear (between shear rates of 0.06 - 10 s^{-1})			Oscillatory Shear		
	Yield Stress, Pa	**Consistency Coefficient, Pa.s**	**Flow Behaviour index**	**Yield Stress, Pa**	**Consistency Coefficient, Pa.s**	**Flow Behaviour index**
MCP1	1.77	14.86	0.84	-168.52	342.36	0.25
MCP2	3.20	26.12	0.80	-123.50	339.53	0.25
MCP3	10.03	55.71	0.77	535.97	773.67	0.20

These techniques have identified differences between the three pastes but due to instabilities at the edge of the plates and at the surface of the vane samples, it was difficult to conclude whether any of the results were a representation of the viscosity. The gap sizes used in both methods were too small relative to the size of the particles. As over half the volume of the solids consisted of large sugar particles, it is hypothesised that jamming is a considerable problem and velocity profiles across the gap will not be achieved. This would prevent the assumptions used to calculate the viscosities from being valid.

a)



b)

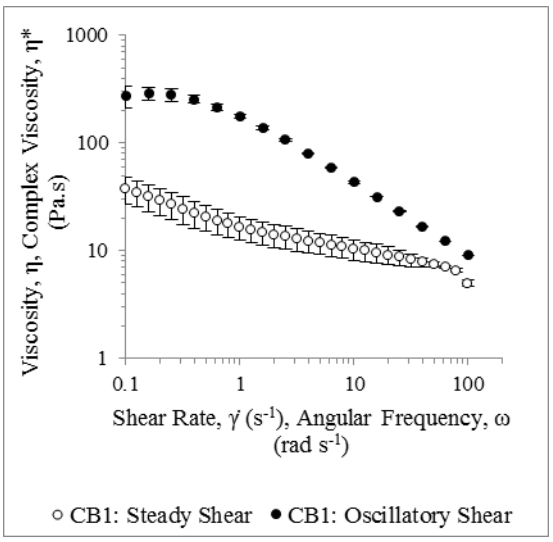
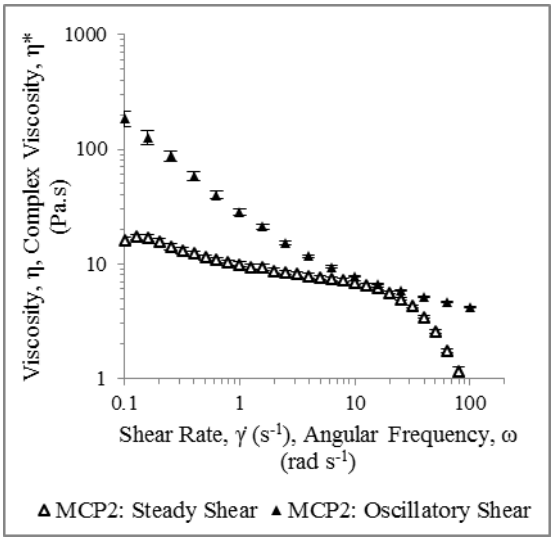


Figure 4.22: Comparisons of viscosity and complex viscosity of MCP1 from steady shear and oscillatory shear tests, respectively, where a) parallel plate geometry and b) vane in cup geometry

a)



b)

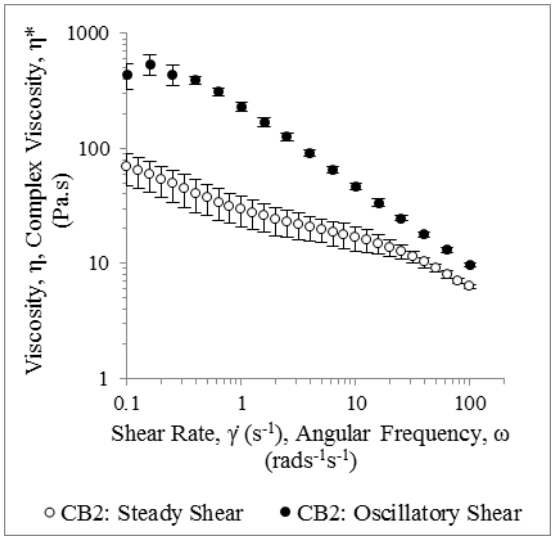
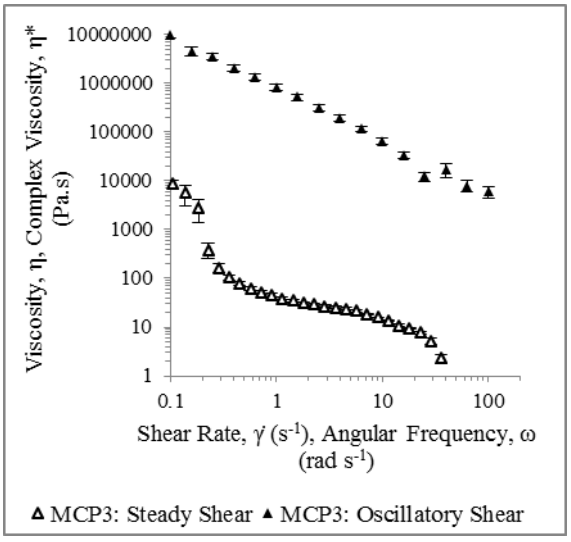


Figure 4.23: Comparisons of viscosity and complex viscosity of MCP2 from steady shear and oscillatory shear tests, respectively, where a) parallel plate geometry and b) vane in cup geometry

a)



b)

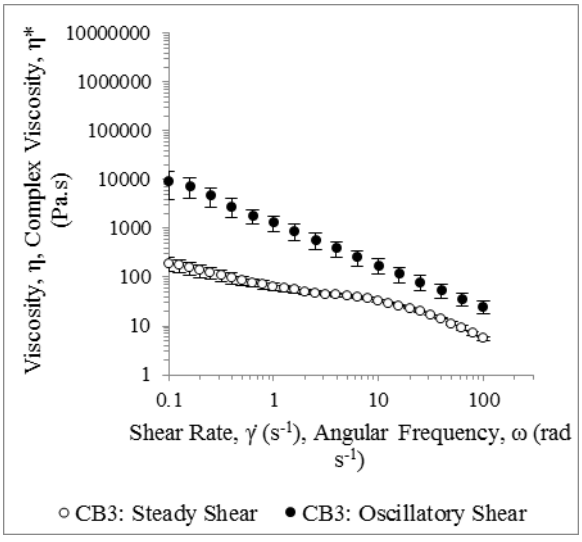


Figure 4.24: Comparisons of viscosity and complex viscosity of MCP3 from steady shear and oscillatory shear tests, respectively, where a) parallel plate geometry and b) vane in cup geometry

4.4 FT4 powder rheometer

The flow energy represents the amount of energy that was put into the sample during the test duration. It is possible to see that most energy was required to move the blade through the lowest fat paste (Figure 4.25). As the liquid content was increased, the quantity of energy

required to move the blade decreased. These results showed a high level of repeatability and each formulation was easily distinguishable.

The relationship with fat content was not linear and the differences between the two pastes with the highest fat contents only showed a small difference. Consequently, this technique may be best suited for comparing the consistencies of pre-refined pastes which are thicker in texture due to reduced particle sizes.

The disadvantage of this technique is that the output is only a measure of "energy consumption" which has no application to other measures and is reliant on the test conditions. The geometry created complex flow patterns and the results were not detailed enough to establish a rheological model that represented the fluid behaviour, such as the Herschel-Bulkley model. As the repeatability was high, this technique may be appropriate for developing an online correlation with plant performance.

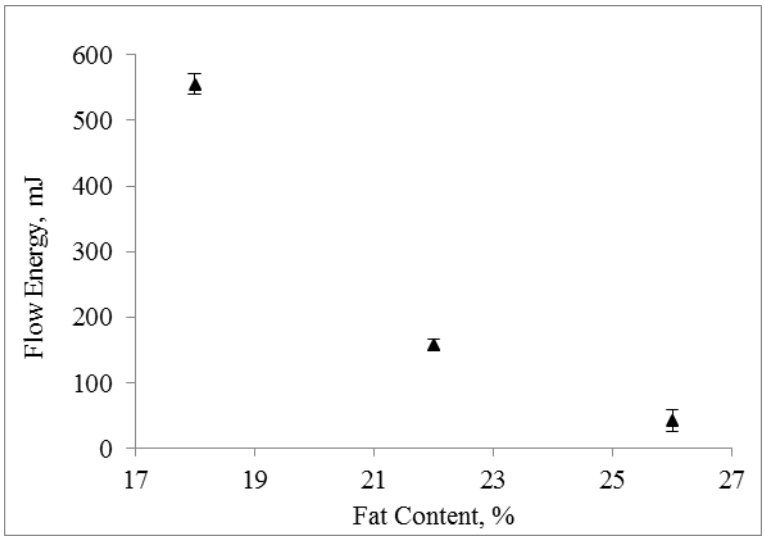


Figure 4.25: Flow energy of three pastes measured on the FT4 powder rheometer. Results of a students t-test showed that all three results are statistically significant.

4.5 Mixer Power

When the mixing shaft in a vessel was set to move at a particular speed, the resistance to the movement of the blades should have been directly related to the viscosity of the material. By recording this resistance, it was possible to determine differences between batches of pastes. Work has been published calculating rheological behaviour from the torque, however this is completely dependent on the geometry of the mixer and blade arrangement (reviewed in section 2.4.10). It has already been discussed that the geometry of the mixer used to combine chocolate ingredients is not standardised and therefore measurements of the power will always be a function of the geometries.

Figure 4.26 shows the averaged current that was measured from three repeated batches of paste over 600 seconds of mixing (voltage remains constant). Two values were determined from this plot: the value of current that was measured at end of the mixing duration and an indication of the total energy input to the paste over the entire mixing duration. Understandably, the latter was significantly influenced by the mixing time and so the value of current at the end of the mixing gave a better representation of the paste consistency prior to entering the refining processes.

This technique had the benefit of providing online and instant data on the consistency of the paste. Although it was not able to compare between equipment with different geometries, this could be used alongside a more in-depth technique, initially to correlate the current with the rheological properties. It would then be useful as an online method to compare between paste batches to understand the variability of material that is produced, perhaps with the potential for controlling the process based on the paste consistency extrapolated from measurements of the current.

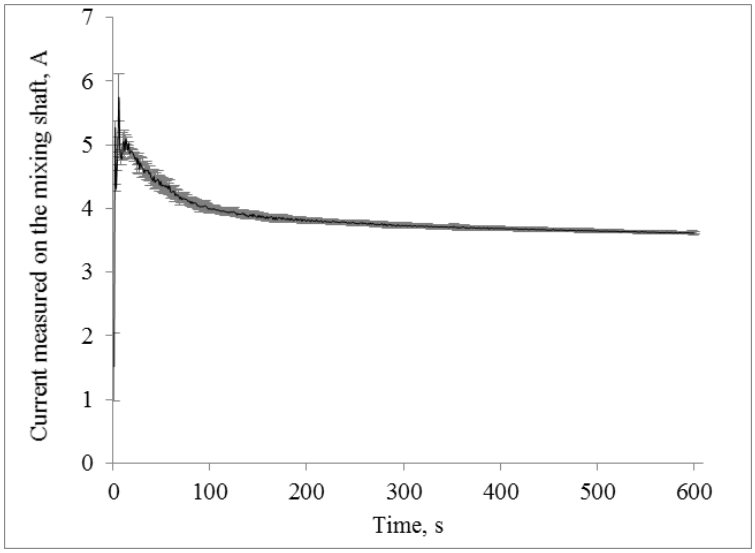


Figure 4.26: Current measured on the mixing shaft during paste manufacture of a standard chocolate recipe in a 200 kg capacity vessel. Error bars are the standard error of three repeated batches.

4.6 Conclusions

Fluids containing high quantities of large particles exist throughout many different industries, including chocolate pastes. Despite a growing need to measure these materials, very few of the techniques discussed in the literature were found to be suitable for chocolate pastes. Although other industries attempt to quantify the consistency of materials similar to chocolate pastes using, for example, penetrometers or slump tests, not enough is understood about the physical interactions of the fluids within these environments in order to fit a rheological model.

The main problem with conventional rheometer tests are the limitations of gap sizes. A parallel plate can be operated with a maximum 4mm gap in order for assumptions to be valid, however the surface tension of the sample also influences whether the sample will hold itself between a gap this large. As some sugar particles can be 1 mm in diameter and these can make up over 50 vol% of the paste, the arrangement and orientation of these particles has a great deal of impact on the measurement. As particles are unable to pack perfectly at the wall,

when the particles are large in comparison to the gap, this will cause apparent slip of the sample at the wall. The measurements of viscosity and shear stress using the parallel plate geometry were lower than when the vane in cup geometry is used, indicating that slip was having more of an effect on the parallel plate measurements.

There were also observed instabilities occurring which meant that homogeneous pastes were no longer being evaluated. Due to radial migration of particles, the edges of the material between parallel plates fractured and as air was drawn down into the paste behind the blades of the vane, material was forced out of the geometry altogether.

To minimise destruction of the structure in the pastes, oscillation tests were used. The Cox-Merz rule is commonly applied to establish values of complex viscosity from oscillation tests although the results have shown that they agreed with literature; the rule did not hold for concentrated suspensions where particle interactions significantly affected the viscosity.

The FT4 Powder Rheometer was able to produce repeatable measurements of how much energy was required to move a helical blade through a sample however this result was then only relevant to those particular testing conditions and would be best used as an offline comparison tool.

There is a potential opportunity for further work involving the measurement of current on the blade shaft of an online mixer. Although the results were relevant only to that particular geometry of mixer, current was instantly output during the mixing stage and did not require any product sampling. Preliminary tests on a pilot scale line indicated that the current varied based on the formulation of the chocolate paste and that the results were repeatable over a range of formulations and mixing speeds. In the future, it would be desirable to correlate the

measurements of current at the end of the mixing duration with offline rheology measurements, generating an online tool for monitoring the performance of a line.

In order overcome the problems found with these offline measurements of rheology, it is critical that larger gaps are used to prevent the largest sugar particles within pastes from affecting the rheological behaviour of the bulk. Measuring the current online or quantifying the paste using the FT4 both are possible techniques that could be used to regularly monitor performance of a line, however they would both be specific to the mixing equipment and would not necessarily provide comparisons between different process lines.

5 ANALYSING THE SUITABILITY OF THE BACK EXTRUSION TECHNIQUE

5.1 Introduction

As has been discussed prior to this chapter, there is currently no known method used within the chocolate manufacturing industry to quantify differences between each batch of paste. Furthermore, it was desirable to develop a measuring technique that not only distinguished between pastes, but was able to identify the rheological characteristics of the paste. It was hoped that by quantifying rheological behaviour of the pastes, these could be related to the behaviour of the material in downstream processes.

As has been discussed in section 2.4.5, work was first published in 1987 by Osorio and Steffe of a back extrusion technique (BET) to predict rheological properties of power law fluids which are difficult to measure in standard geometries (Osorio and Steffe, 1987). This was soon followed by a paper discussing how this can be adapted for a Herschel-Bulkley model (Osorio and Steffe, 1991). Based on these theories, a back extrusion technique was developed to quantify the viscosity of chocolate paste.

The practical considerations of conducting the BET using a Zwick Universal Mechanical Tester were first examined, focussing on the raw data generated in the test. The raw data was then analysed to investigate whether parameters of rheological models, in particular the power law and Herschel-Bulkley models, could be determined from the raw data. Where possible, these results were compared to measurements using a conventional parallel plate rheometer.

Once a method was established, more complex materials which were not suitable for testing using a parallel plate rheometer, such as chocolate pastes, were then evaluated.

Table 5.1 details the formulations of the suspensions which were used to establish the capability of the BET to quantify the rheological behaviour of pastes. In section 5.2.3, the surfaces were roughened by attaching sandpaper around the probe and vessel inner. The grit sizes of sandpaper used are also detailed in Table 5.1.

Table 5.1: Formulations of the suspensions used within this chapter, in vol% (calculated from densities, discussed in section 3.3.8) and the grit size of the sandpaper used for roughening in section 5.2.3

	SMP32	**SMP43**	**SMP47**	**SMP56**	**CP62**	**CP68**	**CP74**	**GS60**	**IS57**
Grit number	*P120*	*P120*	*P120*	*P120*	*P40*	*P40*	*P40*	*P40*	*P1000*
Mean grit diameter, µm	*125*	*125*	*125*	*125*	*400*	*400*	*400*	*400*	*20*
Skimmed milk powder	32	43	47	56	17	19	21	-	-
Granulated sugar	-	-	-	-	39	43	47	60	-
Icing sugar	-	-	-	-	-	-	-	-	57
Vegetable oil	68	57	53	44	-	-	-	40	43
Cocoa butter	-	-	-	-	30	23	16	-	-
Cocoa liquor	-	-	-	-	13	14	16	-	-

5.2 Principle of the technique

A cylindrical barrel of radius R was filled with the test material and the cross-head was manually positioned so that the top of the probe, radius a, was just in contact with the flat surface of the fluid. As the probe was pushed into the fluid at a constant speed, v_p, a known distance, the fluid was displaced by the volume of the plunger which caused the fluid to move upwards through the annulus as the probe moved downwards. During this phase, the total force, F_t, increased as the probe was submerged due to the increasing buoyancy force of the probe, F_b, the resistance due to the shear stress at the wall, $2\pi aL\sigma_w$ and the static pressure of

the test fluid on the base of the probe, $\pi a^2 PL$, according to equation 5.15.1. The buoyancy force was calculated from equation 5.25.2.

$$F_t = 2\pi aL\sigma_w + \pi a^2 PL + F_b \quad (5.1)$$

$$F_b = \rho g L \pi a^2 \quad (5.2)$$

where σ_w = shear stress at the wall, L is the length of probe submerged within the fluid, P= pressure drop per unit length and ρ is the sample density.

The value of peak force corrected for buoyancy was used for the subsequent calculations, calculated using equation 5.3.

$$F_{cb} = F_t - F_b \quad (5.3)$$

A velocity profile develops across the width of the gap; by assuming that there was no slip at the wall, the material at the outer edge should remain stationary at the wall whilst the material contacting the probe surface moves downwards at the same speed as the probe itself. This is further discussed in section 5.3.

Once the probe reached a set plunged distance, the probe was stopped and was then held stationary for 60 seconds whilst the force was continually recorded throughout this period. An example of the idealised force response during a test is shown in Figure 5.1. Ideally, the force should relax to a steady value, F_{t_e}, which is a combination of the buoyancy force and any remaining force is attributed to the effect of a yield stress.

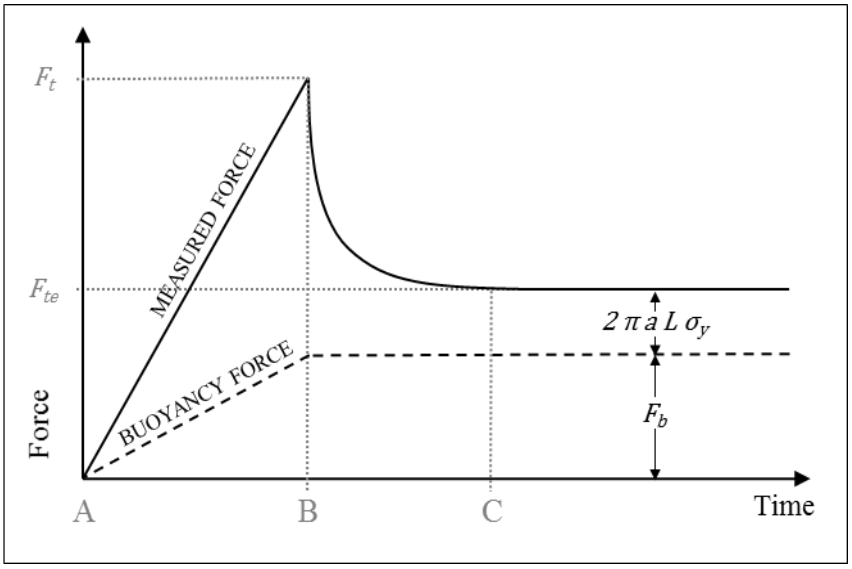


Figure 5.1: Idealise force response produced during a single test run of the back extrusion technique. The force increases initially as the probe is plunged into the sample (A-B) until it reaches a set distance (B). The probe then stops remains stationary for 60 seconds. The material has a short relaxation period where the meniscus relaxes before reaching a steady force at C.

The same sample was tested at four speeds i.e. four nominal wall shear rates, recombined by hand between tests to ensure that the shear history prior to each test is consistent. The wall shear rates were not only dependent on the probe velocity, they were also dependent on the fluid viscosity and the probe to vessel diameter ratio.

At the outset of implementing the test, it was assumed that the motion of the cross head would behave ideally or that any deviations from ideal behaviour would be negligible. Due in part to how the load frame controls itself, a couple of artefacts were identified that need to be "cleaned" from the data.

5.2.1 Initial motion of the probe

The force recorded as the probe begins to move into the sample were compared for three pastes in Figure 5.2. The 7th data point, recorded at 0.46 seconds, was consistently observed to be higher than the moving average, regardless of the test speed, the sample and the probe diameter.

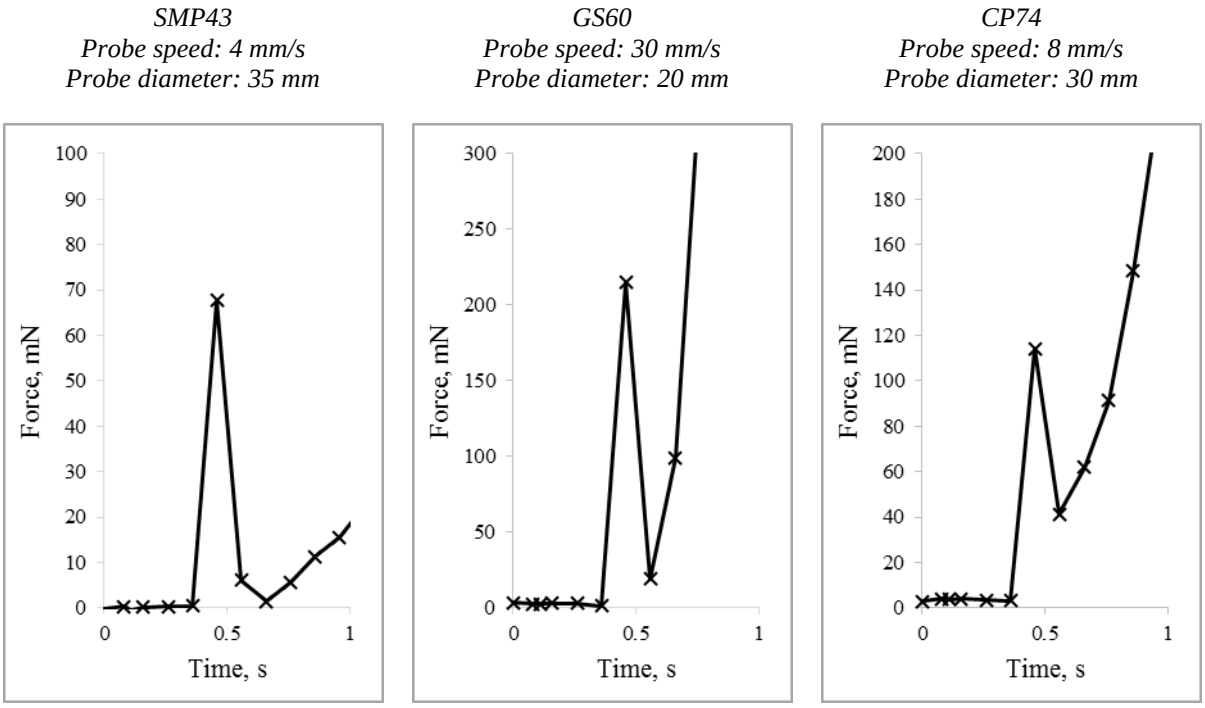


Figure 5.2: Initial force increase at 0.46 seconds after the probe begins to move into the sample.

Figure 5.3 shows plots the forces measured at 0.46 seconds during tests of SMP47 at four speeds using four probe diameters. Based on a time step of 0.09 seconds, the force (mass of the probe × acceleration) was also calculated. The calculated forces (blue symbols in Figure 5.3) correlated well with the forces that were measured (black symbols). This indicated that this peak was exclusively caused by the inertia of the probe as it begins to move, which was larger when a heavier probe began to move quicker.

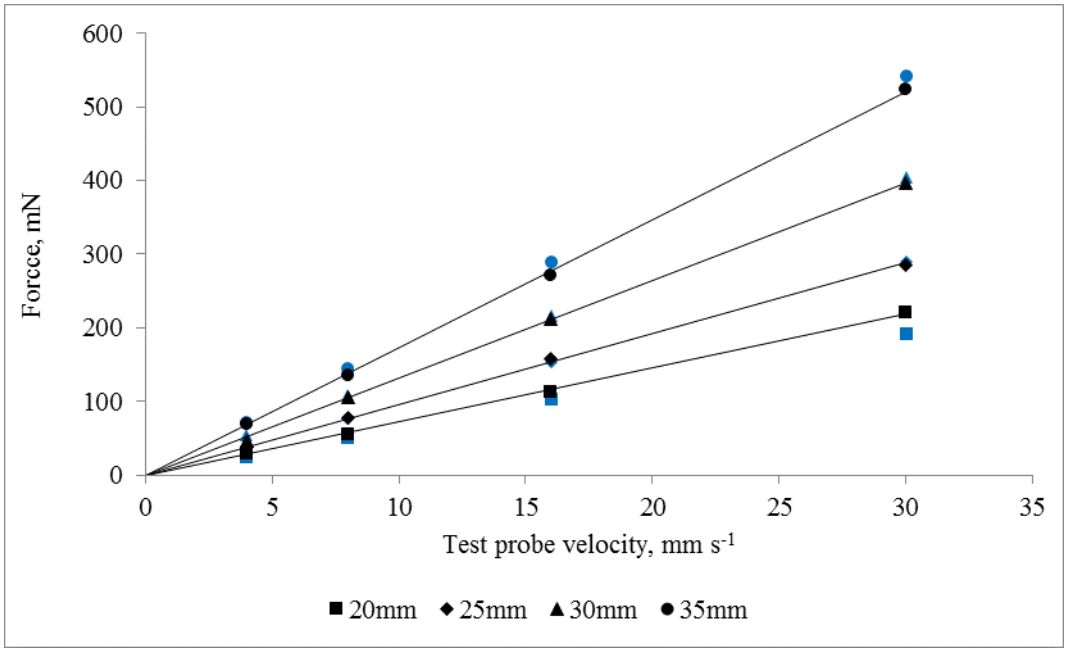


Figure 5.3: Force measured at 0.46 seconds into test phase (black markers) and force calculated from probe mass × acceleration. Reuslts are plotted against the probe velocity set for the test using four probe diameters. Linear trend lines go through the intercept. Results of raw data from testing SMP47.

Table 5.2: The force measured at 0.46 seconds into the test at four different test speeds using four different diameter probes. Averages of the raw data from testing SMP47 are shown with the standard deviation of three measurements.

Probe Diameter (m)	**Probe velocity, m/s**			
	0.004	**0.008**	**0.016**	**0.03**
0.020	29.1 ± 0.380	55.2 ± 2.89	112 ± 2.94	221 ± 4.15
0.025	38.4 ± 2.50	77.9 ± 2.09	158 ± 0.650	285 ± 18.3
0.030	47.2 ± 6.20	106 ± 0.640	212 ± 0.990	396 ± 5.04
0.035	69.2 ± 1.56	135 ± 1.02	272 ± 1.40	524 ± 16.7

The velocity of the probe was then examined in Figure 5.4. The results showed that it required 0.66 seconds for the probe to reach the test velocity which was independent of both the probe velocity and the sample. This figure shows results using SMP47 however the same result was seen for all other materials tested.

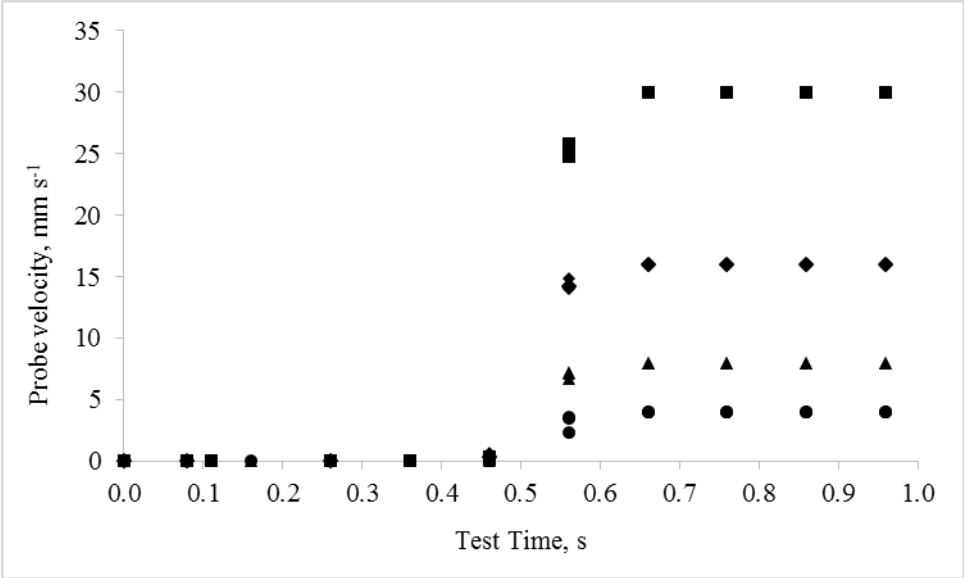


Figure 5.4: Velocities of the probe as the BET begins. Results at four different probe velocities are shown when testing SMP47 using a 30 mm diameter probe within a 90 mm diameter vessel (three repeats at each speed are shown, all tests were on the same sample).

5.2.2 End of the probe motion

Figure 5.5 and Figure 5.6 show the velocities of the probe during tests of SMP47 at 4, 8, 16 and 30 mm s^{-1}. The test time and probe distance were referenced with respect to the point where the probe reached the defined plunged distance, L. Data points were recorded at 0.1 second intervals which created a limitation of identifying precisely when the probe begins to slow.

The results suggested that unlike the start-up forces, the behaviour did not depend on the probe which was used. It was clear that the software was anticipating the approaching plunge distance set point and began to slow the crosshead before this.

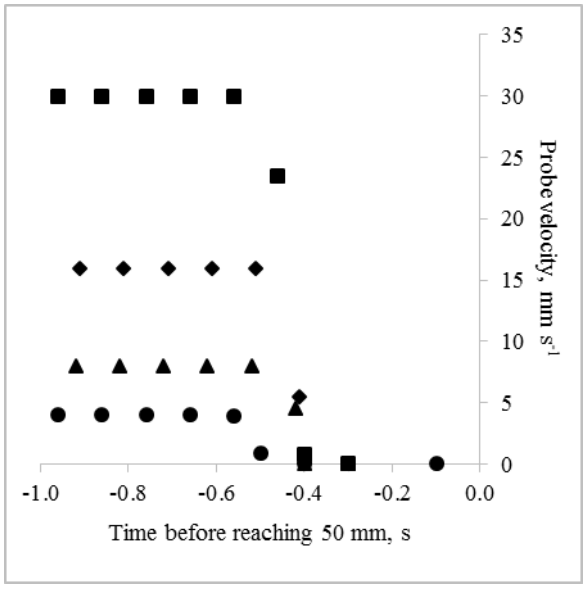


Figure 5.5: Slowing of the probe velocity as the test approaches the time of maximum plunged distance. The test time is normalised with respect to the point where the plunger has moved 50 mm. The data shown is from tests on SMP47 although similar results are seen for all fluids.

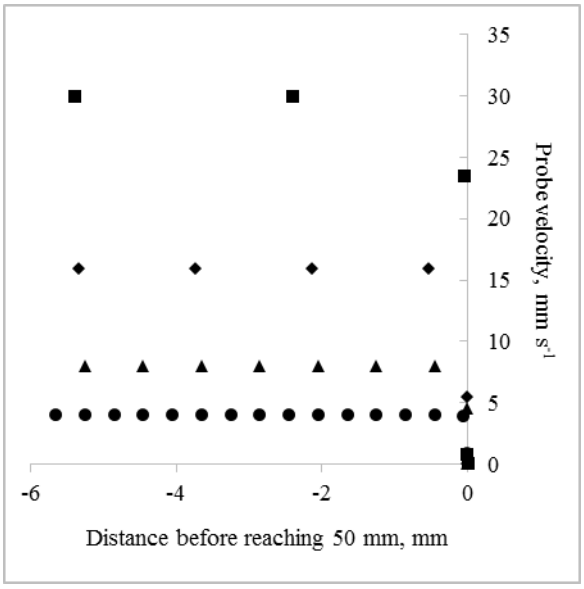


Figure 5.6: Slowing of the probe velocity as the test approaches the maximum plunged distance. The distance moved by the probe is normalised with respect to the point where the plunger has moved 50 mm. The data shown is from tests on SMP47 although similar results are seen for all fluids.

5.2.3 Shape of force increase

As it has already been established that the spike in force at the 7th data point is dependent on the speed; for each run a straight line was calculated between the 8th data point and the value of peak force. Ideally, if the motion is steady through material which does not change in consistency, then the force is expected to increase linearly. The real submerged depth of the probe was determined by extrapolating this linear trend back to zero force; this was used to determine the buoyancy force acting on the probe.

Time and force measurements of three fluids were normalised between the 8th data point and the point where peak force was reached, using equations 5.4 and 5.5. The results of water, GS60 and CP74 are compared in Figure 5.7. The normalised force when water is tested linearly increased as the probe moved into the sample. In contrast, the normalised force increase when GS60 was tested showed a trend which falls lower than the ideal linear trend. This suggests that it became harder for the probe to penetrate the fluid as it was submerged

further. The normalised force when CP74 was tested curved above the linear trend. This result suggests that it became easier for the probe to penetrate as it moved further into the sample. The average deviation from linearity was calculated as a residual to represent how different the raw data was from an ideal linear increase in force.

$$Time_{normalised} = (T_{i+7} - T_8)/(T_{peak\ force} - T_8) \tag{5.4}$$

$$Force_{normalised} = (F_{i+7} - F_8)/(F_t - F_8) \tag{5.5}$$

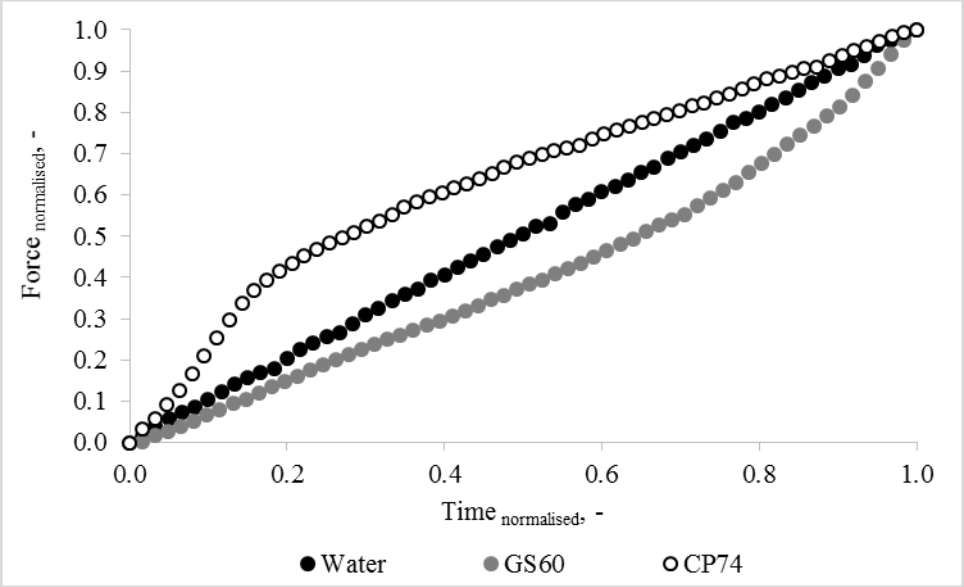


Figure 5.7: Force over time data of three materials, normalised between 0 – 1. Tests were run using a 30 mm diameter probe at 16 mm s^{-1}

To investigate how the measured force increased for each of the suspensions, the deviations of the normal force from linearity were calculated for nine materials, using equation 5.65.6. The following plots show the results, averaged over either the four text velocities or the four probe diameters.

$$Deviation\ from\ Linearity = \frac{\sum(Force_{normalised} - Ideal\ force_{normalised})}{Number\ of\ data\ points} \tag{5.6}$$

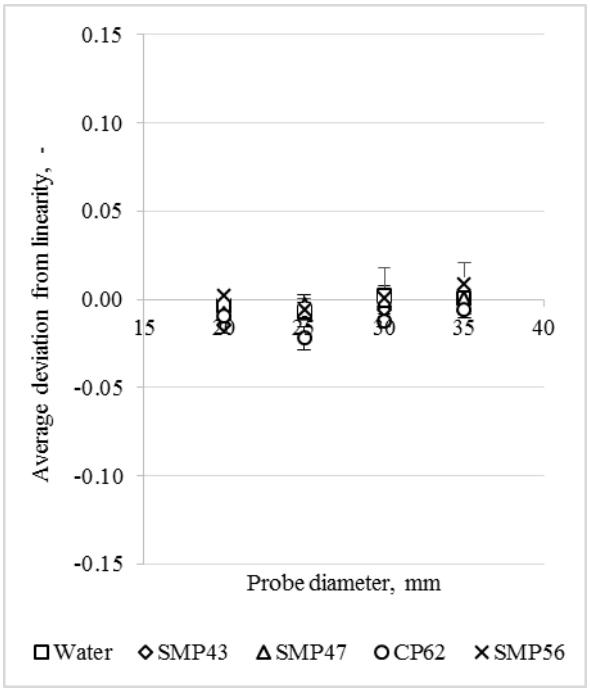


Figure 5.8: Average deviations from linearity over four different probe diameters, averaged over four probe velocities. Error bars are standard error of 3 repeated measurements on each sample.

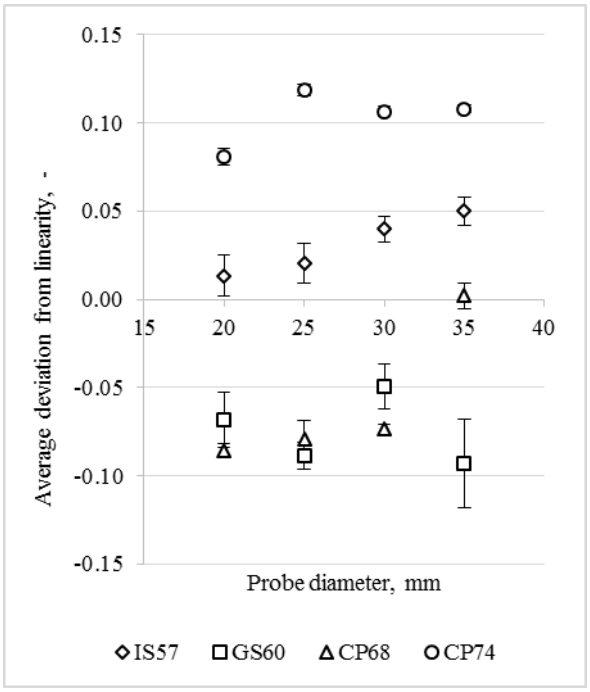


Figure 5.9: Average deviations from linearity over four different probe diameters, averaged over four probe velocities. Error bars are standard error of 3 repeated measurements on each sample.

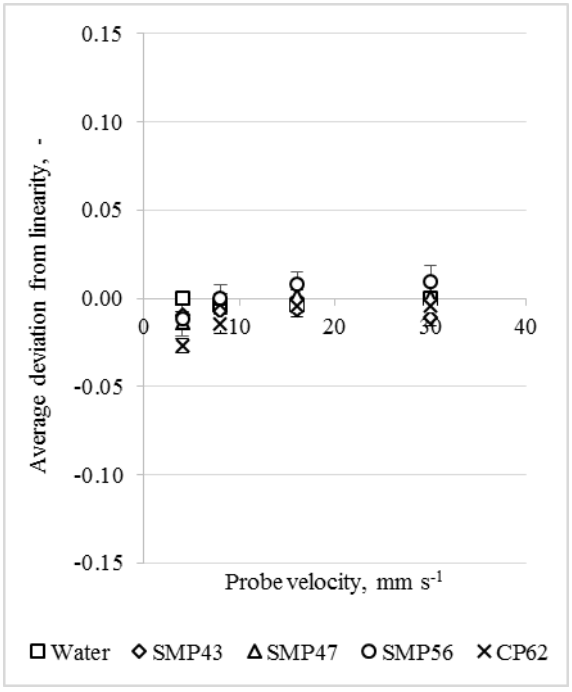


Figure 5.10: Average deviations from linearity over four different test velocities. Error bars are standard error of 3 repeated measurements on each sample at four probe diameters.

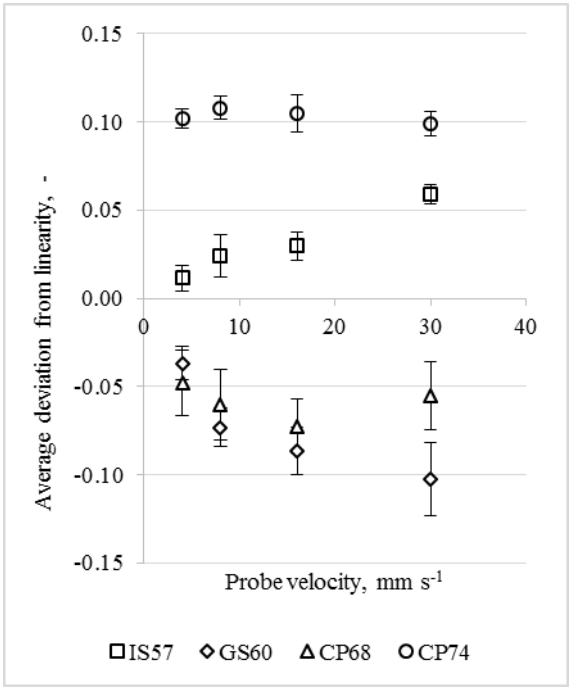


Figure 5.11: Average deviations from linearity over four different test velocities. Error bars are standard error of 3 repeated measurements on each sample at four probe diameters.

It is firstly possible to see that water, SMP43, SMP47, SMP56 and CP62 showed only a small difference from a linear trend (Figure 5.8 and Figure 5.10). IS57 and CP74 both showed positive values of the average devitation from linearity (Figure 5.9 and Figure 5.11). Potentially, some of the resistance was due to the rearrangment of particles near the end of the probe as it first entered the sample. As the probe was further submerged into the fluid, the region where this rearrangement was occurring became a smaller proportion of the total resistance. There may also have been slip developing at the walls; the area affected by slip increased when the probe was submerged further into the fluids. This could have resulted in a decrease of the force required to move the probe further. To investigate this effect, the sufaces of the probe and the wall were roughened by attaching sandpaper of grit sizes relative to the particles within the suspensions.

The positive devitation from linearity of IS57 increased with both probe diameter and probe velocity. As the icing sugar had a narrow PSD, this made it easier for liquid to migrate through the voids. This liquid migration appeared to be sensitive to the size of the geometry gap, similarly to the work discussed by Yaras et al. (1994) regarding capillary extrusion (larger die makes for more stable flows). The trend of the deviation from linearity for IS57 as velocity increased disagreed with observations of Bayfield et al. (1998) who found more stable flows at higher extrusion velocities.

Roughening the walls only slightly reduced the average deviations from linearity (Figure 5.12). This indicates that if slip occurred during the tests using smooth walls, roughening the walls with 20 μm grit sandpaper in this case did not reduce this effect of slip. This therefore suggests that the turbulent region at the end of the probe could have been causing the deviation from linearity.

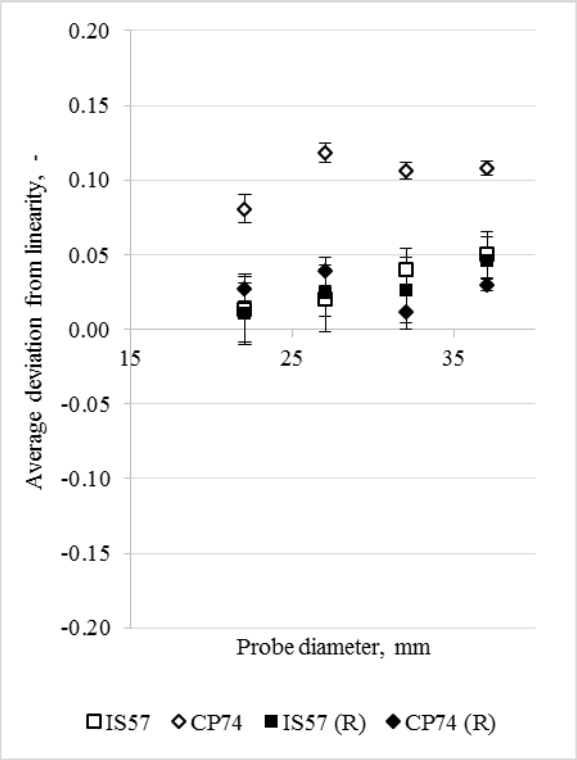


Figure 5.12: Average deviations from linearity for IS57 and CP74 over four different probe diameters using smooth and roughened (R) walls. Error bars are standard error of 3 repeated measurements on each sample at four probe diameters.

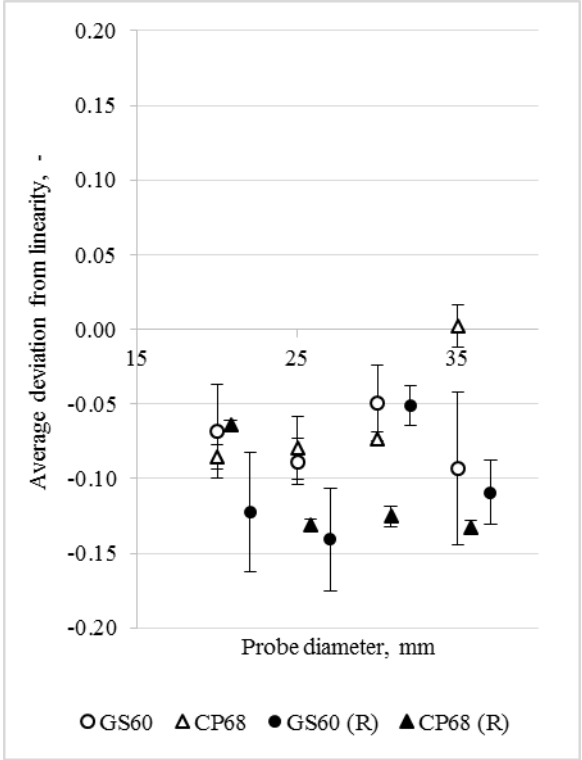


Figure 5.13: Average deviations from linearity for CP68 and GS60 over four different probe diameters using smooth and roughened (R) walls. Error bars are standard error of 3 repeated measurements on each sample at four probe diameters.

The most concentrated paste, CP74, had the most positive deviations from linearity but did not suggest any relationship with the probe velocity or diameter. The comparison of absolute forces was not meaningful because the gap size was reduced when the surfaces were roughened so consequently a plot of the normalised force against the time is shown in Figure 5.14. The force initially increased with a steep upwards curve as the probe initially entered the paste. After a normalised time of 0.2, the gradient reduced by a step change. Figure 5.12 and Figure 5.15 show that once the surfaces were roughened, the average deviation from linearity of CP74 reduced. A comparison of the normalised raw data showed that the roughened surface test had an initial increase in force which was smaller than when smooth surfaces were used (Figure 5.14). Like the smooth walled tests, after a normalised time of 0.2, the force then increased less steeply. As tests with roughened surfaces showed a more linear force

increase, this suggests that slip of CP74 could have been occuring when the surfaces were smooth, which could have been reduced by roughening the walls.

Since the particles are anticipated to be so tightly packed, the initial positively curved force increase as the probe begins to enter the paste could have been due to particle rearrrangement and alignment to allow the probe in.

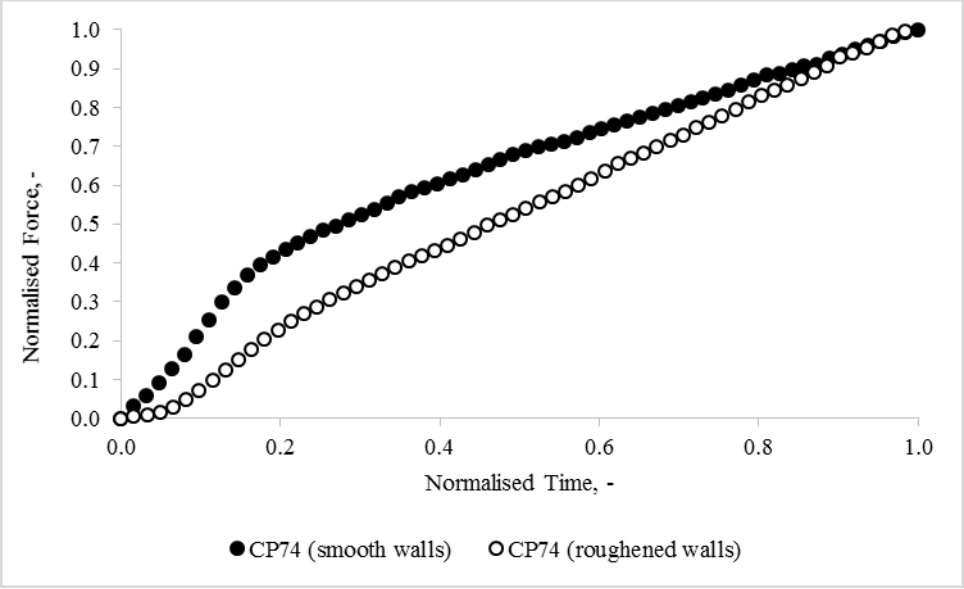


Figure 5.14: Normalised force of CP74, plotted against the normalised time, comparing the results using smooth and roughened surfaces (30 mm diameter probe at 16 mm s^{-1})

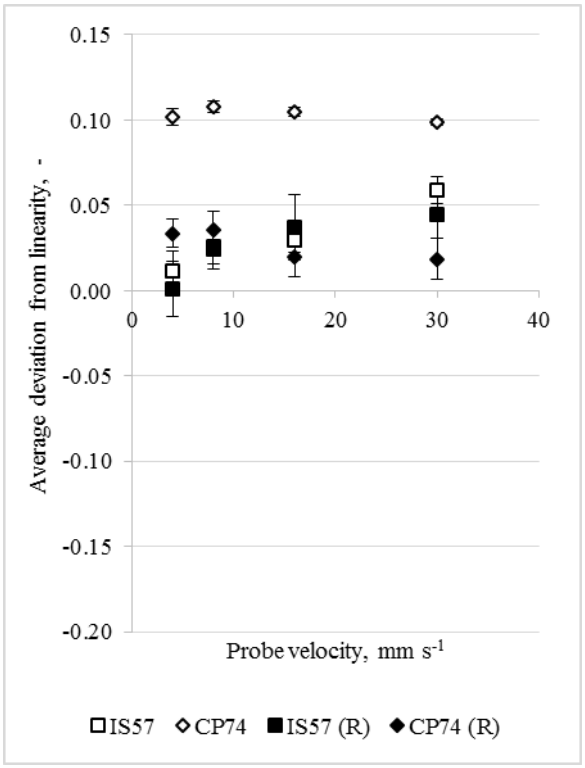


Figure 5.15: Average deviations from linearity for IS57 and CP74 over four different test velocities using smooth and roughened (R) walls. Error bars are standard error of 3 repeated measurements on each sample at four probe diameters.

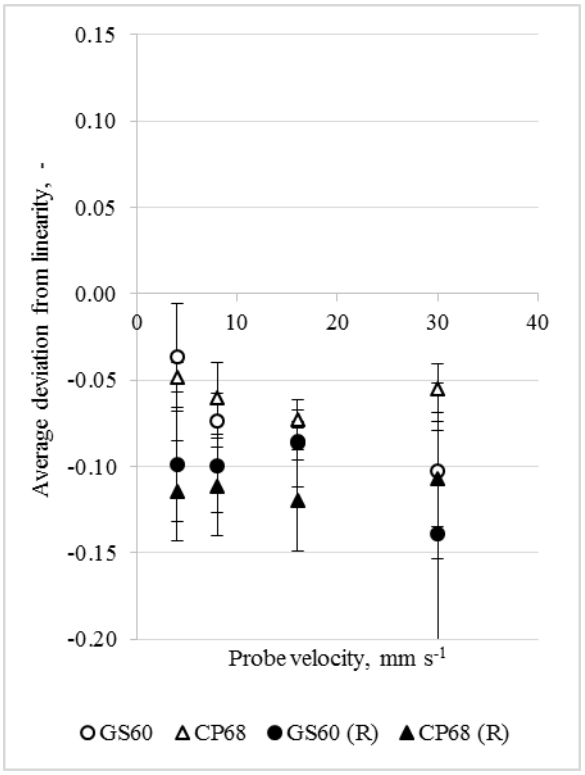


Figure 5.16: Average deviations from linearity for CP68 and GS60 over four different test velocities using smooth and roughened (R) walls. Error bars are standard error of 3 repeated measurements on each sample at four probe diameters.

GS60 and CP68 produced curves which were below the ideal linear trend (Figure 5.16); as the probe moved further into the paste, the resistance on the probe became stronger. It can be seen that as the probe diameter increased, the curvature of the force for CP68 reduced. This trend was similar to IS57 (Figure 5.15); there was more slip occuring when the probe was larger, causing less resistance to the probe moving into the sample. Roughening the probes resulteds in more negative curvatures, suggesting that slip of CP68 was occurring becuase the walls were smooth.

As well as the slip effect, the deviation from linearity overall was negative for CP68 i.e. suggesting that the paste became more viscous as the plunger was further submerged. It was discussed in section 2.4.4 that several studies observed large particles migrating towards regions of low shear, i.e. the centre of the gap. The point where the shear stress is at a

minimum is also where the velocity is the highest. This results in particles that have migrated towards the centre then moving more quickly towards the leading edge, up to the surface (Karnis and Mason, 1967, Ramachandran and Leighton, 2010, Tadier et al., 2014, Azzolini et al., 2014). A higher proportion of large solids will then exist at the surface, leaving behind an area of smaller solids lower down the vessel. The localised PSDs within these regions will be narrower and the particles will be unable to pack as well. This creates localised regions where the fat is trapped within voids and could create higher localised viscosities. The studies that this effect has been seen on is limited to solid volume contents below 50 vol%. The CP74 paste may not have shown this effect at all because the particles were unable to move freely without jamming.

The deviation from linearity of GS60 indicated that there was some dependence on the test velocity. When the probes were roughened, results at 30 mm/s showed a very large variability and the results using the 30 mm diameter probe did not align with the other results. The likelihood of liquid migration within the GS60 suspension was high; the particles were large and as the PSD was fairly narrow, liquid would have easily been able to move within the voids between particles. The particles were jagged and may not have flowed easily past each other, increasing the likelihood of jamming and increasing the migration of liquid. The large variations may have been a result of frequent yet random jamming. Although samples were mixed prior to each test, this suspension in particular was susceptible to settling of the particles which again may have contributed to the variation of results.

Comparing the shape of the force increase as the probe enters the sample highlighted that suspensions of particles which were monomodal above $\varphi = 0.57$ and suspensions of particles which had multimodal PSDs above $\varphi = 0.68$ did not remain homogeneous for the test duration. Slip at the wall due to phase migration of the liquid towards regions of high shear

was a common issue within all rheological measurements. Roughening the vessel and probe surfaces appeared to offer some reduction in the slip, however in practice, roughening of the surfaces was time consuming and could have been introducing more error to the measurement due to varied precision of attaching the sandpaper.

In future studies, it would be beneficial to use visualisation techniques to establish the location of the liquid and the distribution of different sized particles at different points within the test. This would help to test the hypotheses which have been discussed here and would also present the opportunity to develop the method to increase homogeneity during the testing procedure. Micro-XRCT was attempted on samples of SMP and sugar within a fat matrix. Unfortunately, as was discussed in section 3.3.9, there was not enough density contrast between the fat and solids to distinguish the boundaries of each feature.

5.2.4 Probe hold within the sample

Once the probe had reached the targeted plunge distance into the sample, the probe was held at this point for a further 60 seconds. According to the theory by Osorio and Steffe (1991), the residual force, F_{te}, is the buoyancy force of the material resisting the probe, F_b, and any additional force can be attributed to the yield stress of the sample, σ_y. The yield stress was calculated by rearranging equation 5.7.

$$F_{te} = 2\pi aL\sigma_y + F_b \qquad (5.7)$$

During the back extrusion tests, once the probe stopped, there was a short period of time (< 1 second) where the force dropped from the peak force (B – C in Figure 5.1). This period is where the cross head began to slow so that the probe height could accurately reach the set distance. There was also the possibility that some material relaxation occurred as the level of the fluid settled in the annulus.

Over the 60 second hold period, the resistive force of some of the investigated fluids gradually decreased. To investigate this, linear trend lines were fitted to the force during the hold period and the gradients were averaged over three repeated tests using four different probes. Table 5.3 shows the mean of the gradients and the standard error over the twelve sets of data. The yield stresses calculated with a 30 mm diameter probe are shown alongside the results in Table 5.3.

Table 5.3: Linear trend lines are fitted to the residual force as a 30 mm probe was held stationary within the sample for 60 seconds. The yield stresses are the values measured when the residual forces are averaged over the 60 seconds and the Herschel-Bulkley model is applied. All of the results for the gradient and the yield stress are averaged across three repeats at four different speeds for each fluid. It is important to note that practically, materials which have been measured to have negative yield stresses are then only modelled using a power law model.

	Solids Volume Content, %	**Linear gradient of the force whilst the probe is held stationary within the fluid for 60 s**		**Measured Yield Stress from BET**	
		Mean, mN s^{-1}	**Std Error, mN s^{-1}**	**Mean, Pa**	**Std Error, Pa**
CP74	74	-1.30	0.0144	52.8	2.23
IS57	57	-1.07	0.0136	24.4	1.79
SMP56	56	-0.0711	0.00346	14.9	1.21
CP68	68	-0.253	0.0147	5.57	1.07
GS60	60	-0.516	0.0141	3.35	1.61
CP62	62	-0.0882	0.0121	1.62	0.779
SMP43	43	0.00222	0.0061	-3.08	0.246
SMP47	47	-0.0907	0.0084	-12.2	0.329

The samples which were calculated to have the largest yield stresses, CP74 and IS57, showed noticeable decreases in the residual force over the hold period. This suggests that the fluids which were measured to have a yield stress were actually showing some time-dependent relaxation within the 60 seconds hold period. This agrees with the theory that Barnes discussed: the materials that were measured to have a yield stress in the 60 seconds following shearing may actually still be flowing. The material at the surface could have been moving from the shape that was created due to the velocity profile during the plunge phase to the

meniscus due to the surface tension of the fluid. If there was the presence of a very high Newtonian plateau then the material would always flow but the rate would have been much slower than the behaviour of the material during the test. A test was run on CP74 with a hold time of 20 minutes; over this time the residual force showed a consistent decline, approaching the buoyancy force (results not shown).

Although these results suggested that the materials may not have a definitive value of the yield stress, in the time scale that is both experimentally practical and relative to the chocolate manufacturing process, the Herschel-Bulkley model was continued to be used to represent the flow behaviour of the pastes.

5.2.5 Comparisons of raw data

It was important to identify whether this technique was capable of producing repeatable measurements of solid suspensions and that the variation between repeats was much less than the variation between samples. Using the method described above, three chocolate pastes (CP62, CP68 and CP74) were formulated and tested using the back extrusion technique using a 30 mm diameter probe within a 90 mm diameter vessel. Comparisons of the peak forces and relaxation forces achieved at three different test speeds are shown in Table 5.5 and the results are plotted in Figure 5.17 and Figure 5.18.

When the solids content of the paste was higher, the peak force increased. The peak force also increased when the probe velocity increased. The standard error between the peak forces of three repeated tests on the same sample for each fluid was very low in comparison to the forces measured. It was possible to recognise differences between the three pastes, indicating that this method had the potential to distinguish pastes that had not previously been quantified.

Table 5.4: Measured densities, based on the weight of a known volume, of chocolate pastes

Paste	***CP62***	***CP68***	***CP74***
Density, kg m^{-3}	1280.49	1275.18	1273.05

The relaxation forces were averaged over the 60 second hold period once the plunger had stopped. As the densities of each of the pastes only varied slightly (Table 5.4), the average buoyancy force is plotted alongside the relaxation forces in Figure 5.18. Any additional force measured on top of the buoyancy force, once the probe was stationary, could be attributed to the yield stress. CP62 showed values close to the buoyancy force, indicating that this paste displayed minimal yield stress. CP68, containing 6 vol% more solids, only showed a slightly higher relaxation force. Increasing the solids content by a further 6 vol%, CP74 showed a significantly higher relaxation force. The relaxation forces of CP74 also increased when the probe speed was higher, suggesting that the material properties were affected by the shear history during the test.

As the probe was removed from the sample, all three pastes showed a well where the probe had been removed. This well in samples of CP62 and CP68 showed some relaxation of this indent however the wells created in samples of CP74 remained deep and did not relax much.

Table 5.5: Peak and relaxation forces of three model chocolate pastes at four different probe velocities (probe diameter = 30mm, vessel diameter = 90 mm). Average value of the buoyancy force of the probe for all three pastes = 484 ± 5.14 mN

Probe velocities, m/s	**Peak Force, mN ± SE**			**Relaxation Force, mN ± SE**		
	CP62	**CP68**	**CP74**	**CP62**	**CP68**	**CP74**
0.004	650 ± 5.66	1160 ± 2.82	2640 ± 20.6	491 ± 0.652	510 ± 3.00	728 ± 4.01
0.008	704 ± 3.64	1610 ± 7.68	3570 ± 30.3	496 ± 1.01	510 ± 4.68	747 ± 2.31
0.016	877 ± 7.33	2250 ± 12.4	4860 ± 17.9	495 ± 2.81	518 ± 1.99	745 ± 4.39
0.030	1020 ± 3.03	3340 ± 10.7	6960 ± 57.7	493 ± 4.82	517 ± 4.19	791 ± 7.94

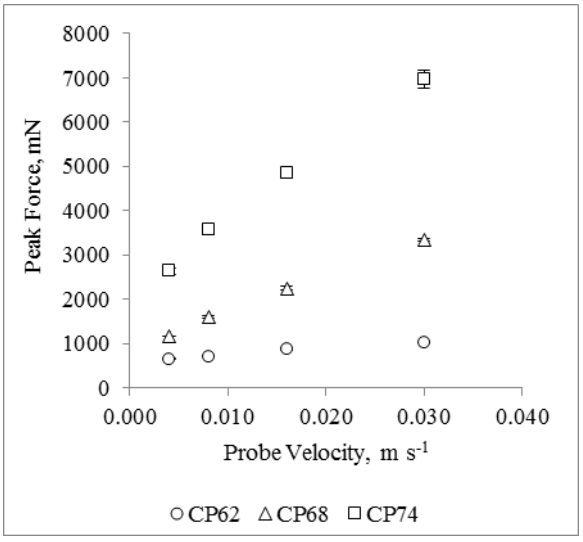


Figure 5.17: Peak forces of three chocolate pastes at four probe velocities with error bars representing the standard error

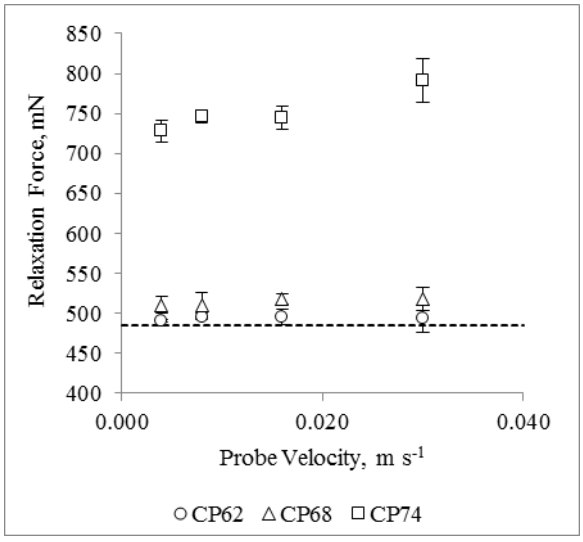


Figure 5.18: Relaxation forces of three chocolate pastes at four probe velocities. The dashed line represents the average value of the buoyancy force of the probe for all three pastes (484 ± 5.14 mN)

5.3 Fitting to rheological models

Since the raw data indicated that the technique could differentiate between pastes, it was now appropriate to calculate rheological model parameters of the pastes. As the solids volume contents were high, a yield stress was expected. Beyond this, the stress response was expected to be non-linear, hence a Herschel-Bulkley model (equation 4.8) was used as the rheological model to represent the flow behaviour of pastes.

Suspensions are likely to show some degree of shear thinning behaviour due to the rearrangement of particles however if the pastes did not display any yield stress behaviour, this work also compared the results using the power law model (equation 4.7). This is a simplified version of the Herschel-Bulkley model when the yield stress is equal to zero.

Osorio and Steffe constructed a force balance on the material within the gap between the probe and the vessel wall; this is a balance of the resistance of the fluid to move through the gap and the pressure drop, ΔP. This generated a shear stress profile; for a power law fluid, this is split into two regions across the width of the gap, separated by λ where the shear rate is

equal to 0. For a Herschel-Bulkley fluid, there are three regions across the width of the gap; the region in the centre, between λ_- and λ_+ is where the yield stress of the fluid is acting hence the shear rate is equal to 0. Following this, either the power law or Herschel-Bulkley model is incorporated into the force balance to develop an expression for the shear rate across the gap. Integrating this results in an expression for the velocity profile, as is illustrated in Figure 5.19.

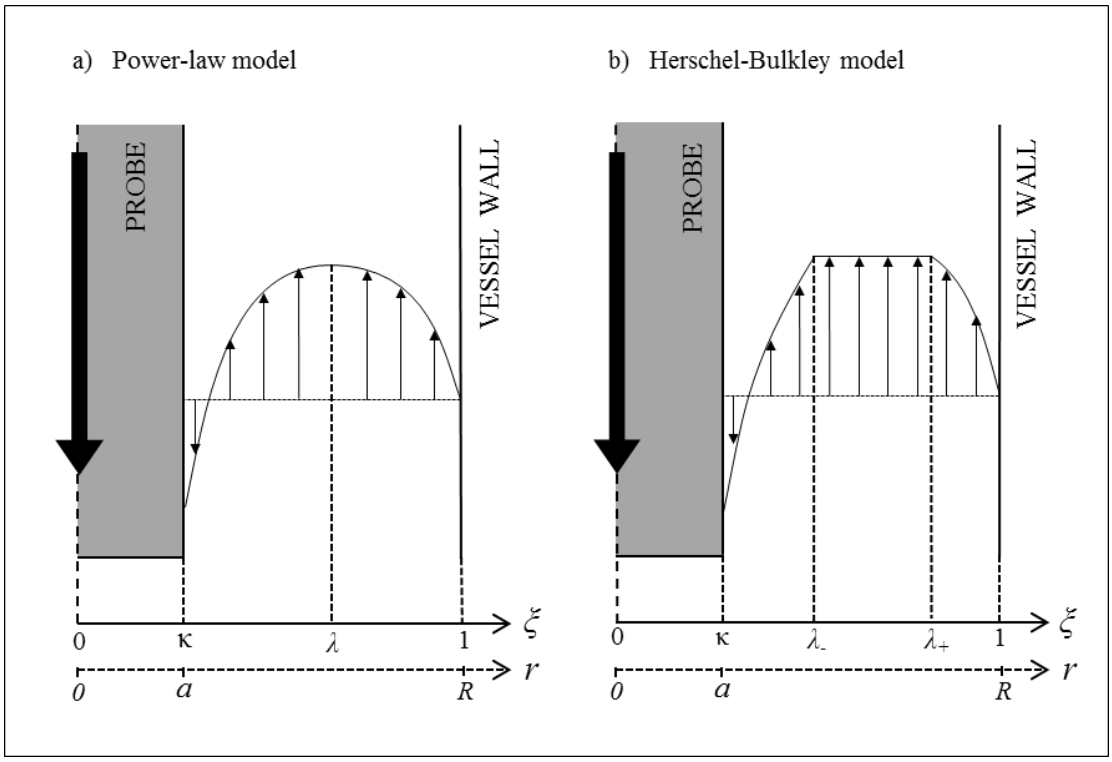


Figure 5.19: Examples of the velocity profiles created within the gap between the probe and the vessel wall as the probe is plunged down into the sample and the material is forced back up through the annulus. Velocities are relative to the vessel wall. R is the radius of the vessel and ξ is the dimensionless radius of the vessel.

The volumetric flow rate through the annulus was established as a function of the velocity profile. For a power law fluid, it was necessary to establish λ which can be found numerically by equating the volumetric flow rate through the annulus to the volumetric flow rate of material displaced by the probe. Knowing the value of λ, the shear stress at the probe wall can be established. The pressure drop, ΔP, is a function of the peak force and the shear stress, which enables the consistency coefficient to be calculated.

For the Herschel-Bulkley model, both ΔP and either λ_- or λ_+ must be established simultaneously. In addition to the two expressions describing volumetric flow rate, it is possible to express ΔP as a function of the peak force measured for each test. Once ΔP has been determined, the shear stress at the probe wall can be established using equation 5.15.15.1, which expresses the resistive force on the probe as the sum of the buoyancy force of the probe, the resistance due to the shear stress at the wall and the static pressure of the test fluid on the base of the probe.

The yield stress of the fluid was quantified from the relaxation force, as the probe was held stationary, submerged within the fluid. The buoyancy force of the probe within the material was removed from the average relaxation force and any remaining resistance was considered to be a product of the yield stress. This was discussed in section 5.2.4.

Knowing the flow behaviour index (as will be discussed in section 5.3.1), Osorio and Steffe demonstrated that the consistency coefficient can be calculated from the expression of the volumetric flow rate as a function of the pressure drop, ΔP.

5.3.1 Calculating the flow behaviour index

5.3.1.1 Technique 1

Analogously to Poiseuille flow, Osorio and Steffe demonstrated that:

$$F_{cb} \propto C \cdot {v_p}^n \qquad (5.8)$$

where F_{cb} is the peak force corrected for buoyancy (equation 5.3), C is a constant, v_p is the probe velocity and n is the flow behaviour index.

For multiple tests on the same fluid, run at different speeds within the same geometries, n can be established from a plot of F_{cb} against v_p. This technique, used by Osorio and Steffe for

calculating the flow behaviour indices, was applied to tomato concentrates, mustard, wheat porridge and sugar suspensions, modelling the flow with a power law model (Alviar and Reid, 1990, Brusewitz and Yu, 1996, Gujral and Sodhi, 2002, Perrot et al., 2011).

This relationship is only valid when the material follows a power law model. When the Herschel-Bulkley model is used, a plug flow region is created in the middle of the gap between the probe and the vessel walls which is affected by the yield stress of the fluid.

5.3.1.2 Technique 2

Alternatively, it was possible to determine at which value of flow behaviour index the consistency coefficient was most consistent. The analysis was run in MATLAB to establish the values of consistency coefficient when the flow behaviour index was set at a particular value. These values tested are between 0.1 – 1.0 at intervals of 0.1. From the tests that were run at different speeds, the coefficients of variance (CoV) of the consistency coefficients were calculated by dividing the standard deviation by the average value from the four different speeds. The minimum CoVs were plotted for each value of the flow behaviour index and a minimum point was established where there is the least variation between the values of consistency coefficient.

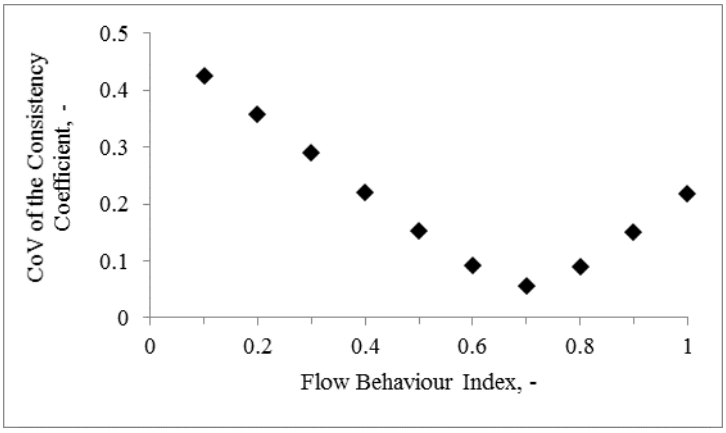


Figure 5.20: Example of the coefficients of variance which occur for the consistency coefficients when different values of flow behaviour indices are analysed

This process was performed on three chocolate pastes and the rheological properties were determined when the CoV of the consistency coefficient was at a minimum. Using three chocolate pastes as examples, the Herschel-Bulkley model parameters are summarised in the following tables and the overall shear stresses are compared on the plots of shear stress against shear rate.

Table 5.6: Parameters of the Herschel-Bulkley model when four different diameter probes are used to test CP62, comparing the values when the power-law theory is used to calculate n and when the variation in k is at a minimum.

Probe diameter, mm	**20**	**25**	**30**	**35**	**20**	**25**	**30**	**35**	**20**	**25**	**30**	**35**
	Flow Behaviour Index, -				**Consistency coefficient, Pa.s^n**				**Yield Stress, Pa**			
Technique 1	0.97 (0.99)	0.75 (0.96)	0.71 (0.95)	0.94 (1.0)	17.36	21.06	23.92	20.42	2.25	2.86	1.62	1.64
Technique 2	0.9	0.5	0.6	0.8	17.35	22.26	25.40	22.55	2.25	2.86	1.62	1.64

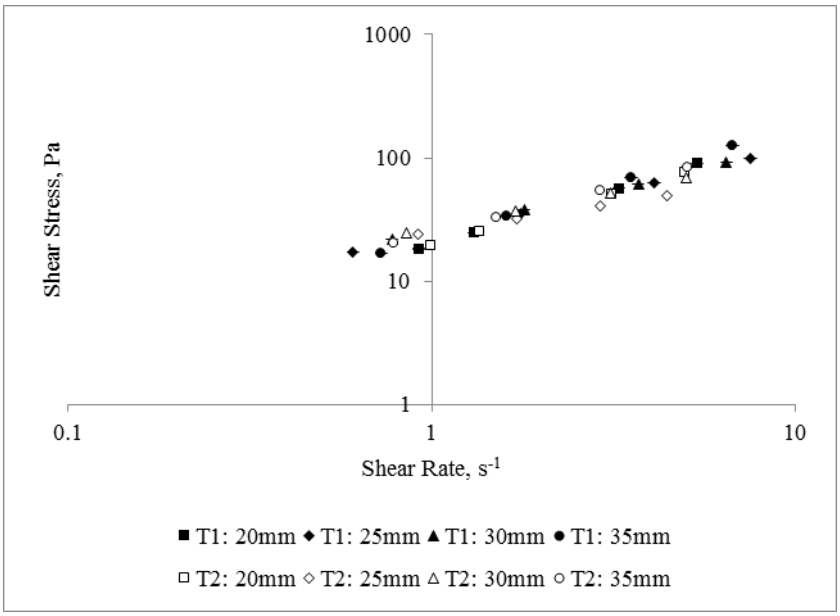


Figure 5.21: Shear stress plotted against shear rate for CP62, comparing the results when two techniques (T1 or T2) have been used to determine the flow behaviour indices using four different probe diameters (20 - 35 mm)

Table 5.7: Parameters of the Herschel-Bulkley model when four different diameter probes are used to test CP68, comparing the values when the power-law theory is used to calculate n and when the variation in k is at a minimum.

Probe diameter, mm	**20**	**25**	**30**	**35**	**20**	**25**	**30**	**35**	**20**	**25**	**30**	**35**
	Flow Behaviour Index, -				**Consistency coefficient, Pa.s^n**				**Yield Stress, Pa**			
Technique 1	0.78 (0.97)	0.69 (1.0)	0.76 (1.0)	0.71 (0.99)	81.55	99.68	108.80	166.29	1.26	4.53	5.57	6.98
Technique 2	0.6	0.7	0.7	0.7	78.78	99.44	112.72	168.18	1.26	4.53	5.57	6.98

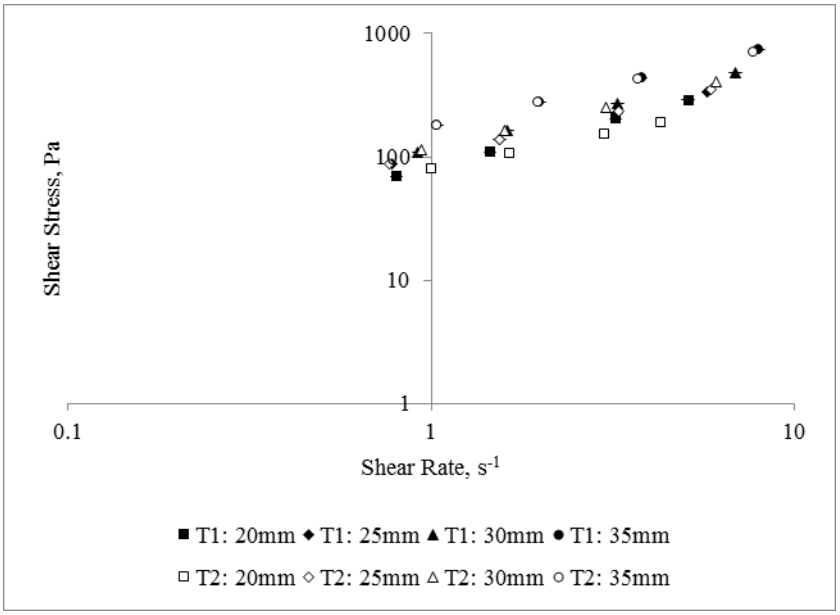


Figure 5.22: Shear stress plotted against shear rate for CP68, comparing the results when two techniques (T1 or T2) have been used to determine the flow behaviour indices using four different probe diameters (20 - 35 mm)

Table 5.8: Parameters of the Herschel-Bulkley model when four different diameter probes are used to test CP74, comparing the values when the power-law theory is used to calculate n and when the variation in k is at a minimum.

Probe diameter, mm	**20**	**25**	**30**	**35**	**20**	**25**	**30**	**35**	**20**	**25**	**30**	**35**
	Flow Behaviour Index, -				**Consistency coefficient, Pa.s^n**				**Yield Stress, Pa**			
Technique 1	0.65 (0.98)	0.64 (0.99)	0.55 (0.94)	0.57 (0.99)	231.64	238.37	258.17	291.58	32.63	38.67	52.76	98.79
Technique 2	0.8	0.6	0.6	0.7	225.45	244.20	243.85	233.36	32.63	38.67	52.76	98.79

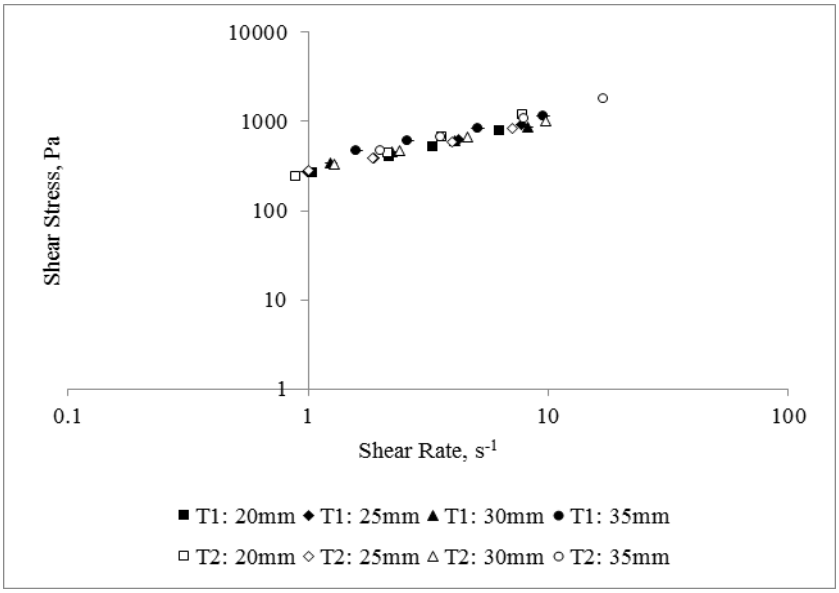


Figure 5.23: Shear stress plotted against shear rate for CP74, comparing the results when two techniques (T1 or T2) have been used to determine the flow behaviour indices using four different probe diameters (20 - 35 mm)

Within the ranges of the shear rates in these back extrusion tests, any error in the value of the flow behaviour indices used was corrected by the consistency coefficient. The predictions of shear stress vs. shear rate curve therefore appeared consistent hence technique 1 will be used for further back extrusion tests.

It is important to be aware that the predicted shear rates were also influenced by the value of the flow behaviour indices. Since the rheological model parameters were only valid at the probe velocities which were tested, it was unwise to extrapolate out of these regions as the results could diverge.

5.3.2 Sensitivity

It was important to consider how the sensitive the processed data was to errors in the measured experimental parameters. The raw data recorded from measurements of a 5% CMC solution using a 30 mm probe was re-analysed, altering the following properties by ± 5 % (original values shown in brackets):

- Probe diameter (0.03 m)
- Vessel diameter (0.04 m)
- Distance Plunged (0.05 m)
- Density of the material (1019 $kg.m^{-3}$)
- Probe velocities (0.004, 0.006, 0.008, 0.01, 0.02 and 0.03 m s^{-1})

Table 5.9 shows that variations in the probe diameter and vessel diameter, affecting the gap width, had more impact on the three Herschel-Bulkley parameters than differences in the density or the distance plunged. The flow behaviour index was relatively unaffected by the changes of any physical parameter because it was calculated from F_{cb}/L, whereas the consistency coefficient and the yield stress both changed significantly.

This highlights that it is crucial to understand the probe and vessel parameters and that small changes in these will have an impact on the result. When the width of the gap is not correct, the assumptions regarding the amount of fluid displaced by the probe, the volume which the fluid is able to move up through and the length of the probe submerged within the fluid will all be incorrect.

Table 5.9: Calculated values of the Herschel-Bulkley parameters of a 5% CMC solution when the probe and vessel diameters, fluid density and the plunge distance are altered by ± 5%. The R^2 value of the flow behaviour index fit for all samples is 0.99.

	Flow behaviour index, -	**Consistency coefficient, Pa.s^n**	**Yield stress, Pa**	**Shear stress at a shear rate of 5 s^{-1}, Pa**
Original	*0.74*	*8.77*	*6.87*	*35.9*
Probe diameter + 5 %	0.79	5.65	-11.0	8.99
Probe diameter - 5 %	0.72	13.1	25.7	67.3
Vessel Diameter + 5 %	0.73	13.4	16.7	60.1
Vessel Diameter - 5 %	0.77	5.27	-4.49	13.7
Density + 5 %	0.75	9.25	3.13	34.1
Density - 5 %	0.74	8.52	10.6	38.5
Distance Plunged + 5 %	0.74	9.61	6.87	38.3
Distance Plunged - 5 %	0.75	7.97	7.07	33.8
Velocity + 5 %	0.74	8.46	6.87	34.9
Velocity - 5 %	0.74	9.11	6.87	37.1

This was most relevant to this research when the probes are roughened. Pieces of sandpaper were attached to the probe and vessel walls which decreased the size of the gap. Although the thickness of the sandpaper was accounted for within the data processing, this technique introduced several errors. Firstly, the sandpaper had to be frequently replaced and each time, there may have been some overlap of the sandpaper positioned around the probe. This decreased the width of the gap in this region, affecting the velocity profile. Fundamentally, the particles within the fluid were designed to fit into troughs between the sandpaper grit particles so that there was no region of apparent slip at the wall where the particles cannot perfectly pack. However in practice, the thickness of the sandpaper was only determined at the surface of the sandpaper particles. This introduced a layer which was not accounted for within the calculations but could be accessed by the suspension. If this method became an established technique to characterise the paste, it is likely that the metal surfaces of probe and vessel would be permanently roughened to suit the paste and to precisely control their diameters.

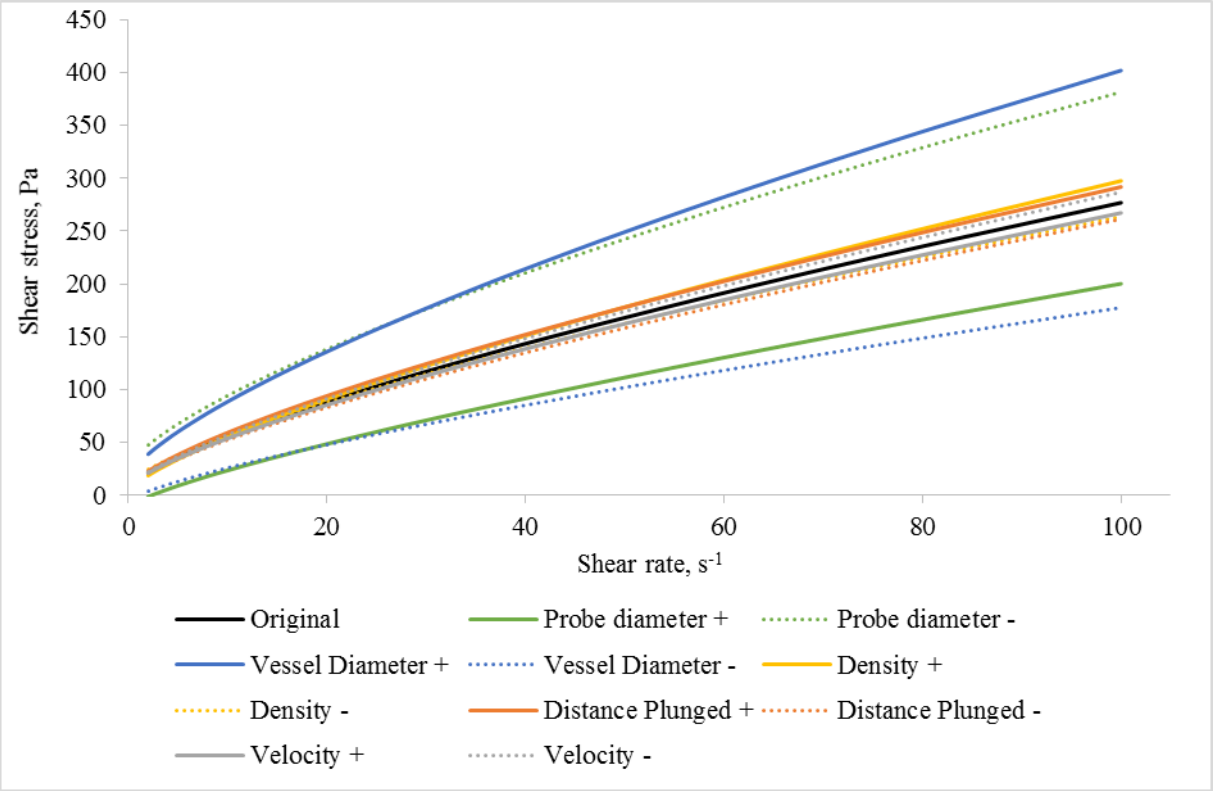


Figure 5.24: Shear stress vs shear rate of a 5% CMC solution when the physical inputs are altered by +/- 5%

5.3.3 Rheological measurements of suspensions

A polymer solution and a range of suspensions were measured using the back extrusion technique. The results presented in Table 5.10 are the results of rheological models which were fitted to the BET results of shear stress against shear rate using all four probe diameters. The polymer solution and the suspensions of SMP particles were also characterised using the Discovery HR-2 Rheometer (TA Instruments, USA). Some suspensions were also tested using the BET when the walls were roughened.

Power law and Herschel-Bulkley models were fitted to the data; if the yield stresses calculated from the raw data of BET tests were positive then the Herschel-Bulkley model was used, otherwise the power law model was fitted.

Table 5.10: Rheological parameters of fluids and suspensions measured using the parallel plate and back extrusion technique (with both smooth and roughened walls).

	Parallel Plate			BET (Smooth walls)			BET (Roughened walls)		
	Yield	**k**	**n**	**Yield**	**k**	**n**	**Yield**	**k**	**n**
CMC	8.58E-09	15.2	0.59	1.33E-07	14.1	0.60	-	-	-
SMP32	-	0.574	0.97	-	0.767	0.83	-	-	-
SMP43[a]	-	3.35	0.91	-	3.39	0.86	-	5.14	0.63
SMP47[a]	-	22.0	0.72	-	15.0	0.78	-	22.0	0.65
SMP56[a]	0.60	15.3	0.80	22.5	14.1	0.69	23.5	34.8	0.40
IS57[b]	-	-	-	1.61E-03	184	0.15	4.19E-06	197	0.23
GS60	-	-	-	1.30	15.7	0.71	-	-	-
CP62[a]	-	-	-	2.09	20.69	0.84	6.59	18.76	0.77
CP68[a]	-	-	-	4.59	114.08	0.74	14.50	156.44	0.70
CP74[a]	-	-	-	55.71	254.94	0.60	57.63	367.85	0.52

a: roughened with P120 grit sandpaper
b: roughened with P1000 grit sandpaper

Note: Materials without a yield stress are modelled using a power law model, materials with a yield stress are based upon the Herschel-Bulkley model. Values are calculated by fitting the relevant rheological model to a plot of the shear stress vs. shear rate of all the data points produced using four probe diameters at all four speeds.

A small vessel (40 mm diameter) was initially used to measure the CMC solution and SMP32. The result for the CMC solution matched closely with the parallel plate measurements (Figure 5.25). This suggests that the back extrusion technique was capable of producing valid results, i.e. the back extrusion technique accurately measured the rheological properties of CMC.

BET measurements of SMP32 did not show a similar result to the parallel plate measurements (Figure 5.26). Reviewing the data indicated that as the gap size decreased, the BET results diverged from the parallel plate results. The gap ranged from 2500 – 10000 μm; at the smallest gap size, this was approximately 10 times the size of the SMP particles within the suspension. This result suggests that the gap must be larger in order to measure the bulk rheological properties. Since the large sugar particles found within chocolate pastes are approximately 1000 μm, which are within suspensions of $\varphi \approx 70$, a larger vessel was used in further tests, with a diameter of 90 mm.

From tests of SMP32 using the larger vessel, the force increase as the probe plunged into the sample was equal to the buoyancy force of the probe. This implies that the resistance of the probe was dominated by the buoyancy and no rheological parameters could be ascertained from this data.

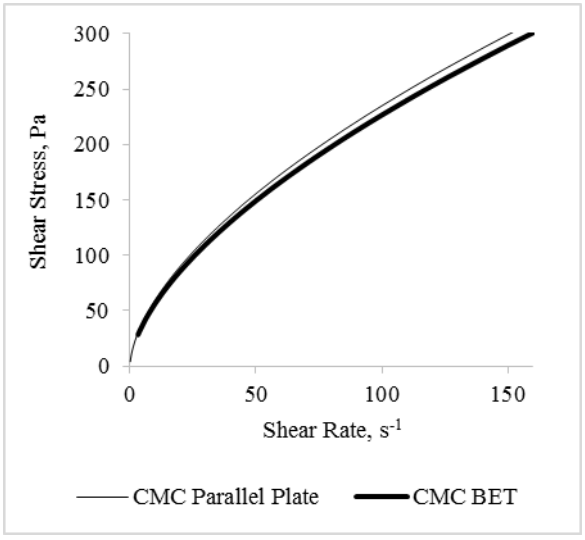


Figure 5.25: Rheological behaviour of a CMC solution measured using a parallel plate and the BET (40mm diameter vessel)

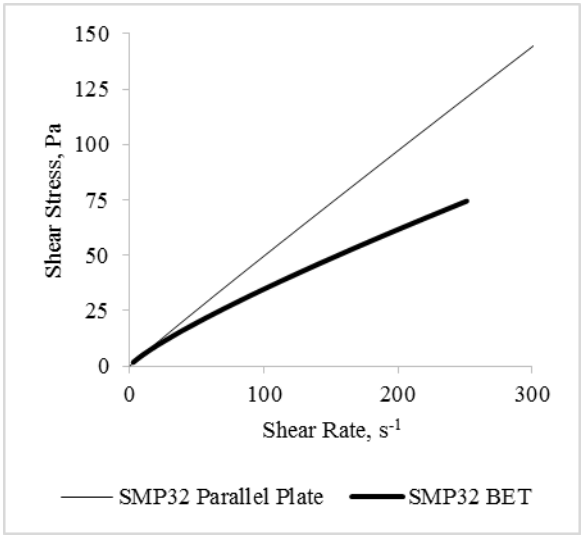


Figure 5.26: Rheological behaviour of SMP32 measured using a parallel plate and the BET (40mm diameter vessel)

Over the range of shear rates measured by the BET, the shear stress of SMP43 was similar to the parallel plate results (Figure 5.27), as were the parameters of the power law model. When the probe was roughened, the data showed more shear thinning behaviour and a higher consistency coefficient which did not fit as well with the parallel plate measurements. Due to the larger vessel being used, it was unavoidable that lower values of shear rate were created at the wall

The BET results of SMP47 were lower than the parallel plate results. Similarly to SMP43, the measurements with roughened walls showed a higher consistency coefficient and greater shear thinning behaviour than with smooth walls.

Increasing the solids content further, BET measurements of SMP56 no longer followed the same trend as measured using the parallel plate rheometer. Similarly to the other suspensions, the roughened wall BET tests showed a higher consistency coefficient and a lower n than with smooth surfaces. As these suspensions had a reasonably high solids content, the parallel plate results may have been less reliable: the gap size within the rheometer was only 3 times the size of the SMP particles, increasing the likelihood of being unable to measure the bulk flow behaviour of the suspensions. Phase migration and instabilities at the edges of the samples were more frequently observed when the solids content of the suspensions is higher. This reduced the confidence we had in the parallel plate measurements and therefore it was not possible to determine which of these techniques may have been correctly measuring the flow behaviour of SMP47 and SMP56.

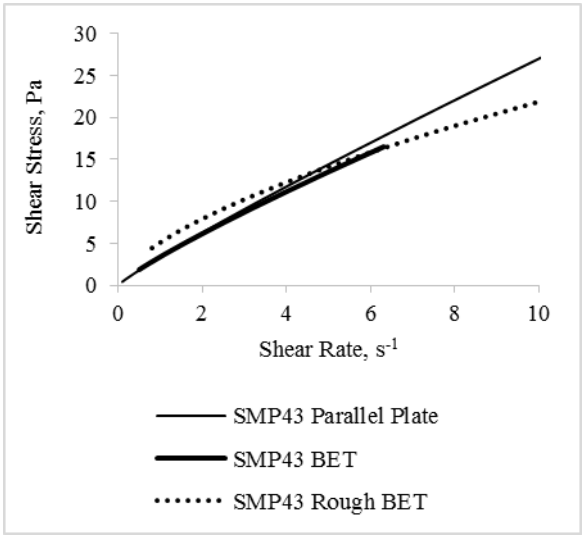


Figure 5.27: Rheological behaviour of SMP43 measured using a parallel plate and the BET (90mm diameter vessel)

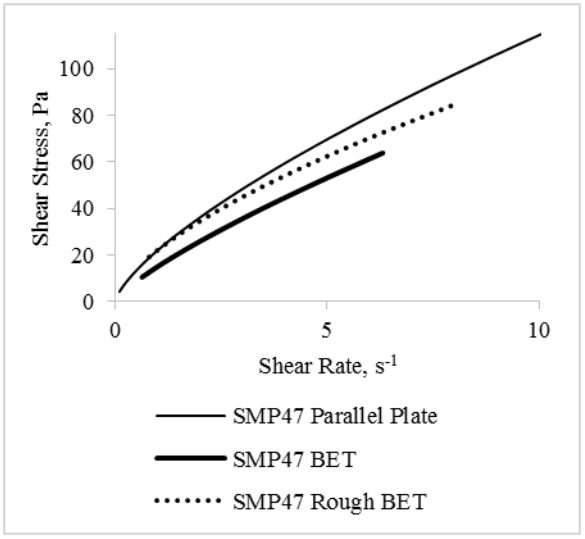


Figure 5.28: Rheological behaviour of SMP47 measured using a parallel plate and the BET (90mm diameter vessel)

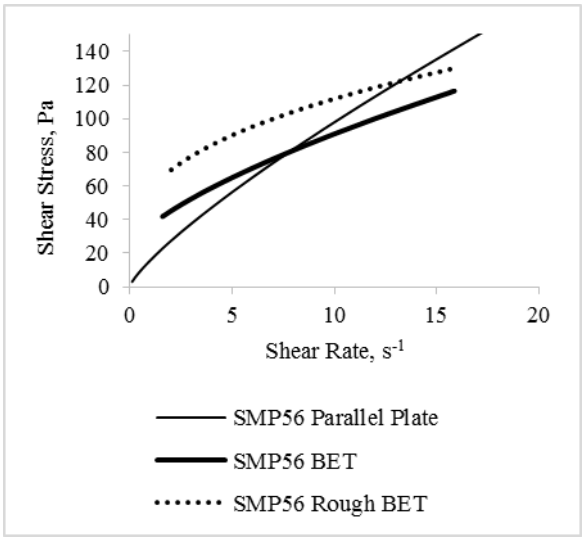


Figure 5.29: Rheological behaviour of SMP56 measured using a parallel plate and the BET (90mm diameter vessel)

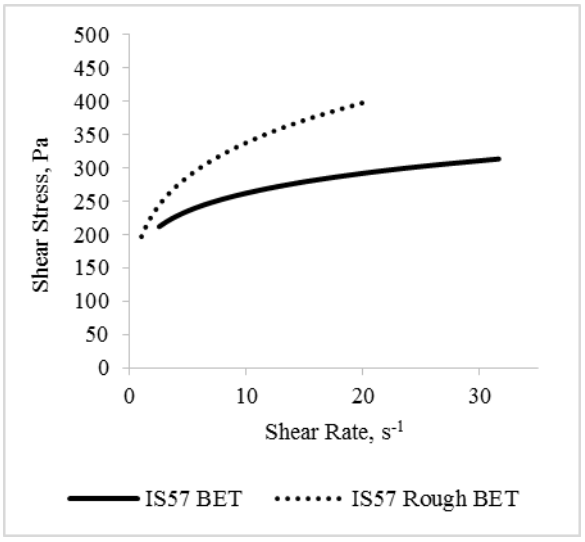


Figure 5.30: Rheological behaviour of IS57 measured using a parallel plate and the BET (90mm diameter vessel)

Phase migration readily occurred when IS57 was sheared between parallel plates, likely due to the high concentration of monomodal particles. The granulated sugar contained particles up to 1000µm, larger than a gap that is practical for parallel plate rheology. It was therefore not possible to compare the BET results to parallel plate measurements for IS57, GS60, CP62, CP68 and CP74.

It was discussed in section 5.2.3 that the positive curvature of the force increase as the plunger entered the sample of IS57 indicated that the material may have been slipping. A similar shaped force increase was observed when the walls were roughened. It was hypothesised that if slip was occurring, it was not reduced by roughening the walls. Conversely, the results of shear stress in Figure 5.30 were lower when the walls were smooth than when the walls were roughened. This suggests that the occurrence of slip was being reduced by roughening the walls however it disagrees with the hypothesis that the curved shape of the force as the probe enters the sample was due to slip at the wall.

This result may be explained by the sensitivity results in section 5.3.2; the probe and vessel diameters when the walls were roughened were established by summing the probe diameter/vessel diameter, respectively, with the thickness of the sandpaper. It may be possible that when the sandpaper was attached to the walls, there may have been some inaccuracy leading to the gap between the probe and the vessel becoming smaller. Several potential causes of experimental error have been listed below:

- It was observed that some fluid at the base flowed into the gap between the wall and the sandpaper, making the gap smaller,
- Sandpaper wrapped around the probe became visibly loose around the bottom end of the probe during the tests which increased the diameter of the probe in some regions,
- Double sided adhesive tape used to hold the sandpaper in place may have decreased the gap further.

These factors may all have contributed to producing a smaller gap than has been used as an input parameter for the data processing. In this case, illustrated by Figure 5.24, the yield stress and consistency coefficient of the material would have been calculated to be larger (the flow behaviour index would be very slightly lower). This may explain why SMP43, SMP47, SMP56, IS57, and CP68 all had higher values of consistency coefficient. Roughened wall tests of SMP74 resulted in a much higher yield stress and Figure 5.34 shows that the shear stress was much higher than when the walls were smooth. SMP62 also had a much higher value of yield stress when the walls were roughened, however Figure 5.32 does not suggest that the overall shear stress is larger.

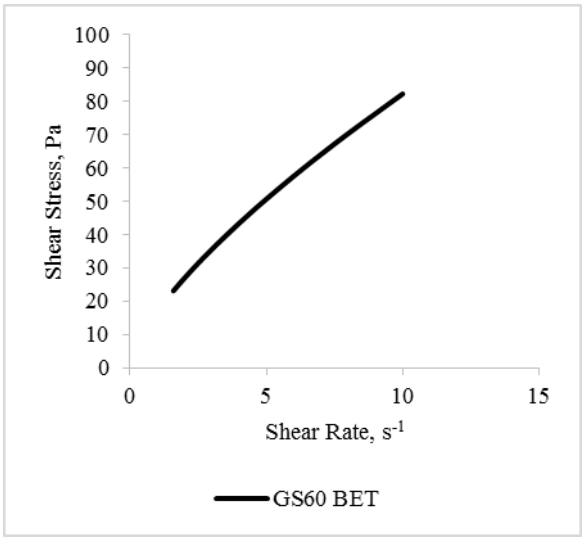


Figure 5.31: Rheological behaviour of GS60 measured using a parallel plate and the BET (90mm diameter vessel)

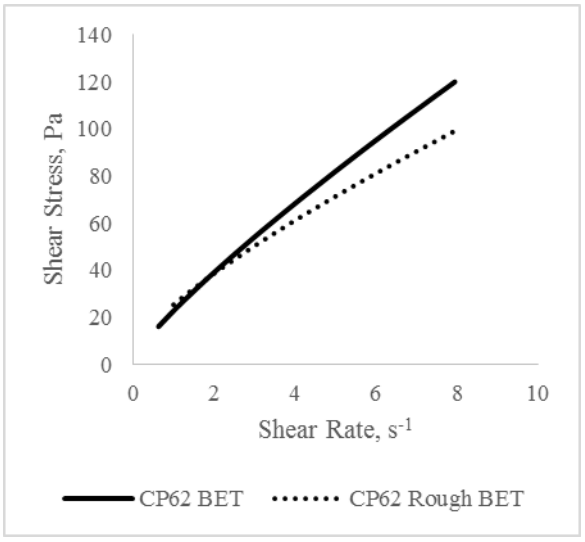


Figure 5.32: Rheological behaviour of CP62 measured using a parallel plate and the BET (90mm diameter vessel)

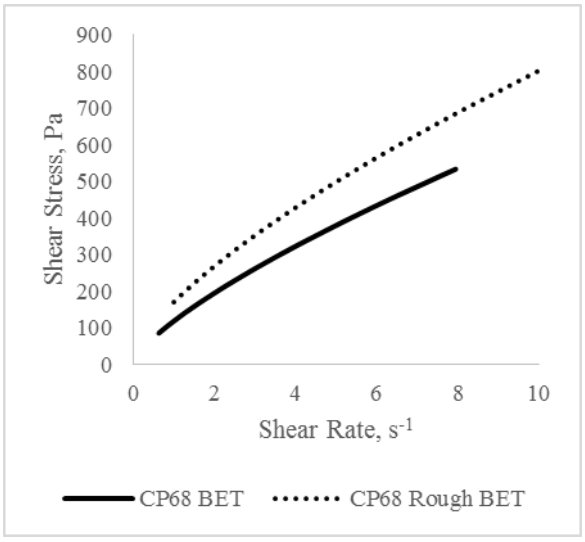


Figure 5.33: Rheological behaviour of CP68 measured using a parallel plate and the BET (90mm diameter vessel)

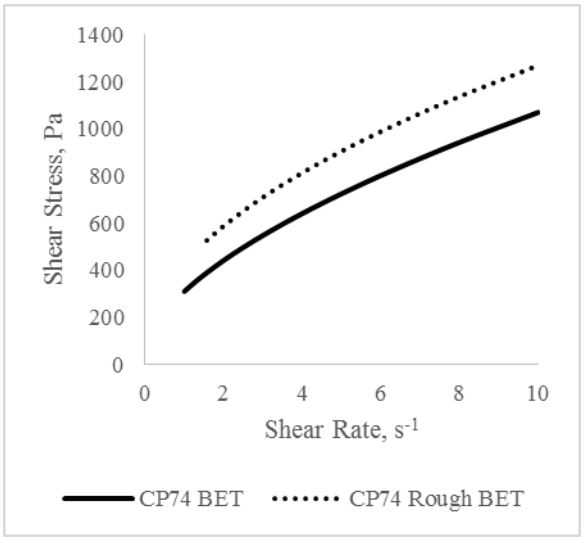


Figure 5.34: Rheological behaviour of CP74 measured using a parallel plate and the BET (90mm diameter vessel)

The BET was able to measure sensible values of the rheological behaviour of these three chocolate pastes that contained particles up to 1000 µm within suspensions containing up to 74 vol% particles. The rheological properties increased as the solids volume content was increased and all three pastes could be distinguished from one another. Roughening of the walls appeared to lead to different results but it was not anticipated that these differences were

due to the reduction in slip at the walls. Instead, experimental error of attaching sandpaper to the cylindrical surfaces of the probe and vessel was thought to be impacting on the width of the annulus which could not be accounted for in the analysis of the raw data. This lead to differences in the results of the rheological model parameters which had been found to be particularly sensitive to the gap width.

To investigate the reliability of the rheological model parameters which were used to fit to the raw BET data, it was possible to look at the spread of repeated results for each test. Figure 5.35, Figure 5.36, Figure 5.37 and Figure 5.38 show the three Herschel-Bulkley parameters describing the three chocolate pastes and the shear stresses of these three chocolate pastes when the shear rate was 10 s^{-1}. Pairwise comparisons were carried out using a Students t-test to identify whether there were statistically significant differences between the three different chocolate pastes. All pairwise comparisons showed a significant difference (p-value < 0.0001) other than the yield stress of CP62 and CP68 (p-value = 0.4765). This indicates that from the repeats which were carried out, a 6 vol% difference in fat content will produce a significantly difference in the rheological behaviour of the chocolate pastes.

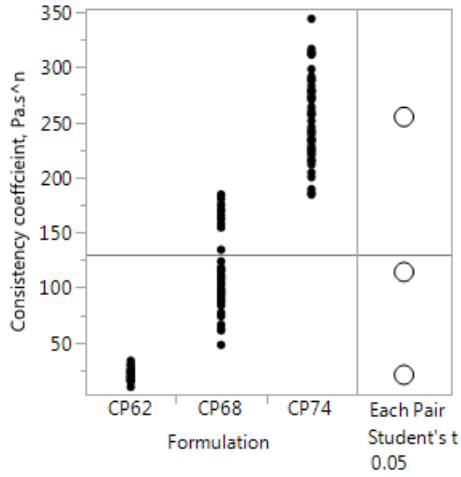


Figure 5.35: Consistency coefficients of each measurement of three chocolate pastes. Comparison circles are shown on the right which indicate that all three formulations are significantly different.

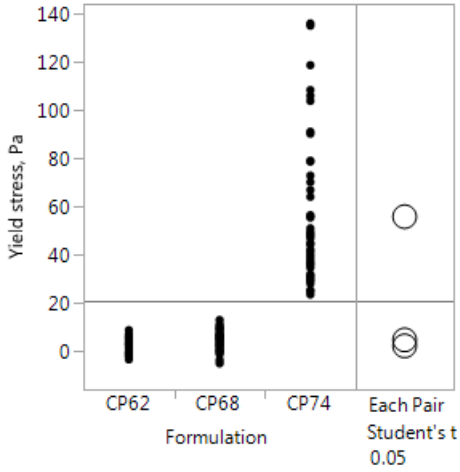


Figure 5.36: Yield stresses of each measurement of three chocolate pastes. Comparison circles are shown on the right which indicate that the yield stress of CP74 is significantly different to the yield stresses of CP62 and CP68.

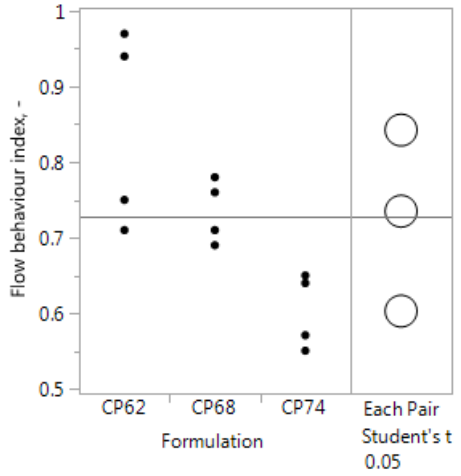


Figure *5.37*: Flow behaviour indices of each measurement of three chocolate pastes. Comparison circles are shown on the right which indicated all three formulations are significantly different.

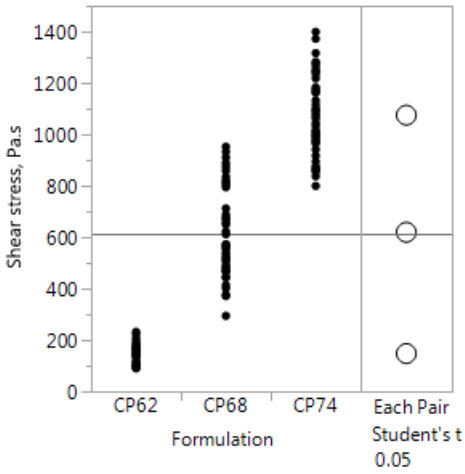


Figure 5.38: Shear stresses, at a shear rate of 10 s^{-1} of each measurement of three chocolate pastes. Comparison circles are shown on the right which indicated all three formulations are significantly different.

5.3.4 Effect of probe ratio

Since the analysis of the raw data should have accounted for changes to the annulus width, the results using four probes with different diameters should have given the same measurements of the flow behaviour. As the measurements of chocolate pastes are relevant to the subsequent

chapters, the results presented here compare measurements of three chocolate pastes: CP62, CP68 and CP74 using four probes with different diameters (20, 25, 30 and 35 mm).

Table 5.11 shows the p-values from nine ANOVAs, designed to establish whether there were significant differences between results produced using the four probe radii for the yield stress, consistency coefficient and the value of shear stress at a shear rate of 10 s^{-1} for the three chocolate pastes. The results could not analyse the results of the flow behaviour indices as for each probe radius, only one value of flow behaviour index was determined. The results indicate that there were statistically significant differences in all the results except for the yield stresses of CP62.

Table 5.11: Results of nine ANOVAs investigating whether there are statistically significant differences between the yield stress, consistency coefficient and shear stress at a shear rate of 10 s^{-1} for the three chocolate pastes when measured at four different probe diameters. Values of p-value are shown and are considered significant if they are below 0.05.

	p-values for the yield stress	p-values for the consistency coefficient	p-values for the shear stress at a shear rate of 10 s^{-1}
CP62	0.7625	0.0128	< 0.0001
CP68	0.0018	< 0.0001	< 0.0001
CP74	< 0.0001	0.0002	0.0048

To further investigate this variation, Tukey HSD tests were run to establish which probe diameters produced significantly different results. To view the results, the connecting letters reports are shown in Table 5.12 - Table 5.19. Comparing the results for the three different suspensions, the results do not strongly indicate whether any of the probes in particular may be unsuitable for measuring the pastes.

Table 5.12: Connecting letters report from a Tukey HSD test of the consistency coefficients of CP62 measured using four different probe diameters.

Probe diameter, mm	Connecting letters			Mean, Pa.s^n
30	A			23.92
25	A	B		21.06
35	A	B		20.42
20		B		17.36

Table 5.13: Connecting letters report from a Tukey HSD test of the shear stresses, measured at a shear rate of 10 s^{-1} of CP62 measured using four different probe diameters.

Probe diameter, mm	Connecting letters		Mean, Pa
35	A		179.49
20	A		164.28
30		B	124.31
25		B	121.30

Table 5.14: Connecting letters report from a Tukey HSD test of the consistency coefficients of CP68 measured using four different probe diameters.

Probe diameter, mm	Connecting letters			Mean, Pa.s^n
35	A			166.29
30		B		108.80
25		B		99.68
20			C	81.55

Table 5.15: Connecting letters report from a Tukey HSD test of the yield stresses of CP68 measured using four different probe diameters.

Probe diameter, mm	Connecting letters		Mean, Pa
35	A		6.98
30	A		5.57
25	A	B	4.53
20		B	1.26

Table 5.16: Connecting letters report from a Tukey HSD test of the shear stresses, measured at a shear rate of 10 s^{-1}, of CP68 measured using four different probe diameters.

Probe diameter, mm	Connecting letters			Mean, Pa.s^n
35	A			859.80
30		B		631.65
25			C	492.73
20			C	492.66

Table 5.17: Connecting letters report from a Tukey HSD test of the consistency coefficients of CP74 measured using four different probe diameters.

Probe diameter, mm	Connecting letters		Mean, Pa
35	A		291.58
30	A	B	258.17
25		B	238.37
20		B	231.64

Table 5.18: Connecting letters report from a Tukey HSD test of the yield stresses of CP74 measured using four different probe diameters.

Probe diameter, mm	Connecting letters			Mean, Pa.s^n
35	A			98.79
30		B		52.76
25		B	C	38.67
20			C	32.63

Table 5.19: Connecting letters report from a Tukey HSD test of the shear stresses, measured at a shear rate of 10 s^{-1}, of CP74 measured using four different probe diameters.

Probe diameter, mm	Connecting letters		Mean, Pa
35	A		1184.25
25	A	B	1078.77
20	A	B	1067.34
30		B	969.46

To further compare results using the four different sized probes, the shear stresses are plotted against the shear rates, based upon the average values of each Herschel-Bulkley parameter at each condition, over the range of shear rates which were calculated to be occurring during the BET. These are shown in Figure 5.39, Figure 5.40 and Figure 5.41. When the 25 mm and 30 mm probes were used to test CP62, the curvature of the result appeared to show more shear thinning behaviour than the results using the 20 mm or 35 mm probes (Figure 5.39). Visually, the results using the 35 mm probe stood out when used for testing CP68 and CP74 (Figure 5.40 and Figure 5.41); the shear stress was much higher than for the other three probes. It was not clear what the reason for these differences was and further investigation is recommended.

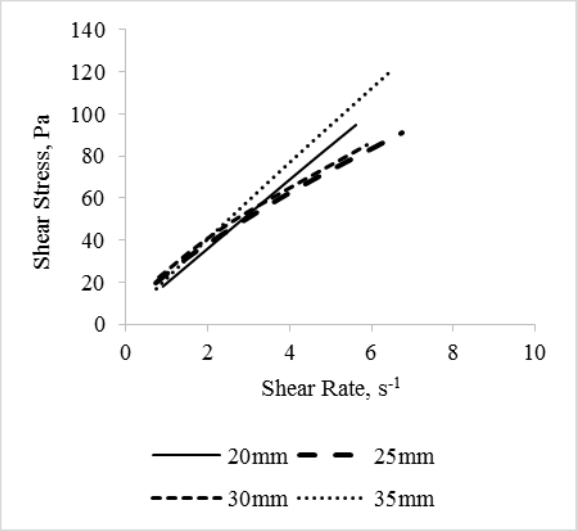


Figure 5.39: Rheological behaviour of CP62 measured using four probes with different diameters

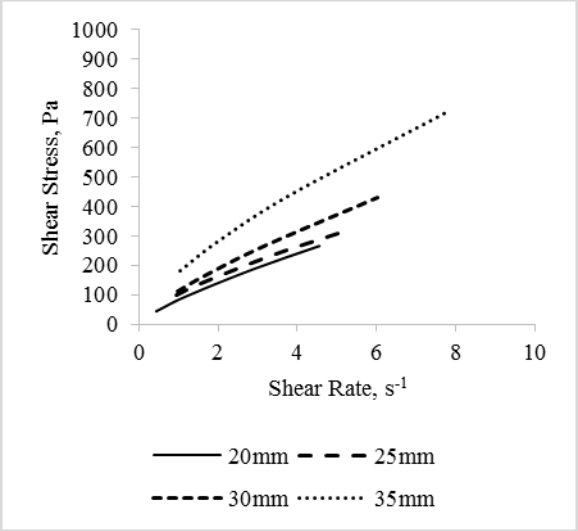


Figure 5.40: Rheological behaviour of CP68 measured using four probes with different diameters

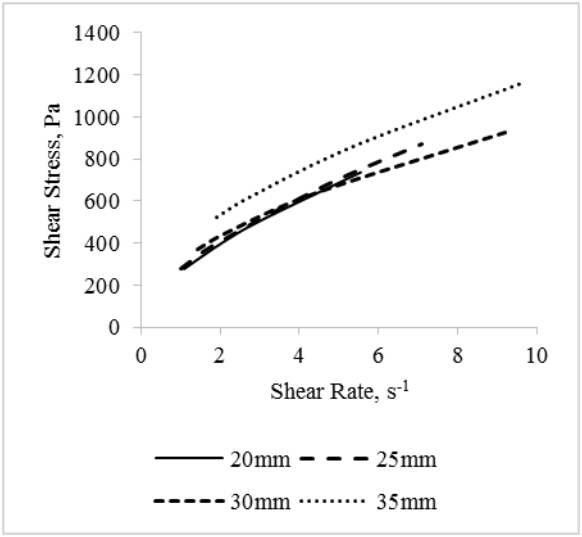


Figure 5.41: Rheological behaviour of CP74 measured using four probes with different diameters

5.3.5 Shear rates relevant within the manufacturing process

The size of the gap in the BET must be large enough to accommodate the large particles within the suspensions however this results in limitations of the shear rates generated within the tests. In a similar manner to Klein et al. (2017), it was possible to estimate characteristic shear rates ($\dot{\gamma}_c$) which were generated within key regions of the chocolate manufacturing process, using equation 5.9.

$$\dot{\gamma}_c = \frac{U_1 - U_2}{d_p} \qquad (5.9)$$

where U_1 and U_2 are linear velocities, calculated from the angular velocity using $U = \omega r$.

In the mixing stage, the highest amount of shear will be generated between the blade edges and the wall. Based upon equation 5.9, the shear rates within this region of the mixers, used for the trials which are discussed in Chapter 6, are reported in Table 5.20. These vary between 43 – 140 s^{-1}.

Table 5.20: Estimated shear rates between the blade and the walls in the mixers which are used to produce the pastes discussed in Chapter 6.

Mixer type	**Paster clearance**	**Blade radius**	**Shaft Velocity**		**Linear velocity at tip**	**Shear rate at tip**
	m	**m**	**rpm**	**rad s^{-1}**	**m s^{-1}**	**s^{-1}**
Buhler	0.005	0.15	14	1.47	0.22	43.98
Buhler	0.005	0.15	25.5	2.67	0.40	80.11
Buhler	0.005	0.15	37	3.87	0.58	116.24
Aoustin	0.002	0.053	50	5.24	0.28	138.75

Table 5.21: Estimated shear rate between the second and third refiner rolls of the Lehmann refiner based upon producing particles with a diameter of 117 µm.

	Roll radius	**Shaft Velocity**		**Linear velocity at roll edge**	**Shear rate between rolls**
	m	***rpm***	***rad* s^{-1}**	***m* s^{-1}**	**s^{-1}**
Roll 2	0.13	60	6.28	0.82	9773.84
Roll 3	0.13	144	15.08	1.96	

The shear rates which were being achieved using the BET were a maximum of approximately 10 s^{-1}. The shear rates which occurred between the rolls in refining are several orders of magnitude higher than what can be measured by the BET. This suggests that the behaviour of the paste within the confines of the back extrusion tests may not be indicative of how the paste behaves within the refiner. The shear rates estimated to occur during the mixing of the pastes is only one order of magnitude higher than are achieved with the BET. It is also important to consider that the shear rates between the blades are localised regions where the shear rate is much higher than the overall batch average. It has not yet been established under what shear conditions the behaviour of paste is important to processing performance, however, these results do provide some confidence that the bulk appearance of the paste whilst it is being mixed is likely to be at a comparable shear rate to that which is achieved in the BET.

5.4 Conclusion

The objective of this chapter was to develop a technique that was able to quantify the rheological behaviour of chocolate pastes that were produced within the first mixing stage of chocolate manufacture. The back extrusion technique was developed, based on published work by Osorio and Steffe, for use with the power law and Herschel-Bulkley rheological models. Using a non-Newtonian polymer solution and particle suspensions of skimmed milk powder, it has been shown that this back extrusion technique can measure the shear stresses of fluids, over a range of shear rates, in agreement with results tested on a parallel plate rheometer. The technique was furthermore used to characterise suspensions of particles that were not possible to measure in conventional rheometers; suspensions containing particles up to 1000 μm at solid volume contents up to 0.72.

Since the force linearly increases as the probe enters the sample, suspensions of monomodal particles below $\varphi = 0.57$ and multimodal particles below $\varphi = 0.68$ were not considered to be affected by slip at the walls. At solids contents above these values, slip was thought to be occurring due to migration of the fat through the voids between particles. A suspension containing a multimodal PSD with $\varphi = 0.68$ was found to thicken as the probe entered the material. It has been hypothesised that the largest particles migrate towards to middle where the shear rate is lowest. Here, the velocity of the paste through the annulus is highest and thus large particles move more quickly than the bulk towards the surface. This created regions of particles with narrow PSDs, increasing the local viscosities. The common solution for preventing slip is to roughen the surfaces so that the packing of particles at the wall is similar to within the bulk. To roughen the walls, sandpaper was attached however the results suggested that this introduced error to the results due to the lack of accuracy of the gap size.

Two methods were compared to calculate the flow behaviour indices and they were both found to show comparable results. The consistency coefficient varied in order to compensate for difference in the flow behaviour index that was calculated first, resulting in comparable flow properties over the region of shear rates. It is therefore not appropriate to extrapolate the rheological model outside of the region of shear rates that have been measured.

Once the probe has fully plunged into the fluid and the probe was held stationary, any residual force additional to the buoyancy force could be attributed to the yield stress of the fluid. Over a 60 second hold, the force attributed to the yield stress showed some degradation. This has not been further investigated however this gradual reduction in force may agree with theories by Barnes and Walters (1985), who believe that fluids have a very viscous Newtonian plateau which would relax to nothing over enough time rather than a yield stress where the material remains completely stationary.

6 IMPACT OF FORMULATION AND PROCESSING CONDITIONS ON PASTE CONSISTENCY

6.1 Introduction

It is currently a challenge for manufacturing sites to produce consistent chocolate mass when the process of combining the raw ingredients produces a paste that frequently varies in consistency. The performance of the roll refiners is hugely dependent on the ability of the paste to resist the forces of the rolls, which will have a direct impact on the final particle size of the chocolate.

The pasting stage is generally regarded as a process simply to combine the raw ingredients together. When manufacturing sites have been built, this stage has not always been standardised and both the size and blade geometry of mixers can vary. There may also be different operating conditions used to mix the raw ingredients at different sites which have become accepted as the norm, despite the lack of underlying theory.

The powder ingredients are usually added at room temperature and the liquid components (cocoa butter, cocoa liquor and milk fat) are added between 40-50°C to ensure they are fully melted. The mixing process is a batch process which feeds multiple, continuous refiners. The operation of the refiners is controlled to achieve a particle size in the chocolate mass, even at the expense of productivity; changes in paste consistency affect the refining performance, often necessitating reductions in throughput. To ensure that the refiners are always full, batches of paste are continually manufactured and then held in the mixing vessel until level sensors on the refiner feed tray measure low levels of paste. As the mixing time of the paste is

not related to the throughput of the refiners, once each paste batch is mixed, it is held in the jacketed vessel and intermittently agitated until it is required by the refiners.

When more paste is required by the refiners, the material is dropped into a two-roll pre-refiner and then transported via an open belt to the feed trays of the five-roll refiners. Some operators will subjectively assess the material after the pre-refiner, based on its appearance and consistency when it is squeezed between their fingers, in order to decide on the best settings for the refiners. As the pre-refined paste passes through the five-roll refiners, it is common for operators to visually evaluate the coverage of materials on the refiner rolls. If the pre-refined paste is not evenly transferring onto each roll, they will change the settings of that particular five-roll refiner. There are guideline procedures to alter the refiner settings but the operators tend to rely on their experience to adjust the settings of each refiner independently.

Batches of the refiner flake from several refiners are then mixed in a conche and more cocoa butter must be added to produce liquid chocolate mass. Along with the PSD, the final viscosity of the conched chocolate is a key performance indicator. Prior to the fat being added, the temperature is increased up to 80°C which helps the moisture to evaporate from the refiner flake and develops the desirable cooked flavours within the chocolate. Since the particles are now very small, the material is stiff. High shear rates are created between the blade and the walls which help to spread the fat over the surface of particles. The increased spreading of the fat and the reduced moisture content both contribute towards lower chocolate mass viscosities. Once the fat is added, the material becomes much runnier and the remaining mixing time is only necessary to combine the solids with the extra fat to produce a homogenous liquid chocolate mass.

It has already been established (in section 5.3.3) that increasing the fat content of the paste will produce a paste with a thinner consistency. If less fat can be added during the pasting stage but by processing the paste differently, the PSD leaving the refiner is the same as a standard fat paste, it may be possible to add the standard quantity of fat into the conching stage, resulting in an overall chocolate mass with a lower fat content.

As cocoa butter is a high cost ingredient, emulsifiers are often added to chocolate to help reduce the viscosity without requiring extra cocoa butter. At some manufacturing sites, a proportion of the emulsifiers are added during the pasting stage and the remaining emulsifier is added into the conching stage however there is no published research which has explicitly determined what effect it would have on the paste, rather than the conched chocolate.

Two studies aimed to quantify how the paste consistency varies when the process settings are different and compare it with altering the fat content or the addition of lecithin, a common emulsifier. The first design of experiments (DoE) involved the manufacture of 19 pastes based on a full factorial design with 3 centred, replicated samples. The design had four factors, each at two levels: fat, lecithin, mixing time and mixing speed. The second trial was a design of experiments involving 21 pastes using a Response Surface Method. This design had four factors at three levels and there were two replicated samples within the design. The factors interrogated were fat, lecithin, mixing time and temperature.

For trial one, the cocoa liquor and cocoa butter were added as molten liquids, the powders were all room temperature. At a manufacturing scale, anhydrous milk fat (AMF), as has already been discussed, is added at 40°C in a liquid form however for experimental ease at pilot scale, the AMF was generally added directly from the fridge. Specific heat capacities were taken from the literature. Based on the mass, heat capacity and addition temperature of

each component, the temperature of the mixture was calculated based on the equation 6.1. A heat balance on the ingredients is shown in Table 6.1, indicating the paste temperature based solely on the ingredients.

$$T_{batch} = \frac{\sum_{i=1}^{n}(m.c_p.T)_i}{\sum_{i=1}^{n}(m.c_p)_i} \quad (6.1)$$

Table 6.1: Heat balance on the components of an average paste formulation used for trial 1, disregarding any heat losses to the environment or gains from the heating jacket

Ingredient	Temperature, T [°C]	Specific Heat Capacity, c_p [kJ/kg °C]
Cocoa butter	45	2.10 (Morad et al., 2000)
Cocoa liquor	45	[a] 2.10
AMF	7	2.10 (NZMP)
Sugar	20	1.24 (Cheméo, 2016)
Skimmed milk powder	20	1.26 (Hui, 2007)
Sweet whey powder	20	[a] 1.26
Lecithin	20	[a] 2.10
Net Property	[c] *27.05*	[b] *1.49*

[a] Could not find values for these within the literature.
[b] Specific heat capacity of the whole batch based on the specific heat capacity and mass of each component
[c] Temperature of the batch without any external heat gains or losses based on equation 6.1.

For trial two, the temperature of the material was a factor in the experimental design hence all the ingredients were pre-heated to the test temperature before they were added to the mixer. The average paste formulations for both trials are shown in Table 3.6.

6.2 Trial 1: Influence of fat content, lecithin content, mixing time and mixing speed

A full factorial design of experiments was created using JMP statistical software (SAS Institute Inc., North Carolina, USA) to understand the impact of fat content, lecithin content, mixing time and mixing speed on the paste consistency. Each factor was at two levels plus

there were three replicated *control* pastes (high, low and control levels listed in Table 6.2). From the replicated pastes, any significant lack of fit could be determined. The results plotted from the predictive models assumed linear dependence on the factors between the low and high levels.

A pilot plant scale line was used to manufacture 19 batches of pastes based on the formulation listed in Table 6.1. The processing conditions/formulation of each paste are detailed in Table 6.3. Each 120kg batch was manufactured in a single shaft blade mixer and the paste consistency was assessed using three techniques (as described in section 3.3):

- Operator assessment on an ordinal scale from 0 - 10
- Mixing shaft measurements of current
- A simple back extrusion technique using the TA.XTplus from Stable Micro Systems

Table 6.2: List of high, low and control points that were used in the full factorial DoE of paste

Factor	Low	Control	High
Fat content, vol %	29.5	32.1	34.5
Lecithin content, vol %	0.00	0.08	0.15
Mixing time, minutes	2	10	18
Mixing speed, rpm	14.0	25.5	37.0

Along with looking at the significant effect of each individual factor, two-way interactions were included in the fit of models using standard least squares regression. Two-way interactions highlighted whether any of the factors affected each other, causing them to respond in a different way.

Table 6.3: Levels of each factor used for the runs of the DoE in trial 1

Run #	Fat content, vol %	Lecithin content, vol %	Mixing time, minutes	Mixing speed, rpm
1	29.5	0.15	18	37
2	34.5	0.15	18	37
3	32.1	0.08	10	25.5
4	29.5	0.15	2	14
5	34.5	0	18	37
6	29.5	0	2	37
7	34.5	0	2	14
8	29.5	0	2	14
9	34.5	0.15	2	37
10	32.1	0.08	10	25.5
11	29.5	0	18	14
12	34.5	0	18	14
13	34.5	0.15	2	14
14	34.5	0.15	18	14
15	32.1	0.08	10	25.5
16	29.5	0.15	18	14
17	29.5	0.15	2	37
18	34.5	0	2	37
19	29.5	0	18	37

6.2.1 Comparisons of the techniques to quantify paste consistency

The measured values of each paste using the simplified back extrusion technique, the values of current draw of the mixing shaft at the end of mixing and the operator ranks of the pastes at the end of the mixing process are summarised in Table 6.4. Values of the Herschel-Bulkley model parameters, calculated from the results of the simplified back extrusion technique, are summarised in Table 6.5.

.

Table 6.4: Measured peak and relaxation forces using the simplified back extrusion technique, values of the current at the end of mixing and operator ranks for each paste produced in trial 1

Run	Peak force at 2 mm s^{-1}	Peak force at 4 mm s^{-1}	Relaxation force at 2 mm s^{-1}	Relaxation force at 4 mm s^{-1}	Mixing Shaft Current	Operator Rank
	N	N	N	N	A	-
1	1.068	1.641	0.321	0.385	0.93	6
2	0.344	0.468	0.187	0.182	0.65	10
3	0.484	0.741	0.184	0.184	0.21	4
4	1.943	2.677	0.321	0.272	1.76	2
5	0.365	0.499	0.19	0.187	0.62	7
6	3.112	3.982	1.329	1.302	1.60	4
7	1.132	1.346	0.459	0.41	0.32	5
8	2.016	2.211	0.559	0.365	1.24	2
9	0.351	0.476	0.184	0.187	1.05	6
10	0.481	0.693	0.182	0.181	0.22	6
11	0.969	1.423	0.221	0.219	0.20	4
12	0.635	0.925	0.192	0.195	0.05	6
13	0.362	0.49	0.186	0.186	0.38	4
14	0.284	0.353	0.191	0.191	0.08	6.5
15	0.464	0.654	0.189	0.189	0.16	6
16	0.565	0.91	0.187	0.187	0.14	5
17	0.729	1.111	0.195	0.195	1.43	4
18	0.357	0.506	0.184	0.181	1.05	5
19	0.567	0.814	0.19	0.189	0.97	7

Table 6.5: Calculated values of Herschel-Bulkley model parameters based upon the measured values using the simplified BET for each paste produced in trial 1

Run	Flow Behaviour Index	Consistency Coefficient	Yield Stress	Shear Stress at 10 s^{-1}
	-	Pa.s	Pa	Pa
1	0.86	59.84	80.96	514.46
2	0.98	11.21	11.48	118.53
3	1.04	43.37	3.09	478.63
4	0.51	230.11	50.55	795.17
5	0.90	10.98	10.53	97.75
6	0.30	22.76	771.93	817.34
7	1.28	16.16	113.59	421.51
8	1.07	92.03	108.43	1189.69
9	0.93	9.32	12.96	92.29
10	0.72	32.80	4.42	176.56
11	0.61	81.50	16.42	348.43
12	0.57	57.61	9.23	223.27
13	0.84	11.10	10.78	87.57
14	1.02	0.64	24.15	30.85
15	0.74	14.73	4.72	85.67
16	0.86	46.35	4.61	340.39
17	0.69	67.81	7.45	339.57
18	1.15	11.24	11.10	169.87
19	0.74	43.68	6.17	246.21

Principal component analysis (PCA) was used to compare the three techniques which were used to quantify differences in the paste consistencies. The principle of this technique was outlined in section 3.4.2. Figure 6.1 shows a summary of the first two principal components when the results of operator rank and mixing shaft current were compared alongside the results of the back extrusion tests (flow behaviour index, consistency coefficient, yield stress and the shear stress at a shear rate of 10 s^{-1}). The first two principal components describe 76.6 % of the variation between the measurement techniques. The third principal component only correlated with the flow behaviour index of the paste therefore it was not of any value to

plot the result of this principal component. In Figure 6.1, the current measured on the mixer is located in the same region as the consistency coefficient and shear stress at a shear rate of 10 s^{-1} of the paste. This is directly opposite the operator ranking of the pastes, indicating that they were measuring similar differences between each formulation. These were not similar to the flow behaviour indices or the yield stresses of pastes; these two measurement values may be inversely correlated with each other.

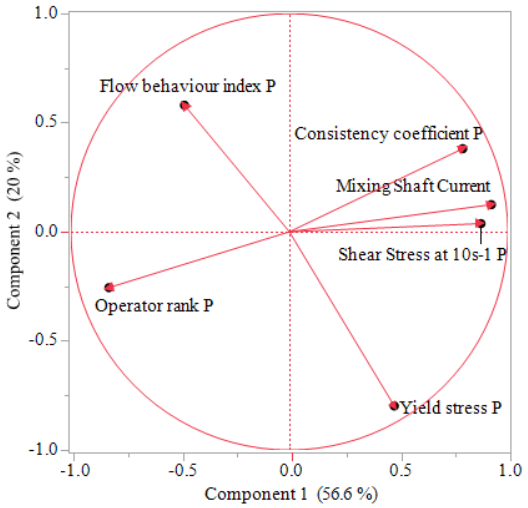


Figure 6.1: Loading plots of the first two principal components which describe 76.6 % of the variation between the operator rank, mixing shaft current, flow behaviour index, consistency coefficient, yield stress and the shear stress at a shear rate of 10 s^{-1} (final four measured using the BET)

6.2.2 Significant effects on the Herschel-Bulkley model parameters measured using the back extrusion technique

Samples were taken of the pastes in order to test them offline using the simplified back extrusion technique (BET) described in section 3.3.6. The Herschel-Bulkley model was used to describe the flow behaviour of the pastes (equation 4.8).

6.2.2.1 Yield stress

Many of the pastes were measured to have yield stresses below 25 Pa. Four pastes were measured to have yield stresses between 50 – 150 Pa and one paste was measured to have a

yield stress of 772 Pa. These are shown on a log plot in Figure 6.2. As the data, on a linear scale, was skewed by the high values of yield stress, the predictive model did not show a significant fit the data ($p\text{-value}_{ANOVA} = 0.27$). If this point is treated as an outlier, it was still not possible to fit a significant model to the remaining data ($p\text{-value}_{ANOVA} = 0.10$)

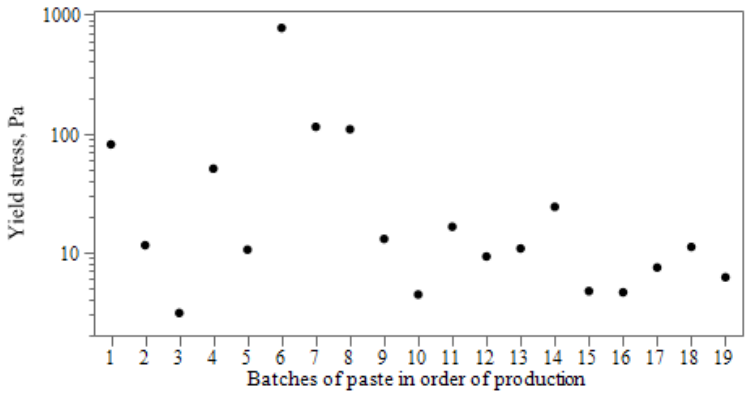


Figure 6.2: Yield stresses of the pastes which were produced in trial 1

6.2.2.2 Flow behaviour index, consistency coefficient and shear stress

Statistical analysis results revealed that the predictive models did not show a significant fit to the flow behaviour indices or the consistency coefficients (p-value = 0.27 and = 0.055, respectively). The flow behaviour indices were established using the results from only two probe velocities hence this may not have been an accurate interpretation of the shear thinning behaviour of the pastes. It was concluded in chapter 0 that the consistency coefficient will compensate for the flow behaviour indices which may also explain why the consistency coefficients cannot be significantly modelled. However, this does suggest that the overall values of shear stress may be more representative of the paste texture variations.

Based upon the values of the three Herschel-Bulkley model parameters, the shear stresses at a shear rate of 10 s^{-1} were calculated. The simplified back extrusion technique determined that the shear rate at the probe wall could reach 14 s^{-1} so values of shear stress at a shear rate of

10 s^{-1} were within the measured region. A predictive model was fit to this data and was found to be significant (p-value = 0.012). From this model, it was shown that increasing the fat content and increasing the mixing time both significantly decreased the shear stress of the pastes (Table 6.6).

Increasing the liquid content of the paste was expected to reduce particle-particle interactions as particles would be spaced further apart. This agrees with comments by Beckett (2008) who discusses that if most of the fat is immobilised at surfaces of particles, small additions of fat content will have a considerable effect on lubricating the particles.

When the mixing time was increased, this was likely to increase the homogeneity of the paste. More particle surfaces will then have been coated by fat which reduces the interactions of particles with each other.

Table 6.6: Significance of factors and interactions on the shear stress at a shear rate of 10 s^{-1} of paste (p-value$_{ANOVA}$ = 0.012)

Term	**p-value**	**Significant**
Fat Content, vol%	0.0009	*
Mixing Time, minutes	0.0166	*
Fat Content * Mixing Time	0.0655	
Lecithin Content * Mixing Time	0.0686	
Lecithin Content, vol%	0.1001	
Mixing Time*Mixing Speed	0.1276	
Mixing Speed, rpm	0.1528	
Lecithin Content * Mixing Speed	0.3396	
Fat Content * Mixing Speed	0.4906	
Fat Content * Lecithin Content	0.9666	

6.2.3 Significant effects on the online measuring techniques

6.2.3.1 Operator rank

Despite the categories used to rank the paste being discrete, a significant predictive model was found to fit the data (p-value = 0.0077) although it was important to take into consideration that there could have been some bias in these results as the operator was aware of the formulation and operating conditions. Similarly to the offline BET measurements, increasing the fat content or the mixing time resulted in a significantly thinner paste consistency. Higher mixing speeds were also shown to significantly decrease the consistency of the paste which could be due to similar principles which create a thinner paste when the mixing time is longer.

Table 6.7: Significance of factors and interactions on the operator rank of paste

Term	p-value	Significant
Mixing Time	0.0008	*
Fat Content, vol%	0.0032	*
Mixing Speed, rpm	0.0047	*
Lecithin Content, vol%	0.3728	
Fat Content *Lecithin Content	0.3770	
Lecithin Content*Mixing time	0.3771	
Lecithin Content *Mixing speed	0.5230	
Mixing time*Mixing speed	0.5230	
Fat Content *Mixing speed	0.6991	
Fat Content *Mixing time	0.8970	

6.2.3.2 Power Draw of the Mixer

A predictive model significantly fits the values of current draw (p-value = 0.015); there was a significant effect of fat content, mixing time and the interaction between fat and mixing time. Overall, these results showed a similar trend to the operator ranking, suggesting that when the consistency appears to be visibly thinner, the mixing shaft was also finding it easier to move

through the paste. Unlike the operator ranking results, there was no significant effect of the mixing speed.

Table 6.8: Significance of factors and interactions on the current draw of the mixer

Term	p-value	Significant
Mixing Time	0.0010	*
Fat Content, vol%	0.0040	*
Fat Content * Mixing time	0.0484	*
Mixing time* Mixing speed	0.2513	
Fat Content * Mixing speed	0.3820	
Mixing Speed, rpm	0.4007	
Lecithin Content * Mixing speed	0.4974	
Lecithin Content * Mixing time	0.6729	
Lecithin Content, vol%	0.7641	
Fat Content * Lecithin Content	0.9009	

The relationship of fat content and mixing time is shown in Figure 6.3. When there was a higher fat content, the effect of mixing time was not as large as when the fat content is low. It is not yet understood why the amount of fat content influences the effect of mixing time.

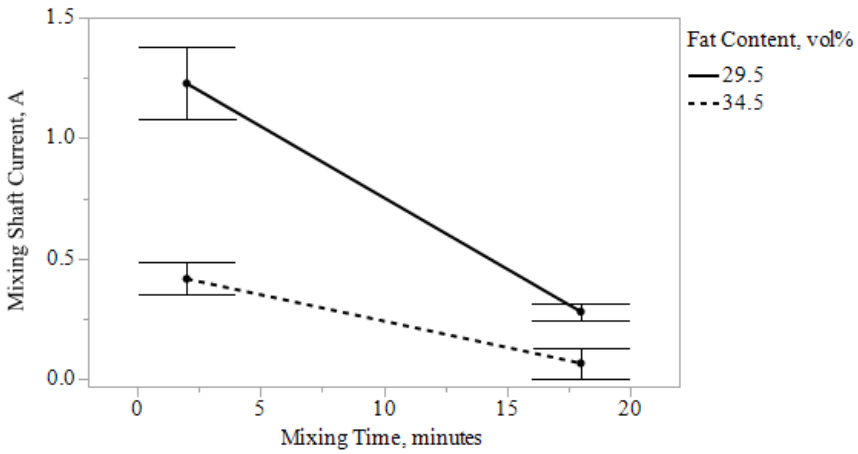


Figure 6.3: Interaction between fat and mixing time significantly impacts the current measured onthe mixer. The results from the predictive model are plotted and the error bars are the standard deviation.

6.2.3.3 Effect of Temperature

Firstly, examining the temperatures measured at the end of each mixing period, although the mixer was jacketed using 45 °C water, Figure 6.4 shows that the paste did not increase above 34 °C after a maximum of 18 minutes of mixing. From the comparisons of the temperature before and after mixing, all the pastes increased in temperature whilst contained within the jacketed vessel (Figure 6.4).

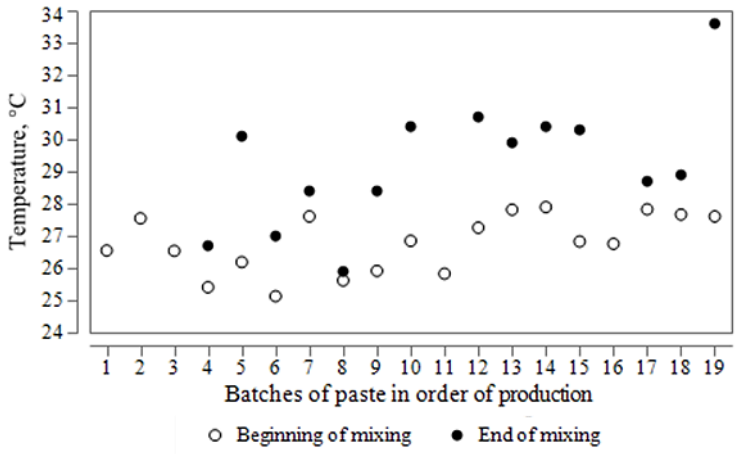


Figure 6.4: Temperatures of the pastes which were produced in trial 1. Temperatures at the beginning were established from the raw ingredients and temperatures were measured using a temperature probe at the end of the mixing duration. Some gaps exist where the temperature was not recorded.

A statistical model was fitted to the temperatures of the pastes measured at the end of the mixing batch and was found to be significant (p-value = 0.043). Despite differences in the fat content causing differences in the initial temperature of the batch, there was no significant effect of the fat content independently. When the mixing time increased, the temperature of the pastes significantly increased confirming that the heated jacket on the vessel was continuously heating the paste whilst it remained within the vessel.

Table 6.9: Significance of factors and interactions on the paste temperature

Term	p-value	Significant
Mixing Time	0.0083	*
Fat Content * Mixing Time	0.0283	*
Fat Content * Mixing Speed	0.1546	
Lecithin Content	0.3364	
Fat Content * Lecithin Content	0.4056	
Mixing Speed	0.6108	
Lecithin Content * Mixing Time	0.6352	
Lecithin Content * Mixing Speed	0.7492	
Mixing Time * Mixing Speed	0.8123	
Fat Content	0.8733	

The interaction between the mixing time and the fat content also significantly impacted the temperature. Based on values from the predictive model, Figure 6.5 shows that when the fat content was low, the temperature increased a greater amount when the paste was mixing for longer than when there was a high fat content (p-value = 0.0279). This difference is unlikely to be due to the heat transfer coefficients of the ingredients varying as between the high and low fat pastes, there were only very small differences. It could have been due to more energy being imparted to the pastes by the mixing shaft, which would have been greater when the fat content was lower. As the blade was moving at a constant speed for the duration of mixing, more power was required to move the blade through a thicker paste. Therefore, more energy, i.e. work done, was imparted to the paste, some of which would have been released as heat. There may also have been more friction between particles, creating more heat when the particles were packed closer together and were more likely to interact with each other.

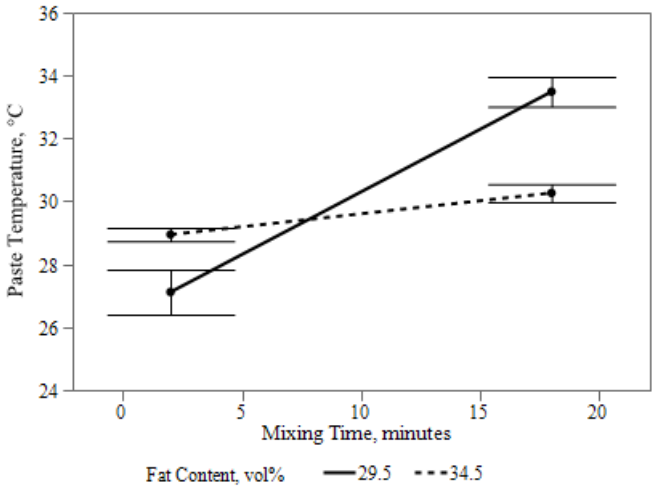


Figure 6.5: Interaction between fat content and mixing time significantly impacts the temperatures of pastes. The results from the predictive model are plotted and the error bars are the standard deviation.

From the plots in Figure 6.6, the operator ranking, the mixing shaft current and the shear stress at 10 s^{-1} measured on the BET all show correlations with the temperature of the paste. Results have shown that pastes mixed for longer became warmer, which was likely to be the cause of why the operator ranking and current of the mixing blade indicated thinner pastes.

The interaction between fat and mixing time also impacted the current measured on the mixing blades and the temperature. Pastes which had a low fat content heated up more if the mixing time was longer and these low fat pastes showed much more of an effect of the mixing time than higher fat pastes.

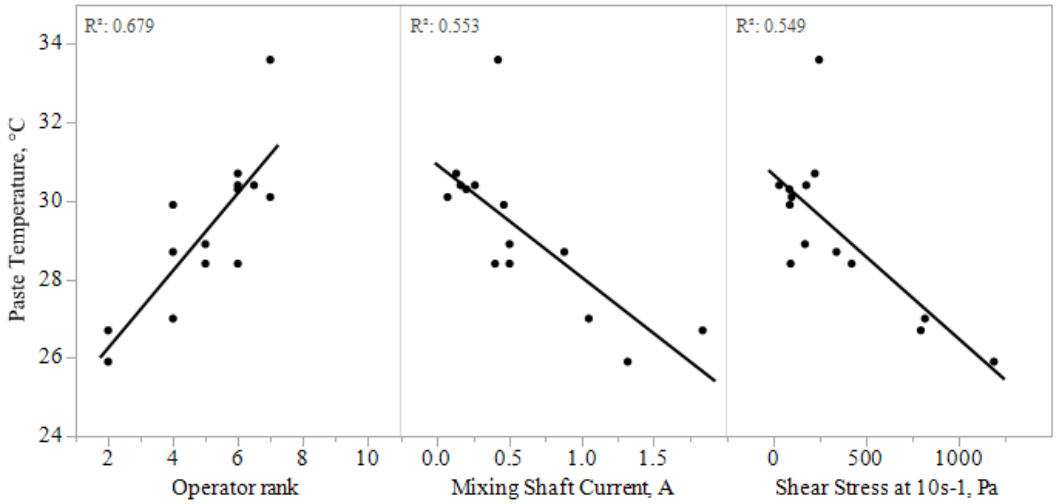


Figure 6.6: Temperatures of the pastes plotted against the consistency measurements. A line of best fit has been drawn and the value of R^2 is quoted.

Both the operator ranking and the current measured on the mixing blades were measured online and there were clear similarities between the consistency of the pastes and the temperatures of the batch. It would be beneficial for future work to establish whether changing the temperature of the paste, in order to manipulate the consistency, has any influence on the refiner performance. Alternatively, the temperature of the paste may be irrelevant to the refining performance as the temperature and pressure within the roll are so high. In this case, the temperature differences may mask the consistency of the paste which is relevant to refining and would cause difficulties for an operator if they assessed the paste visually or focussed on values of the mixing shaft current.

The shear stress of the pastes was measured offline on the BET where all samples were heated up to the same temperature although it still correlated with the temperatures of the paste online. Both measurements were affected by the mixing time; pastes which became warmer during the mixing stage also showed a thinner paste consistency despite the temperature of the measurements being consistent. When the temperature was warmer, the viscosity of the continuous phase was lower so it was likely that it was easier for the fat to coat particles and

flow between smaller gaps so that a greater proportion of the solids were lubricated. This did not indicate that the fat enters pores of the dairy powders as this would have been more likely if the fat was thinner, leading to an increased proportion of immobilised fat and a thicker consistency.

6.2.4 Significant effects on the particle size distributions

The particle size distributions (PSD) of each paste were measured, based on the method described in section 3.3.2. Each measured PSD displayed a tri-modal distribution and was therefore modelled by three weighted log-normal distributions, as was described in section 3.3.2. They were each then represented by nine parameters; standard deviation (S), mean (M), and a weighting (W), of each log-normal distribution. To provide a representation of what the particle sizes are within these pastes, the mean value of each model parameter is shown in Table 6.10 and based upon these, a particle size distribution has been reconstructed, using equation 3.1 (Figure 6.7).

The repeatability of the particle size measurement technique and subsequent modelling of the particle size distributions was discussed in section 3.3.2.3. This will be taken into consideration when discussing the results of the trials since measurements may have shown a statistically significant result (meaning that the difference in results is probably not due to chance) however in practice, the error of the measurements may have been greater than the differences between two results.

Table 6.10: Model PSD parameters averaged over all of the pastes produced in trial 1

Peak 1			Peak 2			Peak 3			SSA, $m^2 kg^{-1}$
S, µm	W	M, µm	S, µm	W	M, µm	S, µm	W	M, µm	
1.01	0.22	10.17	0.79	0.36	154.52	0.41	0.41	556.30	265.7

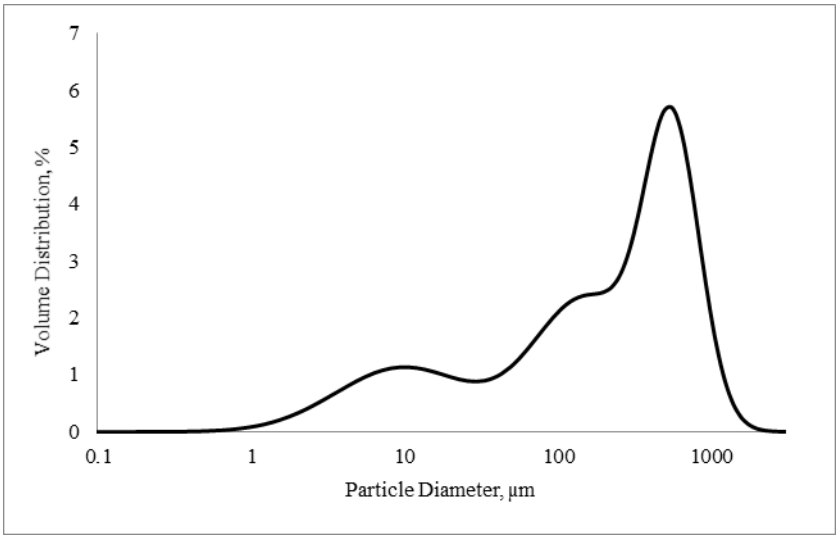


Figure 6.7: Average particle size distribution of all the pastes produced in trial 1

The mean and the weight of the first peak showed statistically significant differences when the fat content or mixing time was increased. There was also a statistically significant reduction of the specific surface area (SSA) when the fat content was increased. The PSDs, based on the predictive statistical models of the parameters when the fat content or mixing time were altered, are shown in Figure 6.8 and Figure 6.9. Although the results indicated statistical significance, considering the error due to the measuring and modelling of the PSDs discussed in section 3.3.2.3, the effects of fat content or mixing time are not thought have an important effect.

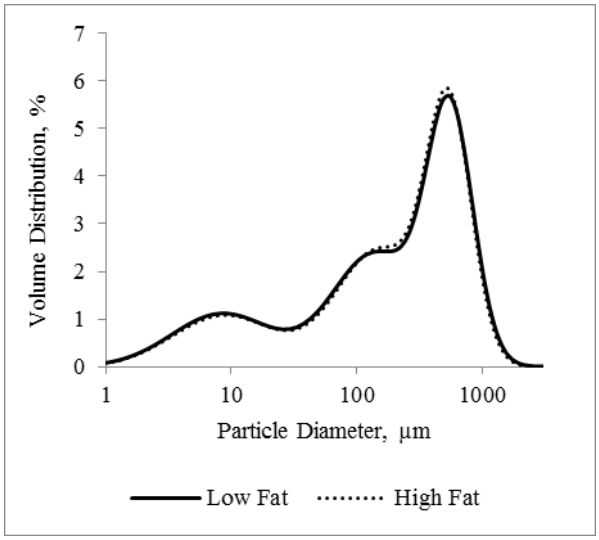


Figure 6.8: Influence of the fat content on the paste PSDs using the average model parameters from the least squares fit ($SSA_{low\ fat}$ = 271.6 $m^2\ kg^{-1}$, $SSA_{high\ fat}$ = 260.0 $m^2\ kg^{-1}$)

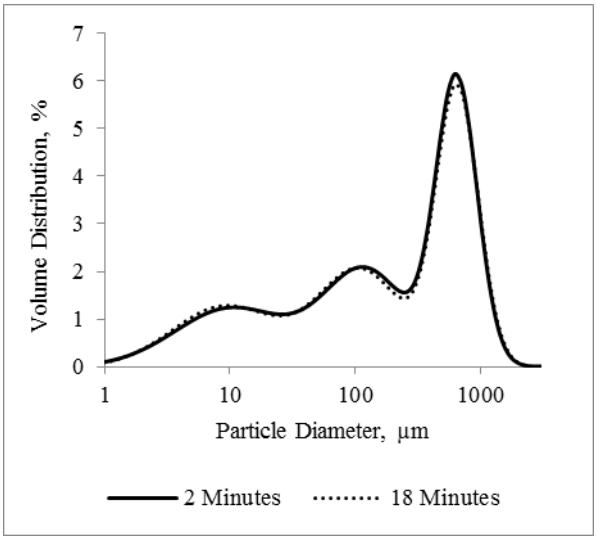


Figure 6.9: Influence of the mixing time on the paste PSDs using the average model parameters from the least squares fit

When the mixing speed was increased, the weighting of the first peak and the SSA both showed a statistically significant increase. From the visualisation of the PSDs in Figure 6.10, and again considering the error discussed in section 3.3.2, it was not possible to conclude that increasing the mixing speed resulted in a meaningful change of the size of the particles.

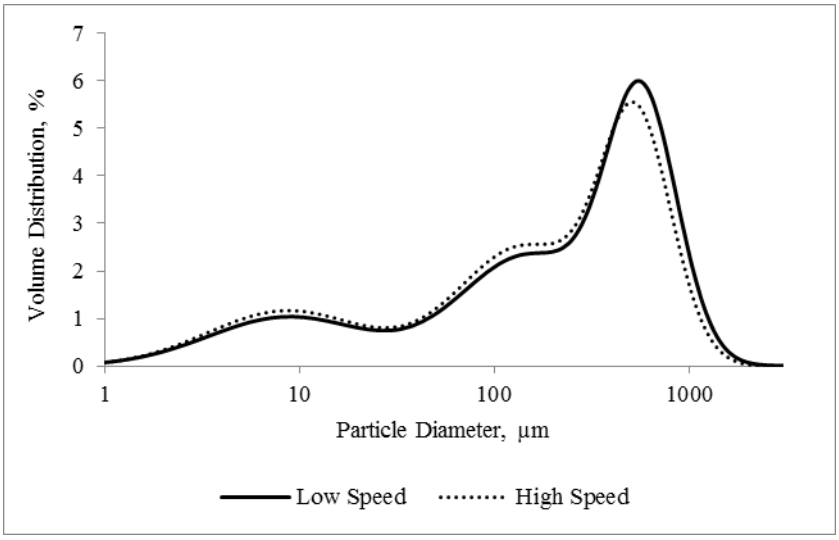


Figure 6.10: Influence of the mixing speed on the paste PSDs using the average model parameters from the least squares fit ($SSA_{low\ speed}$ = 256.1 $m^2\ kg^{-1}$, $SSA_{high\ speed}$ = 275.6 $m^2\ kg^{-1}$)

There was also a statistically significant effect of the interaction between mixing time and mixing speed on the mean of the first peak. The effect of this on the PSDs is shown in Figure 6.11. The two results which differed the most are when the mixing time was high and the mixing speed was varied; a higher mixing speed resulted in a larger proportion of small particles. The results at these conditions showed differences in their PSDs which were larger than the errors associated with the measuring and modelling techniques. However, the results where the mixing time increased from 2 minutes to 18 minutes were not thought to be greater than the inherent error of the technique.

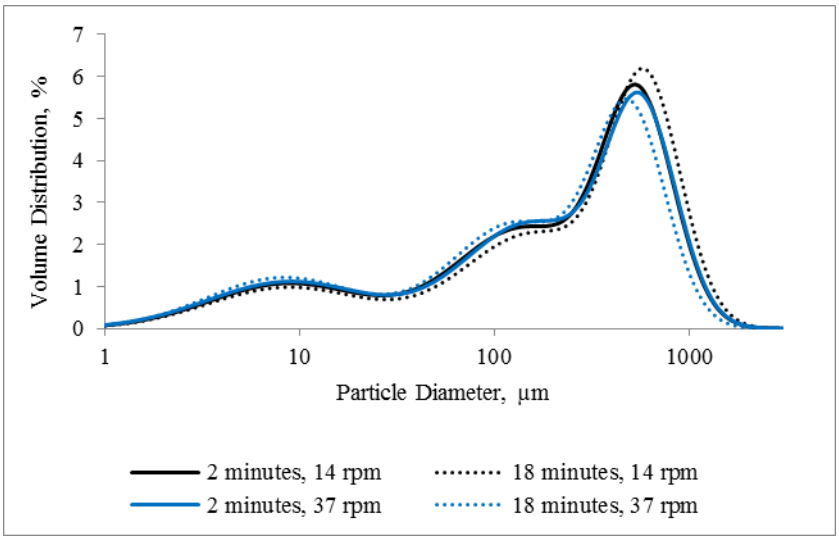


Figure 6.11: Influence of the mixing time and mixing speed on the paste PSDs using the average model parameters from the least squares fit

A significant interaction of the fat and mixing speed was found to have a statistically significant effect on the weighting of the first peak and the SSA (Figure 6.12). Based on the predictive values of the SSA and considering the errors discussed in section 3.3.2, the particles remained largest when there was a high fat content and the paste was mixed at the lowest speed. This does suggest that when the fat content was high, it enabled particles to more easily flow out of regions where they may have been sheared and broken.

There was also a statistically significant effect of the interaction between the lecithin and mixing time which affected the weight of the first peak. However, comparing the entire PSDs in Figure 6.13, it cannot be concluded that this interaction had a meaningful effect on the PSD.

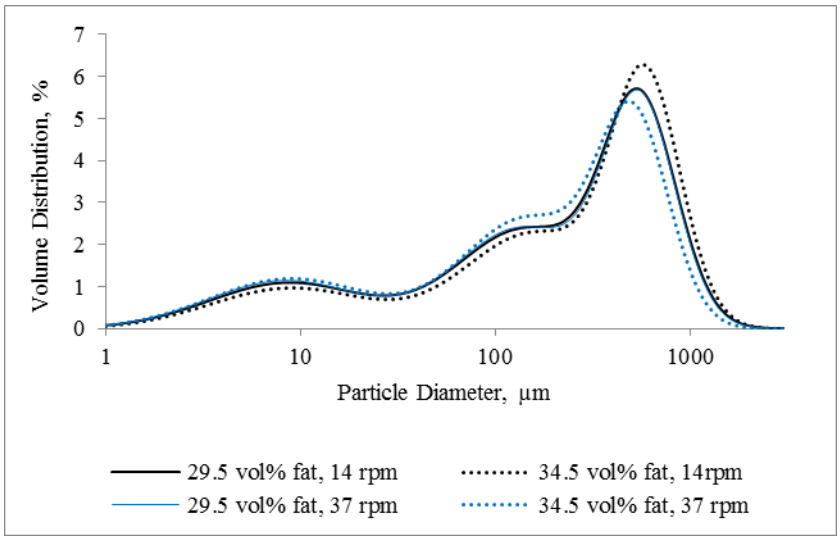


Figure 6.12: Influence of the fat content and mixing speed on the paste PSDs using the average model parameters from the least squares fit ($SSA_{29.5\%\ fat,\ 14\ rpm}$ = 268.5 $m^2\ kg^{-1}$, $SSA_{29.5\%\ fat,\ 37\ rpm}$ = 274.8 $m^2\ kg^{-1}$, $SSA_{34.5\%\ fat,\ 14\ rpm}$ = 243.6 $m^2\ kg^{-1}$, $SSA_{34.5\%\ fat,\ 37\ rpm}$ = 276.3 $m^2\ kg^{-1}$)

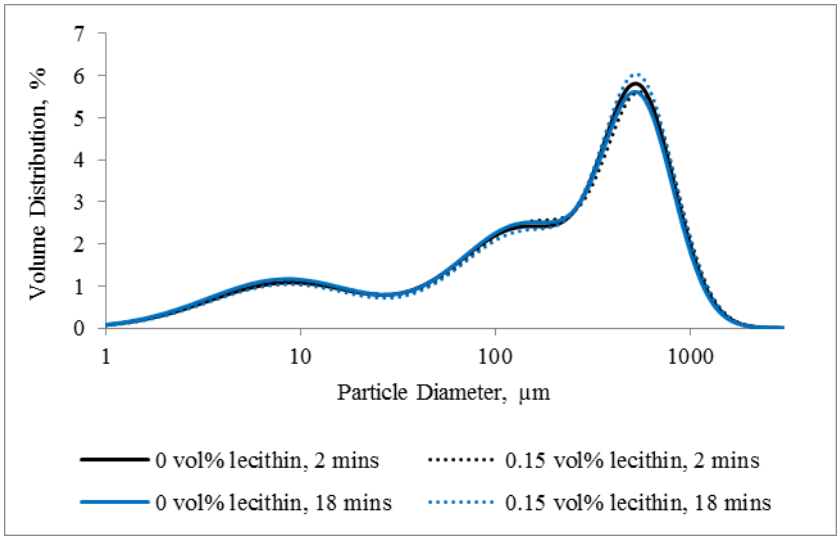


Figure 6.13: Influence of the lecithin content and mixing time on the paste PSDs using the average model parameters from the least squares fit

Table 6.11: Significance of factors and interactions on the standard deviation of the first paste PSD peak (p-value = 0.57)

Term	p-value	Sig.
Mixing time*Mixing speed	0.0848	
Fat Content	0.1785	
Mixing Time	0.2136	
Lecithin content*Mixing time	0.5484	
Fat content*Mixing speed	0.6229	
Lecithin Content, vol%	0.7069	
Fat content*Mixing time	0.7229	
Mixing Speed, rpm	0.7244	
Fat content*Lecithin content	0.7755	
Lecithin content*Mixing speed	0.9166	

Table 6.12: Significance of factors and interactions on the mean of the first paste PSD peak (p-value = 0.032)

Term	p-value	Sig.
Fat Content, vol%	0.0095	*
Mixing Time	0.0100	*
Mixing time*Mixing speed	0.0250	*
Mixing Speed, rpm	0.1573	
Lecithin Content, vol%	0.2249	
Fat content*Mixing speed	0.2688	
Lecithin content*Mixing speed	0.2892	
Fat content*Mixing time	0.3032	
Fat content*Lecithin content	0.4686	
Lecithin content*Mixing time	0.6451	

Table 6.13: Significance of factors and interactions on the weighting of the first paste PSD peak (p-value = 0.025)

Term	p-value	Sig.
Mixing Speed, rpm	0.0035	*
Fat content*Mixing speed	0.0154	*
Lecithin content*Mixing time	0.0284	*
Mixing time*Mixing speed	0.1311	
Fat content*Lecithin content	0.1800	
Lecithin content*Mixing speed	0.1837	
Fat content*Mixing time	0.2219	
Lecithin Content, vol%	0.3147	
Mixing Time	0.5835	
Fat Content, vol%	0.9773	

Table 6.14: Significance of factors and interactions on the standard deviation of the second paste PSD peak (p-value = 0.83)

Term	p-value	Sig.
Mixing time*Mixing speed	0.2263	
Fat content*Mixing time	0.2640	
Mixing Speed, rpm	0.3104	
Fat content*Mixing speed	0.5390	
Fat content*Lecithin content	0.6764	
Lecithin content*Mixing time	0.7071	
Lecithin Content, vol%	0.7884	
Fat Content, vol%	0.7960	
Mixing Time	0.8272	
Lecithin content*Mixing speed	0.8859	

Table 6.15: Significance of factors and interactions on the mean of the second paste PSD peak (p-value = 0.88)

Term	p-value	Sig.
Mixing time*Mixing speed	0.1610	
Fat Content, vol%	0.4777	
Lecithin content*Mixing time	0.5624	
Mixing Speed, rpm	0.5871	
Lecithin Content, vol%	0.5885	
Fat content*Mixing time	0.6005	
Fat content*Lecithin content	0.7204	
Mixing Time	0.7311	
Fat content*Mixing speed	0.8136	
Lecithin content*Mixing speed	0.9715	

Table 6.16: Significance of factors and interactions on the weighting of the second paste PSD peak (p-value = 0.71)

Term	p-value	Sig.
Lecithin content*Mixing time	0.1130	
Mixing Speed, rpm	0.3089	
Fat content*Mixing speed	0.3129	
Fat content*Lecithin content	0.4665	
Mixing Time	0.4820	
Fat Content, vol%	0.6444	
Lecithin content*Mixing speed	0.7974	
Mixing time*Mixing speed	0.8091	
Fat content*Mixing time	0.9277	
Lecithin Content, vol%	0.9888	

Table 6.17: Significance of factors and interactions on the standard deviation of the third paste PSD peak (p-value = 0.57)

Term	p-value	Sig.
Fat content*Lecithin content	0.1673	
Fat Content, vol%	0.2025	
Lecithin content*Mixing time	0.2472	
Fat content*Mixing time	0.2578	
Mixing time*Mixing speed	0.3431	
Fat content*Mixing speed	0.5176	
Mixing Time	0.7892	
Mixing Speed, rpm	0.8293	
Lecithin Content, vol%	0.8951	
Lecithin content*Mixing speed	0.8957	

Table 6.18: Significance of factors and interactions on the mean of the third paste PSD peak (p-value = 0.31)

Term	p-value	Sig.
Mixing time*Mixing speed	0.0473	*
Fat content*Mixing time	0.1314	
Mixing Speed, rpm	0.1564	
Fat content*Mixing speed	0.1616	
Fat content*Lecithin content	0.5863	
Mixing Time	0.6127	
Lecithin Content, vol%	0.6363	
Lecithin content*Mixing time	0.6479	
Lecithin content*Mixing speed	0.6647	
Fat Content, vol%	0.8505	

Table 6.19: Significance of factors and interactions on the weighting of the third paste PSD peak (p-value = 0.19)

Term	p-value	Sig.
Lecithin content*Mixing time	0.0370	*
Mixing Speed, rpm	0.0477	*
Fat content*Mixing speed	0.0814	
Fat content*Lecithin content	0.2778	
Mixing Time	0.4189	
Lecithin content*Mixing speed	0.4862	
Fat Content, vol%	0.6669	
Lecithin Content, vol%	0.7108	
Fat content*Mixing time	0.7246	
Mixing time*Mixing speed	0.7347	

Table 6.20: Significance of factors and interactions on the specific surface area of the paste (p-value = 0.0240)

Term	p-value	Sig.
Mixing Speed, rpm	0.0043	*
Fat content*Mixing speed	0.0296	*
Fat Content, vol%	0.0486	*
Mixing time*Mixing speed	0.0712	
Lecithin content*Mixing speed	0.0791	
Lecithin Content, vol%	0.1076	
Fat content*Mixing time	0.2785	
Mixing Time	0.3146	
Lecithin content*Mixing time	0.3287	
Fat content*Lecithin content	0.4296	

6.2.5 Can the change in consistency due to fat content be replicated by longer mixing time?

It is important that the final formulation of the conched chocolate is maintained. Only a proportion of the final fat content is added into the pasting stage in order to create a paste which will easily refine. The refiner flake is then mixed at high speeds in the conching stage. The material is stiff and dough-like therefore the temperature will more easily heat up due to friction. Moisture will be driven off and the paste is likely to be sheared at the wall, spreading the fat to coat the particle surfaces. When the remaining fat is added, the mixture becomes thinner. If the remaining fat is added too early then it will require more energy to heat the mixture up and particles will be able to more easily move away from the shearing regions within the mixer.

If a paste can be produced with a lower fat content, yet by processing the paste differently, the paste consistency is comparable to a standard fat paste, the resulting PSD from the refiner

might be the same as a standard fat paste and it would be possible to add the same mass of fat into the conche but the final fat content of the chocolate would be lower.

Figure 6.14 and Figure 6.15 are the measured values of current on the mixing blades and shear stress at a shear rate of 10 s^{-1} split in two ways: firstly, each of the four different markers represents paste at a different fat and lecithin content. Secondly, each data point is categorised based on the mixing time and mixing speed combination. The points are staggered within each mixing category in order to see each of the points clearly.

When the mixing occured at a slow speed for a short length of time, the paste with a low level of fat and higher level of lecithin was found to require the largest current to turn the mixing shaft although the measurements of shear stress were even larger when the paste did not contain lecithin. If this sample was mixed at a higher speed or mixed for a longer duration, both cases resulted in a reduction of the paste thickness at the end of the mixing cycle, measured online or offline.

The current measured on the mixing blades was lowest for the low fat pastes when the mixing time was long but the mixing speed was low. It was found that smaller particles are produced when the mixing speed was higher, which would increase the surface area of the solids and could be the cause of a thicker paste when the mixing time and speed were both high.

It was harder to draw conclusions from the measurements of shear stress using the BET however it can be seen that the consistency of a high fat paste without any lecithin, mixing at low speed for a short time, could be recreated by a low fat paste mixed for a long time.

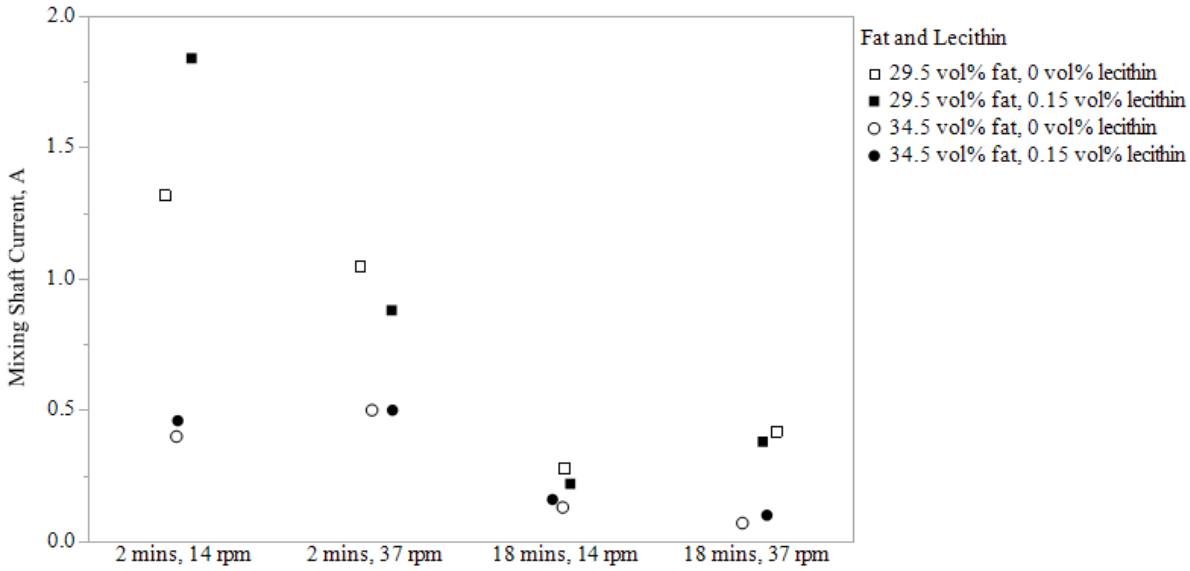


Figure 6.14: Current of the mixer measured at the end of the mixing time of pastes produced in trial 1, varying in fat content, lecithin content, mixing time and mixing speed.

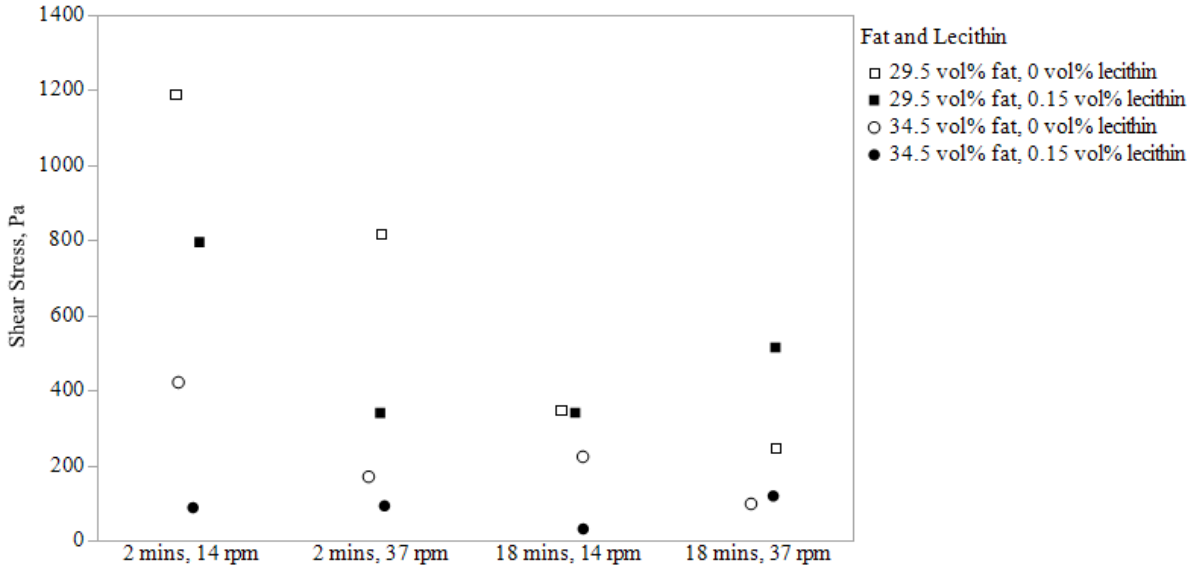


Figure 6.15: Shear stress of pastes, at a shear rate of 10 s^{-1}, produced in trial 1, based on the Herschel-Bulkley parameters measured on the BET, varying in fat content, lecithin content, mixing time and mixing speed.

6.2.6 Discussion

Since the simplified back extrusion technique was used to measure these samples, the flow behaviour indices were only estimated over two test velocities. This does not provide enough information to accurately estimate the shear thinning nature of the paste. During the

evaluation of the rheological model parameters, the consistency coefficient compensated for differences in the flow behaviour indices and therefore it is considered most appropriate to compare the shear stresses at a shear rate of 10 s^{-1} which incorporates all three Herschel-Bulkley components.

When the fat content of pastes was lower, the shear stress, the current draw of the mixing shaft and the operator ranking were all higher; there is less fat available to lubricate particles as most of it becomes immobilised at solid surfaces. This increases the friction between particles and makes it harder for them to flow around each other, consequently increasing the thickness of the paste.

The temperature of the paste was found to significantly increase when the pastes are mixed for a longer time due to the heated water jacket which was higher than the paste temperature. Pastes mixed for a longer time were assessed to be thinner by the operator and by comparing the current on the mixing shaft; both of these measurement techniques were considered to be strongly influenced by the temperatures of the pastes. Increasing the mixing time was also found to significantly affect the shear stress of the pastes when they were measured at a controlled temperature offline. The mixing time was not considered to significantly impact the PSDs of the paste and therefore it was hypothesised that when the system is warmer, the fat is able to coat particles more easily, increasing the lubrication of particles. When the fat content of the pastes is lower, the temperature of the paste increases when they are mixed for longer, much more than high fat pastes. The particles are more closely packed when the fat content is lower which would increase the friction between particles and cause an increase in temperature.

Of the pastes which are mixed for the longest time, there was found to be significantly smaller particles produced when the mixing speed was highest. The operators' assessment of the consistency was the only texture response which indicated a significant effect of the mixing speed, although this may have been vulnerable to bias as the operator knew the mixing conditions and formulation of each batch.

Comparisons of the mixer current at the end of mixing suggested that the online consistency of a high fat paste could be replicated by a paste with 5 vol% less fat when the mixing time was increased from 2 to 18 minutes. Further reductions in consistency were seen when the mixing speed was higher. This was largely due to the temperature increase caused by mixing the paste for longer, particularly when the fat content was lower. There have not been any significant results which have indicated that lecithin impacts the paste behaviour however the results do not suggest that it plays no role in altering the consistency of the pastes.

Currently, operators are relied upon to control the refiner performance based on a visual assessment of the paste consistency. Since it has been established that the temperature of the paste largely contributes to changes in the consistency, this may mean that temperature differences also contribute to how the pastes behave within the refining processes.

In general, there do not seem to be considerable changes in the size of the particles during this mixing process so it is likely that any changes in texture are due to the distribution of fat within the whole system.

6.3 Trial 2: Influence of fat content, lecithin content, mixing time and temperature

Following on from the results from trial 1, a subsequent set of trials was designed to investigate how the paste consistency changed when the fat and lecithin contents, temperature

and mixing time were varied. Within the first trial on a pilot plant scale, the pastes were only found to reach a maximum of 34°C. Despite this, manufacturing lines generally mix within closed vessels and the pastes are expected to rise to temperatures higher than those on a pilot plant scale. As the water jackets are generally controlled at 45°C, it was decided to investigate paste temperatures at 40°C up to 50°C to understand whether heating the pastes higher than normal would beneficially alter the consistency of the paste. All of the ingredients were preheated to the mixing temperature and to be able to control the temperature of the water jacket, it was necessary to use a smaller mixer.

After finding significant effects of the factors on the current drawn by the mixer, it was anticipated that the current would again inform us about the paste consistency and provide comparisons to the offline BET results. Unfortunately, the motor of the mixing vessel available, which allowed the control of the water jacket temperature, was driven by a motor which was much more powerful than the resistance caused by the pastes. Consequently, none of the pastes resulted in any differences of the motor current. The fully developed back extrusion technique, as outlined in section 3.3.6, was therefore the only method that could quantify the consistencies of pastes produced within this trial. This method, described in section 3.3.7, now tested the material at four different speeds to give a better idea of the shear thinning nature of the pastes.

An increased mixing time influenced both online and offline measurements and so it was desirable to determine whether the increased temperature was the main cause of this difference or whether a longer mixing time could also alter the paste consistency. The results of the previous trial were not able to conclude whether lecithin had an influence on the paste consistency. It was again included as a factor in this design of experiments as it was hoped

that using the fully developed BET would allow more precise measurements of the paste consistencies.

A central composite design was created based upon response surface methodology. This technique minimised the number of experimental runs whilst including two-way interactions between factors and curvature of each factor. Models of the responses (measurements) was then fit to the results using least squares analysis. The four factors, each at three levels, are highlighted in Table 6.21 and the processing conditions/formulation of the 21 pastes produced is detailed in Table 6.22. Quantifying the curvature of the factors would allow factors which were not linear across the range (between low and high conditions) to be identified. Plots of the results using the values of the predictive models will be shown at a low, control and high level with a curve fitted between the three.

Table 6.21: List of high, low and control points that were used in the DoE of paste

Factor	Unit	Low	Control	High
Fat content	*vol %*	29.9	32.5	34.9
Lecithin content	*vol %*	0.00	0.07	0.14
Mixing time	*minutes*	2	10	18
Temperature	*°C*	40	45	50

Table 6.22: Levels of each factor used for the runs of the DoE in trial 2

Run #	Fat content, vol %	Lecithin content, vol %	Mixing time, minutes	Temperature, °C
1	34.9	0.14	10	50
2	29.9	0	18	40
3	29.9	0.07	10	45
4	32.4	0.07	2	45
5	34.9	0.14	2	40
6	32.4	0.14	18	40
7	32.4	0.14	10	45
8	32.4	0.07	2	45
9	29.9	0.14	2	40
10	29.9	0	2	50
11	29.9	0.14	18	50
12	32.4	0.07	10	40
13	29.9	0	2	40
14	32.4	0	10	45
15	29.9	0.14	2	50
16	32.4	0	18	50
17	34.9	0	2	50
18	34.9	0.07	18	45
19	34.9	0	10	40
20	29.9	0.07	10	45
21	32.4	0.07	10	50

6.3.1 Back extrusion technique

Samples of the paste were measured at the temperatures which were relevant to the trial temperature. It was hoped that this would be equivalent to the consistency of the paste online. Similarly to the pastes in the preliminary trials, the Herschel-Bulkley model, described in equation 4.8 was used to represent the consistency of these pastes. Table 6.23 shows the calculated values of the Herschel-Bulkley parameters for each paste produced. The values of raw data measured using the back extrusion technique can be found in APPENDIX 2.

Table 6.23: Calculated values of Herschel-Bulkley model parameters based upon the measured values using the BET for each paste produced in trial 2

Run	Flow Behaviour Index	Consistency Coefficient	Yield Stress	Shear Stress at 10 s^{-1}
	-	Pa.s	Pa	Pa
1	0.85	13.48	6.21	101.00
2	0.77	123.69	9.11	744.21
3	0.80	75.31	4.22	480.71
4	0.78	82.09	-1.03	492.82
5	0.78	60.41	6.20	368.62
6	0.77	77.28	2.51	461.59
7	0.80	57.48	6.73	368.06
8	0.73	191.77	13.01	1052.81
9	0.76	467.14	110.67	2781.17
10	0.85	44.52	4.55	320.64
11	0.81	133.22	14.71	870.63
12	0.79	76.93	4.79	482.61
13	0.65	229.49	28.79	1057.36
14	0.77	66.38	6.22	394.98
15	0.86	215.43	25.61	1595.96
16	0.82	46.40	6.66	317.52
17	0.86	43.44	4.56	317.64
18	0.82	25.40	5.48	171.99
19	0.88	41.76	2.92	323.74
20	0.74	106.56	8.51	590.15
21	0.85	48.66	7.48	349.00

6.3.1.1 Yield stress

The model fitted to the yield stress was significant ($p\text{-value}_{ANOVA} = 0.0016$) but also showed a significant lack of fit ($p\text{-value}_{LoF} = 0.0050$); from the plot of the actual values of yield stress against the predicted values based on a least squares fit, one result was considered to be an outlier (Figure 6.16). Removing this outlier produced a model which still significantly fit the data ($p\text{-value}_{ANOVA} = 0.0114$) but no longer had a significant lack of fit ($p\text{-value}_{LoF} = 0.84$).

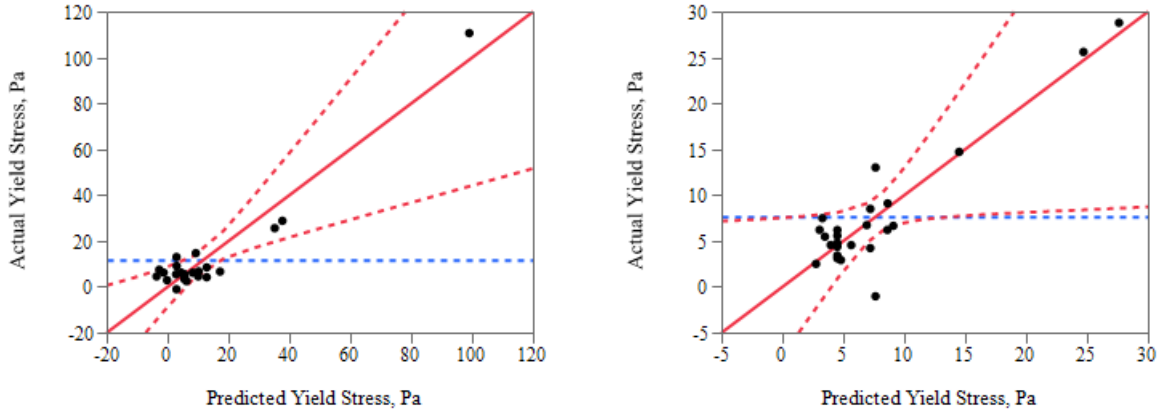


Figure 6.16: Measured yield stresses plotted against values from the predictive model. The plot on the left shows the entire data set where p-value$_{ANOVA}$ = 0.0016 and p-value$_{LoF}$ = 0.005. The outlier is removed and the plot on the right shows the actual and predicted data of the new model with a p-value$_{ANOVA}$ = 0.0114 and p-value$_{LoF}$ = 0.84.

Table 6.24: Significance of factors and interactions on the yield stress of pastes when the largest outlier is removed (p-value$_{ANOVA}$ = 0.0114)

Term	p-value	Significant
Fat content	0.0018	*
Mixing Time	0.0102	*
Mixing time*Temperature	0.0137	*
Fat content*Mixing time	0.0311	*
Fat content*Temperature	0.0513	
Fat content*Lecithin content	0.0518	
Temperature	0.0981	
Mixing time*Mixing time	0.1186	
Lecithin content*Temperature	0.1662	
Temperature*Temperature	0.1890	
Lecithin content*Lecithin content	0.2661	
Lecithin content*Mixing time	0.2967	
Lecithin	0.3012	
Fat content*Fat content	0.5397	

There was a significant effect of the fat content; pastes containing 34.9 vol% fat were shown to have a negligible yield stress and higher yield stresses were measured when the fat content was only 29.9 vol%. This agrees with previous literature discussed within section 2.2.4; that an increase in the solids volume content, here caused by lower fat content, would result in higher yield stresses.

Mixing time was also shown to result in an increased yield stress. Within suspensions of large particles, the literature review indicated that the predominant reason for a yield stress is because of an increase of the solids volume content. It may be possible that air, initially in voids between particles, was becoming entrained within the paste as the liquids were added on top of the solids. Any entrained air would have increased the effective solids volume content which could have increased the yield stresses of the paste. When the pastes were mixed for longer, there were more opportunities for the air to be exposed to the surface and leave the paste which would have decreased the yield stress. This was not hypothesised from the results of the first trial but this could be a result of using the simplified back extrusion technique.

The interaction of fat and mixing time significantly impacted the yield stress, as illustrated in Figure 6.17. The current measured on the mixing shaft in trial 1 was also significantly affected by this interaction however it was mainly hypothesised that this is due to the temperature differences, which are controlled for these trials. When pastes were reheated prior to testing, bubbles were observed at the surface of the samples which appeared most wet. When the fat content was low, air bubbles may have been less able to rise to the surface of pastes because the concentration of solids was greater; rising upwards due to the buoyancy force would be more difficult because particles are more likely to be in the path of the bubble. After short mixing times, pastes containing 34.9 vol% fat had a significantly lower yield stress than if the paste contained only 29.9 vol% fat and bubbles struggled to leave the paste. After a long mixing time, there was no significant difference in the yield stress when the fat content of the pastes were 29.9 or 34.9 vol% as entrained air had been given plenty of opportunities to be released at the surface.

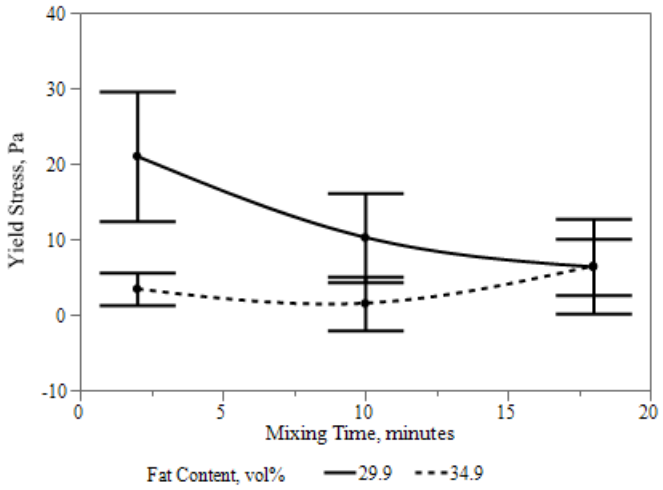


Figure 6.17: Interaction between fat and mixing time significantly impacts the yield stresses of pastes. The results from the predictive model are plotted and the error bars are the standard deviation.

There was also a significant effect of the interaction of mixing time with temperature; when the mixing time was low, mixing the paste at 50 °C resulted in a significantly lower yield stress than when the paste was at 40 °C. When the mixing time was high, mixing the paste at a higher temperature significantly increased the yield stress (Figure 6.18). This may be again due to air entrained within the paste, which was mainly hypothesised to exist after only 2 minutes of mixing. The continuous fat phase has a lower viscosity when the temperature is 50 °C, enabling entrained air to more easily rise to the surface of the sample prior to testing. It is, however, difficult to hypothesise why, after a long mixing time, there was an increase of the yield stress when the temperature was higher, compared to when the temperature was low.

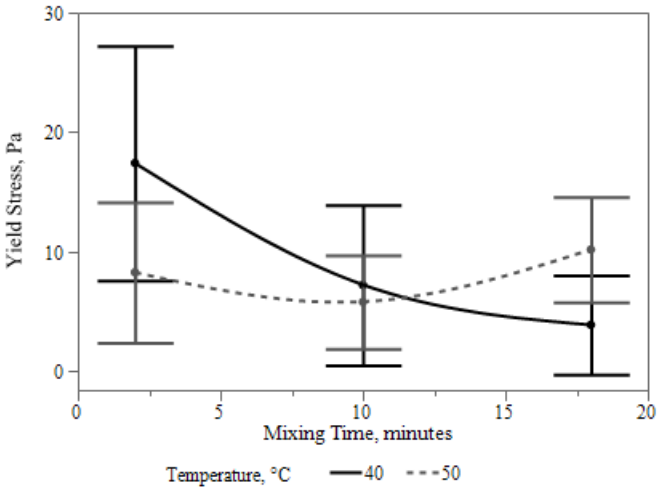


Figure 6.18: Interaction between temperature and mixing time significantly impacts the yield stresses of pastes. The results from the predictive model are plotted and the error bars are the standard deviation.

6.3.1.2 Flow behaviour index

The flow behaviour indices were established from results at four speeds, rather than only two speeds which were relied upon for measuring pastes in trial one. This will have increased the precision of estimating the contribution to flow by the flow behaviour index. The model, using data with the outlier removed, significantly fitted the data ($p\text{-value}_{ANOVA} = 0.05$) and did not show a significant lack of fit ($p\text{-value}_{LoF} = 0.66$) (results detailed in Table 6.25).

All of the pastes had a flow behaviour indices below one, indicating that they all showed shear thinning behaviour. It was discussed in section 2.2.7 that shear thinning may occur due to aggregation or deaggregation due to the shear. Since repeats were done on the same sample that result in comparable measurements, this suggests that the pastes were independent of their shear history and that shear thinning was not caused by aggregation/deaggregation. An alternative hypothesis is that localised viscous heating of the continuous phase occurs between closely packed particles, discussed in section 2.2.7.

Table 6.25: Significance of factors and interactions on the flow behaviour index ($p\text{-value}_{ANOVA} = 0.05$)

Term	p-value	Significant
Temperature*Temperature	0.0279	*
Fat content	0.0296	*
Mixing Time*Temperature	0.0311	*
Temperature	0.0775	
Fat content *Temperature	0.0840	
Mixing Time	0.0936	
Mixing Time*Mixing Time	0.1177	
Lecithin content *Mixing Time	0.4153	
Lecithin content *Lecithin content	0.4163	
Fat content *Lecithin content	0.6408	
Fat content *Fat content	0.7201	
Lecithin content	0.7407	
Lecithin content *Temperature	0.8712	
Fat content *Mixing Time	0.9769	

There was a significant effect of the fat content on the flow behaviour indices; when the fat content was lower, the value of n was lower (Figure 6.19). At lower fat contents, the particles were packed closer together and therefore there may have been more regions where viscous heating would take place.

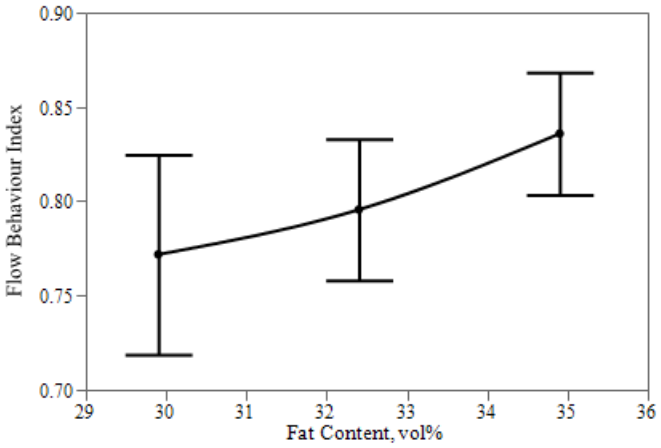


Figure 6.19: The fat content significantly impacts the flow behaviour indices of the pastes. The results from the predictive model are plotted and the error bars are the standard deviation.

There was a significant interaction between mixing time and temperature and the curvature of temperature also had a significant effect. Pastes mixed for a long time showed no difference of the flow behaviour indices although there was some curvature which suggests the flow behaviour indices could have been lowest when the temperature is 45 °C (Figure 6.20). When the pastes were mixed at 40 °C, the flow behaviour indices of pastes mixed for 2 minutes were lower than pastes mixed for 18 minutes. Pastes at 50 °C which were mixed for 2 minutes had flow behaviour indices which were slightly higher than paste mixed for 18 minutes. It is difficult to hypothesise why these differences in the flow behaviour occurred and it must always be considered that the flow behaviour indices and the consistency coefficient are dependent on one another and cannot be considered as completely independent responses.

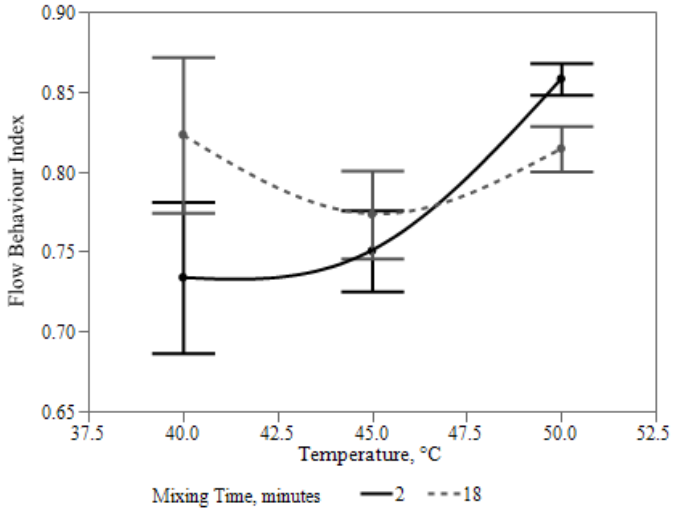


Figure 6.20: Interaction between temperature and mixing time significantly impacts the flow behaviour index of the pastes, plus there is a significant curvature of the temperature. The results from the predictive model are plotted and the error bars are the standard deviation.

6.3.1.3 Consistency coefficient

The model predictive model fitted to the consistency coefficient was significant (p-value$_{ANOVA}$ = 0.0252) and did not show a significant lack of fit (p-value$_{LOF}$ = 0.53). When the fat content was increased, a more dilute system was created so the particles were less likely to

interact and the consistency coefficient was significantly lower (Figure 6.21). Increasing the mixing time from 2 to 18 minutes produced a significant decrease of the consistency coefficient and a significant curvature was also seen for the mixing time (Figure 6.22). After only a short mixing time, it was hypothesised that air bubbles will be present within the paste, increasing the effective solids volume content. This could have increased the number of interactions between particles, resulting in a high consistency coefficient. Mixing paste for 10 minutes will have provided more opportunities for the air to leave the paste at the surface which would have resulted in a decrease of the consistency coefficient. Above 10 minutes, it is not known why the consistency coefficient begins to rise again. This may be due to particle size changes which occurred, affecting the packing of the solids. If the packing fraction decreased due to particle breakages then more of the fat could have been immobilised within the voids between particles and the consistency coefficient would have increased.

Table 6.26: Significance of factors and interactions on the consistency coefficient of pastes ($p\text{-value}_{ANOVA}$ = 0.0252)

Term	p-value	Significant
Mixing Time	0.0053	*
Fat Content, vol%	0.0094	*
Mixing time*Mixing time	0.0102	*
Lecithin content*Temperature	0.1233	
Fat content*Lecithin content	0.1281	
Fat content*Temperature	0.2026	
Temperature	0.2280	
Mixing time*Temperature	0.2771	
Lecithin content*Lecithin content	0.2913	
Temperature*Temperature	0.3794	
Lecithin Content, vol%	0.4545	
Lecithin content*Mixing time	0.4852	
Fat content*Mixing time	0.5157	
Fat content*Fat content	0.7395	

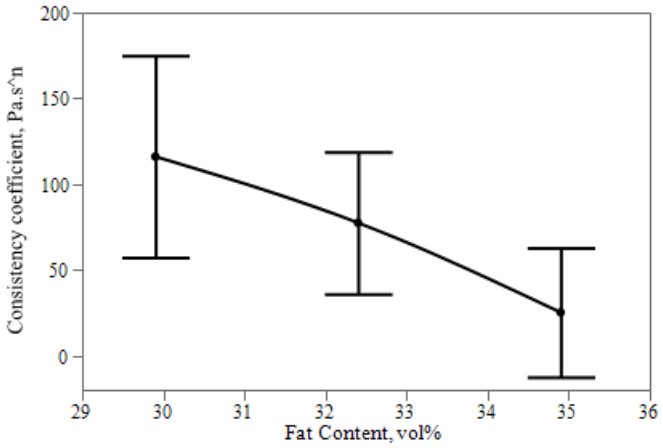


Figure 6.21: The fat content significantly impacts the consistency coefficient of the pastes. The results from the predictive model are plotted and the error bars are the standard deviation.

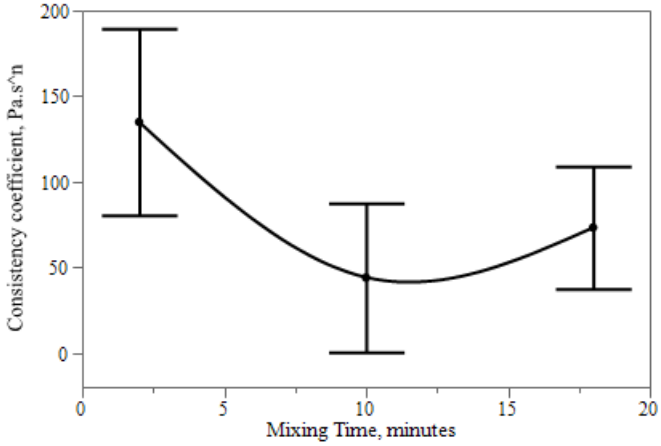


Figure 6.22: The mixing time significantly impacts the consistency coefficient of the pastes, plus there is a significant curvature of the mixing time. The results from the predictive model are plotted and the error bars are the standard deviation.

6.3.1.4 Shear stress

As was observed in trial 1, the consistency coefficient will adapt to differences in the flow behaviour indices, therefore, the shear stress at 10 s^{-1} was also compared. Table 6.27 shows the results of the predictive model which showed a significant fit to the shear stresses ($p\text{-value}_{ANOVA} = 0.011$).

Table 6.27: Significance of factors and interactions on the shear stress at a shear rate of 10 s^{-1} of pastes ($p\text{-value}_{ANOVA}$ = 0.011)

Term	p-value	Significant
Mixing Time	0.0052	*
Fat Content, vol%	0.0065	*
Mixing Time * Mixing Time	0.0078	*
Fat Content * Lecithin Content	0.0376	*
Lecithin Content * Temperature	0.0898	
Lecithin Content * Mixing Time	0.1199	
Lecithin Content, vol%	0.2078	
Lecithin Content * Lecithin Content	0.2517	
Fat Content * Temperature	0.3780	
Temperature	0.4386	
Fat Content * Mixing Time	0.4839	
Temperature * Temperature	0.5882	
Fat Content * Fat Content	0.7589	
Mixing Time * Temperature	0.7787	

Increasing the fat content significantly decreased the shear stress. The mixing time also significantly decreased the shear stress and showed a significant curvature. These were similar to the results found to significantly affect the consistency coefficients; the paste flowed more easily when the fat content was higher as the particles were better lubricated and could interact less. Increasing the mixing time allowed more opportunity for entrained air to leave and also increased homogeneity of the pastes.

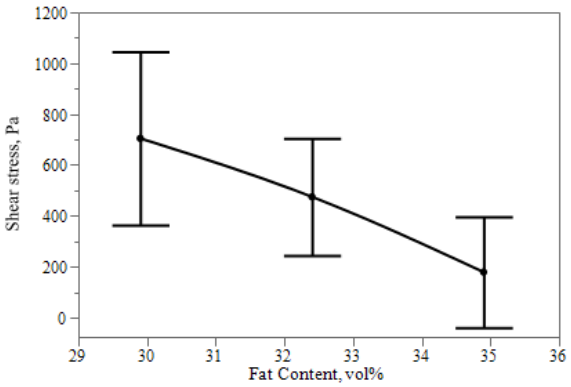


Figure 6.23: The fat content significantly impacts the shear stress of pastes at a shear rate of 10 s^{-1}. The results from the predictive model are plotted and the error bars are the standard deviation.

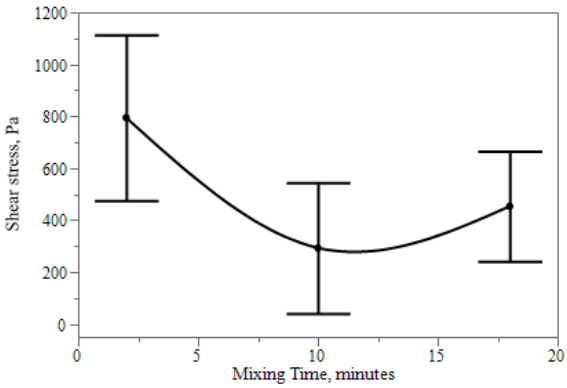


Figure 6.24: The mixing time significantly impacts the shear stress of pastes at a shear rate of 10 s^{-1}. The results from the predictive model are plotted and the error bars are the standard deviation.

There was also a significant interaction between the fat and the lecithin content; when there was lecithin in the paste, the shear stress was much larger at a low fat content and became lower at a high fat content (Figure 6.25). When there was no lecithin in the paste, the shear stress did not show any significant change when the fat content was increased. It may only be possible to hypothesise about the cause of this once the particle sizes have also been considered.

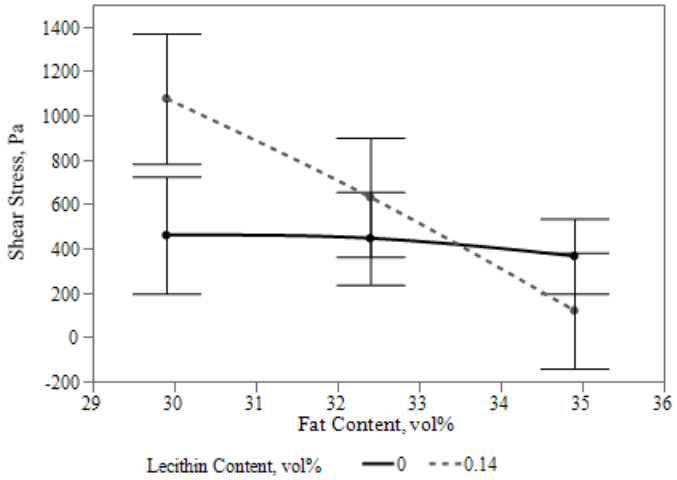


Figure 6.25: Interaction between fat and the lecithin content significantly impacts the shear stress of the pastes, at a shear rate of 10 s^{-1}. The results from the predictive model are plotted and the error bars are the standard deviation.

Unlike the results of the first trial, changing the temperature of the paste did not have any significant effect on the shear stresses of the pastes. When the pastes were mixed in trial one, pastes temperatures were between 25 - 33 °C. In this range, some of the fat may have begun to crystallise, influencing the liquid volume content in the pastes. In these trials, it was likely that all the fat will have been liquid at all temperatures. This highlights that pastes developed in the pilot plant may have been sensitive to the temperature however if the process is scaled up and the pastes are warmer on a manufacturing scale, the paste consistencies could be different.

6.3.2 Significant Effects on the Particle Size Distributions

The particle size distributions (PSD) of each paste were again measured based on the method described in section 3.3.2. The mean values of the pastes produced for these trials is detailed in Table 6.28.

Table 6.28: Model PSD parameters averaged over all of the pastes produced in trial 2

Peak 1			Peak 2			Peak 3			SSA, $m^2 kg^{-1}$
S, µm	W	M, µm	S, µm	W	M, µm	S, µm	W	M, µm	
1.01	0.25	9.90	0.78	0.31	117.65	0.38	0.44	656.87	299.5

None of the predictive models showed a significant fit to any of the PSD parameters at a 95 % confidence interval (results summarised in Table 6.29 - Table 6.38). The predictive model of the mean of the second peak was considered to be marginally significant ($p\text{-value}_{ANOVA}$ = 0.0597). This mean significantly decreased as the mixing time increased (p-value = 0.0315). Comparing the PSDs of pastes after mixing for 2 and 18 minutes, based on the predictive models of each of the PSD parameters, there was very little indication that the mixing time had a meaningful effect on the size of the particles. (Figure 6.26).

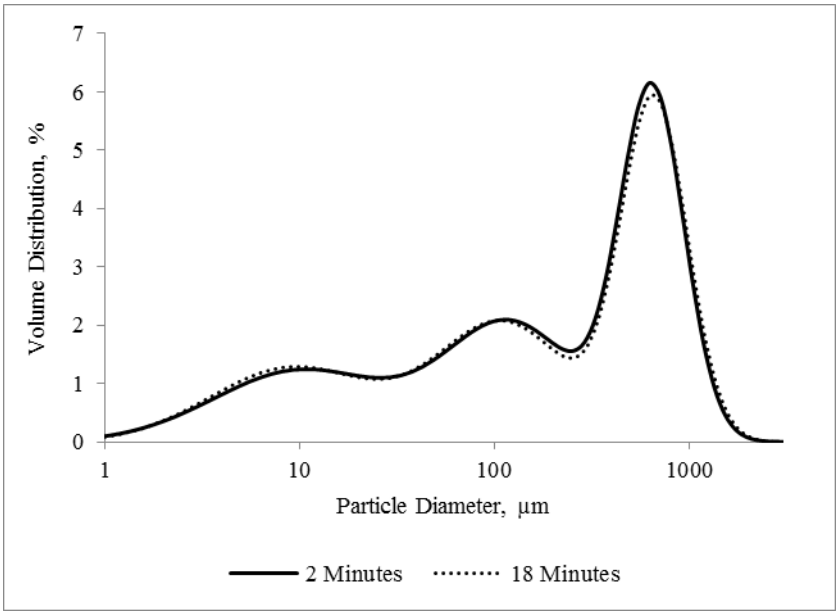


Figure 6.26: Influence of the mixing time on the paste PSDs using the average model parameters from the least squares fit

Table 6.29: Significance of factors and interactions on the mean of the first paste PSD peak (p-value$_{ANOVA}$ = 0.1199)

Term	p-value	Sig.
Mixing Time	0.0043	*
Lecithin content * Lecithin content	0.2040	
Fat content*Mixing time	0.2310	
Temperature	0.3967	
Fat content*Fat content	0.4784	
Lecithin content*Mixing time	0.5170	
Temperature*Temperature	0.5289	
Fat content*Lecithin content	0.5532	
Fat content	0.5803	
Mixing time*Mixing time	0.6118	
Lecithin content	0.8159	
Lecithin content*Temperature	0.8468	
Mixing time*Temperature	0.8805	
Fat content*Temperature	0.9662	

Table 6.30: Significance of factors and interactions on the standard deviation of the first paste PSD peak (p-value$_{ANOVA}$ = 0.1094)

Term	p-value	Sig.
Mixing Time	0.0053	*
Lecithin content * Lecithin content	0.1707	
Fat content*Mixing time	0.2114	
Temperature	0.3116	
Fat content*Fat content	0.3766	
Temperature*Temperature	0.3849	
Lecithin content*Mixing time	0.4232	
Fat content*Lecithin content	0.6973	
Fat content	0.7107	
Mixing time*Mixing time	0.7423	
Lecithin content*Temperature	0.7891	
Fat content*Temperature	0.7975	
Lecithin content	0.8157	
Mixing time*Temperature	0.9954	

Table 6.31: Significance of factors and interactions on the weighting of the first paste PSD peak (p-value$_{ANOVA}$ = 0.6105)

Term	p-value	Sig.
Fat content*Mixing time	0.0761	
Lecithin content*Temperature	0.1924	
Lecithin content	0.2063	
Mixing time*Mixing time	0.5001	
Lecithin content*Lecithin content	0.5458	
Mixing Time	0.5569	
Lecithin content*Mixing time	0.5578	
Temperature*Temperature	0.5604	
Fat content*Temperature	0.5693	
Mixing time*Temperature	0.5870	
Fat content*Lecithin content	0.6100	
Fat content	0.7175	
Temperature	0.8917	
Fat content*Fat content	0.9734	

Table 6.32: Significance of factors and interactions on the mean of the second paste PSD peak (p-value$_{ANOVA}$ = 0.0597)

Term	p-value	Sig.
Mixing Time	0.0315	*
Lecithin content*Lecithin content	0.0557	
Lecithin content*Temperature	0.1128	
Fat content*Lecithin content	0.1251	
Fat content	0.2173	
Mixing time*Mixing time	0.2761	
Fat content*Mixing time	0.3321	
Temperature	0.3801	
Fat content*Temperature	0.4774	
Lecithin content*Mixing time	0.5267	
Temperature*Temperature	0.5389	
Fat content*Fat content	0.5466	
Lecithin content	0.8257	
Mixing time*Temperature	0.9685	

Table 6.33: Significance of factors and interactions on the standard deviation of the second paste PSD peak (p-value$_{ANOVA}$ = 0.3293)

Term	p-value	Sig.
Lecithin content*Lecithin content	0.1226	
Mixing time*Mixing time	0.3441	
Temperature	0.3823	
Lecithin content*Temperature	0.4100	
Fat content*Temperature	0.4249	
Temperature*Temperature	0.4508	
Fat content*Lecithin content	0.5328	
Fat content	0.5349	
Fat content*Mixing time	0.5382	
Lecithin content*Mixing time	0.6561	
Mixing time*Temperature	0.6673	
Lecithin content	0.7552	
Mixing Time	0.8343	
Fat content*Fat content	0.9644	

Table 6.34: Significance of factors and interactions on the weighting of the second paste PSD peak (p-value$_{ANOVA}$ = 0.7316)

Term	p-value	Sig.
Lecithin content*Temperature	0.0805	
Temperature	0.3374	
Temperature*Temperature	0.3490	
Fat content*Mixing time	0.4006	
Fat content*Fat content	0.4709	
Fat content*Lecithin content	0.4953	
Mixing Time	0.7284	
Fat content	0.7567	
Lecithin content*Lecithin content	0.7875	
Lecithin content*Mixing time	0.8366	
Mixing time*Temperature	0.8542	
Lecithin content	0.8591	
Fat content*Temperature	0.8918	
Mixing time*Mixing time	0.9462	

Table 6.35: Significance of factors and interactions on the mean of the third paste PSD peak (p-value$_{ANOVA}$ = 0.4611)

Term	p-value	Sig.
Fat content*Lecithin content	0.0383	*
Fat content*Fat content	0.2220	
Mixing time*Mixing time	0.4201	
Fat content*Mixing time	0.5203	
Lecithin content*Lecithin content	0.5300	
Temperature	0.5551	
Mixing Time	0.6336	
Fat content	0.6411	
Lecithin content	0.6893	
Lecithin content*Mixing time	0.8166	
Lecithin content*Temperature	0.8536	
Fat content*Temperature	0.8724	
Mixing time*Temperature	0.8801	
Temperature*Temperature	0.9317	

Table 6.36: Significance of factors and interactions on the standard deviation of the third paste PSD peak (p-value$_{ANOVA}$ = 0.3984)

Term	p-value	Sig.
Fat content*Lecithin content	0.0982	
Lecithin content*Mixing time	0.1465	
Mixing Time	0.1603	
Mixing time *Mixing time	0.1709	
Mixing time*Temperature	0.3687	
Temperature	0.4300	
Fat content	0.4658	
Temperature*Temperature	0.5840	
Lecithin content	0.6538	
Fat content*Mixing time	0.7233	
Fat content*Temperature	0.7368	
Lecithin content*Lecithin content	0.7561	
Fat content*Fat content	0.9124	
Lecithin content*Temperature	0.9158	

Table 6.37: Significance of factors and interactions on the weighting of the third paste PSD peak (p-value$_{ANOVA}$ = 0.5361)

Term	p-value	Sig.
Lecithin content*Temperature	0.0492	*
Fat content*Mixing time	0.1132	
Lecithin content	0.4061	
Fat content*Lecithin content	0.4291	
Temperature	0.5034	
Fat content*Fat content	0.5920	
Mixing time *Mixing time	0.6764	
Temperature*Temperature	0.6793	
Fat content*Temperature	0.6808	
Lecithin content*Mixing time	0.8721	
Mixing time*Temperature	0.8773	
Lecithin content*Lecithin content	0.9026	
Mixing Time	0.9573	
Fat content	0.9669	

Table 6.38: Significance of factors and interactions on the specific surface area of the paste (p-value$_{ANOVA}$ = 0.9799)

Term	p-value	Sig.
Lecithin content*Temperature	0.3413	
Fat content*Temperature	0.3479	
Mixing time*Temperature	0.5034	
Mixing Time	0.5394	
Lecithin content	0.6054	
Fat content*Lecithin content	0.6485	
Temperature*Temperature	0.6829	
Fat content	0.8166	
Temperature	0.8212	
Mixing time *Mixing time	0.8344	
Lecithin content*Lecithin content	0.8529	
Fat content*Fat content	0.8621	
Lecithin content*Mixing time	0.9607	
Fat content*Mixing time	0.9800	

6.3.3 Comparing consistency with particle size distribution

Principal component analysis (PCA) was used to determine whether there were similarities between how the PSD parameters and the Herschel-Bulkley parameters vary. The first three principal components (PC's) represented 79.3 % of the variation within all the data. PC4 only correlated with the particle size parameters so this was not included in the plots within Figure 6.27. Some of the consistency parameters and the PSD parameters of the first two peaks were clustered together on the plot of PC1 against PC2. These parameters have shown significant effects of the mixing time which was likely to be causing this similarity. These consistency and PSD components were then clustered in separate regions on the plot of PC1 against PC3.

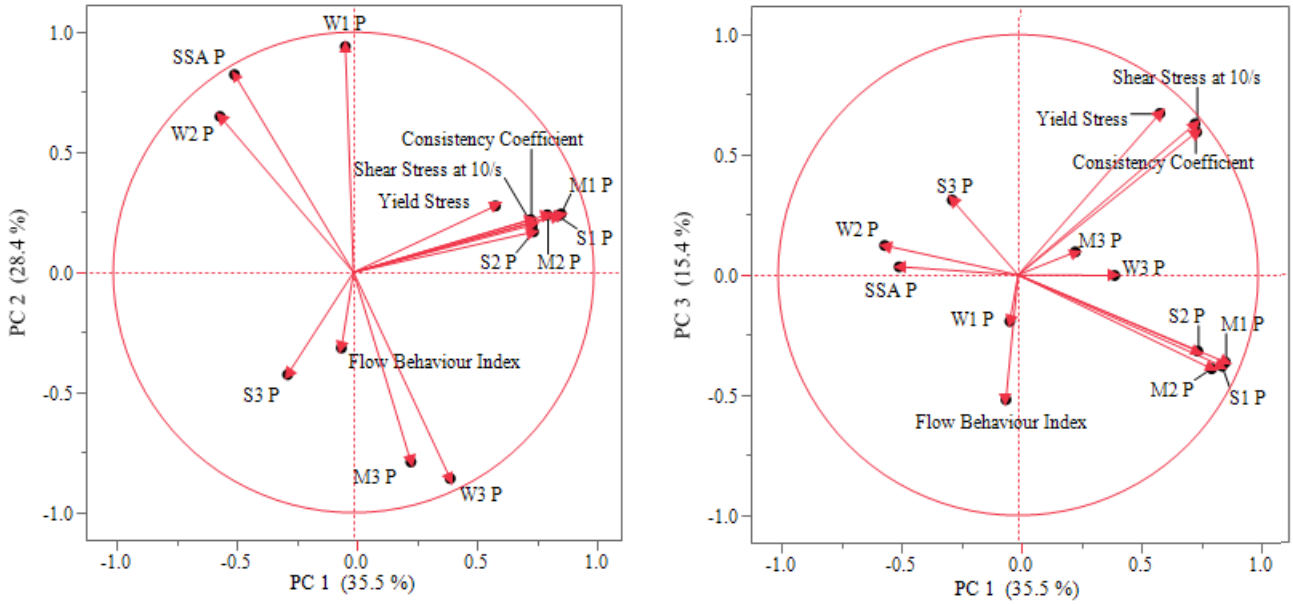


Figure 6.27: Loading plots of the first three principal components which describe 79.3% of the variation between the particle size parameters of the three log-normal distributions (mean, M, standard deviation, S, and weight, W), the specific surface areas (SSA) and the results measured using the BET (flow behaviour index, consistency coefficient, yield stress and the shear stress at a shear rate of 10 s^{-1}). The log-normal peak containing the smallest particles is labelled 1, the largest particles are within the log-normal peak labelled 3.

There did not appear to be any similarities drawn between the mean of the third paste PSD peak (M3 P) and the shear stress of the paste, which were potentially linked by the interaction between fat and lecithin. It therefore remains unknown why the shear stresses of pastes that contain no lecithin were found to be unaffected when the fat content was increased by 5 vol%.

6.3.4 What process settings can be used to change the consistency instead of additional fat?

It was desirable to understand whether varying the process settings of the paste can cause the paste to become thinner in a similar way to the addition of fat to the paste. The results of trial 1 indicated that pastes containing 29.5 vol% fat which were mixed for a long time at a high speed showed similar resistances to mixing as pastes containing 34.5 vol% fat mixed for only 2 minutes. It has been hypothesised that some of this effect is caused by the increased temperature after long mixing times. Since it was only possible to quantify paste consistency with the back extrusion technique (BET), the shear stress at a shear rate of 10 s^{-1} will be used to represent the overall paste consistency. This value is within the shear rates calculated at the walls within the BET tests and therefore was not extrapolated to values which are not tested.

As response surface methodology was used to design the set of experiments, it was not possible to compare each extreme result of raw data, as was done in section 6.2.5. Instead, the predictive model of the shear stress at 10 s^{-1} was used to infer the behaviour of the pastes. Figure 6.28 and Figure 6.29 show the mean values of shear stress based on the predictive models at different fat contents and after mixing for different lengths of time. Since the interaction between fat and lecithin significantly affected the shear stress, the two plots compare the results at different lecithin contents.

When the lecithin content was altered, there was a considerable difference between the results; when pastes did not contain any lecithin, the shear stress of a low fat paste mixed for two minutes was only just higher than a paste containing 5 vol% more fat. After mixing for 10 minutes, the shear stress of high and low fat pastes without lecithin were no different. Conversely, low fat pastes containing lecithin were measured to have very high values of

shear stress, although this decreased as the mixing time was increased from 2 to 10 minutes. Pastes mixed for 2 minutes with 34.9 vol% fat and containing 0.14 vol% lecithin showed a similar shear stress to pastes which did not contain lecithin however mixing these pastes for longer resulted in a significant decrease of the shear stress.

Overall, it was also possible to observe that most of the reduction in the paste consistency occurred between 2 - 10 minutes when there was 0.14 vol% lecithin. The results when there was no lecithin within the paste was surprising as increasing the fat content would generally cause a decrease of the paste consistency. This was the outcome within trial 1, even when lecithin was not present. Measuring the size of particles using the method described in section 3.3.2, the results did not indicate that the solids within the pastes were reduced in size based on any of the process conditions altered in this DoE therefore it was not possible to hypothesis about the cause of this result when there was no lecithin within the paste.

0 vol% lecithin content

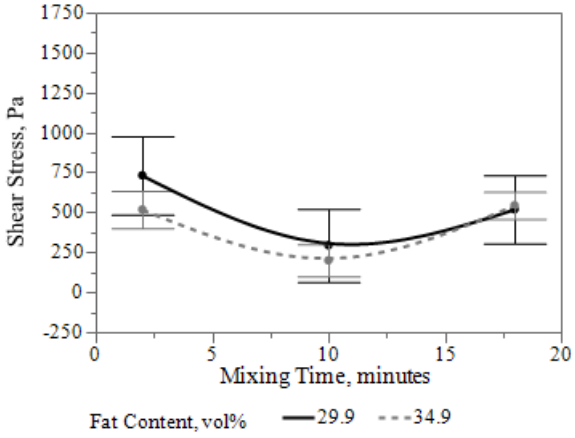


Figure 6.28: Comparing how shear stress at a shear rate of 10 s^{-1} changes depending on the fat content and mixing time when the lecithin content is 0 vol%. The results from the predictive model are plotted and the error bars are the standard deviation.

0.14 vol% lecithin content

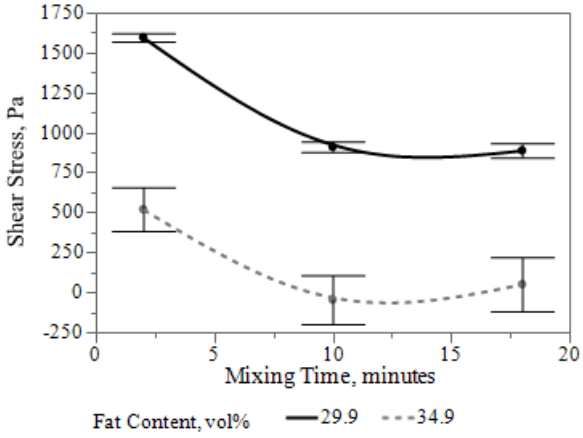


Figure 6.29: Comparing how shear stress at a shear rate of 10 s^{-1} changes depending on the fat content, mixing time when the lecithin content is 0.14 vol%. The results from the predictive model are plotted and the error bars are the standard deviation.

6.3.5 Discussion

Increasing the fat content significantly decreased the yield stress and consistency coefficient and increased the flow behaviour index towards one. This agrees with the literature; when the solids content of the paste was reduced, the yield stress decreased. Increasing the fat content will increase the distance between particles and reduce the number of particle-particle interactions. This lead to less shear thinning behaviour and a lower consistency coefficient.

Research published by Mahaut et al. (2008) has shown that the yield stresses of suspensions of particles between 80 – 2000 μm are only dependent on the total solids volume content. The yield stress was significantly reduced as the mixing time was increased hence it was hypothesised that air, initially between voids of particles prior to the liquid addition, became entrained within the pastes. After a short mixing time, much of the air was not able to leave the paste and as bubbles must be coated by fat, the effective solids content was increased. Mixing for longer provided more opportunities for the air to access the surface of the paste and to escape to the atmosphere. The effective solids volume content and therefore the yield stress were reduced.

There were interactions of the mixing time with the fat content and with the temperature; when there was a high fat content, high mixing time or when the paste was hotter, the yield stresses were much lower. During preparation of the samples for testing, air bubbles were observed at the surface of the pastes when the pastes were thin. Air will have been able to rise to the surface more easily when the fat content or the temperature was higher. If this occurred then the effective solid content and the yield stress were both reduced. With fewer air bubbles within the paste, the particles had more space to move around and the flow behaviour indices was also seen to reduce.

These air bubbles may also have been causing the pastes to display stronger shear thinning behaviour; when the pastes were mixed for a short time, at 40 °C the flow behaviour was significantly lower than pastes at 50 °C. Based upon the literature, it is likely that shear thinning was due to viscous heating of localised regions of fluid between particles when they were in close proximity to each other. It was therefore hypothesised that entrained air bubbles, which might be more prolific in pastes which were cooler, were causing the particles to be packed more tightly, increasing the regions where viscous heating could occur.

There was a significant interaction between the fat and lecithin contents which impacted the shear stress measured using the BET. When the pastes contained 0.14 vol% lecithin, the shear stresses of pastes with higher fat contents were reduced. Unexpectedly, when pastes did not contain lecithin, the shear stresses of the pastes did not show a significant difference when the fat content was increased. In chapter 0, the BET measured differences between the shear stresses of pastes which had a 4 vol% difference in fat content and did not contain lecithin. There was not measured to be any significant variation in the size of particles however it may be advisable to investigate this result in future studies.

6.4 Comparisons between the two trials

Based on the predictive models of the PSD parameters, the average PSDs from trial one and trial two were compared. It is possible to see that the distribution shows quite a different shape; trial two shows a larger proportion of the particles fall within the first two peaks however the third peak has a higher mean value (Figure 6.30). The two trials were run 2 years apart however all the ingredients met the same specifications which were agreed upon by the pilot plant manager at Mondelēz International. The pastes formulated for trial two did not

contain sweet whey powder (d_{10} = 45 μm, d_{90} = 310 μm); the presence of sweet whey powder may have broadened the second PSD peak.

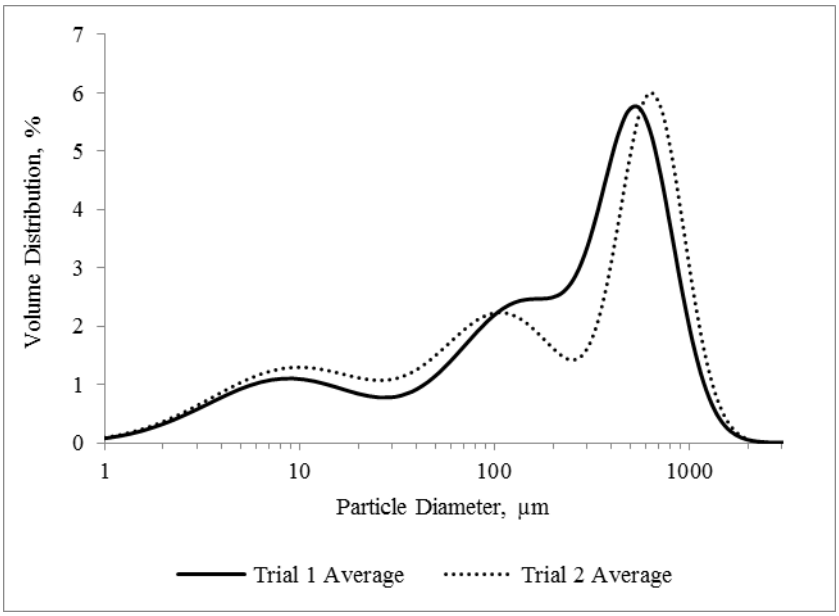


Figure 6.30: Average particle size distributions of the pastes produced in trial 1 and trial 2 using the average model parameters from the least squares fit

The pastes were mixed in vessels with different capacities and different mixing geometries. The smaller mixer used to mix 8 kg batches of pastes for trial two was likely to be able to input more energy into the paste within the same length of mixing time. This could have resulted in more breakages of particles, particularly the large, brittle sugar crystals which may have fractured into a range of particle sizes. It is therefore hypothesised that these fractures could have been masking the variation in particle size between pastes produced at different process conditions.

6.5 Conclusions

Two sets of trials were run on a pilot plant scale in order to investigate how paste consistency varies when the fat and lecithin content were varied and what the influences of mixing time, mixing speed (trial 1 only) and temperature (trial 2 only) were. Pastes were quantified offline

using the back extrusion technique (BET), developed in chapter 0. Using the finalised BET method, the pastes displayed shear thinning behaviour ($n < 1$) and many were measured to have a yield stress. The first trial also involved characterising the paste consistency from the value of the mixing shaft current at the end of mixing and visual assessments/handling of the material by an experienced operator.

The visual assessments of the pastes by an experienced operator were comparable to the measurements of current draw of the mixing shaft at the end of mixing. The results of both of these online techniques correlated with the temperatures of the pastes at the end of the mixing time; the temperature was significantly increased when pastes were mixed for longer, particularly when the fat content of the pastes was low. Given that operators commonly adapt the operating conditions of the refiner based on these visual assessments of paste consistency, which are influenced by the temperature, the temperature of the paste may be contributing to how the pastes refine. On the other hand, the temperature of the paste may be irrelevant to the refining performance and therefore it is problematic to assess the paste consistency without knowing the contribution of temperature. It would be valuable to evaluate the temperatures of pastes across different process lines and draw comparisons with temperatures achieved on a pilot scale line.

Increasing the fat content resulted in pastes with a thinner consistency which had a lower yield stress and were less shear thinning. The current draw of the mixer shaft and the operator rankings also indicated that increasing the fat content resulted in a thinner paste consistency. Adding more fat increased the distance between particles so that it was easier for them to flow around each other and they were less likely to interact.

Pastes which were mixed for a shorter time were measured to have significantly higher values of yield stress. Initially, the solids were placed in the mixer and the liquids were added on top. Since the dry particles were not perfectly packed, air filled the voids. As liquid was added, it is hypothesised that the air may not have been able to escape at the surface and therefore this air becomes entrained, forming bubbles. These voids of air would have increased the effective solids volume content of pastes which was likely to increase the yield stresses of pastes. Mixing the pastes for longer increased the opportunity for air to be released into the atmosphere which would have reduced the yield stress. When pastes were mixed at a higher temperature, surface tension of the fat was lower so entrained air could escape more easily. When the pastes contained more fat, it was easier for air to rise to the surface as fewer particles were in the way.

It is also hypothesised that there were air bubbles in pastes mixed for a short time at 40 °C which caused the paste to have stronger shear thinning behaviour than pastes at 50 °C, where the bubbles were able to leave the fluid. An increase in the effective solids content would have forced particles to be closer together. This would have increased the regions where there were thin layers of fluid between particles. As the strain rate was higher than in the bulk, viscous heating would have occurred; for thin layers, the heat cannot dissipate so the fluid would heat up, leading to shear thinning behaviour.

Based on the current draw of the mixing shafts for pastes in trial one, the consistency of high fat pastes (34.9 vol% fat) mixed for two minutes could be recreated by mixing pastes containing 5 vol% less fat for 18 minutes. It is hypothesised that the decrease was due to the pastes increasing further in temperature over longer mixing times. Additionally, there were more particle-particle interactions when the fat content was lower which could have contributed towards further heating.

Overall, the results of trial two indicated that increasing the mixing time decreased the shear stresses of the pastes however increasing the temperature from 40 – 50 °C did not result in a significant reduction of the paste texture. Although the predictive models indicated that pastes containing lecithin followed this trend, surprisingly, pastes without any lecithin were not found to significantly change in consistency when an additional 5 vol% fat was added. Further investigation is necessary into understanding this result as there was no indication that the sizes of particles were the source of this result.

These results have indicated that there is the possibility of reducing the fat content within the paste whilst maintaining the consistency of the paste, a factor which is thought to have the most effect on the refining performance during chocolate manufacture. It has not yet been established whether pastes of the same consistency will refine to produce refined flake of the same particle size, independently of the fat content of the paste. It is also clear that the effect that lecithin has on the paste is not fully understood and it would be valuable to understand what surfaces lecithin interacts with or whether it remains as micelles.

7 IMPACT OF FORMULATION AND PROCESSING CONDITIONS ON REFINING

7.1 Introduction

Once the ingredients for chocolate have been combined to form pastes, the particle sizes must be reduced so that the chocolate appears smooth. Typically, this is done using roll refiners which can be operated in two different ways: gap driven or pressure driven. A comparison of these two styles of refining can be found within section 1.2. If the refiners are gap driven, then the particles must be crushed so that they become smaller than the gap between the rolls. If the refiners are pressure driven, then the more resistive force that the paste can create to push the rolls apart, the more paste is able to pass through and the larger the particles can remain. The force that can be exerted by the paste is a function of the material friction, essentially the apparent viscosity of the paste, and the friction between the roll and the paste, affected by roll temperature, roughness and roll speeds.

Current operation of the manufacturing process often involves manipulation of the refiner operating conditions based on the manual assessment by operators of the paste consistency and the roll coverage. In chapter 6, it was shown that the paste consistency could be significantly affected by altering the fat content or mixing the paste for a longer time. Processing conditions also impacted the temperature of the paste, potentially influencing the operators' assessment of the paste consistency and the current required by the mixing blade shaft. It would therefore be beneficial to quantify whether the reduction in particle size within the refining stage depended only on the online assessment of paste consistency, regardless of

the mixing conditions, formulation or particle size distribution (PSD) of the paste, or whether the temperature of the paste online masked the actual rheological behaviour of the paste as it entered the refiner rolls.

Following on from chapter 6, the pastes which were produced in trial 1 and 2 were refined. A two-stage refining process was used to reduce the particle sizes of trial 1 pastes. A single pass through a three roll refiner was used to process pastes which were produced in trial 2. The designs of experiments which were discussed in chapter 6 continue to be referenced within this chapter. The refining processes were all operated employing the pressure driven principle; the rolls were initially pressed closed and the paste was only able to pass through if it could overcome the pressing forces between each roll.

7.2 Trial 1: Pre-refined paste

Once a batch of paste was produced, it was emptied from the mixer, directly into the nip between the two rolls of the pre-refiner. This material is now referred to as pre-refined paste; it still showed a paste-like consistency therefore an operator was able to assess the consistency on a scale between 0 - 10 and the back extrusion text was again used to measure the rheological behaviour.

7.2.1 Particle size distributions of pre-refined paste

7.2.1.1 Particle Size Reduction in Pre-Refiner

Similarly to the paste, the pre-refined paste showed a tri-modal log-normal PSD. Based on the predictive models, the average PSDs of the pastes and pre-refined pastes are compared in Figure 7.1. The model PSD parameters, the mean (M), standard deviation (S), and weighting of each log-normal distribution (W), for each log-normal peak, are summarised in Table 7.1.

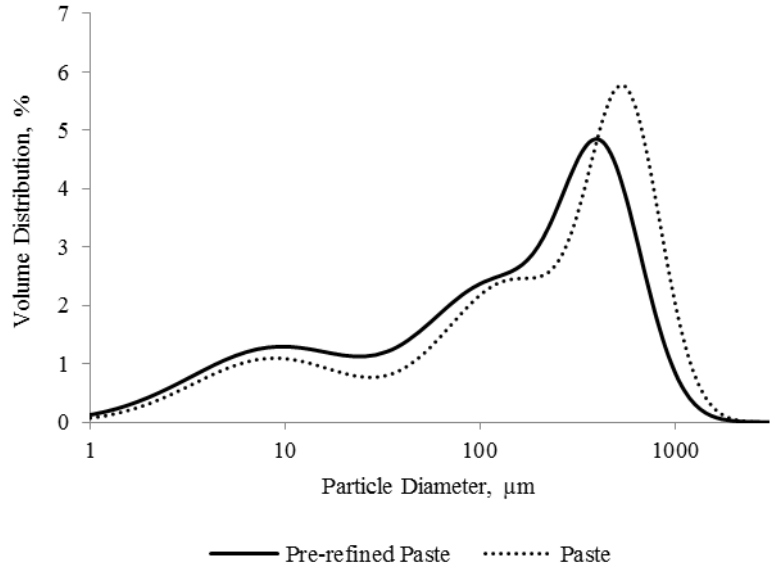


Figure 7.1: Average particle size distributions of the pastes and pre-refined pastes produced in trial 1 using the average model parameters from the least squares fit

Table 7.1: Mean values of the parameters used to model the PSD and the SSA of the pastes to the pre-refined pastes (± the standard deviation).

		Paste	Pre-Refined Paste
Mean (M), µm	**Peak 1**	8.70 ± 0.35	9.23 ± 0.46
	Peak 2	145.59 ± 22.78	121.95 ± 11.85
	Peak 3	551.80 ± 56.77	426.53 ± 19.67
Standard Deviation (S), µm	**Peak 1**	0.94 ± 0.034	1.03 ± 0.030
	Peak 2	0.79 ± 0.040	0.080 ± 0.020
	Peak 3	0.42 ± 0.016	0.47 ± 0.020
Weighting (W)	**Peak 1**	0.20 ± 0.020	0.26 ± 0.021
	Peak 2	0.37 ± 0.029	0.36 ± 0.024
	Peak 3	0.42 ± 0.043	0.38 ± 0.042
SSA, $m^2 kg^{-1}$		265.7 ± 16.9	321.5 ± 23.3

The results show that the large particles were reduced, as was expected after passing through the pre-refiner. There were still some particles above 1000 µm in the pre-refined paste which indicates that not all the particles were crushed in order to pass through the gap. The overall pre-refined paste PSD indicated that the proportion of particles below ≈ 400 µm was increased, suggesting that the large sugar particles were broken into a broad range of particle

sizes. Without further optical or chemical tests on the different sized particles, it cannot be determined whether the particle size of skimmed milk powder (SMP) and sweet whey powder (SWP) was reduced in the pre-refiner. As these particles are far more porous than the sugar crystals, if these particles were broken then this may have dramatically increased the surface area of the solids required to be coated by the fat.

7.2.1.2 Factors affecting Particle Size Distribution of the Pre-Refined Paste

Analysis of the raw data was carried out to establish the significant factors and two-way interactions of each of the model PSD parameters. None of the fits to the parameters were statistically significant (Results of ANOVAs reported in Table 7.3 - Table 7.12. This is a similar result to the results in chapter 6 which suggests that either the factors were not affecting the pre-refined paste PSD more than the inherent variation due to the composition and production method or that the technique introduced more variation which masked differences between samples.

The specific surface area (SSA) was also analysed using least squares regression. Initially, the model was not significant ($p\text{-value}_{ANOVA} = 0.0593$). In order to improve the model, it is common within statistics to remove interactions between factors which are not significant. The interaction between fat and lecithin had a very low significance (p-value = 0.91) hence removing this resulted in a model which statistically fitted the SSA ($p\text{-value}_{ANOVA} = 0.0261$). Increasing the fat content statistically significantly decreased the SSA of the pre-refined paste. Based on predictive values of the PSD model, PSDs of the pre-refined paste were compared at high and low fat contents (Figure 7.2). There appeared to be a greater proportion of particles in the third peak of the higher fat pre-refined paste, however when considering the variation of the measuring technique, discussed in section 3.3.2, this difference cannot be considered to be meaningful.

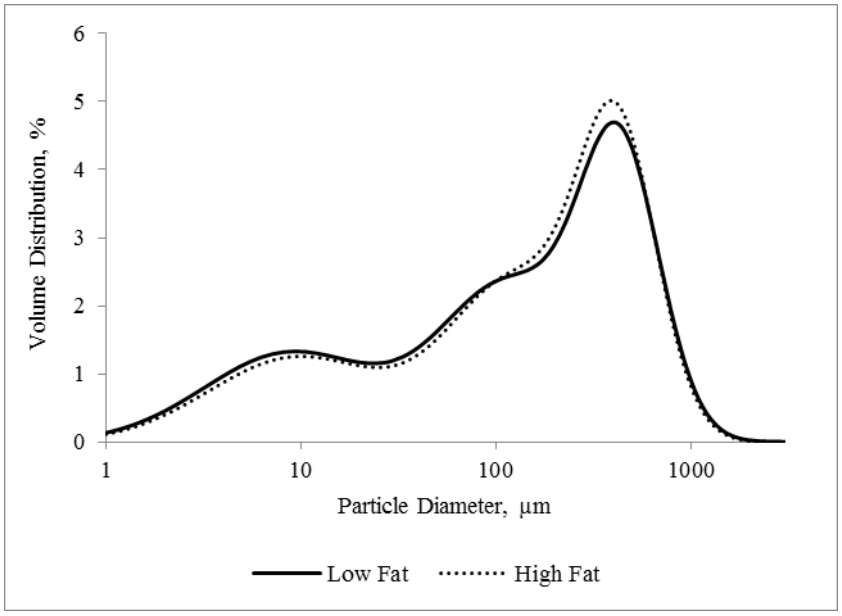


Figure 7.2: Influence of the fat content on the pre-refined paste PSDs using the average model parameters from the least squares fit

The interaction between lecithin and mixing speed was also found to have a statistically significant effects on the SSA, summarised in Table 7.2. When there was no lecithin, increasing the mixing speed resulted in statistically significantly higher SSAs of the pre-refined pastes, indicating that there was a larger proportion of small particles. When the pastes contained 0.15 vol% lecithin, the SSA significantly decreased when the mixing speed was higher.

Table 7.2: Comparing the mean values of paste and pre-refined paste SSA from the predictive models at high and low levels of lecithin content and mixing speed ± the standard deviation

Lecithin Content, vol%	**Mixing Speed, rpm**	**SSA of the Paste, m^2 kg^{-1}**	**SSA of the Pre-Refined Paste, m^2 kg^{-1}**
		p-value = 0.0791	***p-value = 0.0235***
0	37	275 ± 7.77	332 ± 9.14
0.15	14	246 ± 8.47	331 ± 15.5
0.15	37	276 ± 4.58	318 ± 11.8
0	14	266 ± 10.6	304 ± 15.7

Table 7.3: Factors which significantly impact the mean of the first pre-refined paste PSD peak (p-value$_{ANOVA}$ = 0.11)

Term	p-value	Sig.
Fat	0.0065	*
Mixing Time*Mixing Speed	0.0209	*
Mixing Speed	0.2771	
Fat*Lecithin	0.5702	
Fat*Mixing Speed	0.6633	
Lecithin*Mixing Time	0.7036	
Lecithin*Mixing Speed	0.7268	
Mixing Time	0.7355	
Fat*Mixing Time	0.7467	
Lecithin	0.7908	

Table 7.4: Factors which significantly impact the standard deviation of the first pre-refined paste PSD peak (p-value$_{ANOVA}$ = 0.26)

Term	p-value	Sig.
Mixing Time*Mixing Speed	0.0145	*
Lecithin*Mixing Time	0.2213	
Fat	0.2572	
Fat*Lecithin	0.3842	
Lecithin*Mixing Speed	0.3962	
Fat*Mixing Time	0.5099	
Mixing Speed	0.5396	
Lecithin	0.5772	
Mixing Time	0.8489	
Fat*Mixing Speed	0.8531	

Table 7.5: Factors which significantly impact the weight of the first pre-refined paste PSD peak (p-value$_{ANOVA}$ = 0.25)

Term	p-value	Sig.
Lecithin*Mixing Speed	0.0306	*
Fat*Mixing Time	0.1252	
Mixing Time*Mixing Speed	0.1398	
Lecithin*Mixing Time	0.2764	
Fat	0.3213	
Fat*Mixing Speed	0.3774	
Fat*Lecithin	0.7156	
Mixing Speed	0.8213	
Mixing Time	0.8243	
Lecithin	0.9527	

Table 7.6: Factors which significantly impact the mean of the second pre-refined paste PSD peak (p-value$_{ANOVA}$ = 0.31)

Term	p-value	Sig.
Mixing Time*Mixing Speed	0.0202	*
Fat	0.1440	
Lecithin*Mixing Time	0.4035	
Fat*Lecithin	0.4572	
Fat*Mixing Speed	0.4630	
Lecithin*Mixing Speed	0.5200	
Mixing Time	0.6176	
Mixing Speed	0.6861	
Fat*Mixing Time	0.7432	
Lecithin	0.8358	

Table 7.7: Factors which significantly impact the standard deviation of the second pre-refined paste PSD peak ($p\text{-value}_{ANOVA} = 0.70$)

Term	p-value	Sig.
Fat	0.1345	
Fat*Mixing Speed	0.2723	
Mixing Time*Mixing Speed	0.2770	
Fat*Mixing Time	0.4216	
Mixing Time	0.6004	
Fat*Lecithin	0.6122	
Lecithin	0.8968	
Mixing Speed	0.9257	
Lecithin*Mixing Time	0.9828	
Lecithin*Mixing Speed	0.9993	

Table 7.8: Factors which significantly impact the weight of the second pre-refined paste PSD peak ($p\text{-value}_{ANOVA} = 0.61$)

Term	p-value	Sig.
Lecithin	0.2153	
Mixing Time*Mixing Speed	0.2158	
Fat*Mixing Time	0.2385	
Mixing Time	0.3298	
Lecithin*Mixing Time	0.4635	
Lecithin*Mixing Speed	0.4924	
Mixing Speed	0.5883	
Fat*Lecithin	0.5986	
Fat*Mixing Speed	0.6750	
Fat	0.9462	

Table 7.9: Factors which significantly impact the mean of the third pre-refined paste PSD peak ($p\text{-value}_{ANOVA} = 0.11$)

Term	p-value	Sig.
Fat*Mixing Speed	0.0235	*
Mixing Time*Mixing Speed	0.0764	
Fat	0.0884	
Mixing Speed	0.1247	
Lecithin	0.2069	
Lecithin*Mixing Speed	0.3120	
Fat*Lecithin	0.3348	
Lecithin*Mixing Time	0.3820	
Fat*Mixing Time	0.4754	
Mixing Time	0.6589	

Table 7.10: Factors which significantly impact the standard deviation of the third pre-refined paste PSD peak ($p\text{-value}_{ANOVA} = 0.46$)

Term	p-value	Sig.
Lecithin*Mixing Speed	0.1511	
Fat*Mixing Speed	0.1547	
Fat	0.1777	
Mixing Time	0.3062	
Lecithin	0.3896	
Fat*Lecithin	0.5280	
Fat*Mixing Time	0.5336	
Mixing Speed	0.5747	
Lecithin*Mixing Time	0.9200	
Mixing Time*Mixing Speed	0.9283	

Table 7.11: Factors which significantly impact the weight of the third pre-refined paste PSD peak (p-value$_{ANOVA}$ = 0.52)

Term	p-value	Sig.
Lecithin*Mixing Speed	0.1589	
Mixing Time*Mixing Speed	0.1686	
Fat*Mixing Time	0.1716	
Lecithin*Mixing Time	0.3635	
Lecithin	0.4158	
Mixing Time	0.6005	
Fat*Lecithin	0.6335	
Fat	0.6391	
Mixing Speed	0.6680	
Fat*Mixing Speed	0.9038	

Table 7.12: Factors which significantly impact the specific surface area of the pre-refined paste (p-value$_{ANOVA}$ = 0.0261)*

Term	p-value	Sig.
Fat	0.0019	*
Lecithin*Mixing Speed	0.0200	*
Lecithin*Mixing Time	0.0754	
Fat*Mixing Time	0.2552	
Fat*Mixing Speed	0.2682	
Mixing Speed	0.3170	
Lecithin	0.4047	
Mixing Time*Mixing Speed	0.5740	
Mixing Time	0.6305	
Fat*Lecithin	0.9098	

7.2.1.3 PCA of particle size change from paste to pre-refined paste

To establish whether the particle sizes of the pre-refined pastes varied in similar ways to the particle sizes of the pastes, principal component analysis was carried out. Figure 7.3 shows the loading plots of PC1 against PC2 and PC3. These three components represent 78.4 % of the variation in these PSD results. Each PSD peak mean was located in a similar position for both the paste and the pre-refined paste. This suggests that the size of the particles entering the pre-refiner was having an influence on the resulting pre-refined paste particle sizes. There was no clear relationship between the SSA of pastes and the pre-refined pastes or any other parameters which described the PSDs.

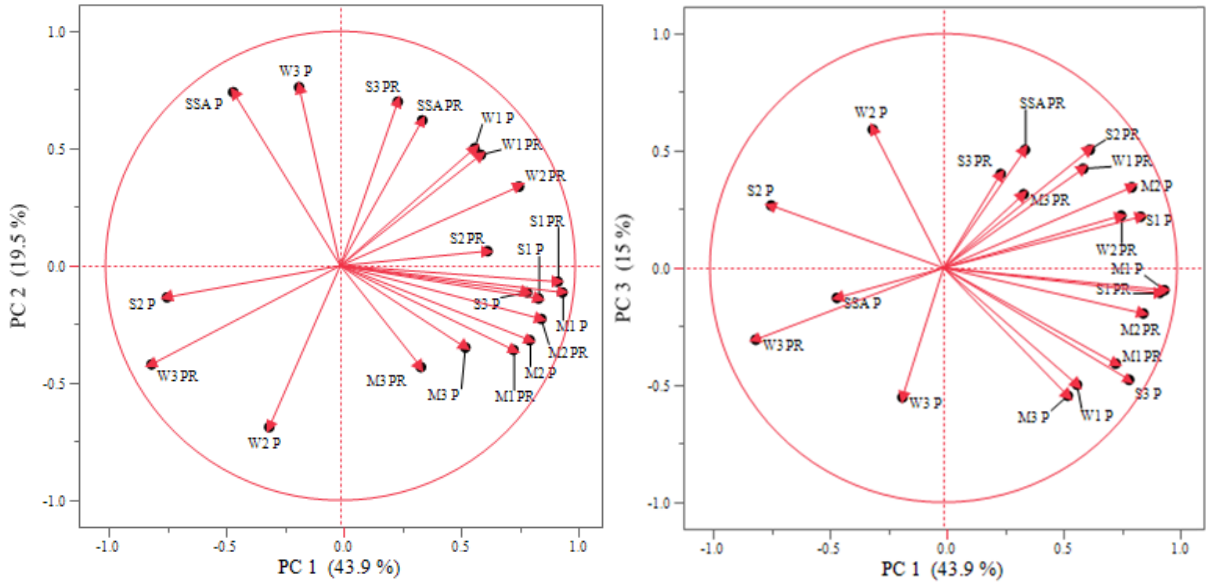


Figure 7.3: Loading plots of the first three principal components which describe 78.4% of the variation between the particle size parameters of the three log-normal distributions (mean, M, standard deviation, S, and weight, W) for the pastes (P) and the pre-refined pastes (PR). The log-normal peak containing the smallest particles is labelled 1, the largest particles are within the log-normal peak labelled 3.

7.2.1.4 PCA of paste consistency and pre-refined PSD

Principal component analysis was again used to identify any similarities between the paste consistency and the resulting particle sizes of the pre-refined pastes. It was anticipated that pastes with a stiffer consistency would be able to resist the pressures of the rolls more, enabling larger particles to pass through. The paste consistency was represented by the results of the simplified BET, assessment of the paste consistency by an operator and the current measured on the mixing shaft at the end of mixing.

The first four principal components represented 81.26 % of the variation in the data. PC4 only correlated with some of the paste consistency parameters whilst PC3 only showed strong correlations with the pre-refined PSD parameters. As there were no links between the paste consistency and PSD parameters for PC3 and PC4, these were not plotted.

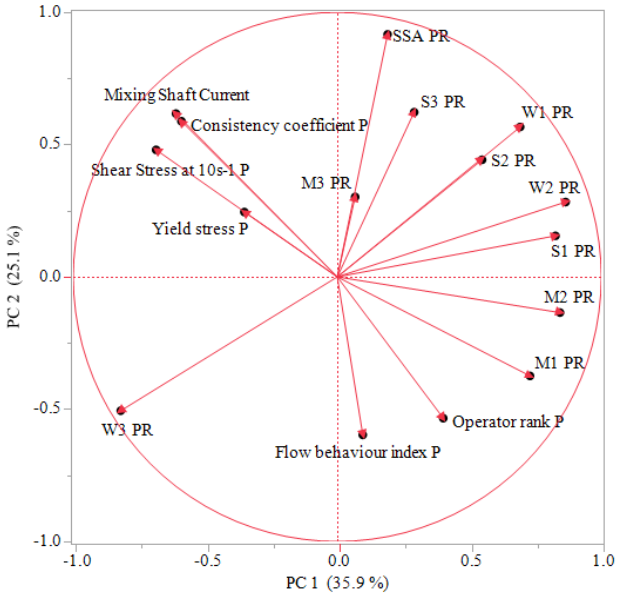


Figure 7.4: Loading plots of the first three principal components which describe 61 % of the variation between the results of the pastes measured using the BET (flow behaviour index, consistency coefficient, yield stress and the shear stress at a shear rate of 10 s^{-1}), the operator ranks of the pastes, the values of current measured at the end of mixing and the particle size parameters of the three log-normal distributions describing the pre-refined pastes (mean, M, standard deviation, S, and weight, W). The log-normal peak containing the smallest particles is labelled 1, the largest particles are within the log-normal peak labelled 3.

The first two principal components, plotted against each other in Figure 7.4, show that the measurements describing the consistency of the paste do not cluster in similar regions to any of the pre-refined paste PSD parameters. This indicated that the consistency of the pastes did not directly link to the particle size leaving the pre-refiner, even though the SSA showed significant effects of the fat and the interaction between the lecithin and mixing time.

7.2.2 Consistency of pre-refined paste

7.2.2.1 Comparing measurement techniques

The measured values of peak force and relaxation force for each paste are detailed in Table 7.13 along with the ranks given to each paste by the operator. The calculated values of the Herschel-Bulkley model parameters are then shown in Table 7.14.

Table 7.13: Measurements of peak and relaxation forces using the simplified back extrusion technique and the operator ranks for each pre-refined paste produced in trial 1

Run	Peak force at 2 mm s^{-1}	Peak force at 4 mm s^{-1}	Relaxation force at 2 mm s^{-1}	Relaxation force at 4 mm s^{-1}	Operator Rank
	N	N	N	N	-
1	1.194	1.829	0.241	0.242	6
2	0.536	0.796	0.189	0.188	10
3	0.996	1.536	0.218	0.226	5
4	6.701	8.97	2.326	2.199	3
5	0.722	1.009	0.205	0.205	5
6	1.611	2.219	0.413	0.363	4
7	0.575	0.867	0.192	0.194	8
8	2.849	3.772	1.243	1.229	3.5
9	0.397	0.59	0.185	0.187	6
10	0.767	1.159	0.2	0.199	5
11	2.17	2.872	0.744	0.732	-
12	0.353	0.43	0.188	0.188	5
13	0.43	0.632	0.187	0.189	6
14	0.337	0.496	0.183	0.189	7
15	-	-	-	-	6
16	1.108	1.727	0.23	0.229	4
17	0.997	1.562	0.218	0.221	4
18	0.44	0.652	0.188	0.188	6
19	1.409	2.008	0.399	0.383	-

Table 7.14: Calculated values of Herschel-Bulkley model parameters based upon the measured values using the simplified BET for each pre-refined paste produced in trial 1

Run	Flow Behaviour Index	Consistency Coefficient	Yield Stress	Shear Stress at 10 s^{-1}
	-	Pa.s	Pa	Pa
1	0.67	113.86	26.76	559.32
2	0.79	39.79	6.52	251.86
3	0.64	98.07	18.65	446.74
4	0.48	211.71	930.16	1569.51
5	0.69	61.51	13.20	314.46
6	0.45	104.88	90.07	385.66
7	0.83	42.42	7.80	294.59
8	0.71	30.00	448.94	602.80
9	0.97	18.48	9.79	182.26
10	0.72	68.52	9.21	368.81
11	0.39	67.35	243.30	408.62
12	1.08	4.99	15.25	75.24
13	0.97	21.30	9.27	208.05
14	1.03	8.34	13.23	102.59
15	-	-	-	-
16	0.72	102.73	21.47	560.60
17	0.67	92.23	17.64	449.03
18	0.87	23.97	9.84	187.53
19	0.52	80.16	91.41	356.84

To evaluate whether the back extrusion results measured similar properties of the pre-refined pastes to how the operator ranked them, the results of a principal component analysis results are shown in Figure 7.5. Principal component 1 represented 70.2 % of the variation; yield stress, consistency coefficient and shear stress all had strong positive relations ships with PC1 and the operator rank and flow behaviour index had strong negative correlations with PC1. On the plot, the operator rank is located closely to the flow behaviour index which may have suggested that the shear thinning behaviour of the paste influenced how the operator perceived the consistency to be. When considering this result, it is important to be reminded

of previous discussions referring to this methodology; as the simplified BET only measured each paste at two speeds, the value of the flow behaviour indices is likely to be unreliable.

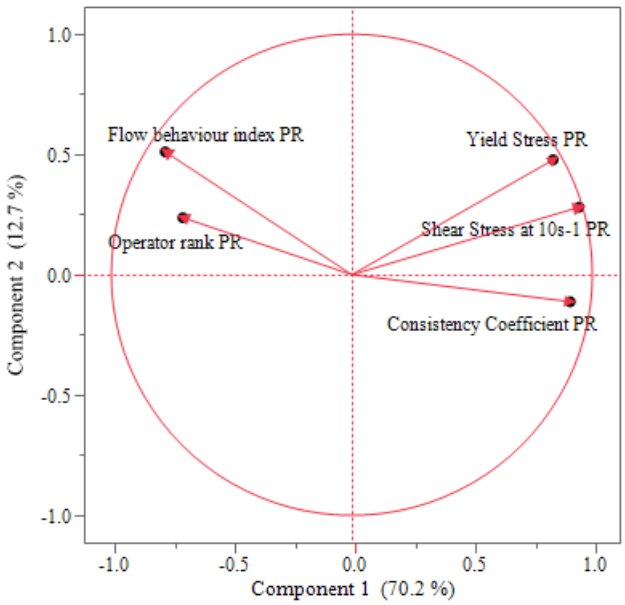


Figure 7.5: Loading plots of the first two principal components which describe 82.9 % of the variation between the results of the pre-refined pastes measured using the BET (flow behaviour index, consistency coefficient, yield stress and the shear stress at a shear rate of 10 s^{-1}) and the operator rank of the pre-refined pastes.

7.2.2.2 Factors affecting the consistency of the pre-refined paste

Using least squares analyses, the parameters of the Herschel-Bulkley model describing the pre-refined pastes were not found to be significantly affected by the formulation or processing conditions changes. However, the shear stresses of the pre-refined pastes at a shear rate of 10 s^{-1} were significantly impacted by the DoE factors ($p\text{-value}_{ANOVA} = 0.0251$). The results of the ANOVAs are presented in Table 7.15 - Table 7.19.

The results showed that the fat content significantly decreased the shear stress at a shear rate of 10 s^{-1} (Figure 7.6). Not only did high fat pastes have a higher volume of fluid, the specific surface area (SSA) was shown to be significantly lower (section 7.2.1.2), hence less fat would have been immobilised at surfaces. There was also a significant effect of the interaction

between mixing time and mixing speed on the shear stress of the pre-refined paste. The pre-refined paste was found to be significantly thicker when the paste was only combined for a short time at a low speed (Figure 7.7). Once it had been either mixed for longer or at a higher speed, the shear stress reduced similarly to increasing the fat content.

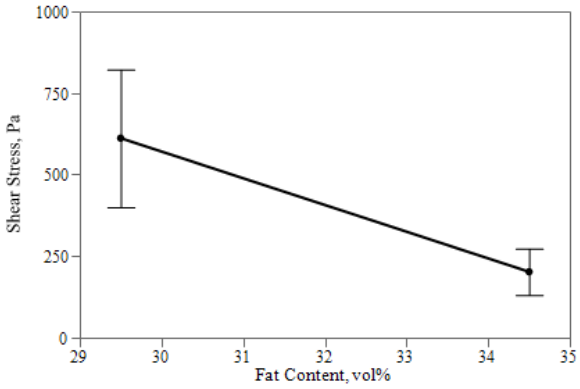


Figure 7.6: The fat content significantly impacts the shear stress of pre-refined paste at a shear stress of 10 s^{-1}. The results from the predictive model are plotted and the error bars are the standard deviation.

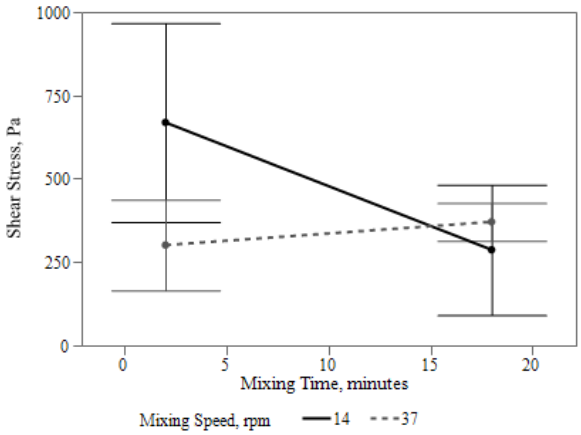


Figure 7.7: Interaction between mixing time and mixing speed significantly impacts the shear stress of pre-refined paste at a shear stress of 10 s^{-1}. The results from the predictive model are plotted and the error bars are the standard deviation.

The predictive model for the yield stress did not significantly fit the data as it was skewed by several high measurements. In Figure 7.8 it is possible to see that five pastes showed a yield stress above 90 Pa whilst the remaining paste yield stresses were relatively low; these five pastes all had a low fat content. Unlike the chocolate pastes, the yield stresses of pre-refined pastes were not anticipated to be caused by entrained air. The particle size reduction in pre-refining caused the overall distribution to become narrower. It is possible that this will have reduced the maximum packing fraction of the solids. The solids volume content within the pre-refined pastes will then have been closer to the maximum packing fraction. When the fat content of the pre-refined pastes was low, the solids volume content may have approached the maximum packing fraction and the results indicated that low fat pastes had a significant yield stress.

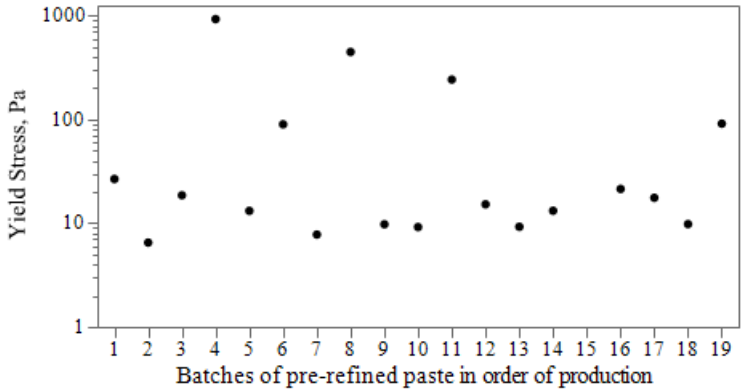


Figure 7.8: Yield stresses of the pre-refined pastes which were produced in trial 1

The predictive model fitted very well to the results of the operator rankings of pre-refined pastes ($p\text{-value}_{ANOVA}$ = 0.0043). The fat content and lecithin content were found to show significant effects; as the content of either the fat or the lecithin increased, so did the operator rank, indicating a thinner paste (Figure 7.9 and Figure 7.10, respectively).

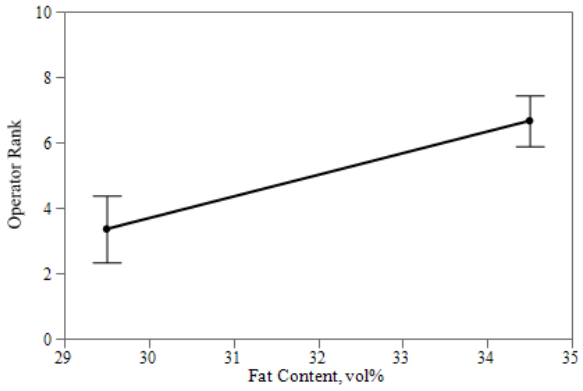


Figure 7.9: The fat content significantly impacts the operator rank of pre-refined paste. The results from the predictive model are plotted and the error bars are the standard deviation.

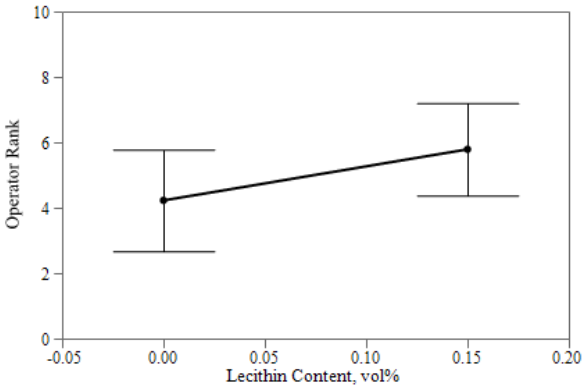


Figure 7.10: The lecithin content significantly impacts the operator rank of pre-refined paste. The results from the predictive model are plotted and the error bars are the standard deviation.

Lecithin content, as an independent factor, did not show a significant effect on the PSD so this result may have been due to the lecithin molecules acting as surfactants to reduce the viscosity. As it was not found to have a significant effect on the BET results however, this may suggest that there was some bias, as the operator was aware of the formulation of each paste.

The operator rank was also significantly affected by an interaction between lecithin and mixing time. Referring to the particle sizes of the pre-refined paste, the specific surface area showed some marginal significance of this interaction (p-value = 0.0754). This could explain why the operator ranking indicated significant differences; when there was no lecithin, increasing the mixing time increased the SSA which would have resulted in a thicker paste. When there is 0.15 vol% lecithin, the SSA reduced when the paste has been mixed for a longer time which resulted in a thinner paste. This suggests that the lecithin may not have been having a direct effect on the consistency, as was also found for paste, but it could have been influencing how the particles refine.

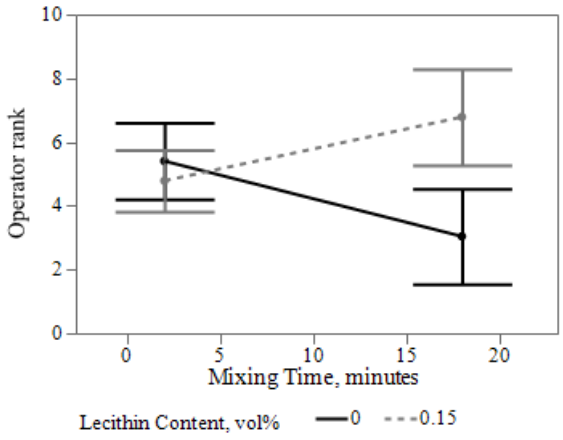


Figure 7.11: Interaction between lecithin content and mixing time significantly impacts the operator rank of pre-refined paste. The results from the predictive model are plotted and the error bars are the standard deviation.

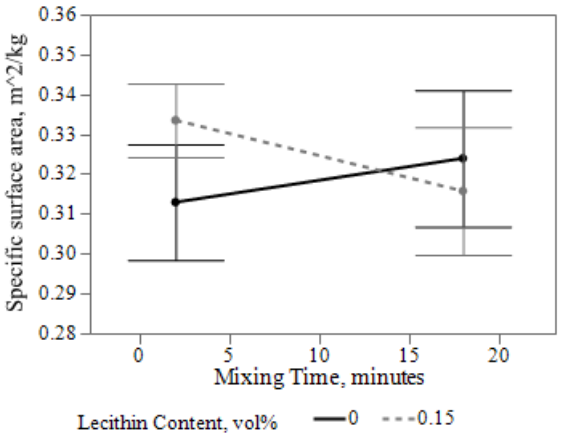


Figure 7.12: Interaction between lecithin content and mixing time significantly impacts the SSA of pre-refined paste. The results from the predictive model are plotted and the error bars are the standard deviation.

Table 7.15: Significance of factors and interactions on the operator ranking of the pre-refined paste (p-value$_{ANOVA}$ = 0.0043)*

Term	p-value	Sig.
Fat Content	0.0002	*
Lecithin Content*Mixing Time	0.0027	*
Lecithin Content	0.0199	*
Mixing Time*Mixing Speed	0.0583	
Lecithin Content*Mixing Speed	0.0739	
Mixing Speed	0.1041	
Fat Content*Mixing Speed	0.2422	
Fat Content*Mixing Time	0.3692	
Fat Content*Lecithin Content	0.5166	
Mixing Time	0.7114	

Table 7.16: Significance of factors and interactions on the flow behaviour index of the pre-refined paste (p-value$_{ANOVA}$ = 0.0977)

Term	p-value	Sig.
Fat Content	0.0022	*
Lecithin Content	0.2154	
Fat Content*Mixing Speed	0.3180	
Mixing Speed	0.3332	
Mixing Time*Mixing Speed	0.3825	
Lecithin Content*Mixing Speed	0.5178	
Lecithin Content*Mixing Time	0.6075	
Fat Content*Lecithin Content	0.7565	
Mixing Time	0.9174	
Fat Content*Mixing Time	0.9449	

Table 7.17: Significance of factors and interactions on the consistency coefficient of the pre-refined paste (p-value$_{ANOVA}$ = 0.0990)

Term	p-value	Sig.
Fat Content	0.0048	*
Fat Content*Lecithin Content	0.0884	
Lecithin Content*Mixing Speed	0.1942	
Lecithin Content	0.2191	
Mixing Time*Mixing Speed	0.2541	
Lecithin Content*Mixing Time	0.5419	
Fat Content*Mixing Speed	0.5608	
Fat Content*Mixing Time	0.5793	
Mixing Time	0.6574	
Mixing Speed	0.7571	

Table 7.18: Significance of factors and interactions on the yield stress of the pre-refined paste (p-value$_{ANOVA}$ = 0.1172)

Term	p-value	Sig.
Fat Content	0.0346	*
Mixing Speed	0.0752	
Fat Content*Mixing Speed	0.0773	
Fat Content*Mixing Time	0.1460	
Mixing Time*Mixing Speed	0.1466	
Mixing Time	0.1533	
Lecithin Content*Mixing Time	0.3355	
Lecithin Content*Mixing Speed	0.5735	
Fat Content*Lecithin Content	0.8547	
Lecithin Content	0.8709	

Table 7.19: Significance of factors and interactions on the shear stress, at a shear rate of 10s-1, of the pre-refined paste ($p\text{-value}_{ANOVA}$ = 0.0251)*

Term	p-value	Sig.
Fat Content	0.0029	*
Mixing Time*Mixing Speed	0.0432	*
Fat Content*Mixing Speed	0.0595	
Fat Content*Lecithin Content	0.0780	
Lecithin Content	0.1298	
Mixing Time	0.1318	
Mixing Speed	0.1653	
Fat Content*Mixing Time	0.2173	
Lecithin Content*Mixing Speed	0.2781	
Lecithin Content*Mixing Time	0.4261	

7.2.2.3 Consistency changes between Paste and Pre-Refined Paste

It was expected that the paste will become thicker after it was pre-refined; the particles were reduced in size and therefore there was a larger surface area of particles required to be coated in fat. Figure 7.13 shows comparisons of the Herschel-Bulkley parameters and the shear stress at a shear rate of 10 s^{-1} for the paste and the pre-refined pastes.

Although the pastes were ranked by the operator on the same number scale of 0 - 10, the expectation for what would appear to be a thick paste compared to a thick pre-refined paste was different. It was therefore not possible to compare these results as the values of maximum and minimum were not equivalent.

The results are plotted over the range of fat contents as many parameters are significantly affected by this factor. The consistency coefficient and overall shear stress of the pre-refined pastes were higher and the flow behaviour indices were lower than the pastes.

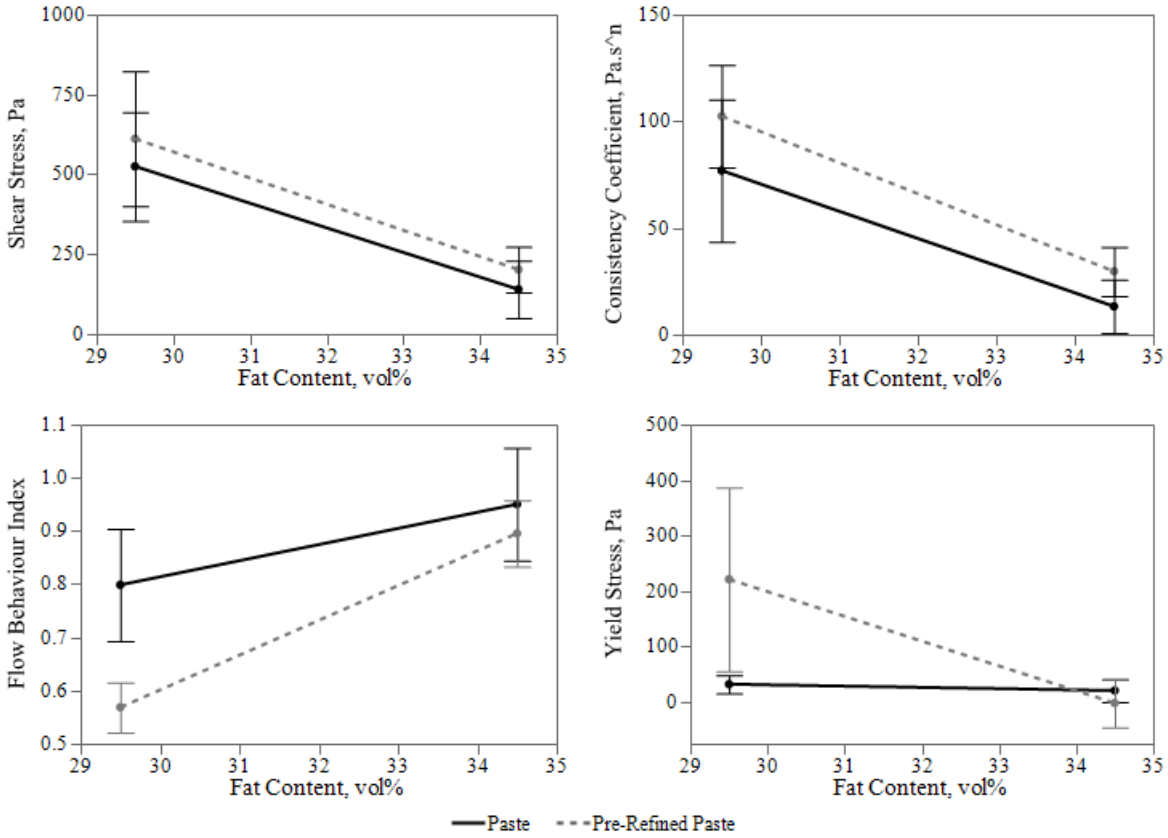


Figure 7.13: Consistency parameters of the paste and pre-refined pastes based on the predictive models for the Herschel-Bulkley model parameters and the shear stress at a shear rate of 10 s^{-1}. The results from the predictive model are plotted and the error bars are the standard deviation.

The yield stress was larger when the pastes were pre-refined when the fat content was low however pre-refined pastes containing 34.5 vol% fat were measured to have lower yield stresses than the pastes. It was hypothesised in chapter 6 that the yield stresses measured in the pastes were caused by entrained air within the paste which increased the effective solids volume of the pastes. Once the pastes pass through the pre-refiner, pockets of air will be able to escape as a thin layer of material is formed and the air will come into contact with the atmosphere. Pre-refined pastes are therefore unlikely to contain entrained air which contribute to additional effective solids volume content.

As the particles within pre-refined pastes were smaller than pastes, although the solids volume content had not changed, the whole distribution became narrower which was likely to

decrease the maximum packing fraction. Fat was forced to remain between voids of particles when the maximum packing fraction was lower therefore less fat was available to aid flow. At a low fat content, the pre-refined pastes displayed high yield stresses.

7.2.2.4 Comparing the consistencies and the PSDs of the pre-refined pastes

To determine if there were any relationships between the pre-refined paste particle sizes and consistencies, principal component analysis was again used. Only the first two principal components correlated with both the consistency and PSD parameters, representing 71.1 % of the variation. Figure 7.14 shows the plot of PC1 against PC2. It is again possible to see that the parameters describing the pre-refined paste consistency were clustered together. The parameters describing the particle sizes were more spread out therefore overall, it did not seem possible to identify any relationships between the pre-refined paste particle sizes and consistency.

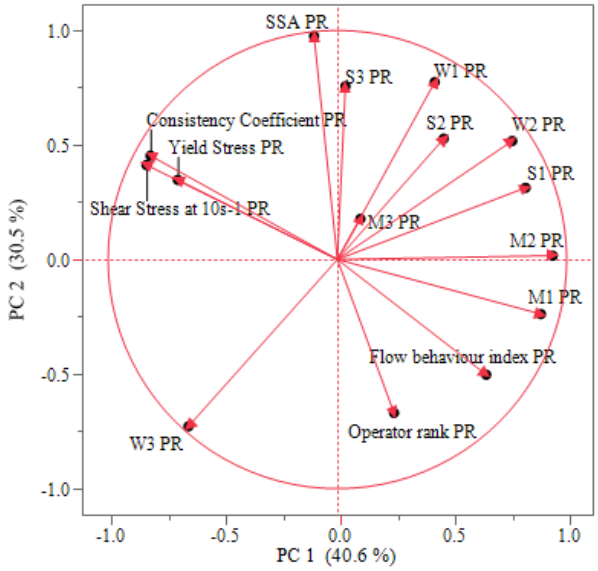


Figure 7.14: Loading plots of the first three principal components which describe 71.1 % of the variation between the results of the pre-refined pastes measured using the BET (flow behaviour index, consistency coefficient, yield stress and the shear stress at a shear rate of 10 s^{-1}), the operator ranks of the pre-refined pastes and the particle size parameters of the three log-normal distributions describing the pre-refined pastes (mean, M, standard deviation, S, and weight, W). The log-normal peak containing the smallest particles is labelled 1, the largest particles are within the log-normal peak labelled 3.

7.2.2.5 Can the change in pre-refined paste consistency due to fat content be replicated by longer mixing time?

The pastes consistencies were compared in section 6.2.5 in order to establish whether intensifying the mixing process will reduce the consistency of the paste similarly to adding a higher proportion of fat. The same method was now used to compare the consistencies of pre-refined pastes (Figure 7.15). The shear stress data is split in two ways: firstly, each of the four different markers represents paste at a different fat and lecithin content. Secondly, each data point is categorised on the x-axis based on the mixing time and mixing speed combination.

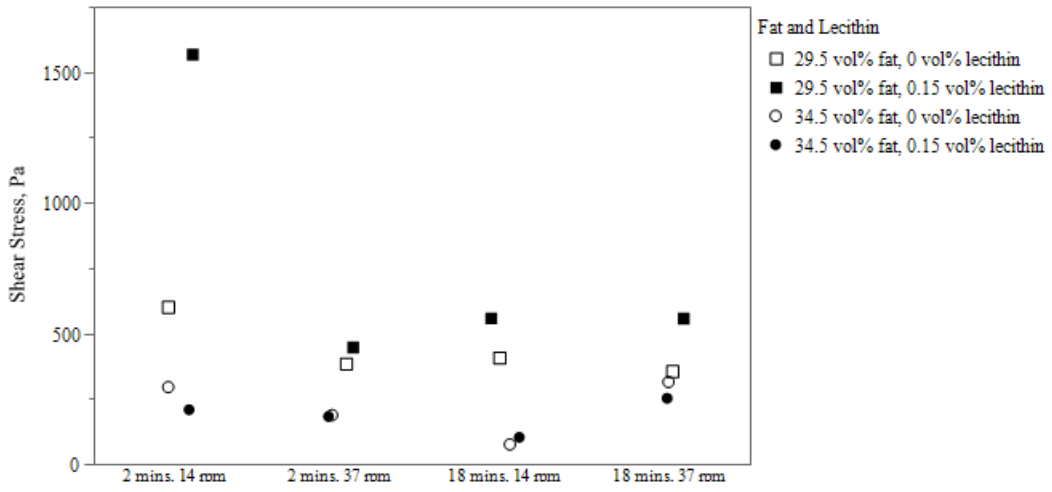


Figure 7.15: Shear stress at a shear rate of 10 s^{-1} of pre-refined pastes produced in trial 1, based on the Herschel-Bulkley parameters measured on the BET, varying in fat content, lecithin content, mixing time and mixing speed. The points are staggered within each mixing category in order to see each of the points clearly.

At all combinations of the mixing conditions, the pre-refined pastes containing a high amount of fat resulted in shear stresses which were lower than the pre-refined pastes containing only 29.5 vol% fat. Both a higher volume of liquid and a lower SSA contributed towards these pastes having a consistently thinner consistency than pastes with a lower fat content. At a high fat content, the presence of lecithin did not have much of an impact on the shear stress of the

pre-refined pastes whereas low fat pre-refined pastes had a higher shear stress when there was lecithin present (particularly after a short mixing time and speed).

7.2.3 Discussion

Overall, the results suggested that the pre-refiner broke down the large sugar particles into a broad range of smaller particles. Without further evaluation of the particles, through either microscopy or centrifugation, it could not be concluded whether the skimmed milk powder or sweet whey powder were affected by the pre-refining stage.

As the flow behaviour index was only measured at two different probe velocities, this parameter could not be independently relied upon. The consistency coefficient compensated in response to the flow behaviour index so that the shear stresses corresponded to the raw data. Hence, the shear stress at a shear rate of 10 s^{-1} was the most appropriate parameter to compare the pre-refined paste consistencies. The shear stress of the paste significantly decreased when there was a greater proportion of fat. This was likely to be due to the increased liquid content, similarly to the results of the pastes. The results did not conclusively show whether the fat content had an effect of the size of the pre-refined paste particles. Differences may have been masked by the variation of the raw ingredients and the error of the measuring technique.

When the pastes were mixed for a short time at a low speed, the shear stresses of the pre-refined pastes were significantly higher but there were no statistically significant effects of the pre-refined PSD. Overall, the parameters describing the consistencies of the pre-refined pastes did not clearly relate to differences of the pre-refined paste PSDs. This could have again been due to the variation in the size of the raw materials, the error of the PSD measurement

technique or that the differences in paste consistency are being caused by other mechanisms such as the location of the fat or presence of agglomerated particles.

There was not a significant fit of the model to the yield stresses of these pre-refined pastes; the pastes with yield stresses above 90 Pa skewed the overall results. Five pastes fell above this value and they all had a low fat content. It has been hypothesised that as the pre-refined paste particle size distribution was narrower than paste, the maximum packing fraction was lower. Low fat pastes will have had a solids volume content close to the maximum packing fraction, leading to a higher yield stress.

The operator ranking was the only measurement to be significantly affected by the lecithin content and there was also a significant interaction between lecithin content and mixing time. As the effect of lecithin on the offline measurements was not measured to be significant, the result may suggest that the lecithin was affected by the temperature of the paste/pre-refined paste online. There was also the possibility that there was bias in the results from the operator as they were aware of the paste formulation.

From comparison of all the pre-refined pastes, unlike the pastes, the high fat pre-refined pastes were measured to have a consistently lower shear stress than the pastes with 5 vol% less fat, regardless of the mixing conditions within the paster.

7.3 Trial 1: Refined flake

Once the paste had passed through the pre-refiner, the material was held in an intermediate mixer which was heated at 50°C before it was transferred on a belt to the five roll refiner. Material was fed on a belt to the bottom of the five-roll refiner. It passed through four gaps and was scraped off the top roll into a collection vessel. Details of this process are discussed in section 3.2.2.2.

The particle size of this material, now known as refiner flake, was assessed using a Malvern Mastersizer 2000 based on the method discussed in section 3.3.2. The particle size distribution of the refiner flake was bi-modal therefore it was modelled by two log-normal peaks which each had a mean (M), standard deviation (S), and a weighting (W). The d_{90} is conventionally used by Mondelēz International to describe differences between bi-modal distributions of refined flake within research and manufacturing environments. It is the particle size at which 90 vol% of the particles are below. It is considered to be adequate at describing differences between the PSD which influence the sensory properties of final chocolate and therefore was used as an additional parameter to compare these refined PSDs.

7.3.1 Refined particle sizes

Least square fits were modelled to the PSD parameters of refiner flake however none of the models fitted the data significantly. Six pastes were not refined which was likely to have caused this issue. Nevertheless, all but one of the parameters describing the refined flake PSDs indicated that the fat content had a significant effect; the standard deviation of the first peak, the means of both the peaks and the d_{90} significantly decreased whilst the SSA significantly increased. Figure 7.16 shows that pastes which had a higher fat content produced refined flakes with significantly smaller particles.

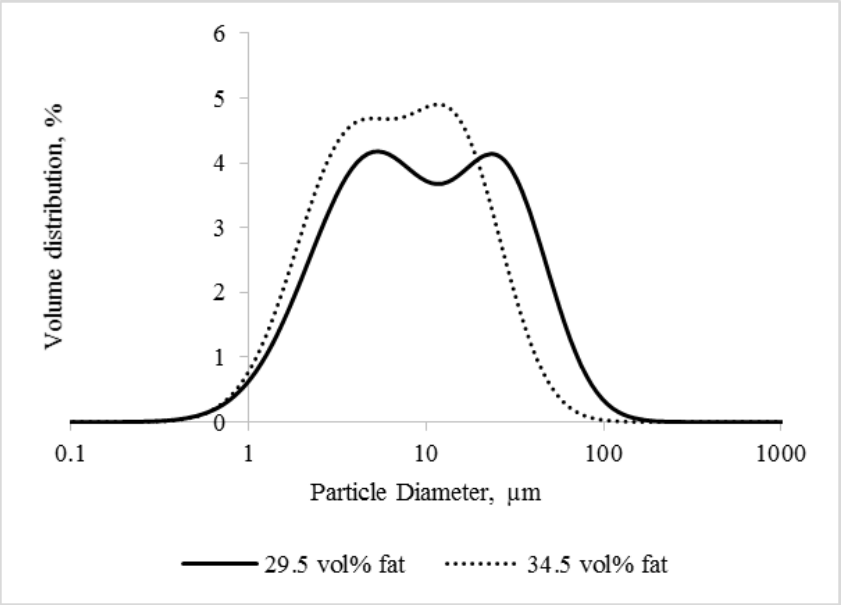


Figure 7.16: Influence of the fat content on the refiner flake PSDs using the average model parameters from the least squares fit

The standard deviation of the second peak was the only parameter which was significantly affected by other interactions of factors. Firstly, the interaction between mixing time and speed significantly affected this parameter (p-value = 0.0406). Viewing the entire PSD at extremes of these conditions suggested that when the standard deviation of the second peak varies, there were big differences to the overall PSD (Figure 7.17).

There were two interactions which significantly impacted the standard deviation of the second peak: mixing time * mixing speed and fat content * mixing speed (p-values = 0.0406 and 0.0454, respectively). Comparing the overall PSD based on the predictive models of each PSD parameter, when the paste had been mixed at a low mixing speed for a short time, the refiner flake was second (Figure 7.17). When the paste was either mixed for longer or the mixing speed was increased, there was a reduction in the volume of particles above 15 µm. When pastes were mixed at a high speed for a long time, the second peak showed a larger proportion of particles but there were much fewer particles above 20 µm.

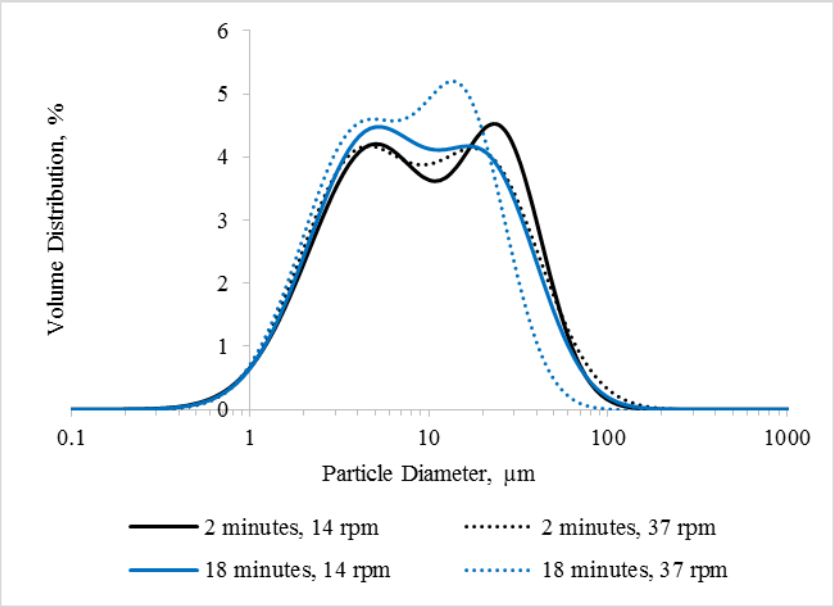


Figure 7.17: Influence of the mixing time and mixing speed on the refined flake PSDs using the average model parameters from the least squares fit

The entire particle size distributions were then plotted to examine the interaction of fat and mixing speed (Figure 7.18). Refiner flakes which had a low fat content and were mixed at a low speed contained the largest particles. When the paste had been mixed at a higher speed, the refiner flake particles above 32 µm were reduced. Pastes which had a higher fat content and were mixed at a low speed were refined to particles with smaller particles and if the pastes were mixed at a higher speed, the refiner flakes were smaller still. This result suggested that the two factors did not interact but mixing speed did appear to contribute towards a refined flake with a smaller PSD.

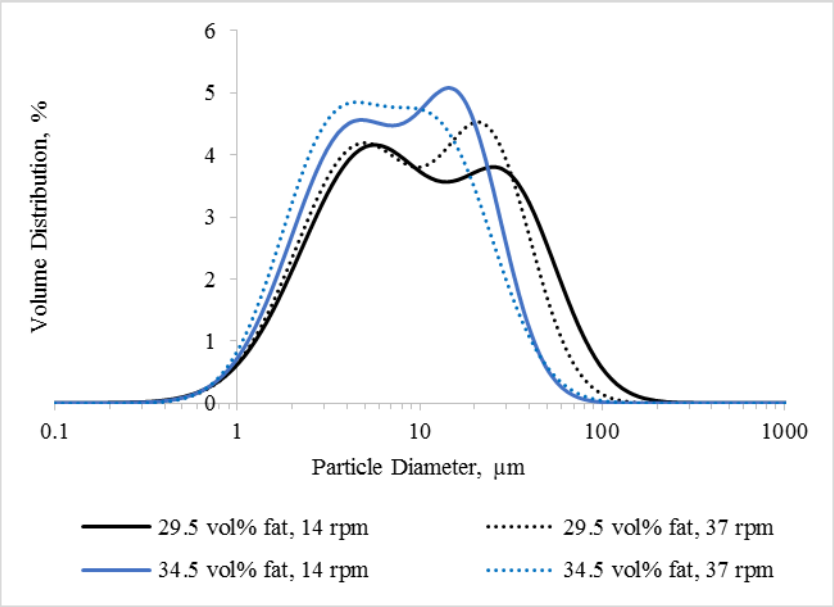


Figure 7.18: Influence of the fat content and mixing speed on the refined flake PSDs using the average model parameters from the least squares fit

Table 7.20: Significance of factors and interactions on the mean of the first refined flake PSD peak ($p\text{-value}_{ANOVA}$ = 0.136)

Term	p-value	Sig.
Fat Content	0.0318	*
Mixing Speed	0.0847	
Lecithin Content	0.2227	
Fat Content *Mixing Time	0.2681	
Fat Content * Lecithin Content	0.3863	
Mixing Time*Mixing Speed	0.6860	
Fat Content *Mixing Speed	0.7147	
Lecithin Content *Mixing Time	0.7391	
Lecithin Content *Mixing Speed	0.7574	
Mixing Time	0.8280	

Table 7.21: Significance of factors and interactions on the standard deviation of the first refined flake PSD peak ($p\text{-value}_{ANOVA}$ = 0.0849)

Term	p-value	Sig.
Fat Content	0.0212	*
Mixing Speed	0.0557	
Lecithin Content	0.1542	
Fat Content *Mixing Time	0.2510	
Fat Content * Lecithin Content	0.2558	
Mixing Time	0.4711	
Mixing Time*Mixing Speed	0.5897	
Fat Content *Mixing Speed	0.6084	
Lecithin Content *Mixing Time	0.8505	
Lecithin Content *Mixing Speed	0.8682	

Table 7.22: Significance of factors and interactions on the weight of the first refined flake PSD peak ($p\text{-value}_{ANOVA} = 0.328$)

Term	p-value	Sig.
Mixing Speed	0.0815	
Fat Content	0.0918	
Lecithin Content *Mixing Speed	0.3573	
Fat Content *Mixing Speed	0.4015	
Fat Content *Mixing Time	0.4101	
Mixing Time*Mixing Speed	0.4178	
Mixing Time	0.5032	
Lecithin Content	0.5751	
Lecithin Content *Mixing Time	0.6052	
Fat Content * Lecithin Content	0.9699	

Table 7.23: Significance of factors and interactions on the mean of the second refined flake PSD peak ($p\text{-value}_{ANOVA} = 0.173$)

Term	p-value	Sig.
Fat Content	0.0479	*
Mixing Speed	0.2113	
Lecithin Content	0.2185	
Fat Content * Lecithin Content	0.2241	
Mixing Time	0.4240	
Fat Content *Mixing Time	0.4283	
Lecithin Content *Mixing Time	0.7189	
Fat Content *Mixing Speed	0.7454	
Mixing Time*Mixing Speed	0.9024	
Lecithin Content *Mixing Speed	0.9607	

Table 7.24: Significance of factors and interactions on the standard deviation of the second refined flake PSD peak ($p\text{-value}_{ANOVA} = 0.162$)

Term	p-value	Sig.
Mixing Time * Mixing Speed	0.0406	*
Fat Content * Mixing Speed	0.0454	*
Fat Content * Mixing Time	0.0712	
Fat Content * Lecithin Content	0.0959	
Mixing Speed	0.1102	
Lecithin Content	0.1111	
Lecithin Content *Mixing Time	0.4451	
Fat Content	0.4588	
Mixing Time	0.5725	
Lecithin Content *Mixing Speed	0.5746	

Table 7.25: Significance of factors and interactions on the d_{90} of the refined flake PSD ($p\text{-value}_{ANOVA} = 0.142$)

Term	p-value	Sig.
Fat Content	0.0393	*
Fat Content * Lecithin Content	0.1529	
Lecithin Content	0.1641	
Mixing Speed	0.2646	
Mixing Time	0.3280	
Fat Content *Mixing Speed	0.4405	
Mixing Time*Mixing Speed	0.5130	
Fat Content *Mixing Time	0.6580	
Lecithin Content *Mixing Time	0.7253	
Lecithin Content *Mixing Speed	0.8161	

Table 7.26: Significance of factors and interactions on the SSA of the refined flake PSD ($p\text{-value}_{ANOVA} = 0.158$)

Term	p-value	Sig.
Fat Content	0.0352	*
Mixing Speed	0.1828	
Lecithin Content * Mixing Time	0.4189	
Lecithin Content	0.4544	
Fat Content * Lecithin Content	0.4674	
Fat Content * Mixing Time	0.5222	
Mixing Time	0.5797	
Lecithin Content *Mixing Speed	0.6058	
Fat Content * Mixing Speed	0.6300	
Mixing Time * Mixing Speed	0.9474	

7.3.2 Comparing Refiner Flake PSD with Paste Consistency

Principal component analysis was again used to identify similarities between the paste consistency and the refined flake PSD's. The loading plot of PC1 and PC2 is shown in Figure 7.19. Except for the standard deviation of the second PSD peak of the refiner flake, the particle size measurements of the flake are clustered together with the consistency coefficient, mixing shaft current and the shear stress at a shear rate of 10 s^{-1}, opposite the operator rank. All of these measurements, except the weight of the first refiner flake peak ($p\text{-value}_{fat}$ = 0.918), were found to be significantly impacted by the fat content. Although the missing samples prevented statistically significant models fitting the refiner PSD parameters, this result suggested that the fat content did have a strong influence on these parameters and provided confidence that the ANOVA results were meaningful.

PC2 strongly correlated with the flow behaviour index and negatively correlated with the standard deviation of the second PSD peak of the refiner flake however the plot did not

suggest that these two were related. The third principal component only correlated strongly with the yield stress and therefore this principal component was not plotted.

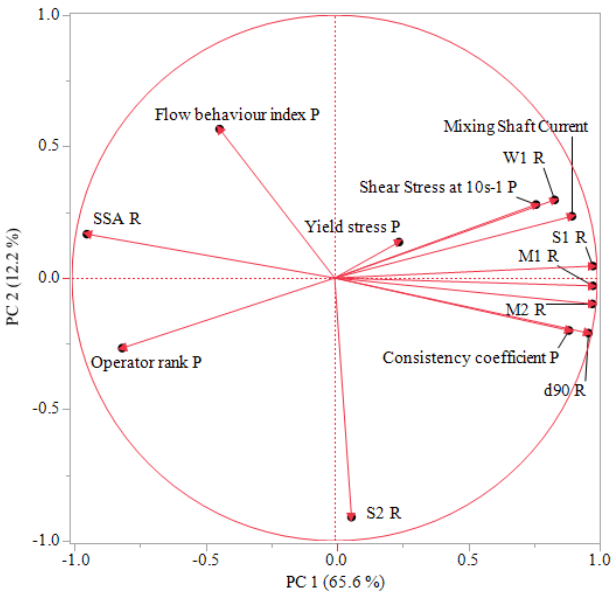


Figure 7.19: Loading plots of the first two principal components which describe 77.8 % of the variation between the results of the pastes measured using the BET (flow behaviour index, consistency coefficient, yield stress and the shear stress at a shear rate of 10 s^{-1}), the operator rank of the pastes, the mixing shaft current and the particle size parameters of the two log-normal distributions describing the refined flake (mean, M, standard deviation, S, and weight, W). The log-normal peak containing the smallest particles is labelled 1, the largest particles are within the log-normal peak labelled 2.

7.3.3 Comparing Refiner Flake PSD with Pre-Refined Paste Consistency

The loading plots of PC1 and PC2 are shown in Figure 7.20, representing the variability in the pre-refined paste consistency parameters and the refined flake PSD parameters. Similarly to the paste consistency comparisons, most of the refined flake PSD parameters showed a strong correlation with PC1, as did the shear stress at 10 s^{-1}, consistency coefficient and yield stress of the pre-refined pastes.

PC2, which represented 16.2% of the variability, showed a strong negative correlation with the standard deviation of the second peak, correlation with the flow behaviour index and some correlation with the consistency coefficient (negative) and the weight of the first peak (positive). Similarly to the results with the paste, plotting the second principal component did

not highlight any further relationships between the particle size parameters of the refiner flake with the pre-refined paste consistency.

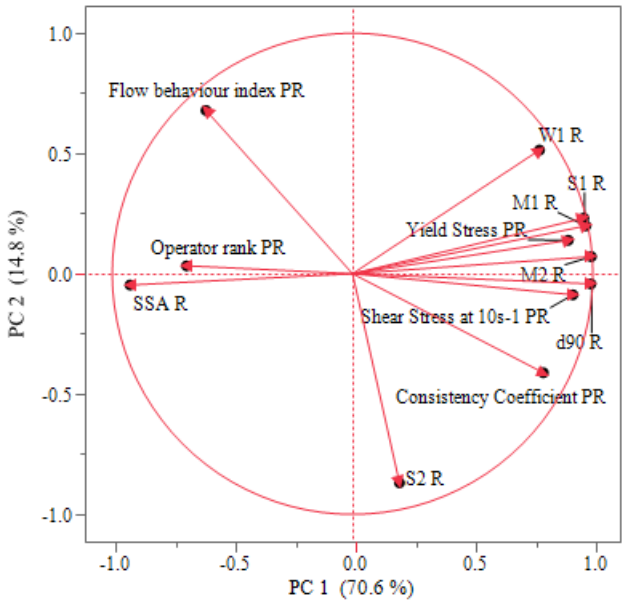


Figure 7.20: Loading plots of the first two principal components which describe 85.4 % of the variation between the results of the pre-refined pastes measured using the BET (flow behaviour index, consistency coefficient, yield stress and the shear stress at a shear rate of 10 s^{-1}), the operator rank of the pre-refined pastes and the particle size parameters of the two log-normal distributions describing the refined flake (mean, M, standard deviation, S, and weight, W). The log-normal peak containing the smallest particles is labelled 1, the largest particles are within the log-normal peak labelled 2.

7.3.4 Contrasting additional fat with more intensive mixing of the paste

The overall PSD of the refiner flakes when the fat content of the paste was high and the mixing conditions of the paste were low are compared to the PSD's when the fat content was 5 vol% lower but the paste was mixed for longer and at a higher speed in Figure 7.21. The refiner flake containing the higher fat content showed a smaller PSD (d_{90} = 24.97 µm) however the results when the paste had been more intensively mixed with only 29.5 vol% fat showed only slightly larger particles which had a similar shaped distribution (d_{90} = 27.92 µm).

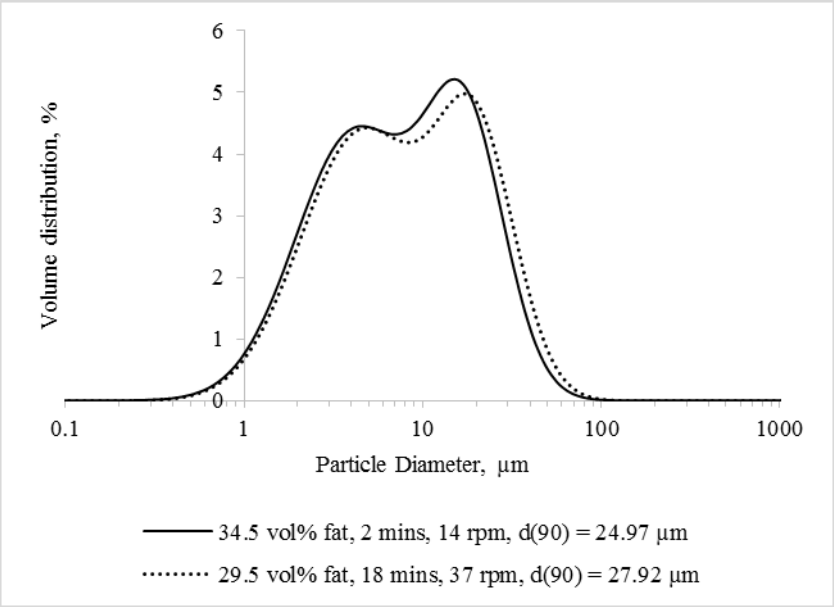


Figure 7.21: Plot of the refined flake PSD comparing low fat flakes which were pasted at intensive conditions and high fat flakes which were gently pasted based on the predictive models of each PSD parameter. Note: the lecithin content is at an average value = 0.075 vol%

7.3.5 Impact of lecithin

It was not yet clear whether there was an impact of lecithin on the paste, pre-refined paste or the refiner flake. Figure 7.22 shows the PSDs of refiner flakes (based on the predictive models of the PSD parameters) without lecithin, containing 29.5 and 32 vol% fat which were intensively mixed, in comparison to a 34.5 vol% refiner flake which was gently mixed. Refiner flakes which contained a low fat content had a greater proportion of small particles and had a lower d_{90} than high fat refiner flakes which were combined gently within the paster.

A similar comparison is made in Figure 7.23 when the lecithin content was 0.15 vol%. Pastes with the highest fat content resulted in the smallest refined particles and the proportion of particles within the second peak was larger than the first. The refined flake which contained only 29.5 vol% fat had a larger d_{90} and the proportion of particles within the two peaks was similar.

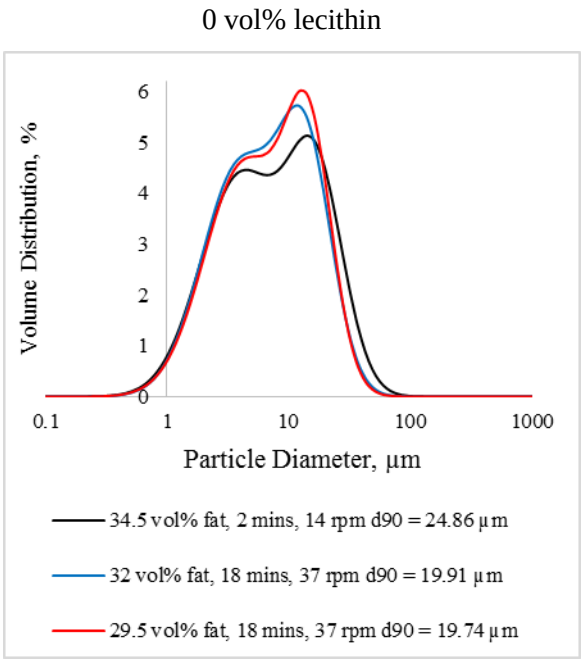


Figure 7.22: Plot of the refiner flake PSD based on the predictive models of each PSD parameter, comparing low fat flakes which were pasted at intensive conditions and high fat flakes which were gently pasted at 0 vol% lecithin.

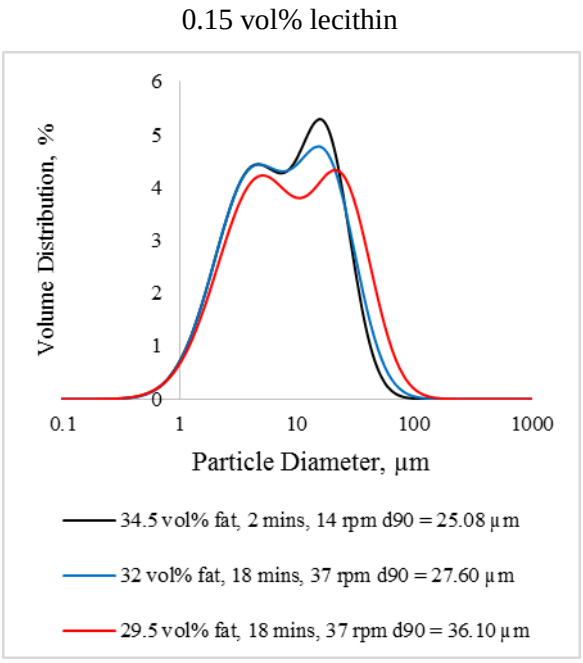


Figure 7.23: Plot of the refiner flake PSD based on the predictive models of each PSD parameter, comparing low fat flakes which were pasted at intensive conditions and high fat flakes which were gently pasted with 0.15 vol% lecithin.

In order to hypothesise why refiner flakes containing lecithin could have different particle sizes to refiner flakes without lecithin, the parameters of the Herschel-Bulkley model describing the pre-refined paste consistencies and the shear stress at a shear rate of 10 s^{-1} were compared in Figure 7.24. The flow behaviour indices of the low fat pre-refined paste increased as lecithin content increased whereas the flow behaviour indices of the high fat pre-refined paste did not change. The yield stresses also showed opposite responses; the yield stress of a high fat pre-refined paste increased when there was more lecithin however the yield stress of a low fat paste which had been intensely mixed showed a small yield stress when there was no lecithin and it decreased further as the pre-refined paste contained more lecithin. The yield stresses here were seen to become negative which was a consequence of using the values from the predictive model. The consistency coefficient increased as lecithin was added at a similar gradient for both high fat pre-refined pastes mixed gently and low fat pre-refined

pastes mixed intensely. At a shear rate of 10 s^{-1}, it was apparent that overall, the results increased similarly for both a high fat and low fat pastes when the lecithin content was larger.

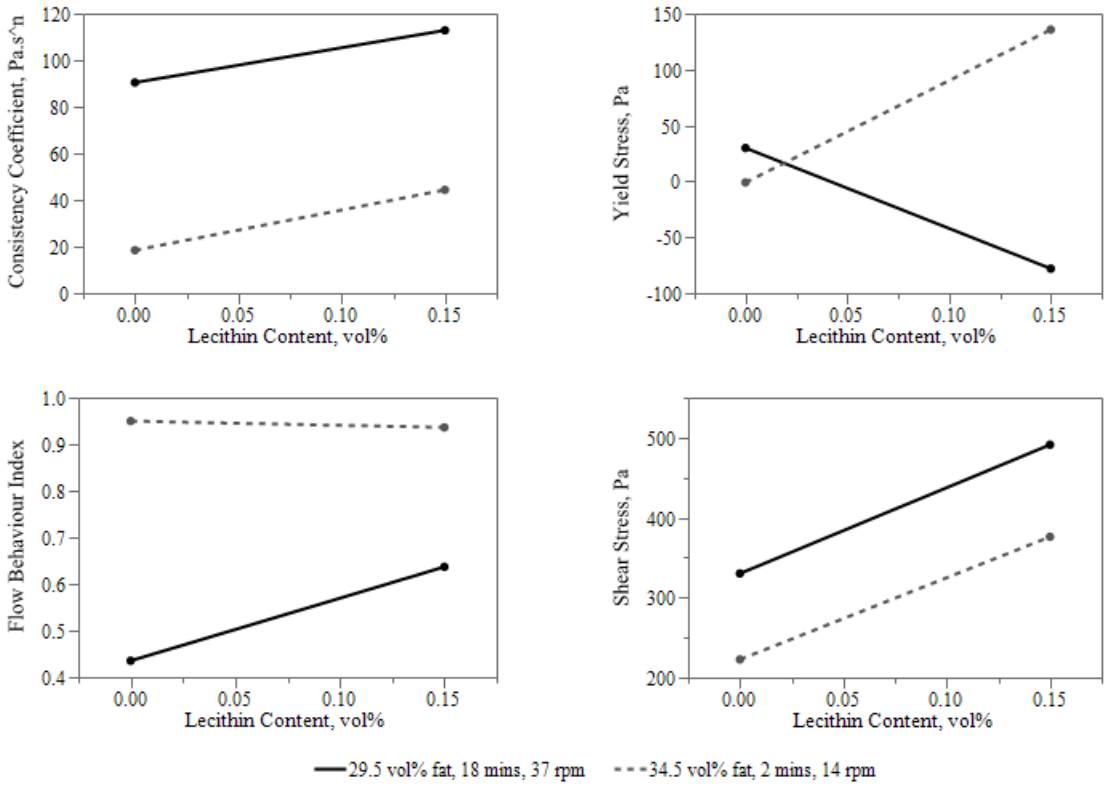


Figure 7.24: Plot of the pre-refined paste consistency measurements on the BET based on the predictive models over a range of the lecithin contents, comparing results of a low fat paste mixed for 18 minutes at 37 rpm and a low fat paste mixed for 2 minutes at 14 rpm.

To the authors' knowledge, there is no published work which established the shear rate the pre-refined paste undergoes as it passes through the refiner. Pastes will also undergo shear elongation as the top roll moves faster than the roll below. Figure 7.25 and Figure 7.26 show the shear stresses at the four extreme conditions which have been discussed in Figure 7.24. These were extrapolated from the Herschel-Bulkley model parameters measured on the BET over a range of shear rates from 0.1 s^{-1} to 5000 s^{-1}.

Overall, the results indicated that refined flakes had a lower d_{90} when the fat content was low and the mixing time/speed were high than when the fat was high and the mixing time/speed were low. This suggests that the pastes with a low fat content were likely to be thinner and

could not resist the pressure of the rolls as much, agreeing with the current anecdotal evidence. Referring to Figure 7.25, the shear stresses of the pre-refined paste with 29.5 vol% fat and 0 vol% lecithin (mixed at a high speed for a long time) was only lower than the high fat pre-refined paste when the shear rate was greater than 18 s^{-1}. When the pastes did contain lecithin, the d_{90} of the refiner flake was lower when the fat content was high and the mixing conditions were low. This suggests that these high fat pastes had a thinner consistency which could not resist the pressure of the rolls. Figure 7.26 shows that pastes only displayed this behaviour when the shear rate was below 250 s^{-1}.

Although it is not ideal to extrapolate the values of shear stress above the shear rates which were measured during the test, this analysis does suggest that the consistency of the pre-refined paste between 18 - 250 s^{-1} may be influencing the refiner flake PSD. It does not, however, provide any extra understanding of why lecithin impacts on the refining process.

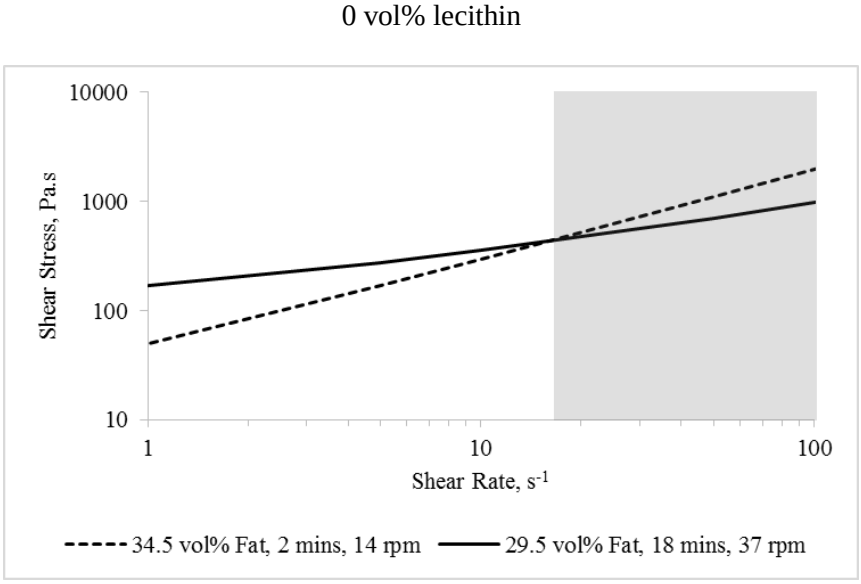


Figure 7.25: Plot of the shear stress and shear rate of two pastes which do not contain lecithin at 1) a high fat content and low mixing time/speed and 2) a high mixing time/speed and a low fat content. The highlighted region is where the behaviour of the paste is similar to what has been observed for refined flakes.

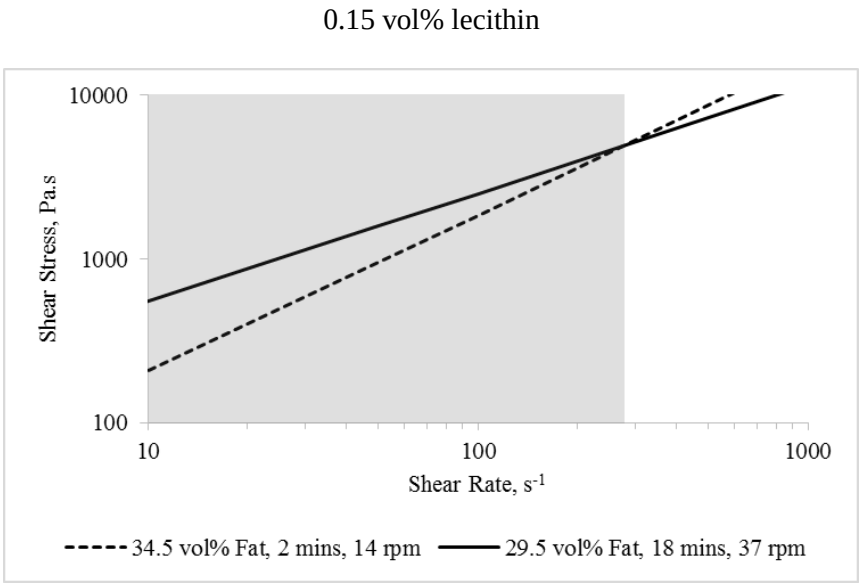


Figure 7.26: Plot of the shear stress and shear rate of two pastes which contain 0.15 vol% lecithin at 1) a high fat content and low mixing time/speed and 2) a high mixing time/speed and a low fat content. The highlighted region is where the behaviour of the paste is similar to what has been observed for refined flakes.

7.3.6 Discussion

PCA highlighted similarities between the PSD parameters of the refiner flakes and the consistency measurements of paste and pre-refined paste. Statistical analysis revealed that when the fat content was high, significantly smaller particles were produced. The pastes and pre-refined pastes had thinner consistencies which could not resist as much of the pressure between the rolls, hence the particles had to be reduced in size in order for the material to pass through the refiner gaps.

One PSD parameter, the standard deviation of the second refiner flake peak, showed no similarities to the other PSD or consistency measurements and it was not significantly affected by the fat content alone. This parameter was significantly impacted by interactions between mixing time and mixing speed and between fat content and mixing speed. The overall plots of refined flake PSDs, based on the model parameters from the predictive models, did not appear to be affected by the interaction of these factors. The results however,

highlighted that pastes which were mixed for longer at a higher speed resulted in a refined flake with smaller particles.

Although there was no significant interaction between the fat and the lecithin contents, plots of the refined flake PSDs at high and low levels of these factors revealed, unexpectedly, that when there was 0 vol% lecithin within the paste, smaller particles were produced when the fat content was lower. Conversely, when there was 0.15 vol% lecithin within the paste, smaller particles were produced when the fat content was higher. As the overall results suggested increasing fat content decreased the size of the refined pastes, agreeing with the anecdotal beliefs of operators, this result of pastes that do not contain lecithin was not anticipated. The interaction between fat and lecithin was not statistically significant and therefore it might be a possibility that this result of refined flakes without lecithin was not meaningful.

Alternatively, as the pastes are not Newtonian, they may have displayed contradicting results depending on the shear stress which the materials were evaluated at. A comparison was made between pre-refined pastes with and without lecithin to try and establish the shear rates of the pre-refined paste which might be relevant to the material behaviour through the refining stage. Although the parameters of the BET were extrapolated beyond the measured shear rates in the test, the comparisons indicate that the behaviour of the pre-refined paste between 18 – 250 s^{-1} was relevant to how the pre-refined pastes behaved within the refiner.

7.4 Trial 2

The two stage refining process used in trial one was complex and the five roll refiner, in particular, required a large amount of material to be processed in order to reach a steady state. It was therefore considered more appropriate to process the pastes through a one-step refining stage. A three-roll Lehmann refiner offered the opportunity to measure the current on the rolls

as the paste passed through two gaps. The operating conditions of the refiner were held constant, each roll rotating faster than the previous roll and the pressure between the three rolls was larger for the second gap than the first.

The design of experiments, described in chapter 6, involved four factors which were used to manufacture the pastes: fat content, lecithin content, mixing time and temperature. An operator manually fed the paste into the refiner, maintaining a constant level of material above the gap between the first two rolls. Prior to refining, the pastes were pre-heated at the temperature set in the DoE.

Lecithin and the mixing conditions showed some interaction affecting the pre-refined paste in trial 1 so it was hoped that this relationship could be better understood from independently assessing the impact of mixing time and temperature. The effect of lecithin on the refined materials was still not clear and its relationship with the fat content was investigated. Additionally, measurements of the current on the refiner rolls was evaluated alongside the resulting PSD of the refined paste to understand if this could offer an online measurement correlating to the resulting particle sizes.

7.4.1 Refiner performance

7.4.1.1 Factors affecting the refining operation

It was observed that the predictive models of the responses measured on the refiner; current on the first refiner roll and time taken to refine a batch represented the spread of data well (Figure 7.27 and Figure 7.28). Despite this, there was a significant *lack of fit* which means that the model did not represent the variation in the data well in comparison to the variation between repeats. This may have been a consequence of the frequency of sampling; only every 10 seconds. This was manually recorded and therefore future work would benefit from

automatic logging of the data more frequently. Visually, the predictive models did represent the raw data measurements and therefore the models were accepted and will be discussed further within this section.

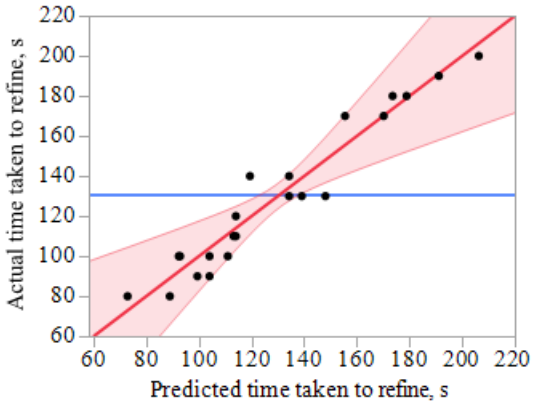


Figure 7.27: Measured times taken to refine plotted against values from the predictive model ($p\text{-value}_{LoF}$ = 0.0049)

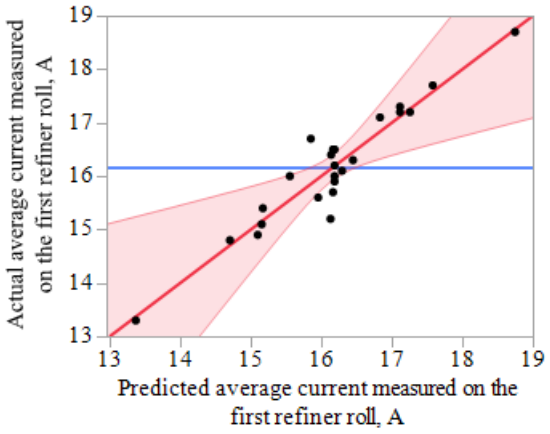


Figure 7.28: Average current measured on the first refiner roll plotted against values from the predictive model ($p\text{-value}_{LoF}$ = 0.0142).

Table 7.27: Significance of factors and interactions on the time taken for pastes to refine ($p\text{-value}_{ANOVA}$ = 0.0007).

Term	p-value	Sig.
Fat Content	<.0001	*
Lecithin Content * Temperature	0.0027	*
Fat Content * Fat Content	0.0111	*
Fat Content * Temperature	0.0353	*
Fat Content * Lecithin Content	0.0375	*
Mixing Time * Mixing Time	0.0430	*
Temperature * Temperature	0.0451	*
Lecithin Content	0.0874	
Mixing Time	0.2039	
Lecithin Content * Lecithin Content	0.2848	
Fat Content * Mixing Time	0.4948	
Lecithin Content * Mixing Time	0.5493	
Temperature	0.8277	
Mixing Time * Temperature	0.9554	

Table 7.28: Significance of factors and interactions on the average current on the first refiner roll ($p\text{-value}_{ANOVA}$ = 0.0113).

Term	p-value	Sig.
Fat Content	0.0004	*
Lecithin Content * Temperature	0.0340	*
Mixing Time	0.1239	
Fat Content * Fat Content	0.1947	
Fat Content * Temperature	0.2416	
Lecithin Content	0.2630	
Lecithin Content * Lecithin Content	0.5411	
Temperature	0.5418	
Mixing Time * Mixing Time	0.5587	
Lecithin Content * Mixing Time	0.5762	
Fat Content * Mixing Time	0.6010	
Fat Content * Lecithin Content	0.6675	
Temperature * Temperature	0.7297	
Mixing Time * Temperature	0.8486	

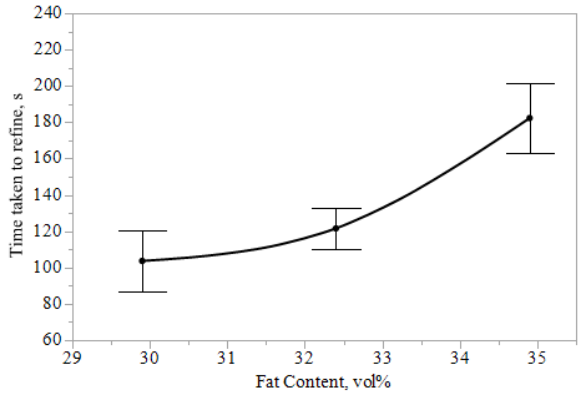


Figure 7.29: The fat content significantly impacts the time taken to refine. The results from the predictive model are plotted and the error bars are the standard deviation.

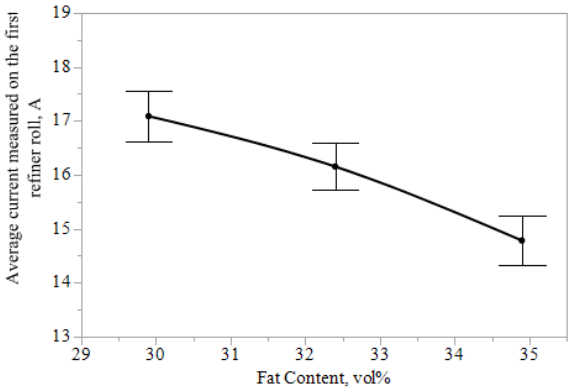


Figure 7.30: The fat content significantly impacts the average current measured on the first refiner roll. The results from the predictive model are plotted and the error bars are the standard deviation.

The most statistically significant effect on the refiner performance measurable was the impact of the fat content; increasing the fat content resulted in significantly lower current on the first roll and also significantly increased the time required to refine a batch of paste (Figure 7.29 and Figure 7.30).

The time taken to refine each paste batch showed a significant impact of the fat * temperature interaction. This interaction also had a marginally significant impact on the paste yield stress (p-value = 0.0513). The effects of this interaction on both the time taken to refine and the paste yield stress are plotted in Figure 7.31 and Figure 7.32. There were no significant differences between the PSD parameters of the paste based on this interaction however Figure 7.33 compares the overall PSDs. Pastes showed the highest yield stresses when the pastes had a low fat content and were at 40 °C. The model PSD of the paste at this condition appeared visually different; a larger proportion of particles fell within the second peak when the fat content was low and had been mixed at 40 °C. This may have been impacting the maximum packing fraction of the pastes. If the maximum packing fraction was reduced then the solids content of the pastes becomes closer to the maximum packing fraction. These pastes were then likely to display a greater yield stress, as was discussed in section 7.2.2.3. When the

yield stress was higher, the time taken for the paste to refine was lower. This suggests that the yield stress of the paste related to how much the paste was able to resist the pressure of the rolls. Pastes with a higher yield stress were able to push the rolls apart, allowing more material through and increasing the throughput of material through the refiner.

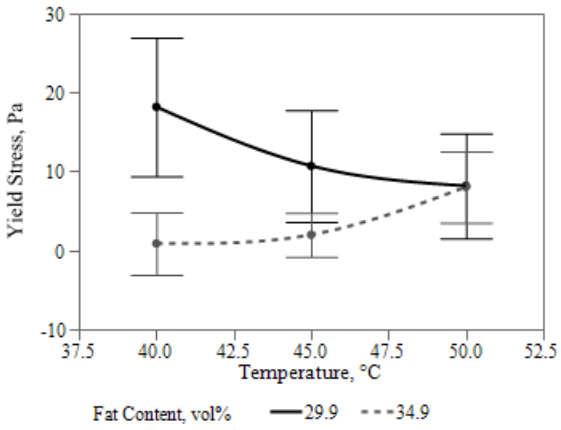


Figure 7.31: Interaction between fat content and temperature had marginally significance on the yield stresses of pastes (p-value = 0.0513). The results from the predictive model are plotted and the error bars are the standard deviation.

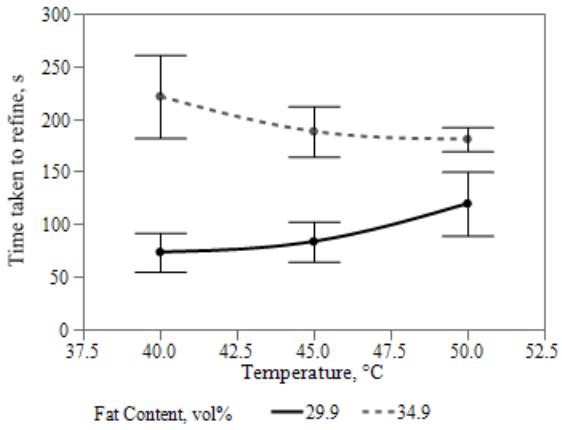


Figure 7.32: Interaction between fat content and temperature significantly impacts the time taken to refine. The results from the predictive model are plotted and the error bars are the standard deviation.

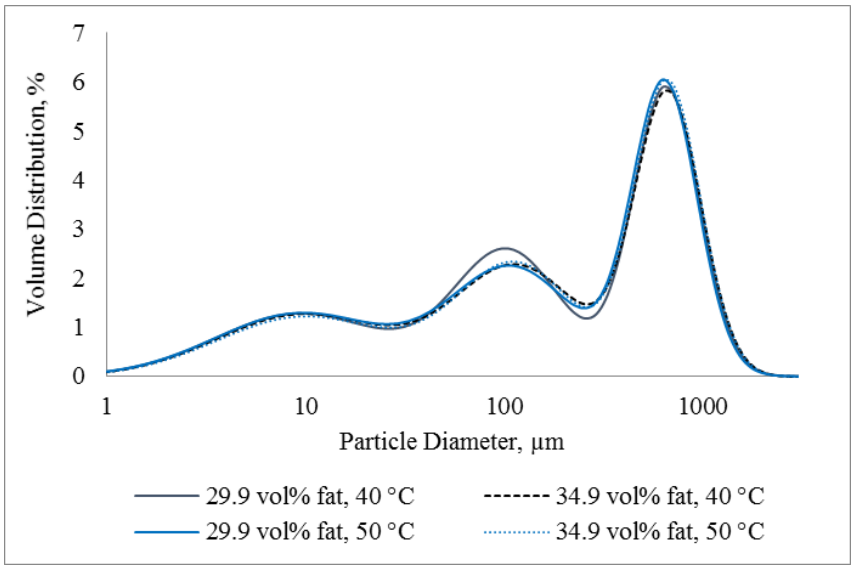


Figure 7.33: Influence of the fat and temperature on the paste PSDs using the average model parameters from the least squares fit

The time taken to refine was also significantly affected by the interaction between lecithin and fat content. The shear stress of the paste at a shear rate of 10 s^{-1}, measured on the BET, showed a significant effect of this interaction (p-value = 0.0376) and the yield stress of the paste showed a marginal significant effect of this interaction (p-value = 0.0518). Comparisons of the predictive model results of these parameters are shown in Figure 7.34. At these conditions, there was no meaningful difference between the paste particle sizes that could have affected the refining performance.

Although the pastes without lecithin were measured to have the same consistencies at both high and low fat contents, the time taken to refine a high fat paste was longer than a low fat paste, which was the result that would be expected. When the fat content of a paste was high, adding lecithin to the paste did not have a significant effect on the paste texture however it significantly increased the time required for the paste to refine. This suggested that the presence of lecithin was hindering the particles from passing through the gaps of the roll refiner. When the fat content was low, adding lecithin to the paste resulted in a more viscous paste and there was a statistically significant reduction of the time taken to refine. This result suggested that the effect of the paste consistency was able to override any influence of the lecithin content; a thicker paste was able to push the rolls apart further and so more material was able to pass through the gap.

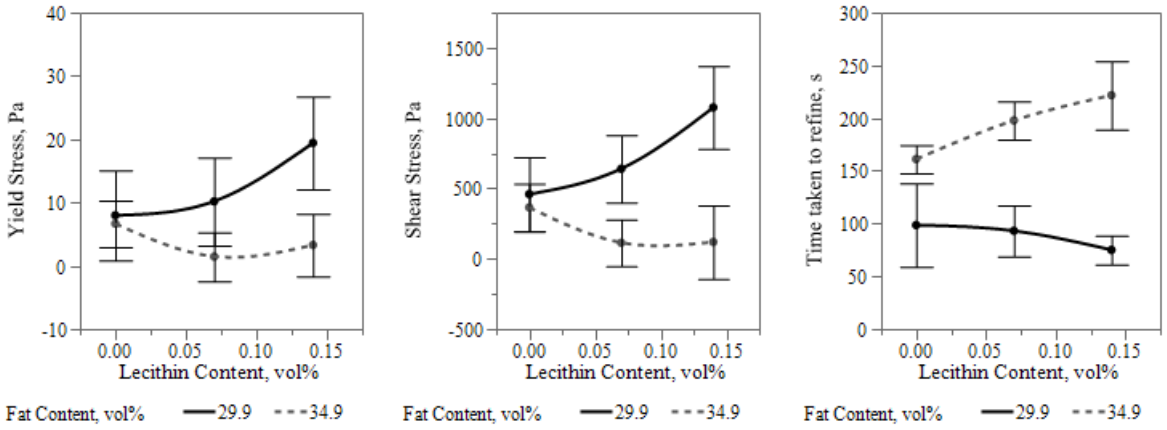


Figure 7.34: Influence of the fat and lecithin content on the yield stress of the pastes, the shear stress of the pastes and the time taken to refine a batch of paste. The results from the predictive model are plotted and the error bars are the standard deviation.

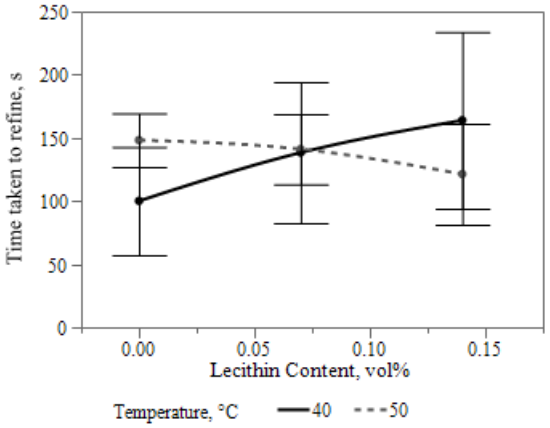


Figure 7.35: Interaction between lecithin content and temperature significantly impacts the time taken to refine. The results from the predictive model are plotted and the error bars are the standard deviation.

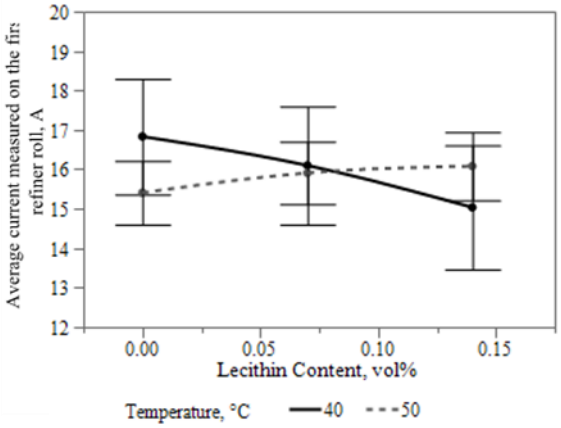


Figure 7.36: Interaction between lecithin content and temperature significantly impacts the average current measured on the first refiner roll. The results from the predictive model are plotted and the error bars are the standard deviation.

There was a significant interaction between lecithin content and the paste temperature affecting both the current on the first refiner roll and the time taken to refine; when there was no lecithin in the paste, increasing the temperature significantly decreased the current on the first roll and increased the time taken for a batch to refine (Figure 7.35). When there was 0.1% lecithin in the paste, increasing the temperature significantly increased the current on the first roll and decreased the time require for a batch to refine. No parameters which described

the PSDs of the pastes showed any significant effects of this interaction, suggesting that lecithin could have affected the interactions between the particles and the fat during refining.

The fat, mixing time and temperature all showed significant curvature when measuring the time taken to refine. From plots of the predictive models, considering the size of the error bars, the curvature over the range of temperatures did not have a substantial effect on the time taken to refine (Figure 7.37). As the fat content and mixing time were increased, the relationships with the time taken to refine were not linear however this curvature may have been a consequence of the rounding errors of measuring each batch time to the nearest 10 seconds.

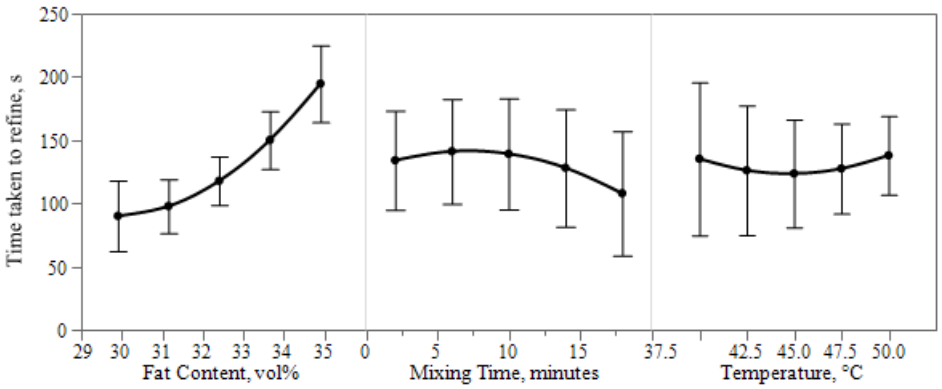


Figure 7.37: Significant curvature is measured for the fat content, mixing time and temperature. The results from the predictive model are plotted and the error bars are the standard deviation.

7.4.1.2 Relationship between the paste particle size distribution and the refiner operation

Principal component analysis (PCA) was carried out to compare the model PSD parameters describing the pastes with the current of the first roll measured during refining and the time taken for each batch of paste to refine. From Figure 7.38, neither PC1 nor PC2 appeared to correlate with the measurements taken on the refiner. PC3 showed a strong correlation with these two refining responses but were not grouped with any of the paste PSD parameters.

These results indicated that the particle size differences between the pastes were not having any impact on how the pastes refine through the three-roll refiner.

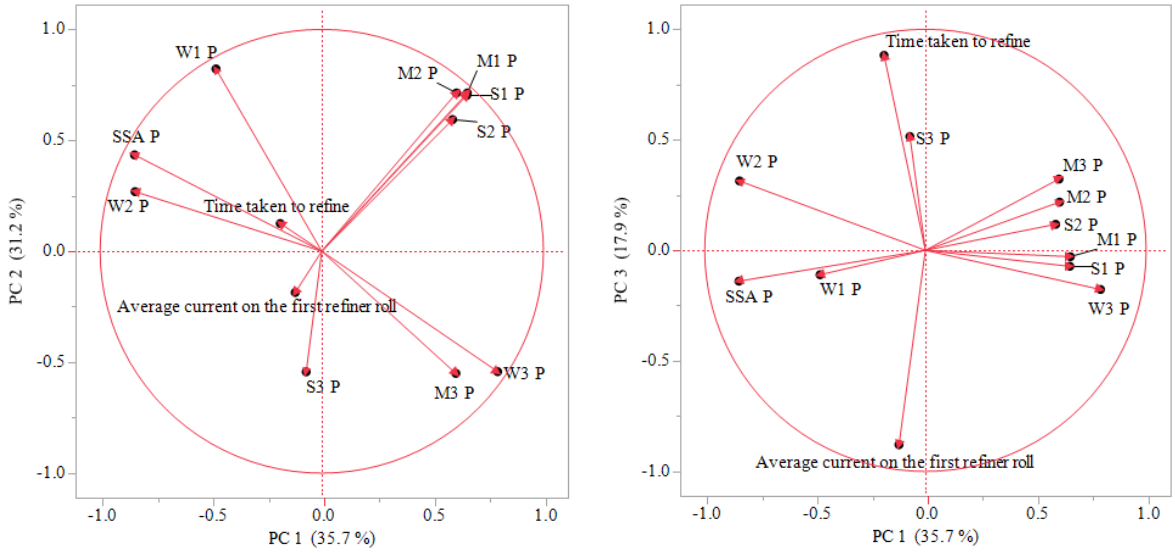


Figure 7.38: Loading plots of the first three principal components which describe 84.8 % of the variation between the time taken for the batch to refine, the average current on the first roll of the refiner and the particle size parameters of the three log-normal distributions describing the pastes (mean, M, standard deviation, S, and weight, W). The log-normal peak containing the smallest particles is labelled 1, the largest particles are within the log-normal peak labelled 3.

7.4.1.3 Relationship between the consistency of the paste and the refiner operation

The Herschel-Bulkley model parameters and the shear stress at a shear rate of 10 s^{-1} of the paste fitted to the BET measurements were compared using PCA to the time taken to refine each batch and the current measured on the first refiner roll. PC1 represented a large proportion of the variation of the results and all of the responses compared using this technique correlated strongly with PC1 (Figure 7.39). From the least square regression analyses, all these responses were significantly affected by the fat content of the paste therefore these PCA results indicated that fat content was the main driving force of the differences of the paste textures and refining performance.

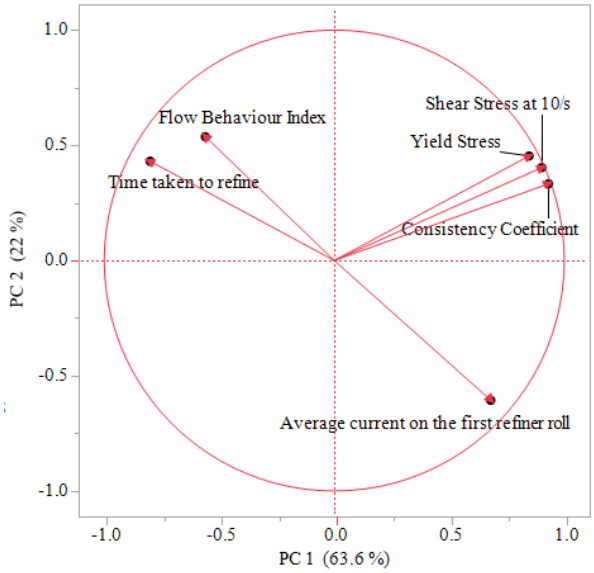


Figure 7.39: Loading plots of the first two principal components which describe 85.6 % of the variation between the time taken for the batch to refine, the average current on the first roll of the refiner, flow behaviour index, consistency coefficient, yield stress and the shear stress at a shear rate of 10 s^{-1} (final four measured using the BET)

7.4.1.4 Discussion

Increasing the fat content of the paste was found to significantly increase the time it took for a batch to refine and decreased the average current recorded on the first refiner roll. Principal component analysis showed that there were similarities between how the Herschel-Bulkley parameters of the paste and the time taken to refine vary. This was likely because the fat content significantly thinned the pastes and also increased the refining time, agreeing with the theory that the counter force pushing the rolls apart is a function of the apparent viscosity of the paste. Increasing the fat content reduced the thickness of the pastes resulting in lower forces resisting the pressure of the rolls. Less material was able to get through the gap so the time taken to refine a batch was longer. Less material within the nip of the rolls meant that there was less friction between the rolls and the current required to turn the rolls was lower. When the yield stresses of the pastes were measured to be high, the time taken to refine was lowest, for example when the fat content and the temperature of a paste was low. The yield

stresses may have helped towards pushing the rolls apart and allowing a greater amount of paste to pass through the gaps.

It was hypothesised that when pastes containing a high fat content were refined, the presence of lecithin prevented the particles from passing through the refiner gaps despite there not being any effect of lecithin content on the paste consistency. It may have been that the lecithin molecules were easily able to move around a system with a lot of free fat and as they resisted particles coming close together, they may have hindered the particles from being pushed closely together as they approached the nip of the roll. When the fat content was low, adding lecithin resulted in a more viscous paste. The more viscous low fat pastes were able to push the rolls apart further and the refining time of batches was reduced.

7.4.2 Particle Size Distributions of the Refined Paste

Each pastes passed through the two gaps, between the three rolls of the refiner. The PSDs of the particles became bimodal, modelled by two log-normal curves. The PSD of each sample was then represented by the mean (M), the standard deviation (S) and the weighting (W) of the two peaks. Here, peak one referred to the first peak and peak two referred to the larger peak. Using the data from the predictive models of the PSD parameters, the average PSDs of the pastes and refined pastes were compared (Figure 7.40).

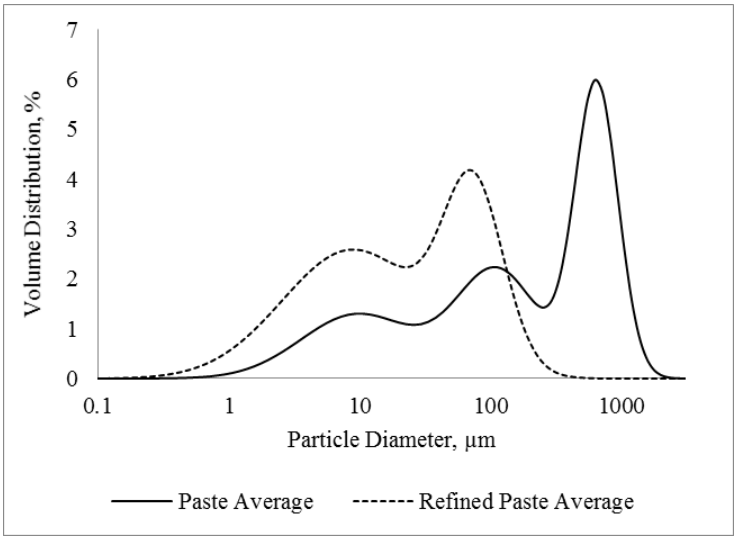


Figure 7.40: Average particle size distributions of the pastes and refined pastes produced in trial 2 using the average model parameters from the least squares fit

7.4.2.1 Factors affecting Particle Size Distribution of the Refined Paste

Analyses of variance were run to assess whether factors significantly impacted any of the refined paste PSD parameters, including the specific surface area (SSA) and the d_{90}. The results are outlines in Table 7.29 to Table 7.35.

Table 7.29: Significance of factors and interactions on the standard deviation of the first refined paste PSD peak ($p\text{-value}_{ANOVA} = 0.2697$)

Term	p-value	Sig.
Fat Content	0.0304	*
Mixing Time*Temperature	0.0946	
Fat Content*Temperature	0.2164	
Fat Content*Lecithin Content	0.2447	
Lecithin Content	0.3247	
Fat Content*Mixing Time	0.3916	
Lecithin Content*Temperature	0.6453	
Temperature	0.7319	
Mixing Time*Mixing Time	0.7761	
Fat Content*Fat Content	0.7783	
Lecithin Content*Lecithin Content	0.8597	
Mixing Time	0.8620	
Temperature*Temperature	0.8761	
Lecithin Content*Mixing Time	0.9769	

Table 7.30: Significance of factors and interactions on the mean of the first refined paste PSD peak ($p\text{-value}_{ANOVA} = 0.1470$)

Term	p-value	Sig.
Fat Content	0.0071	*
Fat Content*Temperature	0.1319	
Mixing Time*Temperature	0.1336	
Fat Content*Lecithin Content	0.3029	
Lecithin Content	0.3906	
Lecithin Content*Temperature	0.4089	
Fat Content*Mixing Time	0.5369	
Temperature*Temperature	0.5632	
Lecithin Content*Mixing Time	0.5960	
Mixing Time	0.5993	
Mixing Time*Mixing Time	0.7522	
Lecithin Content*Lecithin Content	0.7733	
Temperature	0.9069	
Fat Content*Fat Content	0.9194	

Table 7.31: Significance of factors and interactions on the standard deviation of the second refined paste PSD peak ($p\text{-value}_{ANOVA} = 0.8433$)

Term	p-value	Sig.
Lecithin Content*Temperature	0.4319	
Lecithin Content	0.4417	
Temperature*Temperature	0.5007	
Lecithin Content*Lecithin Content	0.5368	
Lecithin Content*Mixing Time	0.5399	
Mixing Time*Mixing Time	0.5711	
Fat Content	0.6235	
Mixing Time*Temperature	0.6878	
Fat Content*Lecithin Content	0.7308	
Temperature	0.7379	
Fat Content*Mixing Time	0.7712	
Mixing Time	0.8889	
Fat Content*Fat Content	0.8947	
Fat Content*Temperature	0.9908	

Table 7.32: Significance of factors and interactions on the mean of the second refined paste PSD peak ($p\text{-value}_{ANOVA} = 0.0134$)

Term	p-value	Sig.
Fat Content	0.0010	*
Fat Content*Temperature	0.0293	*
Lecithin Content*Temperature	0.1692	
Mixing Time*Temperature	0.1949	
Lecithin Content	0.3617	
Fat Content*Mixing Time	0.3666	
Temperature	0.4716	
Fat Content*Lecithin Content	0.4991	
Lecithin Content*Mixing Time	0.5218	
Mixing Time	0.6181	
Fat Content*Fat Content	0.6407	
Mixing Time*Mixing Time	0.7561	
Temperature*Temperature	0.8365	
Lecithin Content*Lecithin Content	0.9819	

Table 7.33: Significance of factors and interactions on the weight of the first refined paste PSD peak ($p\text{-value}_{ANOVA} = 0.3644$).

Term	p-value	Sig.
Fat Content*Lecithin Content	0.2080	
Mixing Time*Temperature	0.2650	
Temperature	0.2868	
Mixing Time	0.3816	
Fat Content*Mixing Time	0.3827	
Lecithin Content*Lecithin Content	0.3927	
Lecithin Content*Temperature	0.4693	
Fat Content	0.6525	
Lecithin Content	0.6845	
Mixing Time*Mixing Time	0.7021	
Lecithin Content*Mixing Time	0.7245	
Fat Content*Temperature	0.7561	
Temperature*Temperature	0.8446	
Fat Content*Fat Content	0.9633	

Table 7.34: Significance of factors and interactions on the d_{90} of the refined paste PSD ($p\text{-value}_{ANOVA} = 0.0039$).

Term	p-value	Sig.
Fat Content	0.0004	*
Fat Content*Temperature	0.0216	*
Lecithin Content*Temperature	0.0429	*
Temperature	0.2080	
Mixing Time*Temperature	0.2400	
Mixing Time	0.3975	
Fat Content*Fat Content	0.5859	
Lecithin Content	0.6245	
Mixing Time*Mixing Time	0.6428	
Temperature*Temperature	0.6472	
Fat Content*Mixing Time	0.7230	
Lecithin Content*Mixing Time	0.7588	
Fat Content*Lecithin Content	0.8615	
Lecithin Content*Lecithin Content	0.9758	

Table 7.35: Significance of factors and interactions on the SSA of the refined paste PSD ($p\text{-value}_{ANOVA}$ = 0.0009).

Term	p-value	Sig.
Fat Content	0.0004	*
Fat Content*Temperature	0.0080	*
Lecithin Content*Temperature	0.0201	*
Mixing Time	0.0498	*
Temperature	0.1338	
Mixing Time*Mixing Time	0.1952	
Mixing Time*Temperature	0.2645	
Lecithin Content*Mixing Time	0.2817	
Lecithin Content*Lecithin Content	0.3595	
Lecithin Content	0.5727	
Temperature*Temperature	0.6529	
Fat Content*Lecithin Content	0.7277	
Fat Content*Mixing Time	0.7568	
Fat Content*Fat Content	0.9170	

The mean of the second peak and the d_{90} were significantly lower when there was a higher fat content, plus the specific surface area (SSA) was significantly higher. The predictive models did not significantly fit the standard deviation and the mean of the first refined paste peak although the fat content was nevertheless found to have a significant effect on the result. From the overall PSD based on the predictive models of each parameter, the distribution was shifted to the left when pastes contained a higher content of fat.

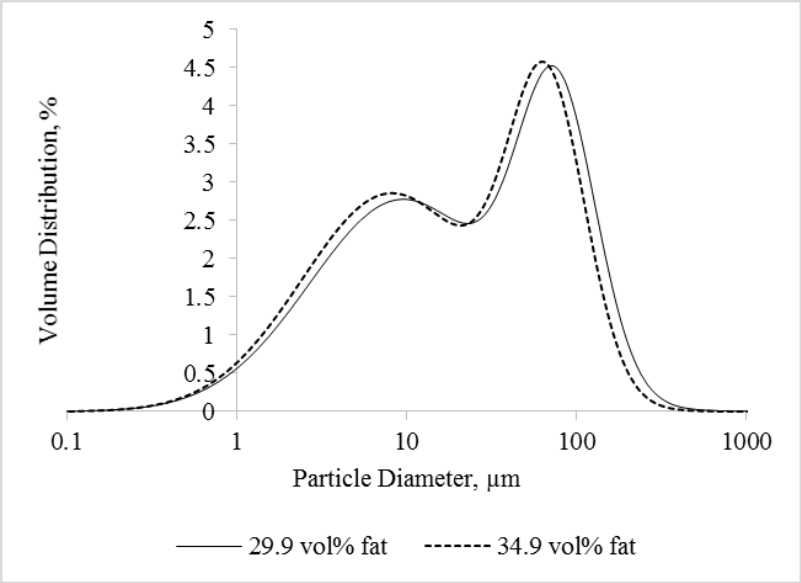


Figure 7.41: Influence of the fat content on the refined paste PSDs using the average model parameters from the least squares fit. At 29.9 vol% fat, d_{90} = 123.0 µm, SSA = 682.1 $m^2 kg^{-1}$. At 34.9 vol% fat, d_{90} = 107.5 µm, SSA = 730.9 $m^2 kg^{-1}$.

The SSA of the refined paste was significantly affected by the mixing time, in the opposite direction to the fat content (Figure 7.42). From the full PSD of the refined paste, reconstructed from the model PSD parameters in Figure 7.43, the pastes mixed for longer contained slightly larger particles than a paste refined for a short time. It was clear that now the particles were much smaller, very slight differences in the entire PSD caused a dramatic impact on the SSA of the refined pastes.

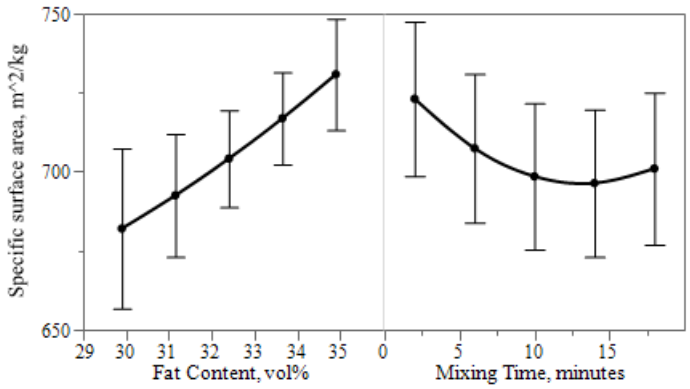


Figure 7.42: The fat content and mixing time significantly impact the SSA of refined pastes. The results from the predictive model are plotted and the error bars are the standard deviation.

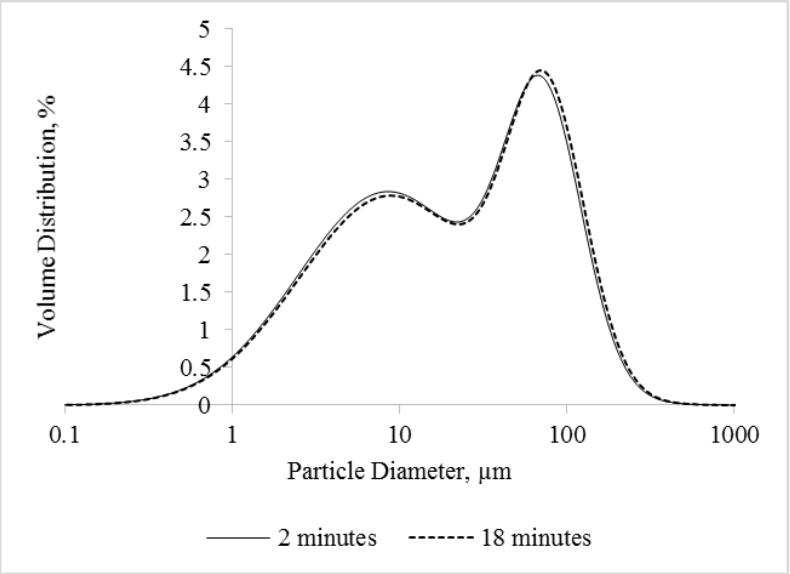


Figure 7.43: Influence of the mixing time on the refined paste PSDs using the average model parameters from the least squares fit

The interaction between fat content and temperature significantly influenced the mean of the second refined paste peak, the d_{90} and the SSA. There was also a marginally significant effect of this interaction on the yield stresses of the pastes, which is summarised in Table 7.36 alongside the refined paste d_{90} and SSA. The predictive model PSDs at the extremes of these conditions are shown in Figure 7.44. When the pastes were at 40 °C, increasing the fat content resulted in smaller particles which had a larger SSA. When the pastes were at 50 °C, both low and high fat pastes showed a similar PSD. This trend was similar to the paste yield stresses, indicating that the yield stresses of the pastes may have been driving the differences in the refined paste particle sizes.

Table 7.36: Comparing the mean values of the paste yield stress and the refined paste SSA and d_{90} from the predictive models at high and low levels of fat content and temperature ± the standard deviation

Fat Content, vol%	**Temperature, °C**	**Yield Stress of the Paste, Pa**	**d_{90} of the Refined Paste, µm**	**SSA of the Refined Paste, $m^2\,kg^{-1}$**
		***p-value*$_{ANOVA}$ = 0.0114**	***p-value*$_{ANOVA}$ = 0.0039**	***p-value*$_{ANOVA}$ = 0.0009**
29.9	40	18.87 ± 8.09	128.84 ± 2.54	654.60 ± 16.20
29.9	50	9.69 ± 6.08	115.97 ± 3.92	714.66 ± 15.32
34.9	40	0.72 ± 4.28	103.18 ± 4.58	746.97 ± 18.19
34.9	50	6.62 ± 4.34	110.64 ± 4.48	719.86 ± 15.28

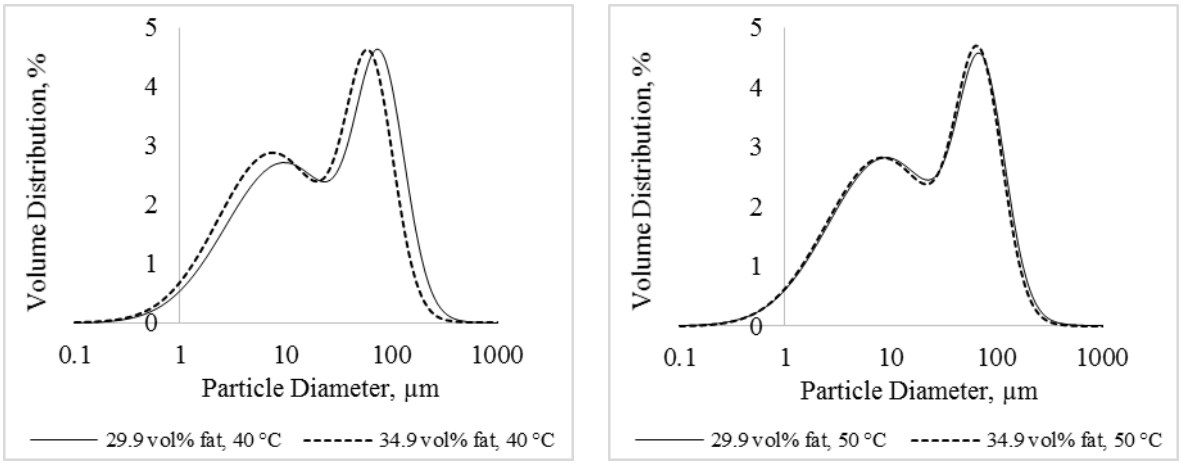


Figure 7.44: Influence of the fat content and temperature on the refined paste PSDs using the average model parameters from the least squares fit.

The d_{90} and the SSA of the refined paste were significantly affected by the interaction between lecithin content and temperature. The time taken to refine and the current measured on the first refiner roll were significantly impacted by this interaction (p-values = 0.0027 and 0.0340, respectively) and the shear stress of the paste at a shear rate of 10 s^{-1} showed some marginal significance of this interaction (p-value = 0.0898). When the paste did not contain lecithin, increasing the temperature decreased the shear stress of the pastes (Figure 7.45). This resulted in an increase of the time taken to refine and a decrease of the current measured on the first refiner roll as the pastes were thinner (Figure 7.46), creating a refined paste with a higher SSA and a lower d_{90} (Figure 7.47). When the pastes contained 0.15 vol% lecithin, there was a lot of variation within the results and it could not be concluded that the consistency changes when the temperature was increased from 40 °C to 50 °C. Similarly, the time taken to refine and the current measured on the refiner roll were also similar for pastes at both 40 and 50 °C. The refined pastes produced also had values of d_{90} and SSA that were alike. As far as the author is aware, there is no literature which has studied the effect of lecithin over these temperature ranges within a lipid environment, despite this emulsifier being a common component of many mass produced products.

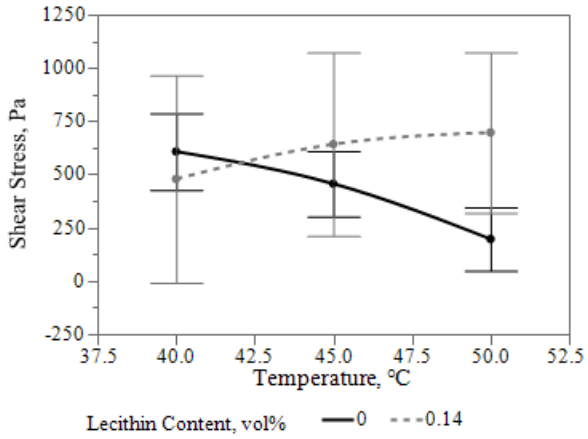


Figure 7.45: Influence of lecithin content and temperature on the shear stress of the paste at a shear rate of 10 s^{-1}. The results from the predictive model are plotted and the error bars are the standard deviation.

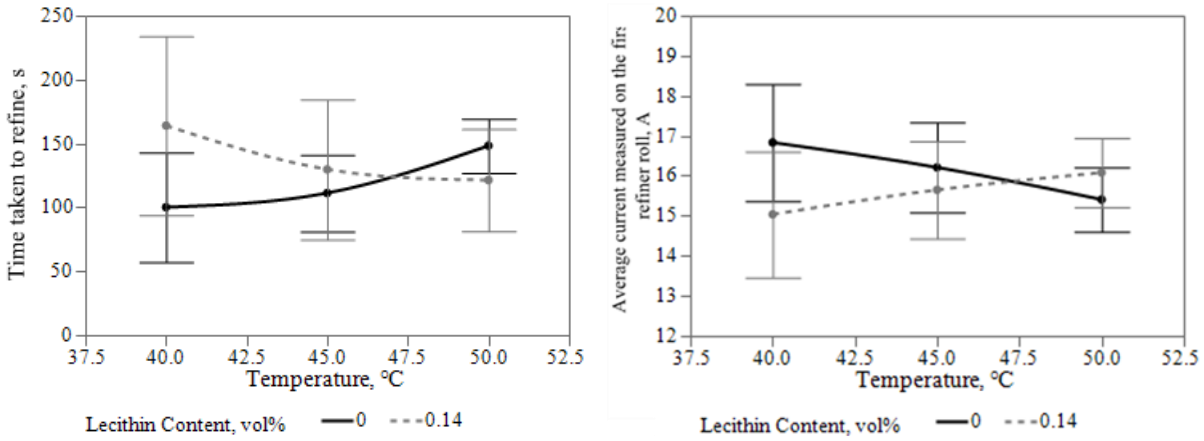


Figure 7.46: Influence of lecithin content and temperature on the time taken to refine and the current measured on the first roll of the refiner. The results from the predictive model are plotted and the error bars are the standard deviation.

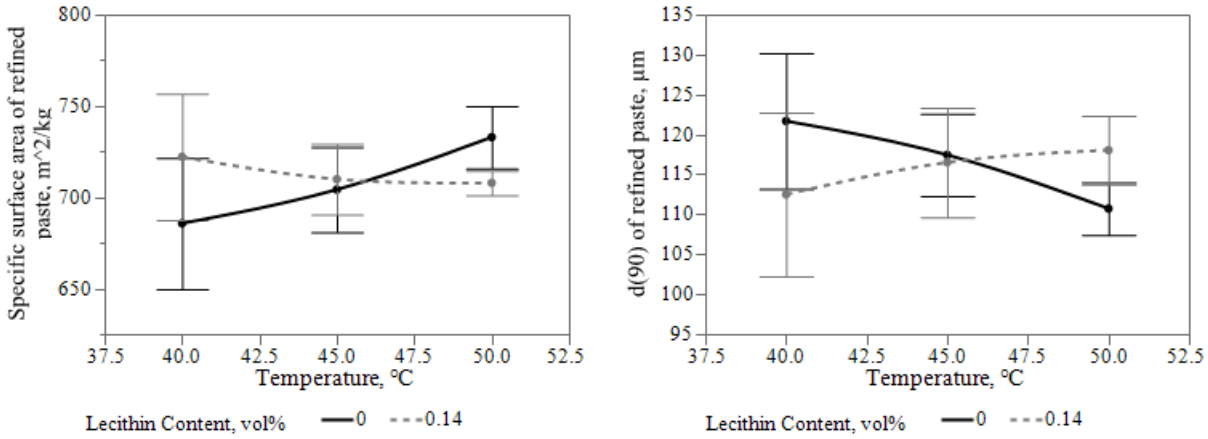


Figure 7.47: Influence of lecithin content and temperature on the d_{90} and the SSA of the refined paste. The results from the predictive model are plotted and the error bars are the standard deviation.

7.4.2.2 Relationship between the paste particle size distribution and the refined paste particle size distribution

The results of trial 1 showed that the means of each peak of the paste were found to vary similarly to the means of each peak of the pre-refined paste (section 7.2.1.3). Principal component analysis was again used to determine whether there were any similarities between the paste and the refined paste PSDs. The loading plot of the first two principal components is shown in Figure 7.48. The main observation linking the paste and the refined pastes was that the means of the largest peaks of the paste and the refined pastes (M3 P and M2 R) were located in a similar position, as were the values of standard deviation (S3 P and S2 R). The values of specific surface area of the pastes and the refined pastes both correlated negatively with PC2 indicating that there was a general trend of pastes containing larger particles to produce refined pastes of larger particles.

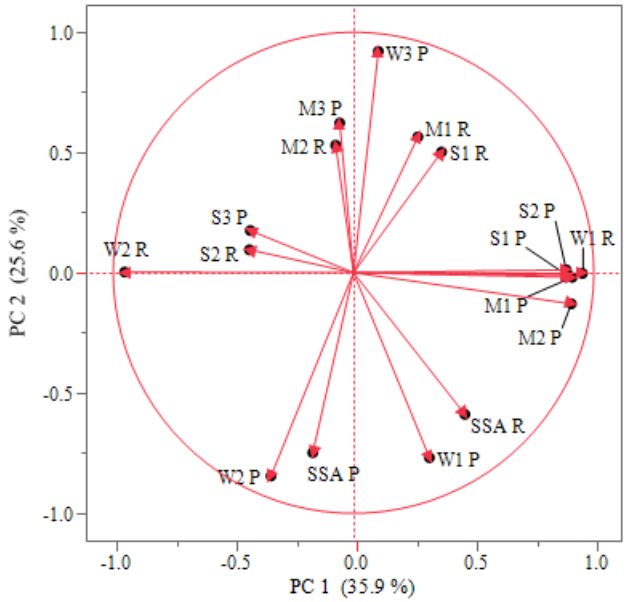


Figure 7.48: Loading plots of the first two principal components which describe 61.5 % of the variation between the particle size parameters of the log-normal distributions (mean, M, standard deviation, S, and weight, W) for the pastes (P) and the refined pastes (R). The log-normal peak containing the smallest particles is labelled 1. The pastes are modelled by three log-normal distributions and the refined pastes are only modelled by two.

Using the values of the predictive models, the SSA of the pre-refined pastes can be plotted against the shear stresses of the pastes, at a shear rate of 10 s^{-1} (Figure 7.49). When the results were highlighted based upon the fat content, the results showed no correlation. Therefore, the consistency of pastes may have varied but the SSA of the refined paste dominated the fat content. When the pastes were highlighted based upon the mixing times, there were stronger correlations between these two variables. This suggests that the relationship between the consistency of the pastes and the particle size of the refined pastes depends on the mixing time. The data split by lecithin content showed similar results, indicating that overall, the presence of lecithin in the paste did not affect the relationship between paste consistency and refined paste SSA. When the data was separated by the temperature, pastes at 40 °C showed some correlation between the paste consistency and the refined particle size. At 50 °C, there was no correlation, indicating that the consistency of the paste may have been different but the particle size produced was not dependent on it.

Overall, these results indicated that the mixing time might have been influencing the interactions between the particles and the fat; if pastes show a similar consistency but one of them has been mixed for longer, it is likely to result in a refined paste with a lower specific surface area i.e. larger particles.

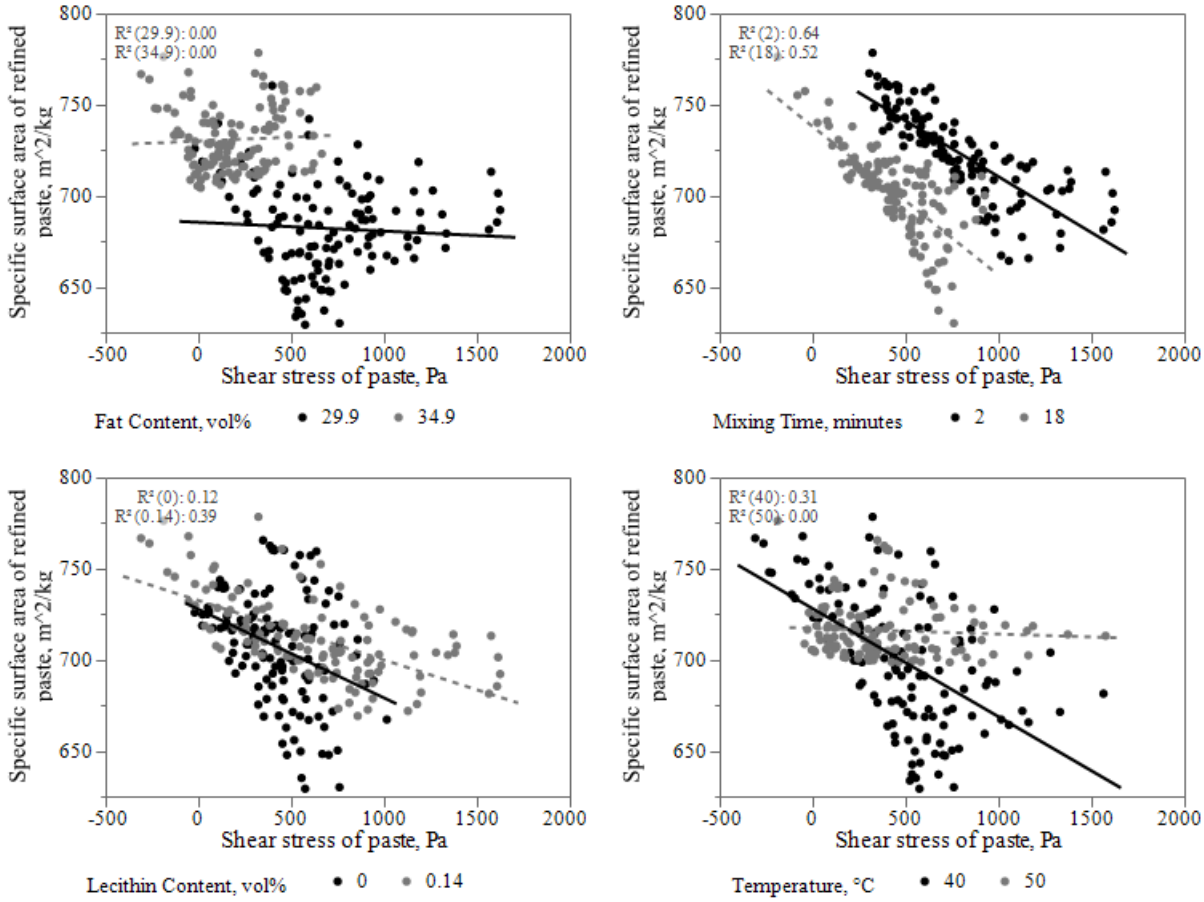


Figure 7.49: Relationships between the shear stresses of the pastes and the SSA of the pre-refined paste when data is separated by each of the DoE factors

7.4.2.3 Relationship between the refiner conditions and the PSD of the refined paste

Principal component analysis was used to examine the relationships between the particle sizes of the resulting refined paste with the two refiner measurements: time taken to refine each batch and the current measured on the first roll (Figure 7.50). The current measured on the first roll was grouped with the means of both peaks (M1 and M2), the standard deviation of

the first peak of the refined paste (S1) and the d_{90}. The SSA is opposite the current measured on the first refining roll, indicating that it negatively correlated.

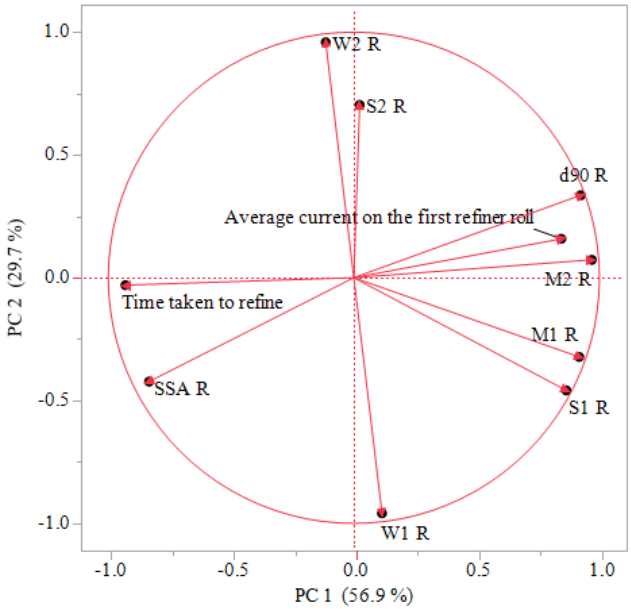


Figure 7.50: Loading plots of the first three principal components which describe 86.6 % of the variation between the time taken for the batch to refine, the average current on the first roll of the refiner with the SSA, d_{90} and the particle size parameters of the two log-normal distributions describing the pastes (mean, M, standard deviation, S, and weight, W) and. The log-normal peak containing the smallest particles is labelled 1, the largest particles are within the log-normal peak labelled 3.

As was done in section 7.4.2.2, the values of SSA of the refined paste are plotted against the current measured on the first refiner roll (Figure 7.51). These were split into four plots, highlighting the correlations at high and low levels of each of the four factors. In comparison to Figure 7.49, high and low levels of each variable had much less effect on the relationship between the current measured on the first refiner roll and the SSA of the refined paste particles.

The fat content showed the most difference in the gradients at high and low levels. The temperature also showed different gradients but overall, the relationship between the current measured on the first refiner roll and the SSA of the refined paste showed a good correlation ($R^2 = 0.766$).

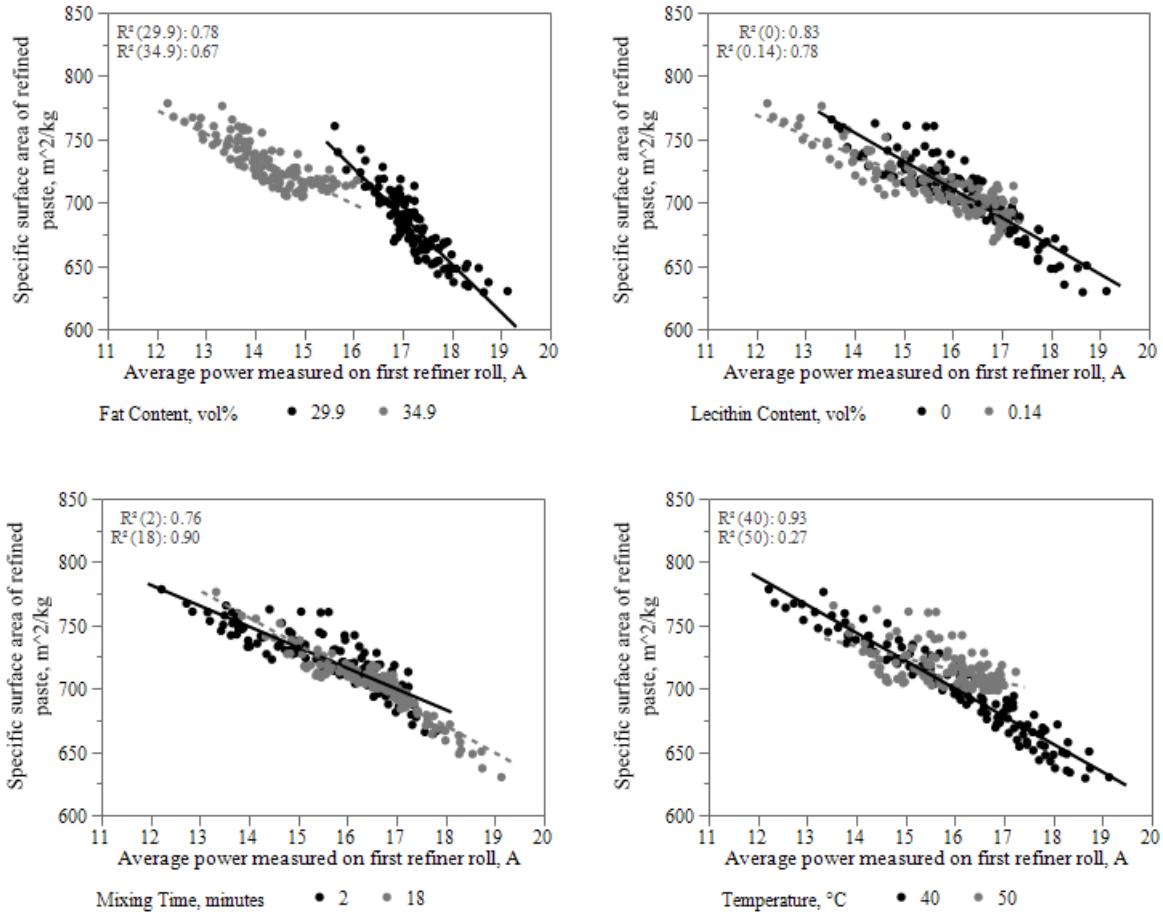


Figure 7.51: Relationships between the current measured on the first refiner rolls and the SSA of the refined paste when data is separated by each of the DoE factors

7.4.2.4 Comparisons of the refined paste particle sizes

Utilising the results of the predictive model of the specific surface area of the refined pastes, Figure 7.52 was created to show the SSA of refined pastes when all four factors are at high or low levels. Out of all these pastes, the high fat paste at 40 °C containing lecithin refined to produce the smallest particles (SSA = 777.4 ± 0.7 m^2/kg). This paste was sensitive to the temperature as an increase of 10 °C resulted in the SSA decreasing to 719.6 ± 2.5 m^2/kg. If no lecithin was added into the paste then the high fat pastes were no longer affected by the temperature, but they did show an effect of the mixing time ($SSA_{2\ minutes}$ = 762.6 ± 2.1 m^2/kg, $SSA_{18\ minutes}$ = 718.4 ± 0.4 m^2/kg).

A paste with only 29.9 vol% fat at 50 °C without any lecithin produced a refined paste with a PSD which was similar to a high fat paste with no lecithin. These pastes were also sensitive to the mixing time, producing refined pastes with a lower SSA when they were mixed for longer; $SSA_{2\ minutes}$ = 763.1 ± 1.8 m^2/kg, $SSA_{18\ minutes}$ = 718.7 ± 0.2 m^2/kg.

Pastes with 29.9 vol% fat and 0.14 vol% lecithin resulted in a comparable refined paste SSA to high fat pastes also containing lecithin at 50 °C. These were sensitive to temperature; when the temperature of the paste was decreased to 40 °C, the SSA of the low fat pastes decreased unlike the SSA of the high fat pastes which increased.

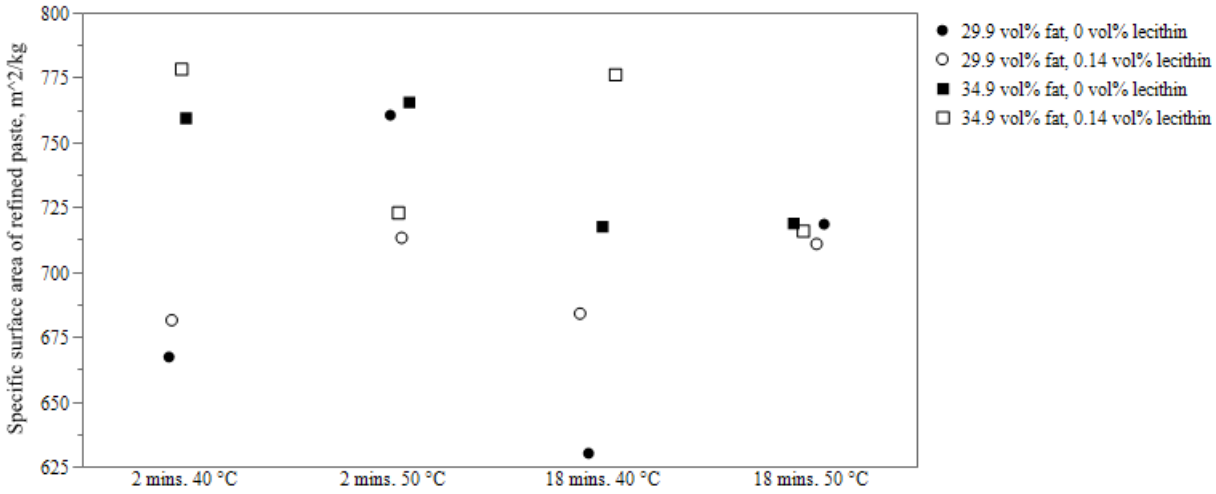


Figure 7.52: Values of SSA of the refined paste based on the results from the predictive model, comparing pastes at high and low levels of each of the four factors: fat content, lecithin content, mixing time and temperature.

7.4.3 Discussion

Ideally the maximum size of particles within chocolates should be 30 µm (Beckett, 2009). The pastes produced through one pass of within a three-roll refiner were larger than this, resulting in a smaller value of SSA than would be expected in chocolate. This refining process was intended to give an idea of what factors affected the refining process in a more controlled refining step than was used for trial 1.

There was a strong effect of the fat content; an increase of the fat content resulted in a decrease of the refined paste SSA and d_{90}. Although increasing the mixing time also resulted in thinner pastes, the results of the ANOVA indicated that longer mixing times lead to refined pastes containing larger particles. Using values of the predictive models, the relationship between the shear stresses of the pastes and the refined paste SSA negatively correlated; a paste with a higher shear stress resulted in a lower refined paste SSA. If the results were segregated by the fat content, the correlation weakened, indicating that the fat content dominated this relationship. In contrast, if the results were split by the mixing time, the correlations remained strong but the intercept of the correlation was altered. This could suggest that the solids and the fat interact when the pastes were mixed for longer, affecting the structure or location of fat within the suspension.

The average current measured on the first refiner roll more strongly correlated with the SSA of the refined pastes than the shear stresses of the pastes, at a shear rate of 10 s^{-1}. The shear stress at another shear rate may be a more appropriate value to relate to the refined paste particle size however these results suggested that the consistency of the paste was not the only physical property which influenced the resulting refined paste PSD when the refiner settings remained constant.

When the pastes did not contain lecithin, increasing the temperature of the paste from 40 °C to 50 °C decreased the shear stress of the paste. The pastes at 50 °C took a longer time to refine and the refined paste particles were smaller. When there was 0.1 vol% lecithin within the paste, there were no longer any significant differences in the paste consistencies, the time taken to refine or the refined paste PSD at the two different temperatures. There is not currently thought to be any research related to how lecithin affects a lipid system whilst it is

still fluid at different temperatures. The research is mainly concerned with how lecithin molecules interact as the fat crystallises.

In chapter 6, measurements using the BET indicated that shear stresses of pastes which did not contain lecithin were unchanged when the fat content increased. This result could not be explained as previous results during the development of the BET in chapter 0 could distinguish pastes with 4 vol% differences in fat content but also did not contain lecithin. The measurements on the refiner presented within this chapter showed that pastes without lecithin do show differences in the time taken to refine, agreeing with the theory that higher fat content pastes are thinner and therefore cannot as easily resist the pressures of the rolls. There was then no significant interaction between the fat and lecithin contents affecting any of the refined paste PSD parameters. This result indicates that further proof of concept is required to ensure accuracy and precision of the BET before it is used alongside a pilot or manufacturing line.

The interaction between the fat content and the temperature had a significant effect on the SSA and d_{90} of the refined pastes and also significantly affected the time taken to refine. The predictive models of the yield stresses of the pastes showed a similar response which may have been causing this relationship. At 40 °C, low fat pastes had a high yield stress and these were thought to be able to resist some of the pressing forces of the rolls, resulting in larger refined paste particles. When the fat content was increased, the pastes no longer had yield stresses. These took a long time to refine and the resulting particle sizes of the refined pastes were small. Pastes at 50 °C, on average, had a marginal yield stress which was unaffected by the fat content between 29.9 and 34.9 vol%. They were able to resist some of the pressing forces of the rolls, took an equivalent time to refine and the resulting PSD was the same.

Pastes manufactured within the pilot plant do not currently reach 40 °C however it is anticipated that on a manufacturing scale, pastes could exceed this temperature, hence why the temperatures were investigated up to 50°C. These results have indicated that there may be an opportunity to alter the particle size of the refined paste by altering the temperature it is mixed or added to the refiner at. These two conditions were not individually tested so it is not known whether there may be physical changes to the structure which occur during the mixing time, or whether the temperature impacts how the fat spreads as the particles are forced between the refiner rolls.

7.5 Conclusions

The work presented in this chapter details the experimental results of two studies; the first was a two stage refining process where the paste was first refined through one gap between two refiner rolls, then this refined paste was fed through a 5-roll refiner. The second study involved a one-step refining process where the paste was passed through two gaps between the three refiner rolls.

Although assumptions were made to estimate the specific surface area from the laser diffraction measurements, it was able to highlight differences between refined flake samples which were observed in plots of the entire particle size distributions. Measurements of the current required by the first roll of the refiner and the time taken to refine had a strong correlation with the refined paste specific surface area. The shear stress of the paste at a shear rate of 10 s^{-1} did not correlate as strongly with the resulting refined paste PSD. This indicated that the behaviour of the paste at 10 s^{-1} may not be relevant to how it behaves during refining. The shear rates anticipated within different process steps was discussed in section 5.3.5; within the refiner the shear rate was estimated to be almost 10000 s^{-1}. It was mainly the

geometry of the back extrusion technique that determines the shear rates which were achieved. Based on the results of chapter 0, the gap size between the probe and the test vessel should not be decreased and therefore the shear rate can only be increased further by using a faster probe velocity; this is currently limited by the equipment however it is unlikely that a shear rate as high as is anticipated within the refiner can ever be achieved.

It was not possible to determine whether altering the fat content had a meaningful effect on the size of the particles within pre-refined pastes since the differences were similar to the variation error of the measurement technique. However, further refining these pastes through a five roll refiner resulted in smaller particles when the fat content was higher as the pre-refined paste had a thinner consistency. Pastes refined within a three roll refiner similarly showed that when the fat content was higher, smaller particles were produced.

Mixing the pastes for longer and at a higher speed in trial 1 resulted in a thinner paste consistency and produced refined flakes with a small PSD, close to the pastes which had a higher fat content. However in trial 1, the effect that mixing time had on the paste could not be distinguished from the impact of temperature. In more extensive trials at controlled temperatures (trial 2), mixing the pastes for longer resulted in a paste of thinner consistency yet the time for these pastes to refine were all the same. Although the paste consistency was thinner, larger refined paste particles were produced when the mixing time was longer which suggested that mixing time could have been influencing the location of fat within the solid-liquid matrix.

In trial 1, as temperature mainly increased when the mixing time was longer, the shear stresses of pastes containing lecithin did not show much difference when the mixing time was increased, in comparison to pastes without lecithin. The use of temperature as a factor in the

DoE of trial 2 helped to highlight the potential interactions that existed between the temperature and the lecithin content. When pastes did not contain any lecithin, increasing the temperature from 40 °C to 50 °C resulted in a thinner paste consistency. The warmer paste took longer to refine as it could not pass through the gaps as easily and produced refined pastes with a smaller PSD. Conversely when there was 0.1 vol% lecithin within the pastes, varying the temperature did not affect the paste consistency, refining time or refined paste particle size.

Unlike in pastes where it hypothesised that entrained air increased the effective solids volume content and caused higher yield stresses, some pre-refined pastes produced in trial 1 were also measured (using the BET) to have a significant yield stresses. As the particles within these pre-refined pastes had a narrower PSD, the maximum packing fraction, φ_p, may have been lowered. Decreasing the fat content caused the solids volume content to approach φ_p, increasing the yield stress. In trial 2, the pastes which displayed a higher yield stress took a shorter time to refine. The results showed that yield stress pastes did not result in larger refined particles however the particles were within more distinct peaks. This would have affected the packing of the particle, ultimately thought to influence the final chocolate viscosity.

Whilst the BET showed several results which were echoed by similar measurements of the pastes within the refiner, there were also some discrepancies which does not agree with the online refiner measurements, such as no significant differences measured between pastes with 5 vol% different fat content but containing no lecithin. Through use of the measurements techniques alongside each other, valuable knowledge was gained through two trials, presented within this chapter. It will, however, be necessary to further develop the BET to ensure measurements of the paste and pre-refined paste consistency are reliable.

Measurements of either the refiner throughput or the current on the rolls is considered to be an invaluable tool for online tracking of the paste performance. It is hoped that relationships can be established between the BET results of the rheological properties and the online measurements of the paste. This would be particularly advantageous within manufacturing environments where only a few different recipes are generally produced, providing the opportunity to collect a large amount of data.

8 CONCLUSIONS AND FUTURE WORK

Reducing the size of the particles and distributing the solids within the fat matrix are considered the key elements in the manufacturing of chocolate. Prior to refining, the ingredients must be combined in a mixing stage; a process step which is almost always overlooked when discussing the manufacture of chocolate. It is currently the sole responsibility of experienced operators to visually assess the consistency differences of these pastes. They must then appropriately manipulate the refiner settings in order to maximise both quality and throughput of the process lines.

The objectives set out at the beginning of this research were:

- to develop a method which can quantify differences between chocolate paste batches that could be used alongside a production line
- to quantify how much the process settings of the mixer and formulation can influence the paste consistency
- to record the impact that varying paste consistency has on the downstream processes, with the aim of quantifying what the ideal paste consistency is

The following sections summarise the outcomes of this investigation into characterisation of chocolate pastes.

8.1 Quantifying chocolate paste rheology

The results of many established methods of measuring the rheological properties of fluids and suspensions were reported in chapter 4. Phase separation at higher shear rates occurred

frequently, leading to inconsistencies in measurements. Capillary rheometry, a common technique used to measure pastes, caused serious phase separation, leading to jamming of the geometry. Practically, the gap size in a parallel plate geometry is limited by the surface tension of the material being able to remain within the gap. Oscillation tests are designed to enable the structures of the suspensions to be maintained however it was not possible to quantify the viscosity from these results as the Cox-Merz transformation, typically applied to polymers, was shown to be inappropriate. This was not improved by using a vane in cup geometry as the gap size remained too small.

The back extrusion technique (BET), developed by Osorio and Steffe (1987), offered the opportunity to use larger geometry gaps. The rheological properties, based on power law and Herschel-Bulkley models, of a polymer solution and suspensions of smaller particles (d_{90} = 146 µm) measured using the BET were comparable to results measured on conventional parallel plate rheometers. The complexity of materials tested on the BET was increased and the technique showed repeatable and realistic results of chocolate pastes containing particles up to 1000 µm with a solids volume content up to 0.72.

Resistive forces measured when the material is stationary are considered by Osorio and Steffe to be representative of the yield stress however the results revealed a very slow, time-dependent decrease in force. This agrees with theories by Barnes and Walters (1985) who believe that perceived results of yield stresses are in fact the slow relaxation of a viscous Newtonian plateau which is present at low shear rates. As the timescale of the pasting process is short, it is still considered beneficial to evaluate the yield stresses of chocolate pastes over a 60 second period.

Considering the application of this technique, experimental ease must be prioritised so that tests are possible within an appropriate timescale. Thus, the most suitable method for evaluating the shear thinning nature of the pastes, represented by the flow behaviour index, assumes that there is no yield stress. The values of flow behaviour indices were compensated for by the calculation of the consistency coefficient hence values of the shear stresses at particular shear rates were still considered to be accurate representations of the fluid behaviour.

It was thought that wall slip, a common issue which plagues many rheological characterisation techniques, occurred during many of the tests of chocolate pastes. Roughening of the walls reduced the impact of the wall slip however attaching sandpaper at the walls lead to experimental errors of the gap size estimations.

The main operational limit of this technique was that the shear stresses of the pastes could only be determined up to a shear rate of 14 s^{-1}. The shear rates which are expected to be achieved within the mixing stage may be within the same order of magnitude as this however, the shear rates estimated to occur within the nip of the refiner rolls are several orders of magnitude higher. This may be problematic since the behaviour of the paste measured by the BET may not be representative of how the material behaves during the refining process.

8.2 Influencing paste consistency

The back extrusion technique was used to determine the rheological properties of chocolate pastes, all of which were found to exhibit shear thinning behaviour and many were also found to have a yield stress. It was hypothesised that yield stresses in pastes are caused by entrained air, which contributes towards increasing the effective solids volume content, discussed further in Chapter 6. Statistical analysis of two pilot plant trials showed that as the fat content

was increased, the consistency of the paste decreases; the shear thinning nature reduces ($n \rightarrow 1$), as does the yield stress. Similarly to the values of resistance that the paste generated on the mixing shaft, an experienced operator was capable of visually identifying differences between the pastes online. Both of these measurement techniques which characterise the pastes online were found to be sensitive to the temperature of the pastes, despite it not currently being measured or controlled.

The viscosity of pastes was also reduced by mixing the pastes for a longer time. It is believed that this was partly a function of the temperature increase which occurs when the mixing duration was increased. Pilot plant trials indicated that the temperature of the paste increased most significantly when the fat content of the paste was lowest and the mixing time was long.

Using the particle size measurement technique that is standardized by Mondelez International, it was not possible to conclude whether there were significant variations in the particle sizes within the pastes due to the processing conditions and thus whether this would affect the paste consistency.

8.3 Impact on downstream performance

Similar factors and interactions of factors were found to influence the consistency of the paste measured using the BET, the current measured on the first roll of the refiner and the time taken for a batch to refine. The fat was the most dominant factor, affecting the paste consistency and how it refined; a higher fat content paste was thinner in consistency and could not easily resist the pressing forces of the refiner rolls.

The current measured on the first roll of the refiner and the throughput of the refiner more strongly correlated with the refined paste particle sizes than the consistencies of the pastes did, suggesting that there may have been more variation in the BET results. Pastes which were

sampled after a two-gap refining stage had significantly smaller particles when the fat content was higher. It was only when the pastes were at 50 °C that the fat content had no impact on the size of the refined particles.

When the temperature was increased from 40 to 50 °C, pastes without lecithin had a lower refiner throughput, producing a much greater proportion of small particles. The refiner throughput of pastes containing lecithin was larger when the temperature was higher, producing refined pastes which were not as fine.

8.4 Future Work

8.4.1 Back extrusion technique

The BET has proven to be a useful technique which is can measure differences in rheological properties between chocolate pastes, contributing to an increased knowledge of the chocolate manufacturing process which is currently not well understood. To further improve the usefulness of this test, the test should be modified so that the shear rates achieved at the walls are comparable to the shear rates which are relevant within the manufacturing process. This may be done by altering the geometry or increasing the velocity of the probe.

In order to increase the confidence that the method does measure the flow properties of a homogeneous paste sample, further visualisation of the paste is recommended. If samples could be solidified and sliced using a microtome, then techniques such as light microscopy or NMR may help to visualise the distribution of solids and fat. If particles could be treated so that their densities were altered, XRCT may be appropriate for imaging of an entire 3D sample.

Similarly to other rheological techniques, results have indicated that slip can potentially be reduced by roughening the probe and the inner walls of the vessel however future work

should look to permanently alter the surfaces through sand blasting. It would also be beneficial to create a roughened surface which has a comparable size to the mix of particles within chocolate pastes.

Following the development of this technique within this project, Mondelēz International have demonstrated that the technique is sensitive enough to distinguish pastes with a 1 vol% fat difference. They are currently validating this technique for several different chocolate paste formulations with the intention of rolling out the method to their manufacturing sites across Europe.

8.4.2 Chocolate paste processing

Overall, no clear factor showed that it could reduce the particle size of the refined chocolates more efficiently than increasing the fat content. Through this research however, significant interactions of the fat content with the temperature have continually been identified. Currently, monitoring or altering the temperature of the pastes is not considered on both pilot plant and manufacturing scales. Through prioritising the temperature of the paste, it may be possible to manipulate the particle sizes of chocolate.

The presence of lecithin within the paste was found to prevent any differences in the consistency of the pastes when the temperature was altered. This was the only significant effect of the lecithin however there is not currently enough understanding about the presence of this emulsifier within a solid-fat system to hypothesis about the cause of this result. It is thus crucial that there is further research undertaken to identify how lecithin molecules interact with the system and how this is influenced by the temperature. This could be done by continuing the work done by Middendorf et al. (2016), who characterised the thickness of lecithin layers on sugar particles.

Recording the current required to turn the mixing shaft through the paste and required by the refiner rolls to rotate have both provided valuable information about differences between pastes. Neither of these measurements necessitate additional equipment or operation. Requiring only small modifications, this data can be continually logged on production lines, creating an abundance of information that could relate the consistency of the pastes to the particle size of the chocolates.

Using the BET to analyse chocolate pastes, the consistency coefficient and the shear stress similarly trend for most pastes and are able to give a good indication of differences between paste consistencies. When the fat content was reduced, yield stresses began to become significant; as yet, the results are unclear as to whether this will have an additional effect on how pastes pass through the refiners. As the shear thinning behaviour of the paste has been found to have little significance on the refining performance, running BET tests at different velocities may not be necessary. Instead, the peak force and relaxation force at one test velocity could be measured without further processing of the data to attain the shear stresses. This would offer a reliable technique to easily and rapidly compare pastes alongside a manufacturing line.

If further particle size analysis of the paste is desirable, it is recommended that there is a detailed validity study on the use of the Malvern Mastersizer technique since the particles range over a broad spectrum of sizes. It may be appropriate to compare results with dynamic image analysis techniques or through visual assessments. This would allow the identification of any particle agglomerates or aggregates which may be relevant to the behaviour of the pastes as they are refined.

This work was unsuccessful at determining the ideal paste consistency that would refine to create a material with the desired particle size since there was a large amount of process variability which may have masked significant results. It is therefore necessary to determine the process repeatability by producing a large number of identical batches. This would allow further studies to ascertain whether factors which are altered have an effect on the process which is greater than the process variability. An extensive study, similar to the design of experiments reported in this work, would then be required to study the effect of the refiner settings and paste consistency on the particle size of refined material.

It has been recommended to Mondelēz International that results from the back extrusion technique are recorded in conjunction with continuous logging of the current on both the mixing blades and the refiner rolls. Particularly on manufacturing lines, a large amount of data can be collated within a short time scale as only a few different products are continually produced. As this data can be compared with the particle size and viscosity of the final chocolate, this should greatly increase the understanding of the variation which currently exists on manufacturing lines.

REFERENCES

AERTS, L. & VERSPAILLE, M. 2001. Absolute Rheometry in the Brabender Viscograph by Mixer Viscometry Calibration. *Starch - Stärke,* 53**,** 59-63.

AFOAKWA, E. O. 2016. *Chocolate Science and Technology: Second Edition,* Wiley-Blackwell.

AÏT-KADI, A., MARCHAL, P., CHOPLIN, L., CHRISSEMANT, A. S. & BOUSMINA, M. 2002. Quantitative Analysis of Mixer-Type Rheometers using the Couette Analogy. *The Canadian Journal of Chemical Engineering,* 80**,** 1166-1174.

ALEJO, B. & BARRIENTOS, A. 2009. Model for yield stress of quartz pulps and copper tailings. *International Journal of Mineral Processing,* 93**,** 213-219.

ALI, A. R. M. & DIMICK, P. S. 1994. Melting and solidification characteristics of confectionery fats: Anhydrous milk fat, cocoa butter and palm kernel stearin blends. *Journal of the American Oil Chemists' Society,* 71**,** 803-806.

ALVIAR, M. S. B. & REID, D. S. 1990. Determination of Rheological Behaviour of Tomato Concentrates Using Back Extrusion. *Journal of Food Science,* 55.

AMMARCHA, C., GATUMEL, C., DIRION, J. L., CABASSUD, M. & BERTHIAUX, H. 2017. Continuous powder mixing of segregating mixtures under steady and unsteady state regimes: Homogeneity assessment by real-time on-line image analysis. *Powder Technology,* 315**,** 39-52.

ANCEY, C., LÈ, H. & JORROT, N. 2001. Yield stress for particle suspensions within a clay dispersion. *Journal of Rheology,* 45.

ARNOLD, G., SCHULDT, S., SCHNEIDER, Y., FRIEDRICHS, J., BABICK, F., WERNER, C. & ROHM, H. 2013. The impact of lecithin on rheology, sedimentation and particle interactions in oil-based dispersions. *Colloids and Surfaces A: Physicochemical and Engineering Aspects,* 418**,** 147-156.

ARVANITI, E. C., JUENGER, M. C. G., BERNAL, S. A., DUCHESNE, J., COURARD, L., LEROY, S., PROVIS, J. L., KLEMM, A. & DE BELIE, N. 2015. Determination of particle size, surface area, and shape of supplementary cementitious materials by different techniques. *Materials and Structures,* 48**,** 3687-3701.

ATTAIE, H., BREITSCHUH, B., BRAUN, P. & WINDHAB, E. J. 2003. The functionality of milk powder and its relationship to chocolate mass processing. *International Journal of Food Science and Technology,* 38**,** 325-335.

AUTY, M. A. E., TWOMEY, M., GUINEE, T. P. & MULVIHILL, D. M. 2001. Development and application of confocal scanning laser microscopy methods for studying the distribution of fat and protein in selected dairy products. *Journal of Dairy Research,* 68**,** 417–427.

AYAZI SHAMLOU, P. & KOUTSAKOS, E. 1989. Solids suspension and distribution in liquids under turbulent agitation. *Chemical Engineering Science,* 44**,** 529-542.

AZZOLINI, A., SGLAVO, V. M. & DOWNS, J. A. 2014. Novel method for the identification of the maximum solid loading suitable for optimal extrusion of ceramic pastes. *Journal of Advanced Ceramics,* 3**,** 7-16.

BANFILL, P. F. G. 1994. Rheological methods for assessing the flow properties of mortar and related materials. *Construction and Building Materials,* 8**,** 43-50.

BARNES, H. A. 1995. A review of the slip (wall depletion) of polymer solutions, emulsions and particle suspensions in viscometers: its cause, character, and cure. *Journal of Non-Newtonian Fluid Mechanics,* 56**,** 221-251.

BARNES, H. A. 2000. Measuring the viscosity of large-particle (and flocculated) suspensions — a note on the necessary gap size of rotational viscometers. *Journal of Non-Newtonian Fluid Mechanics,* 94**,** 213-217.

BARNES, H. A. 2007. The 'Yield stress myth?' paper - 21 years on. *Applied Rheology,* 17**,** 43110.

BARNES, H. A. & CARNALI, J. O. 1990. The vane-in-cup as a novel rheometer geometry for shear thinning and thixotropic materials. *Journal of Rheology,* 34**,** 841-866.

BARNES, H. A. & HOLBROOK, S. A. 1993. *Processing of Solid-Liquid Suspensions,* Oxford, UK, Butterworth-Heinemann Ltd.

BARNES, H. A., HUTTON, J. F. & WALTERS, K. 1989. *An Introduction to Rheology,* Amsterdam, Elsevier.

BARNES, H. A. & NGUYEN, Q. D. 2001. Rotating vane rheometry — a review.pdf. *Journal of Non-Newtonian Fluid Mechanics,* 98**,** 1-14.

BARNES, H. A. & WALTERS, K. 1985. The yield stress myth? *Rheologica Acta,* 24**,** 323-326.

BAYFIELD, M., HAGGETT, J. A., WILLIAMSON, M. J., WILSON, D. I. & ZARGAR, A. 1998. Liquid Phase Migration in the Extrusion of Icing Sugar Pastes. *Food and Bioproducts Processing,* 76**,** 39-46.

BECKETT, S. T. 2008. *The Science of Chocolate,* Cambridge, UK, The Royal Society of Chemistry.

BECKETT, S. T. 2009. *Industrial chocolate manufacture and use,* Chichester, UK, Blackwell Publishing.

BENBOW, J. & BRIDGWATER, J. 1993. *Paste flow and extrusion,* Oxford, UK, Clarendon Press.

BENCHABANE, A. & KARIM, B. 2008. Rheological properties of carboxymethyl cellulose (CMC) solutions. *Colloid Polym Sci,* 286**,** 1173-1180.

BERTHIAUX, H., MOSOROV, V., TOMCZAK, L., GATUMEL, C. & DEMEYRE, J. F. 2006. Principal component analysis for characterising homogeneity in powder mixing using image processing techniques. *Chemical Engineering and Processing: Process Intensification,* 45**,** 397-403.

BOLENZ, S. & MANSKE, A. 2013. Impact of fat content during grinding on particle size distribution and flow properties of milk chocolate. *European Food Research and Technology,* 236**,** 863-872.

BOLENZ, S., MANSKE, A. & LANGER, M. 2014. Improvement of process parameters and evaluation of milk chocolates made by the new coarse conching process. *European Food Research and Technology,* 238**,** 863-874.

BOLENZ, S., THIESSENHUSEN, T. & SCHÄPE, R. 2003. Influence of milk components on properties and consumer acceptance of milk chocolate. *European Food Research and Technology,* 216**,** 28-33.

BOUSMINA, M., AIT-KADI, A. & FAISANT, J. B. 1999. Determination of shear rate and viscosity from batch mixer data. *Journal of Rheology,* 43**,** 415-433.

BROCKBANK, K., ARMSTRONG, B., CHANDORKAR, Y. & FREEMAN, T. 2015. Understanding Powder Caking as a Consequence of a Range of Mechanisms by Means of Powder Rheometry. *Particulate Science and Technology,* 33**,** 102-108.

BROUWERS, H. J. 2010. Viscosity of a concentrated suspension of rigid monosized particles. *Phys Rev E Stat Nonlin Soft Matter Phys,* 81**,** 051402.

BRUSEWITZ, G. H. & YU, H. 1996. Back extrusion method for Determining Properties of Mustard Slurry. *Journal of Food Engineering,* 27**,** 259-265.

BUMA, T. J. 1971. Free fat in spray-dried whole milk- A final report with a physical model for free fat in spray-dried milk. *Neth. Milk Dairy J.,* 25**,** 159-174.

BYLUND, G. 2015. *Dairy Processing Handbook* Tetra Pak.

CARIC, M. & KALAB, M. 1987. Effects of Drying Techniques on Milk Powders Quality and Microstructure: A Review. *Food Structure,* 6.

CASTELL-PEREZ, M. E. & STEFFE, J. F. 1990. Evaluating shear rates for power law fluids in mixer viscometry. *Journal of Texture Studies,* 21**,** 439-452.

CEPURITIS, R., GARBOCZI, E. J., FERRARIS, C. F., JACOBSEN, S. & SØRENSEN, B. E. 2017. Measurement of particle size distribution and specific surface area for crushed concrete aggregate fines. *Advanced Powder Technology,* 28**,** 706-720.

CHATZIMINA, M., GEORGIOU, G. & ALEXANDROU, A. 2009. Wall Shear Rates in Circular Couette Flow of a Herschel Bulkley Fluid. *Applied Rheology,* 19.

CHEMÉO. 2016. *Chemical Properties of Sucrose (CAS 57-50-1)* [Online]. Available: https://www.chemeo.com/cid/18-498-0/Sucrose.

CHOI, M., PARK, K. & OH, T. 2016. Viscoelastic Properties of Fresh Cement Paste to Study the Flow Behavior. *International Journal of Concrete Structures and Materials,* 10**,** 65-74.

CHOW, A., SINTON, S., H. IWAMIYA, J. & STEPHENS, T. 1994. Shear-induced particle migration in Couette and parallel-plate viscometers: NMR imaging and stress measurements. *Physics of Fluids,* 6**,** 2561-2576.

CILAS n.d. Choosing the most Suitable Theory in Laser Diffraction.

COLBOURNE, A. A., BLYTHE, T. W., BARUA, R., LOVETT, S., MITCHELL, J., SEDERMAN, A. J. & GLADDEN, L. F. 2018. Validation of a low field Rheo-NMR instrument and application to shear-induced migration of suspended non-colloidal particles in Couette flow. *Journal of Magnetic Resonance,* 286**,** 30-35.

COX, W. P. & MERZ, E. H. 1958. Correlation of dynamic and steady flow viscosities. *Journal of Polymer Science,* 28**,** 619-622.

CULLEN, P. J. 2009. *Food Mixing: Principles and Applications*, Wiley-Blackwell.

DABAK, Y. & YUCEL, O. 1986. Shear Viscosity behaviour of highly concentrated suspensions at low and high shear rates. *Rheologica Acta,* 25**,** 527-533.

DAVID, J., FILIP, P. & KHARLAMOV, A. A. 2013. Back Extrusion of Vocadlo-Type Fluids. *Applied Rheology,* 23**,** 45366.

DEBACKER, A., MAKARCHUK, S., LOOTENS, D. & HEBRAUD, P. 2014. Imbibition kinetics of spherical colloidal aggregates. *Phys Rev Lett,* 113**,** 028301.

DESHPANDE, K. V. & SHAPLEY, N. C. 2010. Particle migration in oscillatory torsional flows of concentrated suspensions. *Journal of Rheology,* 54**,** 663-686.

DONTULA, P., MACOSKO, C. W. & SCRIVEN, L. E. 2005. Origins of concentric cylinders viscometry. *Journal of Rheology,* 49**,** 807-818.

DORAISWAMY, D., MUJUMDAR, A. N., TSAO, I., BERIS, A. N., DANFORTH, S. C. & METZNER, A. B. 1991. The Cox–Merz rule extended: A rheological model for concentrated suspensions and other materials with a yield stress. *Journal of Rheology,* 35**,** 647-685.

DÖRR, A., SADIKI, A. & MEHDIZADEH, A. 2013. A discrete model for the apparent viscosity of polydisperse suspensions including maximum packing fraction. *Journal of Rheology,* 57**,** 743-765.

DRAPER, O., BLACKBURN, S., DOLMAN, G., SMALLEY, K. & GRIFFITHS, A. 1999. A comparison of paste rheology and extrudate strength with respect to binder formulation and forming technique. *Journal of Materials Processing Technology,* 92-93**,** 141-146.

DUFFY, J. J., HILL, A. J. & MURPHY, S. H. 2015. Simple Method for Determining Stress and Strain Constants for Non Standard Measuring Systems. *Applied Rheology,* 25**,** 42670.

DZUY, N. Q. & BOGER, D. V. 1983. Yield Stress Measurement for Concentrated Suspensions. *Journal of Rheology,* 27**,** 321-349.

EWOLDT, R. H., JOHNSTON, M. T. & CARETTA, L. M. 2015. Experimental Challenges of Shear Rheology: How to Avoid Bad Data. *In:* SPAGNOLIE, S. E. (ed.) *Complex Fluids in Biological Systems: Experiment, Theory, and Computation.* New York, NY: Springer New York.

FARRIS, R. J. 1968. Prediction of the Viscosity of Multimodal Suspensions from Unimodal Viscosity Data. *Transactions of the Society of Rheology,* 12**,** 281-301.

FERRARIS, C. & DE LARRARD, F. 1998. Modified Slump Test to Measure Rheological Parameters of Fresh Concrete. *Cement Concrete and Aggregates,* 20.

FISCHER, P. & WINDHAB, E. J. 2011. Rheology of food materials. *Current Opinion in Colloid & Interface Science,* 16**,** 36-40.

FISHER, D. T., CLAYTON, S. A., BOGER, D. V. & SCALES, P. J. 2007. The bucket rheometer for shear stress-shear rate measurement of industrial suspensions. *Journal of Rheology,* 51**,** 821-831.

FRANKE, K. & HEINZELMANN, K. 2008. Structure improvement of milk powder for chocolate processing. *International Dairy Journal,* 18**,** 928-931.

GARTI, N. & ASERIN, A. 2012. 12 - Effect of Emulsifiers on Cocoa Butter and Chocolate Rheology, Polymorphism, and Bloom. *Cocoa Butter and Related Compounds.* AOCS Press.

GLEISSLE, W. & HOCHSTEIN, B. 2003. Validity of the Cox–Merz rule for concentrated suspensions. *Journal of Rheology,* 47**,** 897-910.

GLICERINA, V., BALESTRA, F., DALLA ROSA, M. & ROMANI, S. 2015. Effect of manufacturing process on the microstructural and rheological properties of milk chocolate. *Journal of Food Engineering,* 145**,** 45-50.

GOLDSZAL, A. & BOUSQUET, J. 2001. Wet agglomeration of powders. *Powder Technology,* 117**,** 221–231.

GOODRICH, J. E. & PORTER, R. S. 1967. A rheological interpretation of torque-rheometer data. *Polymer Engineering & Science,* 7**,** 45-51.

GUILLEMIN, J. P., MENARD, Y., BRUNET, L., BONNEFOY, O. & THOMAS, G. 2008. Development of a new mixing rheometer for studying rheological behaviour of concentrated energetic suspensions. *Journal of Non-Newtonian Fluid Mechanics,* 151**,** 136-144.

GUJRAL, H. S. & SODHI, N. S. 2002. Back extrusion properties of wheat porridge (Dalia). *Journal of Food Engineering,* 52**,** 53-56.

GUTIÉRREZ, T. J. 2017. State-of-the-Art Chocolate Manufacture: A Review. *Comprehensive Reviews in Food Science and Food Safety,* 16**,** 1313-1344.

HAFID, H., OVARLEZ, G., TOUSSAINT, F., JEZEQUEL, P. H. & ROUSSEL, N. 2016. Effect of particle morphological parameters on sand grains packing properties and rheology of model mortars. *Cement and Concrete Research,* 80**,** 44-51.

HANCOCK, B. C., YORK, P. & ROWE, R. C. 1994. An assessment of substrate-binder interactions in model wet masses. 1: Mixer torque rheometry. *International Journal of Pharmaceutics,* 102**,** 167-176.

HARNBY, N. 2000. An engineering view of pharmaceutical powder mixing. *Pharmaceutical Science & Technology Today,* 3**,** 303-309.

HARRISON, S. T. L., STEVENSON, R. & CILLIERS, J. J. 2012. Assessing solids concentration homogeneity in Rushton-agitated slurry reactors using electrical resistance tomography (ERT). *Chemical Engineering Science,* 71**,** 392-399.

HAYLOCK, S. J. & DODDS, T. M. 2009. Ingredients From Milk. *In:* BECKETT, S. T. (ed.) *Industrial chocolate manufacture and use.* 4th ed. Chichester, UK: Blackwell Publishing.

HEIRMAN, G., VANDEWALLE, L., VAN GEMERT, D. & WALLEVIK, Ó. 2008. Integration approach of the Couette inverse problem of powder type self-compacting concrete in a wide-gap concentric cylinder rheometer. *Journal of Non-Newtonian Fluid Mechanics,* 150**,** 93-103.

HEYMANN, L., PEUKERT, S. & AKSEL, N. 2002. On the solid-liquid transition of concentrated suspensions in transient shear flow. *Rheologica Acta,* 41**,** 307-315.

HOGEKAMP, S. & SCHUBERT, H. 2003. Rehydration of Food Powders. *Food Science and Technology International,* 9**,** 223-235.

HOSSEINI, S., PATEL, D., EIN-MOZAFFARI, F. & MEHRVAR, M. 2010. Study of solid–liquid mixing in agitated tanks through electrical resistance tomography. *Chemical Engineering Science,* 65**,** 1374-1384.

HOU, T. H. 1981. On the flow field of Newtonian liquids in the truncated cone and plate rheometer. *Rheologica Acta,* 20**,** 14-22.

HUANG, A.-N. & KUO, H.-P. 2014. Developments in the tools for the investigation of mixing in particulate systems – A review. *Advanced Powder Technology,* 25**,** 163-173.

HUI, Y. H. 2007. *Handbook of Food Products Manufacturing: Health, Meat, Milk, Poultry, Seafood, and Vegetables, Volume 2,* Wiley-Interscience.

INGBER, M. S., GRAHAM, A. L., MONDY, L. A. & FANG, Z. 2009. An improved constitutive model for concentrated suspensions accounting for shear-induced particle migration rate dependence on particle radius. *International Journal of Multiphase Flow,* 35**,** 270-276.

J. STICKEL, J. & L. POWELL, R. 2005. Fluid mechanics and rheology of dense suspensions. *Annual Review of Fluid Mechanics,* 37**,** 129-149.

JANA, S. C., KAPOOR, B. & ACRIVOS, A. 1995. Apparent wall slip velocity coefficients in concentrated suspensions of noncolloidal particles. *Journal of Rheology,* 39**,** 1123-1132.

JÁNOSI, I. M., TÉL, T., WOLF, D. E. & GALLAS, J. A. C. 1997. Chaotic particle dynamics in viscous flows. *Physical Review E,* 56**,** 2858.

JI, J., FITZPATRICK, J., CRONIN, K., MAGUIRE, P., ZHANG, H. & MIAO, S. 2016. Rehydration behaviours of high protein dairy powders: The influence of agglomeration on wettability, dispersibility and solubility. *Food Hydrocolloids,* 58**,** 194-203.

JOMHA, A. I. & REYNOLDS, P. A. 1993. An experimental study of the first normal stress difference — shear stress relationship in simple shear flow for concentrated shear thickening suspensions. *Rheologica Acta,* 32**,** 457-464.

JONES, D. & KUNZE, M. 2004. Guide to Sampling Soil Compaction Using Hand-Held Soil Penetrometers.

JONES, J. R., PRIME, D., LEAPER, M. C., RICHARDSON, D. J., RIELLY, C. D. & STAPLEY, A. G. F. 2013. Effect of processing variables and bulk composition on the surface composition of spray dried powders of a model food system. *Journal of Food Engineering,* 118**,** 19-30.

KABAGIRE, K., DIEDERICH, P., YAHIA, A. & CHEKIRED, M. 2017. Experimental assessment of the effect of particle characteristics on rheological properties of model mortar. *Construction and Building Materials,* 151**,** 615-624.

KALÁB, M. 2010. The Beauty of Milk at High Magnification. *infocus.* Royal Microscopical Society.

KARNIS, A. & MASON, S. G. 1967. The flow of suspensions through tubes VI. Meniscus effects. *Journal of Colloid and Interface Science,* 23**,** 120-133.

KEENTOK, M. & XUE, S.-C. 1999. Edge fracture in cone-plate and parallel plate flows. *Rheologica Acta,* 38**,** 321-348.

KELLY, G. M., O'MAHONY, J. A., KELLY, A. L. & O'CALLAGHAN, D. J. 2014. Physical characteristics of spray-dried dairy powders containing different vegetable oils. *Journal of Food Engineering,* 122**,** 122-129.

KELLY, J., KELLY, P., M. & HARRINGTON, D. 2002. Influence of processing variables on the physicochemical properties of spray dried fat-based milk powders. *Lait,* 82**,** 401-412.

KIM, E. H.-J., CHEN, X. D. & PEARCE, D. 2002. Surface characterization of four industrial spray-dried dairy powders in relation to chemical composition, structure and wetting property. *Colloids and Surfaces B: Biointerfaces,* 26**,** 197-212.

KIM, E. H. J., CHEN, X. D. & PEARCE, D. 2009. Surface composition of industrial spray-dried milk powders. 2. Effects of spray drying conditions on the surface composition. *Journal of Food Engineering,* 94**,** 169-181.

KIM, J. M., LEE, S. G. & KIM, C. 2008. Numerical simulations of particle migration in suspension flows: Frame-invariant formulation of curvature-induced migration. *Journal of Non-Newtonian Fluid Mechanics,* 150**,** 162-176.

KLEIN, R. J., LORENZINI, G., ZINANI, F. S. F. & ROCHA, L. A. O. 2017. Dimensionless pressure drop number for non-newtonian fluids applied to Constructal Design of heat exchangers. *International Journal of Heat and Mass Transfer,* 115**,** 910-914.

KOOS, E., LINARES-GUERRERO, E., HUNT, M. L. & BRENNEN, C. E. 2012. Rheological measurements of large particles in high shear rate flows. *Physics of Fluids,* 24**,** 013302.

KRISHNAN, G. P., BEIMFOHR, S. & LEIGHTON, D. T. 2006. Shear-induced radial segregation in bidisperse suspensions. *Journal of Fluid Mechanics,* 321**,** 371-393.

KROMKAMP, J., VAN DEN ENDE, D., KANDHAI, D., VAN DER SMAN, R. & BOOM, R. 2006. Lattice Boltzmann simulation of 2D and 3D non-Brownian suspensions in Couette flow. *Chemical Engineering Science,* 61**,** 858-873.

KROUPA, M., SOOS, M. & KOSEK, J. 2017. Slip on a particle surface as the possible origin of shear thinning in non-Brownian suspensions. *Physical Chemistry Chemical Physics,* 19**,** 5979-5984.

LARSON, R. G. 1999. The structure and rheology of complex fluids. New York: Oxford University Press.

LAY MA, U. V., ZIEGLER, G. R. & FLOROS, J. D. 2008. Effect of Sucrose on Physical Properties of Spray-Dried Whole Milk Powder. *Journal of Food Science,* 73**,** E431-E438.

LEUENBERGER, H. & BETZ, G. 2007. Chapter 15 Granulation process control — production of pharmaceutical granules: The classical batch concept and the problem of scale-up. *Handbook of Powder Technology,* 11**,** 705-733.

LEUENBERGER, H., PUCHKOV, M., KRAUSBAUER, E. & BETZ, G. 2009. Manufacturing pharmaceutical granules: Is the granulation end-point a myth? *Powder Technology,* 189**,** 141-148.

LIANG, B. & HARTEL, R. W. 2004. Effects of Milk Powders in Milk Chocolate. *Journal of Dairy Science,* 87**,** 20-31.

LIU, S. & HA, Z. 2002. Prediction of random packing limit for multimodal particle mixtures. *Powder Technology,* 126**,** 283-296.

LUUKKONEN, P., SCHÆFER, T., HELLÉN, L., JUPPO, A. M. & YLIRUUSI, J. 1999. Rheological characterization of microcrystalline cellulose and silicified microcrystalline cellulose wet masses using a mixer torque rheometer. *International Journal of Pharmaceutics,* 188**,** 181-192.

MAGELLI, F., FAJNER, D., NOCENTINI, M. & PASQUALI, G. 1990. Solid distribution in vessels stirred with multiple impellers. *Chemical Engineering Science,* 45**,** 615-625.

MAHAUT, F., MOKÉDDEM, S., CHATEAU, X., ROUSSEL, N. & OVARLEZ, G. 2008. Effect of coarse particle volume fraction on the yield stress and thixotropy of cementitious materials. *Cement and Concrete Research,* 38**,** 1276-1285.

MALVERN INSTRUMENTS LIMITED. *Smarter Particle Sizing* [Online]. [online]. Available: https://www.malvernpanalytical.com/en/products/product-range/mastersizer-range/mastersizer-3000/ [Accessed 15 Feb 2017].

MARTIN, R. A. 1988. Chocolate. *In:* CHICHESTER, C. O., MRAK, E. M. & SCHWEIGERT, B. S. (eds.) *Advances in Food Research.* Academic Press.

MATUSZEK, D. & WOJTKIEWICZ, K. 2017. Application of fluorescent markers for homogeneity assessment of grain mixtures based on maize content. *Chemical and Process Engineering,* 38**,** 505-512.

MAVROS, P. 2001. Flow Visualization in Stirred Vessels: A Review of Experimental Techniques. *Chemical Engineering Research and Design,* 79**,** 113-127.

MEHDIPOUR, I. & KHAYAT, K. 2017. Effect of Particle-Size Distribution and Specific Surface Area of Different Binder Systems on Packing Density and Flow Characteristics of Cement Paste. *Cement and Concrete Composites,* 78.

MERHI, D., LEMAIRE, E., BOSSIS, G. & MOUKALLED, F. 2005. Particle migration in a concentrated suspension flowing between rotating parallel plates: Investigation of diffusion flux coefficients. *Journal of Rheology,* 49**,** 1429-1448.

METZGER, B. & BUTLER, J. E. 2010. Irreversibility and chaos: role of long-range hydrodynamic interactions in sheared suspensions. *Phys Rev E Stat Nonlin Soft Matter Phys,* 82**,** 051406.

MEZGER, T. G. 2006. *The rheology handbook : for users of rotational and oscillatory rheometers,* Hannover, Vincentz Network.

MIDDENDORF, D., BINDRICH, U., MISCHNICK, P., JUADJUR, A., FRANKE, K. & HEINZ, V. 2016. Atomic Force Microscopy study on the effect of different lecithins in cocoa-butter based suspensions. *Colloids and Surfaces A: Physicochemical and Engineering Aspects,* 499**,** 60-68.

MILLQVIST-FUREBY, A. & SMITH, P. 2007. In-situ lecithination of dairy powders in spray-drying for confectionery applications. *Food Hydrocolloids,* 21**,** 920-927.

MIRBOD, P. 2016. Two-dimensional computational fluid dynamical investigation of particle migration in rotating eccentric cylinders using suspension balance model. *International Journal of Multiphase Flow,* 80**,** 79-88.

MISTRY, V. V., HASSAN, H. N. & ROBISON, D. J. 1992. Effect of Lactose and Protein on the Microstructure of Dried Milk. *Food Structure,* 2**,** 73-82.

MØLLER, P. C. F., FALL, A. & BONN, D. 2009. Origin of apparent viscosity in yield stress fluids below yielding. *EPL (Europhysics Letters),* 87**,** 38004.

MONGIA, G. & ZIEGLER, G. R. 2000. The role of particle size distribution of suspended solids in defining the flow properties of milk chocolate. *International Journal of Food Properties,* 3**,** 137-147.

MONTANTE, G., MICALE, G., MAGELLI, F. & BRUCATO, A. 2001. Experiments and CFD Predictions of Solid Particle Distribution in a Vessel Agitated with Four Pitched Blade Turbines. *Chemical Engineering Research and Design,* 79**,** 1005-1010.

MOON, J. Y., DAI, S., CHANG, L., LEE, J. S. & TANNER, R. I. 2015. The effect of sphere roughness on the rheology of concentrated suspensions. *Journal of Non-Newtonian Fluid Mechanics,* 223**,** 233-239.

MORAD, N. A., KAMAL, A. A. M., PANAU, F. & YEW, T. W. 2000. Liquid Specific Heat Capacity Estimation for Fatty Acids, Triacylglycerols, and Vegetable Oils Based on Their Fatty Acid Composition. *Journal of the American Oil Chemists' Society,* 77**,** 1001-1005.

MUELLER, S., LLEWELLIN, E. W. & MADER, H. M. 2009. The rheology of suspensions of solid particles. *Proceedings of the Royal Society A: Mathematical, Physical and Engineering Sciences,* 466**,** 1201-1228.

MUKHERJEE, A. & PISUPATI, S. V. 2015. Interparticle Interactions in Highly Concentrated Coal–Water Slurries and Their Effect on Slurry Viscosity. *Energy & Fuels,* 29**,** 3675-3683.

MURATA, J. 1984. Flow and deformation of fresh concrete. *Matériaux et Construction,* 17**,** 117-129.

MURRIETA-PAZOS, I., GAIANI, C., GALET, L. & SCHER, J. 2012. Composition gradient from surface to core in dairy powders: Agglomeration effect. *Food Hydrocolloids,* 26**,** 149-158.

MUTHUKUMARAPPAN, K. 2009. *Food Mixing: Principles and Applications,* Wiley-Blackwell.

MWASAME, P. M., WAGNER, N. J. & BERIS, A. N. 2016. Modeling the viscosity of polydisperse suspensions: Improvements in prediction of limiting behavior. *Physics of Fluids,* 28**,** 061701.

NEBESNY, E. & ŻYŻELEWICZ, D. 2005. Effect of lecithin concentration on properties of sucrose-free chocolate masses sweetened with isomalt. *European Food Research and Technology,* 220**,** 131-135.

NGUYEN, H.-V., ANDREASSEN, E., KRISTIANSEN, H., JOHANNESSEN, R., HOIVIK, N. & AASMUNDTVEIT, K. E. 2013. Rheological characterization of a novel isotropic conductive adhesive – Epoxy filled with metal-coated polymer spheres. *Materials & Design,* 46**,** 784-793.

NZMP. *AMF Properties* [Online]. Global Dairy Trade. Available: https://globaldairytrade.info/en/gdt-events/gdt-events-sellers-and-products/nzmp/ [Accessed 11.05.2018.

OSORIO, F. A. & STEFFE, J. F. 1987. Back extrusion of power law fluids. *Journal of Texture Studies***,** 43-63.

OSORIO, F. A. & STEFFE, J. F. 1991. Evaluating Herschel-Bulkley fluids with the back extrusion (annular pumping) technique. *Rheologica Acta,* 30**,** 579-558.

OVARLEZ, G., BERTRAND, F., COUSSOT, P. & CHATEAU, X. 2012. Shear-induced sedimentation in yield stress fluids. *Journal of Non-Newtonian Fluid Mechanics,* 177-178**,** 19-28.

OVARLEZ, G., COHEN-ADDAD, S., KRISHAN, K., GOYON, J. & COUSSOT, P. 2013. On the existence of a simple yield stress fluid behavior. *Journal of Non-Newtonian Fluid Mechanics,* 193**,** 68-79.

OVARLEZ, G., MAHAUT, F., BERTRAND, F. & CHATEAU, X. 2011. Flows and heterogeneities with a vane tool: Magnetic resonance imaging measurements. *Journal of Rheology,* 55**,** 197.

PALANUWECH, J., POTINENI, R., ROBERTS, R. F. & COUPLAND, J. N. 2003. A method to determine free fat in emulsions. *Food Hydrocolloids,* 17**,** 55-62.

PERROT, A., MÉLINGE, Y., ESTELLÉ, P., RANGEARD, D. & LANOS, C. 2011. The Back Extrusion Test as a Technique for Determining the Rheological and Tribological Behaviour of Yield Stress Fluids at Low Shear Rates. *Applied Rheology,* 21**,** 53642.

PHAM, P., METZGER, B. & BUTLER, J. E. 2015. Particle dispersion in sheared suspensions: Crucial role of solid-solid contacts. *Physics of Fluids,* 27**,** 051701.

PIAU, J. M. 2006. Consistometry slump and spreading tests: Practical comments. *Journal of Non-Newtonian Fluid Mechanics,* 135**,** 177-178.

PIAU, J. M. & DEBIANE, K. 2005. Consistometers rheometry of power-law viscous fluids. *Journal of Non-Newtonian Fluid Mechanics,* 127**,** 213-224.

PIETSCH, W. 1997. Size Enlargement by Agglomeration. *In:* FAYED, M. E. & OTTEN, L. (eds.) *Handbook of Powder Science & Technology.* Boston, MA: Springer US.

R. ABBOTT, J., TETLOW, N., GRAHAM, A., A. ALTOBELLI, S., FUKUSHIMA, E., MONDY, L. & STEPHENS, T. 1991. Experimental Observations of Particle Migration in Concentrated Suspensions: Couette Flow. *Journal of Rheology,* 35**,** 773-795.

RAMACHANDRAN, A. & LEIGHTON, D. T. 2010. Particle migration in concentrated suspensions undergoing squeeze flow. *Journal of Rheology,* 54**,** 563-589.

REEVE, P. 2010. Yield Stress: A Predictive Tool for Determining Suspending Properties? *Applied Rheology,* 20**,** 33009.

ROUSSEL, N. & COUSSOT, P. 2005. "Fifty-cent rheometer" for yield stress measurements: From slump to spreading flow. *Journal of Rheology,* 49**,** 705-718.

ROWE, R. C. & SADEGHNEJAD, G. R. 1987. The rheology of microcrystalline cellulose powder/water mixes — measurement using a mixer torque rheometer. *International Journal of Pharmaceutics,* 38**,** 227-229.

RUMPF, H. 1959. Beanspruchungstheorie der Prollzerkleinerung. *Chem-Ingenieur Technik,* 31.

SAAK, A. W., JENNINGS, H. M. & SHAH, S. P. 2004. A generalized approach for the determination of yield stress by slump and slump flow. *Cement and Concrete Research,* 34**,** 363-371.

SANTI, C. R., JR., E. H., VLACHOPOULOS, J. & CORREA, C. A. 2009. Torque Viscometry of Molten Polymers and Composites. *Applied Rheology,* 19.

SCHANTZ, B., LINKE, L. & ROHM, H. Effects of different emulsifiers on rheological and physical properties of chocolate. 3rd International Symposium on Food Rheology and Structure, 2003 Zurich, CZ.

SCICOLONE, J. V., METZGER, M., KOYNOV, S., ANDERSON, K., TAKHISTOV, P., GLASSER, B. J. & MUZZIO, F. J. 2016. Effect of liquid addition on the bulk and flow properties of fine and coarse glass beads. *AIChE Journal,* 62**,** 648-658.

SELOMULYA, C. & FANG, Y. 2013. 15 - Food powder rehydration. *Handbook of Food Powders.* Woodhead Publishing.

SHARIFI, M. & YOUNG, B. 2013. Electrical Resistance Tomography (ERT) applications to Chemical Engineering. *Chemical Engineering Research and Design,* 91**,** 1625-1645.

SHARMA, A., JANA, A. H. & CHAVAN, R. S. 2012. Functionality of Milk Powders and Milk-Based Powders for End Use Applications-A Review. *Comprehensive Reviews in Food Science and Food Safety,* 11**,** 518-528.

SHAULY, A., WACHS, A. & NIR, A. 1998. Shear-induced particle migration in a polydisperse concentrated suspension. *Journal of Rheology,* 42**,** 1329-1348.

SHI, F. 2016. A review of the applications of the JK size-dependent breakage model. *International Journal of Mineral Processing,* 155**,** 118-129.

STANLEY, S. J. & BOLTON, G. T. 2008. A Review of Recent Electrical Resistance Tomography (ERT) Applications for Wet Particulate Processing. *Particle & Particle Systems Characterization,* 25**,** 207-215.

SUBBANNA, M., PRADIP & MALGHAN, S. G. 1998. Shear yield stress of flocculated alumina–zirconia mixed suspensions: effect of solid loading, composition and particle size distribution. *Chemical Engineering Science,* 53**,** 3073-3079.

SUMITA, I. & MANGA, M. 2008. Suspension rheology under oscillatory shear and its geophysical implications. *Earth and Planetary Science Letters,* 269**,** 468-477.

SZYDŁOWSKA-CZERNIAK, A., RABIEJ, D. & PAWŁOWICZ, R. 2017. Comparison of the crystallization behaviors of different types of cocoa butters and chocolates. *Journal of Food Processing and Preservation,* 41**,** e13154-n/a.

TA.INSTRUMENTS. *Rheology: Theory and Applications* [Online]. [Accessed 16/06/17.

TADIER, S., GALEA, L., CHARBONNIER, B., BAROUD, G. & BOHNER, M. 2014. Phase and size separations occurring during the injection of model pastes composed of β-tricalcium phosphate powder, glass beads and aqueous solutions. *Acta Biomaterialia,* 10**,** 2259-2268.

TAVARES, L. M. & KING, R. P. 1998. Single-particle fracture under impact loading. *International Journal of Mineral Processing,* 54**,** 1-28.

TETLOW, N., GRAHAM, A. L., INGBER, M. S., SUBIA, S. R., MONDY, L. A. & ALTOBELLI, S. A. 1998. Particle migration in a Couette apparatus: Experiment and modeling. *Journal of Rheology,* 42**,** 307-327.

TWOMEY, M., KEOGH, M. K., O'KENNEDY, B. T., AUTY, M. & MULVIHILL, D. M. 2000. Effect of Milk Composition on Selected Properties of Spray-Dried High-Fat and Skim-Milk Powders. *Irish Journal of Agricultural and Food Research,* 39**,** 79-94.

VÁZQUEZ-QUESADA, A., MAHMUD, A., DAI, S., ELLERO, M. & TANNER, R. I. 2017. Investigating the causes of shear-thinning in non-colloidal suspensions: Experiments and simulations. *Journal of Non-Newtonian Fluid Mechanics,* 248**,** 1-7.

VIGNOLLES, M.-L., JEANTET, R., LOPEZ, C. & SCHUCK, P. 2007. Free fat, surface fat and dairy powders: interactions between process and product. A review. *Le Lait,* 87**,** 187-236.

WELLS, M. A. 2009. Chocolate Crumb. *In:* BECKETT, S. T. (ed.) *Industrial chocolate manufacture and use.* 4th ed. Chichester, UK: Blackwell Publishing.

WILLIAMS, R. W. 1979. Determination of viscometric data from the Brookfield R.V.T. viscometer. *Rheologica Acta,* 18**,** 345-359.

WILSON, D. I. & ROUGH, S. L. 2006. Exploiting the curious characteristics of dense solid–liquid pastes. *Chemical Engineering Science,* 61**,** 4147-4154.

WINDHAB, E. 2000. Fluid immobilization-a structure-related key mechanism for the viscous flow behavior of concentrated suspension systems. *Applied Rheology,* 10**,** 134-144.

WINTER, H. H. 2008. Three views of viscoelasticity for Cox–Merz materials. *Rheologica Acta,* 48**,** 241-243.

XU, A., SHI, L. & ZHAO, T. S. 2018. Lattice Boltzmann simulation of shear viscosity of suspensions containing porous particles. *International Journal of Heat and Mass Transfer,* 116**,** 969-976.

YARAS, P., KAYLON, D. M. & YILMAZER, U. 1994. Flow instabilities in capillary flow of concentrated suspensions *Rheologica Acta,* 33**,** 48-59.

YILMAZER, U. & KALYON, D. M. 1989. Slip Effects in Capillary and Parallel Disk Torsional Flows of Highly Filled Suspensions. *Journal of Rheology,* 33**,** 1197-1212.

YOO, B. & RAO, M. A. 1994. Effect of unimodal particle size and pulp content on rheological properties of tomato puree. *Journal of Texture Studies,* 25**,** 421-436.

YOSHIMURA, A. S., PRUD'HOMME, R. K., PRINCEN, H. M. & KISS, A. D. 1987. A Comparison of Techniques for Measuring Yield Stresses. *Journal of Rheology,* 31**,** 699-710.

YU, B., CHEN, Y. & LIU, Q. 2016. Experimental Study on the Influence of Course Particle on the Yield Stress of Debris Flows. *Applied Rheology,* 26**,** 42997.

YU, Z., SHAO, X. & ROGER, T. 2007. Dynamic Simulation of Shear-induced Particle Migration in a Two-dimensional Circular Couette Device. *Chinese Journal of Chemical Engineering,* 15**,** 333-338.

YUAN, Y., LIU, L., ZHANG, Y., JIN, W. & LI, S. 2018. Coupling effects of particle size and shape on improving the density of disordered polydisperse packings. *PHYSICAL REVIEW E*.

ZHOU, J. Z. Q., FANG, T., LUO, G. & UHLHE, P. H. T. 1995. Yield stress and maximum packing fraction of concentrated suspensions. *Rheologica Acta,* 34**,** 544-561.

ZIMBONE, S. M., VICKERS, A., MORGAN, R. P. C. & VELLA, P. 1996. Field investigations of different techniques for measuring surface soil shear strength. *Soil Technology,* 9**,** 101-111.

ZIYI, H., PENG, P., JINDE, X., YEZHEN, Y. & SHAOPENG, Z. 2014. Study on Test Methods for Intelligence-based Monitoring of Fresh Cement Concrete Quality *Advanced Materials Research,* 857**,** 3-9.

APPENDIX 1

MATLAB code to determine rheological parameters from the back extrusion technique:

Power Law model

```
clc;
clear;
close all;

% Number of tests:
nrepeats = 3;
nspeeds = 4;
ntests = nrepeats * nspeeds;

% Import the time, load and distance from Excel
    filename = 'InsertFilenameHere.xlsx';

    % 4mmps
    TimeRun14mmps = xlsread(filename,10,'C4:C738');
    LoadRun14mmps = xlsread(filename,10,'B4:B738');
    DistRun14mmps = xlsread(filename,10,'A4:A738');
    TimeRun24mmps = xlsread(filename,11,'C4:C738');
    LoadRun24mmps = xlsread(filename,11,'B4:B738');
    DistRun24mmps = xlsread(filename,11,'A4:A738');
    TimeRun34mmps = xlsread(filename,12,'C4:C738');
    LoadRun34mmps = xlsread(filename,12,'B4:B738');
    DistRun34mmps = xlsread(filename,12,'A4:A738');

    % 8mmps
    TimeRun18mmps = xlsread(filename,7,'C4:C677');
    LoadRun18mmps = xlsread(filename,7,'B4:B677');
    DistRun18mmps = xlsread(filename,7,'A4:A677');
    TimeRun28mmps = xlsread(filename,8,'C4:C677');
    LoadRun28mmps = xlsread(filename,8,'B4:B677');
    DistRun28mmps = xlsread(filename,8,'A4:A677');
    TimeRun38mmps = xlsread(filename,9,'C4:C677');
    LoadRun38mmps = xlsread(filename,9,'B4:B677');
    DistRun38mmps = xlsread(filename,9,'A4:A677');

    % 16mmps
    TimeRun116mmps = xlsread(filename,4,'C4:C646');
    LoadRun116mmps = xlsread(filename,4,'B4:B646');
    DistRun116mmps = xlsread(filename,5,'A4:A646');
    TimeRun216mmps = xlsread(filename,5,'C4:C646');
    LoadRun216mmps = xlsread(filename,5,'B4:B646');
    DistRun216mmps = xlsread(filename,5,'A4:A646');
    TimeRun316mmps = xlsread(filename,6,'C4:C646');
    LoadRun316mmps = xlsread(filename,6,'B4:B646');
    DistRun316mmps = xlsread(filename,6,'A4:A646');

    %30mmps
    TimeRun130mmps = xlsread(filename,1,'C4:C630');
```

```
    LoadRun130mmps = xlsread(filename,1,'B4:B630');
    DistRun130mmps = xlsread(filename,1,'A4:A630');
    TimeRun230mmps = xlsread(filename,2,'C4:C630');
    LoadRun230mmps = xlsread(filename,2,'B4:B630');
    DistRun230mmps = xlsread(filename,2,'A4:A630');
    TimeRun330mmps = xlsread(filename,3,'C4:C630');
    LoadRun330mmps = xlsread(filename,3,'B4:B630');
    DistRun330mmps = xlsread(filename,3,'A4:A630');

% Make a matrix of the results
    Time = NaN(length(TimeRun14mmps),ntests);
    Load = NaN(length(TimeRun14mmps),ntests);
    Dist = NaN(length(TimeRun14mmps),ntests);

    Time(1:numel(TimeRun14mmps),1) = TimeRun14mmps;
    Time(1:numel(TimeRun24mmps),2) = TimeRun24mmps;
    Time(1:numel(TimeRun34mmps),3) = TimeRun34mmps;
    Time(1:numel(TimeRun18mmps),4) = TimeRun18mmps;
    Time(1:numel(TimeRun28mmps),5) = TimeRun28mmps;
    Time(1:numel(TimeRun38mmps),6) = TimeRun38mmps;
    Time(1:numel(TimeRun116mmps),7) = TimeRun116mmps;
    Time(1:numel(TimeRun216mmps),8) = TimeRun216mmps;
    Time(1:numel(TimeRun316mmps),9) = TimeRun316mmps;
    Time(1:numel(TimeRun130mmps),10) = TimeRun130mmps;
    Time(1:numel(TimeRun230mmps),11) = TimeRun230mmps;
    Time(1:numel(TimeRun330mmps),12) = TimeRun330mmps;

    Load(1:numel(LoadRun14mmps),1) = LoadRun14mmps;
    Load(1:numel(LoadRun24mmps),2) = LoadRun24mmps;
    Load(1:numel(LoadRun34mmps),3) = LoadRun34mmps;
    Load(1:numel(LoadRun18mmps),4) = LoadRun18mmps;
    Load(1:numel(LoadRun28mmps),5) = LoadRun28mmps;
    Load(1:numel(LoadRun38mmps),6) = LoadRun38mmps;
    Load(1:numel(LoadRun116mmps),7) = LoadRun116mmps;
    Load(1:numel(LoadRun216mmps),8) = LoadRun216mmps;
    Load(1:numel(LoadRun316mmps),9) = LoadRun316mmps;
    Load(1:numel(LoadRun130mmps),10) = LoadRun130mmps;
    Load(1:numel(LoadRun230mmps),11) = LoadRun230mmps;
    Load(1:numel(LoadRun330mmps),12) = LoadRun330mmps;

    Dist(1:numel(DistRun14mmps),1) = DistRun14mmps;
    Dist(1:numel(DistRun24mmps),2) = DistRun24mmps;
    Dist(1:numel(DistRun34mmps),3) = DistRun34mmps;
    Dist(1:numel(DistRun18mmps),4) = DistRun18mmps;
    Dist(1:numel(DistRun28mmps),5) = DistRun28mmps;
    Dist(1:numel(DistRun38mmps),6) = DistRun38mmps;
    Dist(1:numel(DistRun116mmps),7) = DistRun116mmps;
    Dist(1:numel(DistRun216mmps),8) = DistRun216mmps;
    Dist(1:numel(DistRun316mmps),9) = DistRun316mmps;
    Dist(1:numel(DistRun130mmps),10) = DistRun130mmps;
    Dist(1:numel(DistRun230mmps),11) = DistRun230mmps;
    Dist(1:numel(DistRun330mmps),12) = DistRun330mmps;

% Test velocities for each run:
    vp(1,1) = 0.004;
    vp(2,1) = 0.004;
    vp(3,1) = 0.004;
    vp(4,1) = 0.008;
```

```
    vp(5,1) = 0.008;
    vp(6,1) = 0.008;
    vp(7,1) = 0.016;
    vp(8,1) = 0.016;
    vp(9,1) = 0.016;
    vp(10,1) = 0.030;
    vp(11,1) = 0.030;
    vp(12,1) = 0.030;

% Test variables:
    a = 0.0175;     % Probe radius, m
    R = 0.045;      % Vessel radius, m
    k = a/R;        % Gap ratio
    OB = 0.05;      % Distance probe plunged, m
    density = 1280;     % Density of sample, kg/m3
    L = OB/(1-k^2);     % Length of plunger which is submerged
    Fb = density*9.81*L*pi*(a^2);   % Buoyancy Force

% Plot of raw data, Force vs Time
    figure( 'Name', 'Plot of Raw Data' );
    hold on
    for i = 1:ntests;
        plot(Time(:,i),Load(:,i))
        hold on
    end
    hold on
    xlabel('Time, seconds');
    ylabel('Load, mN');

% As there is some variation of how far the plunger has really entered the
% material, we need to calculate the gradient of the line and then
calculate % what the actual peak force would be if the probe had plunged
exactly from
% the surface
    for i = 1:ntests
        [~,indFt1] = max(Load(:,i));
        MaxForce(i) = max(Load(:,i));
        DistanceAtMaxForce(i) = Dist(indFt1,i);
        TimeAtMaxForce(i) = Time(indFt1,i);
        ForceInCell8(i) = Load(8,i);
        TimeInCell8(i) = Time(8,i);
        DistInCell8(i) = Dist(8,i);

        % 1. Work out the gradient of the line
        m(i) = (MaxForce(i)-ForceInCell8(i))/(TimeAtMaxForce(i)-
TimeInCell8(i));
        mTime1(i) = m(i)*TimeInCell8(i);
        c1T(i) = ForceInCell8(i) - mTime1(i);
        mTime2(i) = m(i)*TimeAtMaxForce(i);
        c2T(i) = MaxForce(i) - mTime2(i);

        % 2. Work out when it would hit the value of force that it started
at
        ForceAtStart(i) = Load(1,i);
        TimeAtStart(i) = (ForceAtStart(i)-c2T(i))/m(i);

        % 3. Work out what the distance between the start and max force is
        [~,indTime] = min(abs(Time(:,i) - TimeAtStart(i)));
```

```
        DistanceAtStart(i) = Dist(indTime,i);
        DistanceOfTest(i) = DistanceAtMaxForce(i) - DistanceAtStart(i);

        % 4. Calculate force at OB (Calculate gradient with respect to
        % distance)
        m2(i) = (MaxForce(i)-ForceInCell8(i))/(DistanceAtMaxForce(i)-
DistInCell8(i));
        mDist1(i) = m2(i)*DistInCell8(i);
        c1D(i) = ForceInCell8(i) - mDist1(i);
        mDist2(i) = m2(i)*DistanceAtMaxForce(i);
        c2D(i) = MaxForce(i) - mDist2(i);
        ForceAtOB(i) = m2(i)*OB*1000;
    end

% Average peak forces at each speed
    FtAv(1) = mean(ForceAtOB(1:3));
    FtAv(2) = mean(ForceAtOB(4:6));
    FtAv(3) = mean(ForceAtOB(7:9));
    FtAv(4) = mean(ForceAtOB(10:12));

% Plot the values of force which would have been at OB on the same plot as
% the raw data
    hold on
    for i = 1:ntests;
    plot ((OB/vp(i)),ForceAtOB(i),'x')
    grid on
    end
    x = [0, max(TimeRun14mmps)];
    y = [Fb*1000, Fb*1000];
    saveas(gcf, 'Plot_Raw_Data_InsertFilenameHere.jpg')
    hold off

% Calculate what the actual buoyancy force would be at the distance that
was
% plunged in the test
    for i = 1:ntests
        LReal(i) = (DistanceOfTest(i)/1000)/(1-k^2);
        FbReal(i) = density*9.81*LReal(i)*pi*(a^2);
        FbAv = mean(FbReal);
    end

% Calculate n from this plot using force corrected for bouyancy, Fcb
    for i = 1:ntests
        Fcb(i) = abs(ForceAtOB(i))/1000 - FbReal(i);
        A(i) = log(vp(i));
        B(i) = log(Fcb(i)/L);
    end
    [xData, yData] = prepareCurveData( B, A );
    % Set up fittype and options.
    ft = fittype( {'x', '1'}, 'independent', 'x', 'dependent', 'y',
    'coefficients', {'b', 'c'} );
    % Fit model to data.
    [fitresult1, gof1] = fit( xData, yData, ft );
    figure( 'Name', 'Calculating value of n' );
    plot(fitresult1,B,A,'x');
    xlabel ln(Fcb/L)
    ylabel ln(plunger speed)
    legend( 'Data Points', 'Fitted Curve', 'Location', 'southeast' );
```

```
    grid on
    saveas(gcf, 'HB_Calculating_n_InsertFilenameHere.jpg')
    Gof1 = struct2cell(gof1);
    n = 1/(fitresult1.b)
    s = 1/n;

% Calculate the residual force once the plunger is stationary, Fte
    for i = 1:ntests
        indOB = find(Dist(:,i) > (OB-0.0001)*1000);
        Fte(i) = mean(Load(indOB,i));
    end

% Average relaxation forces
    FteAv(1) = mean(Fte(1:3));
    FteAv(2) = mean(Fte(4:6));
    FteAv(3) = mean(Fte(7:9));
    FteAv(4) = mean(Fte(10:12));

% Calculate the yield stress from the relaxation force and the calculated
% buoyancy force
% NOTE: yield is only calculated here to check that there is not a large
% yield stress, which would indicate that the Power-Law model is unsuitable
    for i = 1:ntests
        yield(i) = (Fte(i)/1000 - FbReal(i))/(2*pi*LReal(i)*a);
    end
    yieldAv = mean(yield)

% To calculate consistency coefficient, eta, we need to find the value of
% lambda which satisfies equation 5.13
    points = 50;    % Number of lambdas to estimate

    % Below sets up blank matrices
        q1 = zeros(1,points);
        q2 = zeros(1,points);
        phip = zeros(points,1);
        Phi = zeros(points,1);
        Phi1 = zeros(points,1);
        Phi2 = zeros(points,1);
        PhiTarget = zeros(points,1);

    % Estimate lambdaP between two values:
    lambda = linspace(k,1,points);

    for i= 1:points

        fun1 = @(dimr) (((lambda(i).^2)./dimr) - dimr).^s ;
        q1(i) = integral(fun1,k,lambda(i));

        fun2 = @(dimr) (dimr - (lambda(i).^2)./dimr).^s;
        q2(i) = integral(fun2,lambda(i),1);

        phip(i)= q1(i) - q2(i);

        Phi1(i) = 1/(s+3)*(((1-lambda(i).^2).^(s+1))-((k^(1-
s))*((lambda(i).^2)-k^2).^(s+1)));
```

```
        Phi2(i) = phip(i)*((2*(s+1)/(s+3)*lambda(i).^2) - ((lambda(i)^2)-
(k^2)));

        Phi(i) = Phi1(i) + Phi2(i);

        PhiTarget(i) = phip(i)*k^2;
    end

% Now minimise the difference between Phi and PhiTarget and find LambdaP at
% that point
    Difference = abs(Phi - PhiTarget);
    [minimum,ind_min] = min(Difference);    % minimum is the lowest value
and ind_min is the index of where that value is
    lambdamin = lambda(ind_min);            % value of lambda at the index
ind_min
    Phimin = Phi(ind_min);                  % value of Phi at the index
ind_min

% To plot the results of the differences between the two phi estimates at
% each lambda+:
    figure( 'Name', 'Finding the minimum value of Phi and lambda - Power
Law Fluid' );
    plot(lambda,Phi,'b', lambda, PhiTarget, 'r', lambdamin,Phimin,'x')
    xlabel('Lambda');
    ylabel('Phi and phip*k^2');
    legend( '', '', 'Location', 'southeast' );
    grid on
    saveas(gcf, 'PL_Minimum_of_Phi_Lambda_InsertFilenameHere.jpg')

% Dimensionless Shear Stress at the Plunger Wall
    Tw = ((lambdamin.^2)/k)-k;
% Dimensionless Shear Rate at the wall
    dphidq = (((lambdamin^2)/k)-k)^s;
% Calculate the final value of the consistency coefficient
    P = zeros(1,ntests);
    eta = zeros(1,ntests);
    toww = zeros(1,ntests);
    dvdr = zeros(1,ntests);
    ShearStress = zeros(1,ntests);

    for i = 1:ntests
        P(i) = Fcb(i)/((Tw+k)*pi()*L*R*a);
        eta(i) = (P(i)*R/2)*(Phimin*R/(vp(i)*k^2))^n;
        toww(i) = P(i)*R*Tw/2;
        dvdr(i) = ((P(i)*R/(2*eta(i)))^s)*dphidq;
        ShearStress(i) = eta(i) * dvdr(i)^n;
        etaAv = mean(eta)
    end
    Tw = ((lambdamin.^2)/k)-k;
    dphidq = (((lambdamin^2)/k)-k)^s;

% The shear stress vs shear rate can be plotted and saved
    figure('Name','Power Law Predictions of Shear Stress')
    plot (dvdr, eta.*dvdr.^n,'o')
    x = [0, max(dvdr)];
    y = [0, max(etaAv*dvdr.^n)];
    xlabel('Shear Rate, s^-1')
    ylabel('Shear Stress, Pa')
```

```
    grid on
    saveas(gcf, 'PL_Fit_to_Data_InsertFilenameHere.jpg')

% Write to Excel
filename = '5%CMC_PlungerD_PowerLaw';
%Sheet 1
xlswrite(filename, {'Plunger Radius (a), m'}, 1, 'A1')
xlswrite(filename, {'Outer Cyclinder Radius (R), m'}, 1, 'B1')
xlswrite(filename, {'k (a/R)'}, 1, 'C1')
xlswrite(filename, {'Distance moved by probe (L), m'}, 1, 'D1')
xlswrite(filename, {'Density, kg/m^3'}, 1, 'E1')
xlswrite(filename, {'Length of probe submerged (OB), m'}, 1, 'F1')
xlswrite(filename, {'Buoyancy Force (Fb), N'}, 1, 'G1')
xlswrite(filename, {'Flow behaviour index (n)'}, 1, 'I1')
xlswrite(filename, {'Average Consistency Coefficient (etaAv), Pa.s^n'}, 1,
'H1')
xlswrite(filename, {'lambdamin'}, 1, 'J1')
xlswrite(filename, {'Phimin'}, 1, 'K1')
xlswrite(filename, {'Dimensionless Shear Stress at Plunger Wall (Tw)'}, 1,
'L1')
xlswrite(filename, {'Dimensionless Shear Rate (dphidq)'}, 1, 'M1')
xlswrite(filename, a, 1, 'A2')
xlswrite(filename, R, 1, 'B2')
xlswrite(filename, k, 1, 'C2')
xlswrite(filename, L, 1, 'D2')
xlswrite(filename, density, 1, 'E2')
xlswrite(filename, OB, 1, 'F2')
xlswrite(filename, Fb, 1, 'G2')
xlswrite(filename, n, 1, 'H2')
xlswrite(filename, etaAv, 1, 'I2')
xlswrite(filename, lambdamin, 1, 'J2')
xlswrite(filename, Phimin, 1, 'K2')
xlswrite(filename, Tw, 1, 'L2')
xlswrite(filename, dphidq, 1, 'M2')

%Sheet 2
xlswrite(filename, {'Probe Velocity (vp),m/s'}, 2, 'A1')
xlswrite(filename, vp, 2, 'A2')
xlswrite(filename, {'Peak Force Average (Ft), mN'}, 2, 'B1')
xlswrite(filename, FtAv', 2, 'B2')
xlswrite(filename, {'Relaxation Force (Fte), mN'}, 2, 'C1')
xlswrite(filename, FteAv', 2, 'C2')
xlswrite(filename, {'Residual Corrected for Buoyancy (Fcb), N'}, 2, 'D1')
xlswrite(filename, Fcb, 2, 'D2')
xlswrite(filename, {'Pressure drop per unit length (P), Pa/m'}, 2, 'E1')
xlswrite(filename, P', 2, 'E2')
xlswrite(filename, {'Consistency Coefficient (eta), Pa.s^n '}, 2, 'F1')
xlswrite(filename, eta', 2, 'F2')
xlswrite(filename, {'Shear Rate (dvdr), s^-1'}, 2, 'G1')
xlswrite(filename, dvdr', 2, 'G2')
xlswrite(filename, {'Shear Stress at Plunger Wall (toww), Pa'}, 2, 'H1')
xlswrite(filename, toww', 2, 'H2')
xlswrite(filename, {'Hypothetical Yield Stress (should be minimal)'}, 2,
'I1')
xlswrite(filename, yield', 2, 'I2')
xlswrite(filename, {'Consistency coefficient (eta), Pa.s^n'}, 2, 'J1')
xlswrite(filename, eta', 2, 'J2')
```

MATLAB code to determine rheological parameters from the back extrusion technique:

Herschel-Bulkley model

```
clc;
clear;
close all;

% Number of tests:
    nrepeats = 3;
    nspeeds = 4;
    ntests = nrepeats * nspeeds;

% Import the time, load and distance from Excel
    filename = 'ChocPasteFresh_Recipe1_BigVessel_Probe25.xlsx';

    % 4mmps
    TimeRun14mmps = xlsread(filename,10,'C4:C738');
    LoadRun14mmps = xlsread(filename,10,'B4:B738');
    DistRun14mmps = xlsread(filename,10,'A4:A738');
    TimeRun24mmps = xlsread(filename,11,'C4:C738');
    LoadRun24mmps = xlsread(filename,11,'B4:B738');
    DistRun24mmps = xlsread(filename,11,'A4:A738');
    TimeRun34mmps = xlsread(filename,12,'C4:C738');
    LoadRun34mmps = xlsread(filename,12,'B4:B738');
    DistRun34mmps = xlsread(filename,12,'A4:A738');

    % 8mmps
    TimeRun18mmps = xlsread(filename,7,'C4:C677');
    LoadRun18mmps = xlsread(filename,7,'B4:B677');
    DistRun18mmps = xlsread(filename,7,'A4:A677');
    TimeRun28mmps = xlsread(filename,8,'C4:C677');
    LoadRun28mmps = xlsread(filename,8,'B4:B677');
    DistRun28mmps = xlsread(filename,8,'A4:A677');
    TimeRun38mmps = xlsread(filename,9,'C4:C677');
    LoadRun38mmps = xlsread(filename,9,'B4:B677');
    DistRun38mmps = xlsread(filename,9,'A4:A677');

    % 16mmps
    TimeRun116mmps = xlsread(filename,4,'C4:C646');
    LoadRun116mmps = xlsread(filename,4,'B4:B646');
    DistRun116mmps = xlsread(filename,5,'A4:A646');
    TimeRun216mmps = xlsread(filename,5,'C4:C646');
    LoadRun216mmps = xlsread(filename,5,'B4:B646');
    DistRun216mmps = xlsread(filename,5,'A4:A646');
    TimeRun316mmps = xlsread(filename,6,'C4:C646');
    LoadRun316mmps = xlsread(filename,6,'B4:B646');
    DistRun316mmps = xlsread(filename,6,'A4:A646');

    %30mmps
    TimeRun130mmps = xlsread(filename,1,'C4:C630');
    LoadRun130mmps = xlsread(filename,1,'B4:B630');
    DistRun130mmps = xlsread(filename,1,'A4:A630');
```

```
    TimeRun230mmps = xlsread(filename,2,'C4:C630');
    LoadRun230mmps = xlsread(filename,2,'B4:B630');
    DistRun230mmps = xlsread(filename,2,'A4:A630');
    TimeRun330mmps = xlsread(filename,3,'C4:C630');
    LoadRun330mmps = xlsread(filename,3,'B4:B630');
    DistRun330mmps = xlsread(filename,3,'A4:A630');

% Make a matrix of the results
    Time = NaN(length(TimeRun14mmps),ntests);
    Load = NaN(length(TimeRun14mmps),ntests);
    Dist = NaN(length(TimeRun14mmps),ntests);

    Time(1:numel(TimeRun14mmps),1) = TimeRun14mmps;
    Time(1:numel(TimeRun24mmps),2) = TimeRun24mmps;
    Time(1:numel(TimeRun34mmps),3) = TimeRun34mmps;
    Time(1:numel(TimeRun18mmps),4) = TimeRun18mmps;
    Time(1:numel(TimeRun28mmps),5) = TimeRun28mmps;
    Time(1:numel(TimeRun38mmps),6) = TimeRun38mmps;
    Time(1:numel(TimeRun116mmps),7) = TimeRun116mmps;
    Time(1:numel(TimeRun216mmps),8) = TimeRun216mmps;
    Time(1:numel(TimeRun316mmps),9) = TimeRun316mmps;
    Time(1:numel(TimeRun130mmps),10) = TimeRun130mmps;
    Time(1:numel(TimeRun230mmps),11) = TimeRun230mmps;
    Time(1:numel(TimeRun330mmps),12) = TimeRun330mmps;

    Load(1:numel(LoadRun14mmps),1) = LoadRun14mmps;
    Load(1:numel(LoadRun24mmps),2) = LoadRun24mmps;
    Load(1:numel(LoadRun34mmps),3) = LoadRun34mmps;
    Load(1:numel(LoadRun18mmps),4) = LoadRun18mmps;
    Load(1:numel(LoadRun28mmps),5) = LoadRun28mmps;
    Load(1:numel(LoadRun38mmps),6) = LoadRun38mmps;
    Load(1:numel(LoadRun116mmps),7) = LoadRun116mmps;
    Load(1:numel(LoadRun216mmps),8) = LoadRun216mmps;
    Load(1:numel(LoadRun316mmps),9) = LoadRun316mmps;
    Load(1:numel(LoadRun130mmps),10) = LoadRun130mmps;
    Load(1:numel(LoadRun230mmps),11) = LoadRun230mmps;
    Load(1:numel(LoadRun330mmps),12) = LoadRun330mmps;

    Dist(1:numel(DistRun14mmps),1) = DistRun14mmps;
    Dist(1:numel(DistRun24mmps),2) = DistRun24mmps;
    Dist(1:numel(DistRun34mmps),3) = DistRun34mmps;
    Dist(1:numel(DistRun18mmps),4) = DistRun18mmps;
    Dist(1:numel(DistRun28mmps),5) = DistRun28mmps;
    Dist(1:numel(DistRun38mmps),6) = DistRun38mmps;
    Dist(1:numel(DistRun116mmps),7) = DistRun116mmps;
    Dist(1:numel(DistRun216mmps),8) = DistRun216mmps;
    Dist(1:numel(DistRun316mmps),9) = DistRun316mmps;
    Dist(1:numel(DistRun130mmps),10) = DistRun130mmps;
    Dist(1:numel(DistRun230mmps),11) = DistRun230mmps;
    Dist(1:numel(DistRun330mmps),12) = DistRun330mmps;
%%
% Test velocities (m/s) for each run:
    vp(1,1) = 0.004;
    vp(2,1) = 0.004;
    vp(3,1) = 0.004;
    vp(4,1) = 0.008;
    vp(5,1) = 0.008;
    vp(6,1) = 0.008;
```

```
    vp(7,1) = 0.016;
    vp(8,1) = 0.016;
    vp(9,1) = 0.016;
    vp(10,1) = 0.030;
    vp(11,1) = 0.030;
    vp(12,1) = 0.030;

% Test variables:
    a = 0.0125;      % Probe radius, m
    R = 0.045;       % Vessel radius, m
    k = a/R;         % Gap ratio
    OB = 0.05;       % Distance probe plunged, m
    density = 1280.49;  % Density of sample, kg/m3
    L = OB/(1-k^2);     % Length of plunger which is submerged
    Fb = density*9.81*L*pi*(a^2);   % Buoyancy Force

% Plot of raw data, Force vs Time
    figure( 'Name', 'Plot of Raw Data' );
    hold on
    for i = 1:ntests;
        plot(Time(:,i),Load(:,i))
        hold on
    end
    hold on
    xlabel('Time, seconds');
    ylabel('Load, mN');

% As there is some variation of how far the plunger has really entered the
% material, we need to calculate the gradient of the line and then
calculate
% what the actual peak force would be if the probe had plunged exactly from
% the surface
    for i = 1:ntests
        [~,indFt1] = max(Load(:,i));
        MaxForce(i) = max(Load(:,i));
        DistanceAtMaxForce(i) = Dist(indFt1,i);
        TimeAtMaxForce(i) = Time(indFt1,i);
        ForceInCell8(i) = Load(8,i);
        TimeInCell8(i) = Time(8,i);
        DistInCell8(i) = Dist(8,i);

        % 1. Work out the gradient of the line
        m(i) = (MaxForce(i)-ForceInCell8(i))/(TimeAtMaxForce(i)-
TimeInCell8(i));
        mTime1(i) = m(i)*TimeInCell8(i);
        c1T(i) = ForceInCell8(i) - mTime1(i);
        mTime2(i) = m(i)*TimeAtMaxForce(i);
        c2T(i) = MaxForce(i) - mTime2(i);

        % 2. Work out when it would hit the value of force that it started
at
        ForceAtStart(i) = Load(1,i);
        TimeAtStart(i) = (ForceAtStart(i)-c2T(i))/m(i);

        % 3. Work out what the distance between the start and max force is
        [~,indTime] = min(abs(Time(:,i) - TimeAtStart(i)));
        DistanceAtStart(i) = Dist(indTime,i);
        DistanceOfTest(i) = DistanceAtMaxForce(i) - DistanceAtStart(i);
```

```
        % 4. Calculate force at OB (Calculate gradient with respect to
        % distance)
        m2(i) = (MaxForce(i)-ForceInCell8(i))/(DistanceAtMaxForce(i)-
DistInCell8(i));
        mDist1(i) = m2(i)*DistInCell8(i);
        c1D(i) = ForceInCell8(i) - mDist1(i);
        mDist2(i) = m2(i)*DistanceAtMaxForce(i);
        c2D(i) = MaxForce(i) - mDist2(i);
        ForceAtOB(i) = m2(i)*OB*1000;
    end

% Average peak forces at each speed
    FtAv(1) = mean(ForceAtOB(1:3));
    FtAv(2) = mean(ForceAtOB(4:6));
    FtAv(3) = mean(ForceAtOB(7:9));
    FtAv(4) = mean(ForceAtOB(10:12));

% Plot the values of force which would have been at OB on the same plot as
% the raw data
    hold on
    for i = 1:ntests;
    plot ((OB/vp(i)),ForceAtOB(i),'x')
    grid on
    end
    x = [0, max(TimeRun14mmps)];
    y = [Fb*1000, Fb*1000];
    saveas(gcf,
'Plot_Raw_Data_ChocPasteFresh_Recipe1_BigVessel_Probe25.jpg')
    hold off
% Calculate what the actual buoyancy force would be at the distance that
was
% plunged in the test
    for i = 1:ntests
        LReal(i) = (DistanceOfTest(i)/1000)/(1-k^2);
        FbReal(i) = density*9.81*LReal(i)*pi*(a^2);
        FbAv = mean(FbReal);
    end

% Calculate n from this plot using force corrected for bouyancy, Fcb
    for i = 1:ntests
        Fcb(i) = abs(ForceAtOB(i))/1000 - FbReal(i);
        A(i) = log(vp(i));
        B(i) = log(Fcb(i)/L);
    end
    [xData, yData] = prepareCurveData( B, A );
    % Set up fittype and options.
    ft = fittype( {'x', '1'}, 'independent', 'x', 'dependent', 'y',
    'coefficients', {'b', 'c'} );
    % Fit model to data.
    [fitresult1, gof1] = fit( xData, yData, ft );
    figure( 'Name', 'Calculating value of n' );
    plot(fitresult1,B,A,'x');
    xlabel ln(Fcb/L)
    ylabel ln(plunger speed)
    legend( 'Data Points', 'Fitted Curve', 'Location', 'southeast' );
    grid on
    saveas(gcf, 'HB_Calculating_n_ChocPasteFresh_Recipe1_BigVessel.jpg')
```

```
    Gof1 = struct2cell(gof1);
    n = 1/(fitresult1.b)
    s = 1/n;

% Calculate the residual force once the plunger is stationary, Fte
    for i = 1:ntests
        indOB = find(Dist(:,i) > (OB-0.0001)*1000);
        Fte(i) = mean(Load(indOB,i));
    end

% Average relaxation forces
    FteAv(1) = mean(Fte(1:3));
    FteAv(2) = mean(Fte(4:6));
    FteAv(3) = mean(Fte(7:9));
    FteAv(4) = mean(Fte(10:12));

% Calculate the yield stress from the relaxation force and the calculated
% buoyancy force
    for i = 1:ntests
        yield(i) = (Fte(i)/1000 - FbReal(i))/(2*pi*LReal(i)*a);
    end
    yieldAv = mean(yield)

% To calculate consistency coefficient, eta, we need to find values of To
and
% lambda which satisfies equation 5.13:
    pointsL = 50;          % lambda+
    pointsTo = 50;         % To

    % Below sets up blank matrices
        To = zeros(1,pointsTo);
        To1 = zeros(1,pointsTo);
        To1Alt = zeros(1,pointsTo);
        To2 = zeros(1,pointsTo);
        To2Alt = zeros(1,pointsTo);
        To3 = zeros(1,pointsTo);
        To3Alt = zeros(1,pointsTo);
        To4 = zeros(1,pointsTo);
        To4Alt = zeros(1,pointsTo);
        To5 = zeros(1,pointsTo);
        To5Alt = zeros(1,pointsTo);
        To6 = zeros(1,pointsTo);
        To6Alt = zeros(1,pointsTo);
        q1 = zeros(1,pointsTo);
        q2 = zeros(1,pointsTo);
        q3 = zeros(1,pointsTo);
        q4 = zeros(1,pointsTo);
        q5 = zeros(1,pointsTo);
        q6 = zeros(1,pointsTo);
        phip = zeros(pointsL,pointsTo);
        Phi1 = zeros(pointsL,pointsTo);
        Phi2 = zeros(pointsL,pointsTo);
        lambdaM = zeros(pointsL,pointsTo);
        lambdasq = zeros(pointsL,pointsTo);
        Tw = zeros(1,pointsTo);
        Equation31Calc = zeros(1,pointsTo);
        DifferenceP = zeros(1,pointsTo);
```

```
    for j = 1:pointsTo
        %First estimate To between two values:
        To = linspace(0,1-k,pointsTo);
        %Then estimate lambdaP between two values:
        lambdaP = linspace(k,1,pointsL);

        for i= 1:pointsL
            lambdaM(i,j) = lambdaP(i) - To(j) ;
            lambdasq(i,j) = lambdaP(i) * (lambdaP(i) - To(j)) ;

            fun1 = @(dimr) abs(lambdasq(i,j) - (dimr.^2) -
(To(j).*dimr)).^s.*(dimr).^(-s);
            q1(i,j) = integral(fun1,k,lambdaM(i,j));

            fun2 = @(dimr) (dimr.^2 - lambdasq(i,j) -
To(j).*dimr).^s.*dimr.^(-s);
            q2(i,j) = integral(fun2,lambdaP(i),1);

            phip(i,j)= q1(i,j) - q2(i,j);

            fun3 = @(dimr) abs(lambdasq(i,j) - (dimr.^2) -
(To(j).*dimr)).^s.*(dimr).^(2-s);
            q3(i,j) = integral (fun3,k,lambdaM(i,j));

            fun4 = @(dimr) ((dimr.^2) - lambdasq(i,j) -
(To(j).*dimr)).^s.*(dimr).^(2-s);
            q4(i,j) = integral (fun4,lambdaP(i),1);

            Phi1(i,j) = ((k.^2)*phip(i,j)) - q3(i,j) + q4(i,j);

            Phi2(i,j) = phip(i,j)*k.^2;
        end
    end

% Now minimise the difference between Phi and PhiTarget and find LambdaP at
% that point
    DifferencePhi = abs(Phi1 - Phi2);
    [minimum,ind_min] = min(DifferencePhi);
    lambdaPmin = lambdaP(ind_min);

% In order to see how To could change based on Lambda+ at the four plunger
% speeds:
    for i = 1:ntests
        C(i) = (k*Fcb(i))/(2*pi()*L*a*yield(i));
            for j = 1:pointsL
            ToC(i,j)=lambdaP(j)^2/(lambdaP(j)+C(i));
        end
    end

% To find the minimum combination of To and Lamba+, firstly we need to plot
% the 12 curves of how To and lambdaP can relate to each other:
    figure( 'Name', 'Finding the minimum of To and Lambda +' );
    for i = 1:ntests
        plot(ToC(i,:),lambdaP)
        hold on
    end
```

```
% Then, from where Phi = phip*K^2, we can plot the points and a line of
best
% fit of lambdaPmin at each value of To:
    [xData, yData] = prepareCurveData( To, lambdaPmin );
    % Set up fittype and options.
    ft = fittype( 'poly1' );
    % Fit model to data.
    [fitresult, gof2] = fit( xData, yData, ft );
    % Plot fit with data.
    plot( fitresult, xData, yData );
    xlabel('To')
    ylabel('Lambda+')
    legend( 'Data Points', 'Fitted Curve', 'Location', 'southeast' );
    hold on

% Then to work out where the two lines cross for each experiment:
    for i = 1:ntests
        lambdaPTemp(:,i) = fitresult(ToC(i,:));
        lambdaPCross = lambdaPTemp';
        Diff(i,:) = lambdaPCross(i,:) - lambdaP;
        [minDiff,ind_minDiff] = min(abs(Diff(i,:)));
        ToMin(i,:) = ToC(i,ind_minDiff);
        lambdaPMin(i,:) = lambdaP(ind_minDiff);
        plot(ToMin(i,:),lambdaPMin(i,:),'x')
        hold on
    end
    saveas(gcf,
'HB_Minimum_of_To_Lambda_ChocPasteFresh_Recipe1_BigVessel_Probe25.jpg')

% Then to find pressure drop:
    for i = 1:ntests
        PMin(i)= (2*yield(i))/(ToMin(i)*R);
        lambdaMMin(i) = lambdaPMin(i) - ToMin(i);
        lambdaSMin(i) = lambdaPMin(i)*lambdaMMin(i);

        fun1Min = @(dimr) abs(lambdaSMin(i) - (dimr.^2) -
(ToMin(i).*dimr)).^s.*(dimr).^(-s);
        q1Min(i) = integral(fun1Min,k,lambdaMMin(i));

        fun2Min = @(dimr) abs(dimr.^2 - lambdaSMin(i) -
ToMin(i).*dimr).^s.*dimr.^(-s);
        q2Min(i) = integral(fun2Min,lambdaPMin(i),1);

        phipMin(i)= q1Min(i) - q2Min(i);

        fun3Min = @(dimr) abs(lambdaSMin(i) - (dimr.^2) -
(ToMin(i).*dimr)).^s.*(dimr).^(2-s);
        q3Min(i) = integral (fun3Min,k,lambdaMMin(i));

        fun4Min = @(dimr) abs((dimr.^2) - lambdaSMin(i) -
(ToMin(i).*dimr)).^s.*(dimr).^(2-s);
        q4Min(i) = integral (fun4Min,lambdaPMin(i),1);

        PhiMin(i) = ((k.^2)*phipMin(i)) - q3Min(i) + q4Min(i);
        PhiMin2(i) = phipMin(i)*(k^2);
```

```
        eta(i) = (PMin(i)*R/2)*(PhiMin(i)*R/(vp(i)*k^2))^n;              %
Consistency coefficient
        TwMin(i) = (Fcb(i)/(pi()*L*a*R*PMin(i)))-k;                      %
Dimensionless shear stress at the plunger wall
        dPhidq(i) = (((lambdaPMin(i)*lambdaMMin(i))/k)-k-ToMin(i)).^s;   %
Dimensionless shear rate at the wall
        dvdr(i) = ((PMin(i)*R/(2*eta(i)))^s)*dPhidq(i);                  %
Shear rate at the plunger wall
        ShearStress(i) = (eta(i) * dvdr(i)^n)+yield(i);                  %
Shear stress
    end
    etaAv = mean(eta)

% The shear stress vs shear rate can be plotted and saved
    figure('Name','Herschel-Bulkley Model of Shear Stress')
    plot (dvdr, eta.*dvdr.^n + yield,'o')
    % Label axes
    x = [0, max(dvdr)];
    y = [0, max(etaAv*dvdr.^n + yieldAv)];
    xlabel('Shear Rate, s^-1')
    ylabel('Shear Stress, Pa')
    grid on
    saveas(gcf, 'HB_Fit_to_Data_ChocPasteFresh_Recipe1_BigVessel_Probe25.jp
filename = 'CMC_PlungerD_HerschelBulkley';

%Sheet 1
xlswrite(filename, {'Plunger Radius (a), m'}, 1, 'A1')
xlswrite(filename, {'Outer Cyclinder Radius (R), m'}, 1, 'B1')
xlswrite(filename, {'k (a/R)'}, 1, 'C1')
xlswrite(filename, {'Distance moved by probe (L), m'}, 1, 'D1')
xlswrite(filename, {'Density, kg/m^3'}, 1, 'E1')
xlswrite(filename, {'Length of probe submerged (OB), m'}, 1, 'F1')
xlswrite(filename, {'Buoyancy Force (Fb), N'}, 1, 'G1')
xlswrite(filename, {'Flow behaviour index (n)'}, 1, 'H1')
xlswrite(filename, {'Consistency Coefficient (etaAv), Pa.s^n '}, 1, 'I1')
xlswrite(filename, {'Yield Stress Average(yieldAv), Pa'}, 1, 'J1')

xlswrite(filename, a, 1, 'A2')
xlswrite(filename, R, 1, 'B2')
xlswrite(filename, k, 1, 'C2')
xlswrite(filename, L, 1, 'D2')
xlswrite(filename, density, 1, 'E2')
xlswrite(filename, OB, 1, 'F2')
xlswrite(filename, Fb, 1, 'G2')
xlswrite(filename, n, 1, 'H2')
xlswrite(filename, etaAv, 1, 'I2')
xlswrite(filename, yieldAv, 1, 'J2')

%Sheet 2
xlswrite(filename, {'Probe Velocity,m/s'}, 2, 'A1')
xlswrite(filename, vp, 2, 'A2')
xlswrite(filename, {'Measured Peak Force (Ft), mN'}, 2, 'B1')
xlswrite(filename, Ft', 2, 'B2')
xlswrite(filename, {'Peak Force at OB , mN'}, 2, 'C1')
xlswrite(filename, ForceAtOB', 2, 'C2')
xlswrite(filename, {'Relaxation Force (Fte), mN'}, 2, 'D1')
xlswrite(filename, Fte', 2, 'D2')
xlswrite(filename, {'Residual Corrected for Buoyancy (Fcb), N'}, 2, 'E1')
```

```
xlswrite(filename, Fcb, 2, 'E2')
xlswrite(filename, {'Dimensionless Yield Stress, To'}, 2, 'E1')
xlswrite(filename, ToMin, 2, 'E2')
xlswrite(filename, {'Dimensionless Shear Rate at the Wall, s^-1'}, 2, 'F1')
xlswrite(filename, dPhidq', 2, 'F2')
xlswrite(filename, {'Dimensionless Shear Stress at the Wall, (Tw)'}, 2,
'G1')
xlswrite(filename, TwMin', 2, 'G2')
xlswrite(filename, {'Shear Rate at the Wall, s^-1'}, 2, 'H1')
xlswrite(filename, dvdr', 2, 'H2')
xlswrite(filename, {'Shear Stress at the Wall, Pa'}, 2, 'I1')
xlswrite(filename, ShearStress', 2, 'I2')
xlswrite(filename, {'Lambda +'}, 2, 'J1')
xlswrite(filename, lambdaPMin, 2, 'J2')
xlswrite(filename, {'Lambda -'}, 2, 'K1')
xlswrite(filename, lambdaMMin, 2, 'K2')
xlswrite(filename, {'Pressure drop per unit length, Pa/m'}, 2, 'L1')
xlswrite(filename, PMin, 2, 'L2')
xlswrite(filename, {'Yield Stress at each Speed, Pa'}, 2, 'M1')
xlswrite(filename, yield', 2, 'M2')
xlswrite(filename, {'Consistency coefficient (eta), Pa.s^n'}, 2, 'N1')
xlswrite(filename, eta', 2, 'N2')
```

APPENDIX 2

Measured peak and relaxation forces using the BET for each paste produced in trial 2

Run	Peak force at:				Relaxation force at:			
	4 mm s^{-1}	8mm s^{-1}	16 mm s^{-1}	30 mm s^{-1}	4 mm s^{-1}	8mm s^{-1}	16 mm s^{-1}	30 mm s^{-1}
	N	N	N	N	N	N	N	N
1	585.82	670.77	807.22	1076.18	487.52	507.47	507.63	496.37
2	1205.20	1826.91	2649.42	3930.39	496.83	514.62	523.43	538.81
3	949.64	1245.86	1818.55	2751.39	509.95	506.76	509.54	495.62
4	949.66	1316.20	1898.32	2676.90	467.16	474.41	478.94	463.25
5	857.14	1132.84	1585.04	2341.75	503.48	502.57	483.16	479.78
6	942.88	1248.47	1776.39	2676.87	463.16	466.40	486.09	492.65
7	849.05	1097.07	1566.06	2319.81	502.46	504.19	508.67	497.27
8	1662.21	2520.93	3860.33	5600.21	544.27	547.00	549.93	528.87
9	3691.52	6377.41	10459.75	14941.09	758.34	904.94	1142.24	1317.28
10	757.98	973.70	1359.86	1967.76	493.67	508.74	507.34	488.31
11	1370.55	1974.67	3090.74	4918.90	545.38	560.23	553.24	572.65
12	951.32	1273.56	1824.80	2763.68	499.76	505.03	503.56	509.25
13	2097.41	3345.88	4995.84	6221.21	598.94	626.40	652.15	591.00
14	891.48	1182.27	1668.93	2426.19	493.31	496.38	510.31	494.03
15	1782.39	2734.96	4819.81	7719.05	549.81	566.65	604.83	673.23
16	800.23	1028.58	1435.30	2118.11	499.50	516.46	521.72	517.29

17	753.64	949.22	1347.43	2045.23	487.85	483.89	486.89	481.93
18	668.14	797.07	1040.65	1473.84	496.45	494.96	493.72	483.32
19	740.38	938.57	1333.66	1968.91	483.74	494.99	493.29	500.59
20	1190.74	1652.16	2457.38	3522.28	517.72	520.01	531.85	532.02
21	773.51	1009.81	1432.59	2111.21	497.88	495.91	508.90	512.54